

Monomer Recovery from Nylon Carpets via Reactive Extrusion

A Thesis
Presented to
The Academic Faculty

by

Latoya G. Bryson

In Partial Fulfillment
of the Requirements for the Degree
Doctor of Philosophy in the
School of Chemical & Biomolecular Engineering

Georgia Institute of Technology
April 2008

Monomer Recovery from Nylon Carpets via Reactive Extrusion

Approved by:

Dr. John D. Muzzy, Advisor
School of Chemical & Biomolecular
Engineering
Georgia Institute of Technology

Dr. Christopher W. Jones
School of Chemical & Biomolecular
Engineering
Georgia Institute of Technology

Dr. Matthew J. Realf
School of Chemical & Biomolecular
Engineering
Georgia Institute of Technology

Dr. F. Joseph Schork
School of Chemical & Biomolecular
Engineering
Georgia Institute of Technology

Dr. Fred L. Cook
School of Polymer, Textile and Fiber
Engineering
Georgia Institute of Technology

Dr. J. Rhett Mayor
School of Mechanical Engineering
Georgia Institute of Technology

Date Approved: January 22, 2008

Say yes as often as you can. . . .

Now, will saying yes get you in trouble at times? Will saying yes lead you to doing some foolish things? Yes it will. But don't be afraid to be a fool. Remember, you cannot be both young and wise. Young people who pretend to be wise to the ways of the world are mostly just cynics. Cynicism masquerades as wisdom, but it is the farthest thing from it. Because cynics don't learn anything. Because cynicism is a self-imposed blindness, a rejection of the world because we are afraid it will hurt us or disappoint us.

Cynics always say no. But saying yes begins things. Saying yes is how things grow. Saying yes leads to knowledge. "Yes" is for young people. So for as long as you have the strength to, say yes.

...So say "yes." And if you're lucky, you'll find people who will say "yes" back.

Stephen Colbert, Knox College commencement June 3, 2006.

For mi Mada, Breda, Sistas, Ants, ah Cozun dem; nuff rispeck, ah tanx fi ebreyting

ACKNOWLEDGEMENTS

This dissertation would not have been possible without the guidance, assistance, understanding and patience from my advisor Dr. John D. Muzzy. I am indebted to him. My deepest gratitude to Dr. Christopher W. Jones, Dr. Matthew J. Realff, Dr. F. Joseph Schork, Dr. Fred L. Cook, and Dr. J. Rhett Mayor for serving on the thesis reading committee and for providing extremely valuable advice. I would like to thank Dr. Jonathan Colton for his contribution as well.

Special thanks to Dr. Beckham's group for their assistance with the thermogravimetry (TG) equipment, especially Chris Hubbell for training me in TG analysis. Results from SEM would not have been possible without the aid of Yolanda Berta and Lisa Detter-Hoskin. Completion of this project would not have been possible for the assistance of: Trudy Walker, Phyllis Jones, Kevin Guger, the staff at the Bioanalytical Mass Spectrometry Facility, my current and past group members especially Bryan Shaw, Valli Subbiah, Samba Jarju, Lariscia Bryan, Pritesh Patel, Susnata Samanta, and Courtney Woods.

I would also like to thank the Consortium on Competitiveness for the Apparel, Carpet, and Textile Industries (CCACTI), for providing the funds for this research.

The support of my family and friends was also vital to completing this long road. I would especially like to thank my Mom (Juliet) for never giving upon me; my brother (Greg) for being so competitive which only helped to bring out the best in me; my sisters (Alva and Tudy), cousins (Trudy, Andre, Keron, Shane), aunts (Peggy, Gayon, Saline) and uncle (Eric) for their encouragement and involvement in my education. Special

thanks also to Paul Barnswell, Dave Muir, Andrew Robinson, Oneil Gibbs and Dain Walker for their assistance, ear and guidance.

To the Colbert Nation, the staff of the Daily Show with Jon Stewart and the staff of the Colbert Report, particularly Dr. Stephen T. Colbert, D.F.A. (according to him), thanks for uplifting my spirit with laughter and serve as a distraction when I desperately needed to break from the complexities of this project.

Above all, I would like to thank God for all the blessings He has bestowed upon me, for all the struggles He has helped me to overcome, and for allowing me to see this project to completion.

TABLE OF CONTENTS

ACKNOWLEDGEMENTS	v
LIST OF TABLES	x
LIST OF FIGURES	xii
SUMMARY	xx
CHAPTER I: INTRODUCTION	1
Part I: Reaction Characterization	
CHAPTER 2: LITERATURE OVERVIEW	4
2.1. Carpet Waste Sources and Composition	4
2.2. Depolymerization	6
2.3 Catalysts Characterization	13
2.4 Probable Mechanisms	36
CHAPTER 3: EXPERIMENTAL METHODS	48
3.1 Catalyst Screening	48
3.2 Kinetic Determination	51
CHAPTER 4: EXPERIMENTAL RESULTS	52
4.1 Dispersion of Catalysts in Nylon Mixture	52
4.2 Catalyst Effect on Thermal Properties of Nylon 6	57
4.3 Catalyst Screening: Degradation onset	81
4.4 Kinetics Results	89
4.5 Differential Thermogravimetry (DTG)	108
4.6 Differential Thermal Analysis (DTA)	120

Part II: Reactive Extrusion

CHAPTER 5: EXTRUSION THEORY	133
5.1 Extruders	133
5.2 Reactive Extrusion	143
5.3 Solid Conveying	145
5.4 Plasticating/Melting	149
5.5 Metering/Melt Pumping	158
5.6 Mixing	170
5.7 Energy Balance	173
5.8 Devolatilization	183
5.9 Scale up	196
CHAPTER 6: MODEL DEVELOPMENT AND EXPERIMENT METHODS	199
6.1 Basis of the Extruder	199
6.2 Variables in the Model	202
6.3 Functions in the Model	204
6.4 Cost Analysis	224
6.5 Extrusion	226
CHAPTER 7: SIMULATION RESULTS AND VERIFICATION	233
7.1 Effect of Screw Design and Operation Limit	233
7.2 Effect of Scaling on Cost	236
7.3 Extruder Results	239
CHAPTER 8: CONCLUSIONS AND RECOMMENDATIONS	247
APPENDIX	249

A.1	Parameters Used in Modeling	249
A.2	Reactive Extrusion Model Codes	251
	REFERENCES	324

LIST OF TABLES

Table 2.1: Commonly used kinetic models of solid state eactions.....	20
Table 4.1: Comparison of the composition of different catalyst in nylon 6 after mixing using energy-dispersive spectrometry (EDS)	55
Table 4.2: Percent char from dynamic TG with heating 500°C for different catalyst in nylon 6 (cr means carpet ratio)	57
Table 4.3: Thermal transitions of pure nylon 6.....	58
Table 4.4: Melting temperature for different catalyst mass composition in nylon 6.....	60
Table 4.5: Crystallization peak temperature of different mass compositions in nylon 6 .	60
Table 4.6: Melting temperature for different catalyst mole ratio to 30 grams of nylon 6	61
Table 4.7: Crystallization peak temperature for different catalyst mole ratios to 30 grams of nylon 6	62
Table 4.8: Comparison of melting temperatures for each catalyst loading in Nylon 6	63
Table 4.9: Coefficient of determination (R^2) and model for nylon 6 with different temperatures from using isothermal data.....	90
Table 4.10: Determination, E_a and A from the best fitting model from using isothermal data for pure N6	90
Table 4.11: Models and kinetics parameters for different heating rate of pure N6	91
Table 4.12: Kinetic parameters found by using the ASTM standard for pure n6.....	92
Table 4.13: Corresponding temperatures for the E_a , A and Fractions found for pure N6 using DAE model.....	93
Table 4.14: Summary of E_a and A for different catalysts amounts in pure N6.....	97
Table 4.15: Summary of time to get 90% conversion for some catalyst combinations of N6	97
Table 4.16: Kinetic parameters found by using the ASTM standard with the 100:1 ratio of N6:KOH	98

Table 4.17: Kinetic parameters found by using the ASTM standard for 10:1 ratio of N6:KOH.....	99
Table 4.18: Summary of E_a and A for different catalysts amounts in pure N66.....	103
Table 4.19: Summary of time to get 90% conversion for some catalyst combinations with N66 using ASTM kinetic parameters	103
Table 4.20: Kinetic parameters found by using the ASTM standard for carpet N6	107
Table 4.21: Comparison of time to get 90% conversion for some catalyst combinations of N6 and carpet N6	108
Table 4.22: Calculated heat of reaction in mJ/mg for pure N6 with various concentration of several catalysts at different heating rates	131
Table 6.1: Composition of carpet used in model	207
Table A.1: Solid density and melt density of reactor components.	249
Table A.2: Heat capacity of reactor component at room temperature.....	249
Table A. 3: Heat capacity of reactor components at different temperature ranges.....	249
Table A.4: Dimensions given by NFM used in the model	250

LIST OF FIGURES

Figure 2.1: Schematic of tufted carpet.....	5
Figure 2.2: The mass per area for the different components of carpet and the percent make up of used carpet.	6
Figure 2.3: Different types of computational methods used in determining kinetic parameters from isothermal and dynamic TG data.....	15
Figure 2.4: Proposed crosslinking mechanism 1 for nylon 6.....	38
Figure 2.5: Proposed crosslinking mechanism 2 for nylon 6.....	39
Figure 2.6: Proposed intramolecular backbiting mechanism for nylon 6.....	40
Figure 2.7: Proposed mechanism for neighboring H abstraction/ β -C-N hydrogen transfer for nylon 6.....	41
Figure 2.8: Proposed mechanism for end group nitrile formation for nylon 6.....	42
Figure 2.9: Proposed mechanism for single site scission of nylon 6.....	43
Figure 2.10: Proposed mechanism for single site scission of nylon 6.....	44
Figure 2.11: Proposed mechanism for single site KOH attack on nylon 6.....	45
Figure 2.12: Proposed mechanism for neighboring site KOH attack on nylon 6.....	46
Figure 2.13: Formation of imine impurity through a base-catalyzed Claisen-type condensation reaction.....	47
Figure 4.1: Scanning Electron Microscope image of a sample of 10:1 N6:KOH	52
Figure 4.2: Spectrum of a 10:1 ratio of N6:KOH using energy-dispersive spectrometry showing the peaks at energies of characteristic elements present.	54
Figure 4.3: DSC curve for pure nylon 6: 1 st heating at 10 °C/min, 2 nd heating and cooling at 3°C/min	58
Figure 4.4: Second heating curves for different KOH loadings in Nylon 6 (heating at 3 °C per min).....	64

Figure 4.5: Cooling curves for different KOH loadings in Nylon 6 (cooling at 3 °C per min)	65
Figure 4.6: Comparison of the second heating curves for different KOH loadings in Nylon 6 and their residues after catalyst extraction (heating at 3 °C per min)	66
Figure 4.7: Comparison of the cooling curves for different KOH loadings in Nylon 6 and their residues after catalyst extraction (cooling at 3 °C per min).....	67
Figure 4.8: Second heating curves for different K ₂ CO ₃ loadings in Nylon 6 (heating at 3 °C per min).....	68
Figure 4.9: Cooling curves for different K ₂ CO ₃ loadings in Nylon 6 (cooling at 3 °C per min).....	69
Figure 4.10: Comparison of the second heating curves for 10:1 K ₂ CO ₃ loading in Nylon 6 and its residue after catalyst extraction (heating at 3 °C per min) .	69
Figure 4.11: Second heating curves for different NaOH loadings in Nylon 6 (heating at 3 °C per min).....	71
Figure 4.12: Cooling curves for different NaOH loadings in Nylon 6 (cooling at 3 °C per min).....	71
Figure 4.13: Comparison of the second heating curves for different NaOH loadings in Nylon 6 and their residue after catalyst extraction (heating at 3 °C per min).....	72
Figure 4.14: Comparison of the cooling curves for different NaOH loadings in Nylon 6 and their residue after catalyst extraction (cooling at 3 °C per min).....	72
Figure 4.15: Second heating curves for different Na ₂ CO ₃ loadings in Nylon 6 (heating at 3 °C per min).....	73
Figure 4.16: Cooling curves for different Na ₂ CO ₃ loadings in Nylon 6 (cooling at 3 °C per min).....	74
Figure 4.17: Second heating curves for different Cs ₂ CO ₃ loadings in Nylon 6 (heating at 3 °C per min).....	75
Figure 4.18: Cooling curves for different Cs ₂ CO ₃ loadings in Nylon 6 (cooling at 3 °C per min).....	75

Figure 4.19: Second heating curves for different CaCO ₃ loadings in Nylon 6 (heating at 3 °C per min).....	76
Figure 4.20: Cooling curves for different CaCO ₃ loadings in Nylon 6 (cooling at 3 °C per min).....	77
Figure 4.21: GC of the methanol wash extract from a 100:1 ratio of N6 to K ₂ CO ₃ mixture	79
Figure 4.22: Mass spectrum scan of the second peak, which has a retention time of around 3.5 minutes, from the GC of a 100:1 ratio of N6 to K ₂ CO ₃ mixture	79
Figure 4.23: Mass spec scan of the third peak, which has a retention time of around 5 minutes, from the GC of a 100:1 ratio of N6 to K ₂ CO ₃ mixture	80
Figure 4.24: Mass spec scan of the fourth peak, which has a retention time of around 7 minutes, from the GC of a 100:1 ratio of N6 to K ₂ CO ₃ mixture	81
Figure 4.25: Comparison of 10:1 ratios of pure nylon 6 to that of hydroxides catalysts; eut. means eutectic	83
Figure 4.26: Comparison of 10:1 ratios of pure nylon 6 to that of carbonates catalysts.....	84
Figure 4.27: Comparison of 10:1 and 100:1 ratios of nylon 6 to KOH and K ₂ CO ₃ catalysts.....	85
Figure 4.28: Comparison of 200:1 ratios of N6:to KOH and K ₂ CO ₃ catalysts.....	86
Figure 4.29: Comparison of 10:1 ratio of pure nylon 6, 6 to hydroxides and carbonates catalysts.....	87
Figure 4.30: Comparison of 10:1 and 100:1 ratios of Nylon 66 to hydroxide catalysts...	88
Figure 4.31: Comparison of different ratios of nylon 66 to carbonate catalysts.....	88
Figure 4.32: Simulated and experimental conversion curves for dynamic heating of pure N6 using the kinetic parameters found by using the ASTM method.....	92
Figure 4.33: E _a /R, A and Fraction allocated for the 50 possible reactions against the normalized mass of the pure N6.	94
Figure 4.34: The normalized mass remaining for heating at 5 and 10 degrees per minute using the kinetic parameters from the DAE method for pure N6....	95

Figure 4.35: Simulated and experimental conversion curves for dynamic heating of 100:1 ratio of N6:KOH using the kinetic parameters found by using the ASTM method.....	98
Figure 4.36: Simulated and experimental conversion curves for dynamic heating of 10:1 ratio of N6:KOH using the kinetic parameters found by using the ASTM method	99
Figure 4.37: Simulated and experimental conversion curves for dynamic heating of 100:1 N6:K ₂ CO ₃ using the kinetic parameters found by using the ASTM method	100
Figure 4.38: Simulated and experimental conversion curves for dynamic heating of 10:1 N6:K ₂ CO ₃ using the kinetic parameters found by using the ASTM method.....	101
Figure 4.39: Simulated and experimental conversion curves for dynamic heating of carpet ratio (1.8:1) N6:CaCO ₃ using the kinetic parameters found by using the ASTM method.....	102
Figure 4.40: Simulated and experimental conversion curves for dynamic heating of Pure N66 using the kinetic parameters found by using the ASTM method.....	104
Figure 4.41: Simulated and experimental conversion curves for dynamic heating of 100:1 N66:KOH using the kinetic parameters found by using the ASTM method	104
Figure 4.42: Simulated and experimental conversion curves for dynamic heating of 10:1 N66:KOH using the kinetic parameters found by using the ASTM method	105
Figure 4.43: Simulated and experimental conversion curves for dynamic heating of 10:1 N6:K ₂ CO ₃ using the kinetic parameters found by using the ASTM method	105
Figure 4.44: Simulated and experimental conversion curves for dynamic heating of 100:1 N66:NaOH using the kinetic parameters found by using the ASTM method	106
Figure 4.45: Simulated and experimental conversion curves for dynamic heating of carpet ratio (1.8:1) of N66:CaCO ₃ using the kinetic parameters found by using the ASTM method.....	106

Figure 4.46: Simulated and experimental conversion curves for dynamic heating of carpet N6 using the kinetic parameters found by using the ASTM method.....	107
Figure 4.47: DTG of pure N6 with a heating rate of 5 degrees per minute with KOH and CaCO ₃ in different ratios.....	111
Figure 4.48: DTG of pure N6 with heating rate of 5 degrees per minute with different ratios of K ₂ CO ₃ and Cs ₂ CO ₃	111
Figure 4.49: DTG of pure N6 with heating rate of 10 degrees per minute with different ratios of KOH and CaCO ₃	112
Figure 4.50: DTG of pure N6 with heating rate of 10 degrees per minute with different ratio of K ₂ CO ₃ , Cs ₂ CO ₃ NOH and Na ₂ CO ₃	112
Figure 4.51: DTG of N6 carpet with heating rate of 5 degrees per minute 100:1 N6:KOH.....	114
Figure 4.52: DTG of pure N66 with a heating rate of 5 degrees per minute with different ratios of K ₂ CO ₃	115
Figure 4.53: DTG of pure N66 with a heating rate of 5 degrees per minute with different ratios of KOH, NaOH and CaCO ₃	116
Figure 4.54: DTG of pure N66 with a heating rate of 10 degrees per minute with different ratios of K ₂ CO ₃	116
Figure 4.55: DTG of pure N66 with a heating rate of 10 degrees per minute with different ratios of KOH and NaOH.....	117
Figure 4.56: DTG of pure N66 with a heating rate of 10 degrees per minute with different ratios of Cs ₂ CO ₃ , CaCO ₃ , and Na ₂ CO ₃	117
Figure 4.57: DTG of N66 carpet with heating rate of 5 degrees per minute 100:1 N66:KOH.....	119
Figure 4.58: DTA of pure N6 with a heating rate of 5 degrees per minute with different ratios of KOH and CaCO ₃	121
Figure 4.59: DTA of pure N6 with a heating rate of 5 degrees per minute with different ratios of K ₂ CO ₃ and Cs ₂ CO ₃	121
Figure 4.60: DTA of pure N6 with heating rate of 10 degrees per minute with different ratios of KOH, CaCO ₃ and Cs ₂ CO ₃	122

Figure 4.61: DTA of pure N6 with a heating rate of 10 degrees per minute with different ratios of K_2CO_3 , NaOH and Na_2CO_3	122
Figure 4.62: DTA of N6 carpet with heating rate of 5 degrees per minute 100:1 N6:KOH.....	124
Figure 4.63: DTA of pure N66 with heating rate of 5 degrees per minute with different ratios of KOH, NaOH, and $CaCO_3$	125
Figure 4.64: DTA of pure N66 with heating rate of 5 degrees per minute with different ratios of K_2CO_3	126
Figure 4.65: DTA of pure N66 with heating rate of 10 degrees per minute with different ratios of K_2CO_3 and KOH.....	126
Figure 4.66: DTA of pure N66 with a heating rate of 10 degrees per minute with different ratios of NaOH and Cs_2CO_3	127
Figure 4.67: DTA of pure N66 with a heating rate of 10 degrees per minute with different ratios of $CaCO_3$ and Na_2CO_3	127
Figure 4.68: DTA of N66 carpet with heating rate of 5 degrees per minute and 100:1 N66:KOH.....	128
Figure 5.1: Classification of twin screw extruders	134
Figure 5.2: Arrangements of different twin screws	135
Figure 5.3: Contact types in twin screw extruders; left column - counter rotating; right column - co-rotating	136
Figure 5.4: CRNI showing different screw lengths	136
Figure 5.5: Illustration of a screw with its important geometry shown	137
Figure 5.6: Examples of multi-flighted screws.....	139
Figure 5.7: (A) Staggered screw flights; (B) Matched screw flights.....	141
Figure 5.8: Idealized cross section of a channel showing the grow of the film and the direction of flow.....	151
Figure 5.9: Profiles of the temperature and velocity of the differential volume which is perpendicular to the solid melt interface.....	152
Figure 5.10: Vector directions used in describing flow in the extruder.....	152

Figure 5.11: Three plate model used for flow in a CRNI extruder.....	159
Figure 5.12: Apex area of a CRNI extruder.....	160
Figure 5.13: Elements that consumes power in an extruder	175
Figure 5.14: Jacketed barrel.....	177
Figure 5.15: Approximation of the inner diameter for twin screw extruders	178
Figure 5.16: Design of vent for vacuum extraction	191
Figure 5.17: Vent port showing undercut	191
Figure 6.1: Operating range of the 30 mm NFM twin screw extruder	200
Figure 6.2: Screw profile of the 30 mm counter-rotating non-intermeshing twin screw NFM extruder used in the depolymerization process.....	201
Figure 6.3: Variables accounted for in extruder depolymerization model	203
Figure 6.4: Part A of the Flowchart of the “rxnzone2” function.	205
Figure 6.5: Part B of the Flowchart of the “rxnzone2” function.	206
Figure 6.6: Flowchart of the “feedinfo” function.	209
Figure 6.7: NFM/WE Machine diameter with one tenth of their regular capacity.....	211
Figure 6.8: Flowchart of the “screwdim” function.	213
Figure 6.9: Cross-sectional area of the CRNI extruder barrel.	214
Figure 6.10: Barrel cross section showing the gap removed.	215
Figure 6.11: Geometry used in calculation of barrel gap area.....	216
Figure 6.12: Shape of a flight, where R is the radius of the screw root, and $e=0.14$ ”	217
Figure 6.13: Flowchart of the “Meltzone” function.....	218
Figure 6.14: Flowchart of the “Pressure” function.	220
Figure 6.15: Flowchart of the “integrator3” function.	222

Figure 6.16: Flowchart of the “Rxndiff2” function.	224
Figure 6.17: Picture of extruder without vacuum system attachment	227
Figure 6.18: Picture of extruder with vacuum system attachment 1.....	228
Figure 6.19: Picture of die attachment for collection of residual product.	229
Figure 6.20: Picture of extruder with vacuum system with sample collection with bypass.....	230
Figure 6.21: Schematic of the vacuum system with sample collection with bypass	231
Figure 7.1: Conversion of N6 using the un-scaled extruder dimensions at the two boundary operating conditions at 325 (°C).....	234
Figure 7.2: Average temperature in using the un-scaled extruder dimensions at the two boundary operating conditions at 325 (°C).....	235
Figure 7.3: Cost of manufacturing of caprolactam using the un-scaled extruder dimensions at the two boundary operating conditions at 325 (°C).....	236
Figure 7.4: Temperature and N6 Conversion profile of 10 lb/hr of carpet using un-scaled extruder dimensions at 325 (°C)	237
Figure 7.5: Temperature and N6 Conversion profile of 1500lb/hr of carpet using scaled extruder dimensions at 325 (°C)	238
Figure 7.6: Cost of Manufacturing caprolactam and present value ratio of using scaled extruder dimensions at 325 (°C); 10lb/hr not scaled	239
Figure 7.7: Pictures of vent lines clogged with product	240
Figure 7.8: Product collected in the cooling tank	241
Figure 7.9: Close up on cooling collection tank product; the product collected on the steel wool	242
Figure 7.10: Gas chromatograph of the product collected from the extruder.....	243
Figure 7.11: Mass spectra of the main peak from the gas chromatograph of the product collected from the extruder.....	244

SUMMARY

The catalytic depolymerization/pyrolysis of nylon 6 and 66 were investigated with the prospect of helping to curb the amount of carpet landfilled. Thermogravimetric analysis (TGA) was used to determine which catalysts (and their nylon/catalyst ratio) were most suited for the depolymerization. By adding bases, the onset of degradation for some bases was 100 °C lower than that of the pure nylons. Potassium hydroxide and sodium hydroxide were found to be the most effective catalysts at a catalyst ratio of 100:1 of nylon 6 and nylon 66 to catalyst, respectively.

After determining the most efficient catalyst, kinetic models/parameters from the TGA data were determined. These parameters were used in a reactive extrusion model for depolymerizing nylon 6 in carpet. Data from the model was then used to do cost analysis for the process. It was found that to get a Present Value Ratio (PVR) greater than 1, the flow rate has to be greater than or equal to 500 lb/hr. At even higher flow rates up to the model's limit (1500 lb/hr), the Net Present Value (NPV) shows that this process is economically viable.

Extrusion of a 100:1 ratio of pure N6 and KOH was done in a 30 mm counter-rotating non-intermeshing twin screw extruder. The material collected from the vents of the extruder was tested with a gas chromatograph- mass spectrum (GC-MS) in tandem. There was only one significant peak from the GC and the primary molecular weight on the MS was 113, the molecular weight of caprolactam. This shows that the process could be profitable and require little purification if done industrially.

CHAPTER 1

INTRODUCTION

The average lifetime of carpet is between 8 and 12 years [1]. This short lifetime and new constructions have caused the waste stream of carpet to be ever increasing [2]. In 2006, approximately 5.3 billion pounds of carpet was discarded; this number is projected to reach 6.8 billion pounds in 2012 [3]. Of the current carpet wastes, 95% ends up in landfills even though most carpet components are recyclable [2, 3]. Since carpet fibers are not generally biodegradable, land-filling is not an environmentally friendly way to dispose of them [4]. Other disadvantages of using landfills include: the material and energy wasted; and the tipping fees required (which are increasing because of limited capacity) [1, 4].

In response to government regulations, environmental concerns, and consumers demand for recycled products, a variety of technologies have been developed to recycle carpet components [1, 4]. Over the past decades, several carpet/polymer recycling technologies have emerged; they include:

- converting the polymer into products with properties similar to those made from virgin polymer [1, 2, 4]
- melting the carpet waste and forming other products of lower quality [4]
- transforming the waste to chemicals or fuels by processes such as pyrolysis and hydrolysis [4]
 - recovering the energy by incineration of the waste [2].

The inhomogeneity of carpet makes most of these processes difficult and costly to operate; so for economic reasons they are not currently viable to divert most of the carpet from landfills [1].

Of the techniques used to recycle carpet, depolymerization is the preferred method since it allows for recovery of useful monomers. Many efforts have been made in this area, but a cost effective method has not been found. The goal of this research was to develop a method that will efficiently recover monomers from nylon carpet wastes.

Part I:

Reaction Characterization

CHAPTER 2

LITERATURE OVERVIEW

Depolymerization of the nylon in carpet is not a trivial matter. To begin the process, one has to take into account several factors that may affect the reaction outcome. For example, the composition and source of the carpet will affect diffusion and heat transfer, which can either aid or retard the reaction. Having considered these factors, it is also essential to examine previous depolymerization efforts. From these efforts, new ideas may be born, which requires different techniques to characterize the outcomes of these new ideas. In this chapter, reviews of these factors are covered.

2.1. *Carpet Waste Sources and Composition*

To efficiently depolymerize waste carpet, the source and composition of waste carpet must be taken into account. Figure 2.1 shows a schematic of tufted carpet (90% of carpets produced are made this way) [4, 5]. In tufted carpets, the face yarns (typically either nylon 6 or nylon 6,6) are held in place by two layers of mostly polypropylene backing, which are jointed by latex [styrene-butadiene rubber (SBR)] filled with CaCO_3 [4, 5]. Other components added during manufacturing include (but not limited to): dyes, soil repellents and stabilizers.

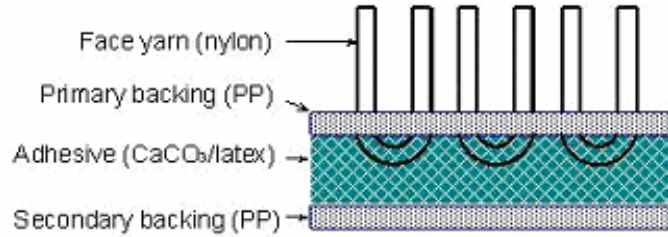


Figure 2.1: Schematic of tufted carpet [5]

Carpet waste can be divided in two categories: pre- and post- consumer waste. Pre-consumer waste includes manufacturing waste in the form of trimmings and cuts, which is approximately 12% of total carpet produced [1]. A large contribution of this waste comes from the automotive industry where millions of pounds of scrap carpet are generated from forming and cutting the carpet into irregular shapes [2]. The other source of carpet wastes is used carpet known as Post-consumer carpet (PCC). PCC generally contains dirt, cleaning chemicals and other materials that accumulate while being used; this causes PCC to be 30% heavier than new carpet [1].

Figure 2.2 shows the mass per area for the different components of carpet and the approximate percent make up of used carpet which is: 40% face yarn, 25% dirt, 5% polypropylene and 30% SBR/CaCO₃ [5]. Since nylon fibers are normally used in the face yarn, recovery of their monomers will reduce the amount of synthetic fibers landfilled from waste carpet by at least 75%.

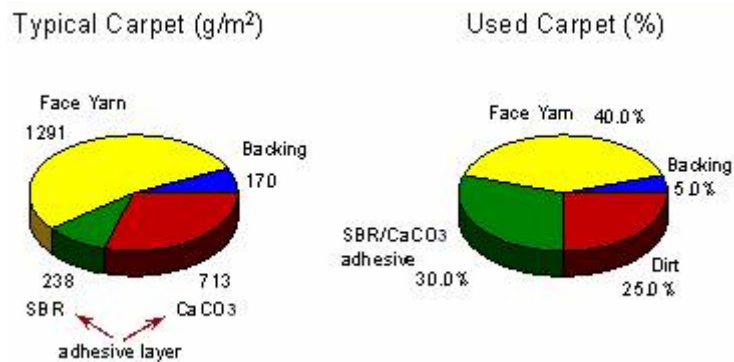


Figure 2.2: The mass per area for the different components of carpet and the percent make up of used carpet [5]

Both nylon 6 and nylon 6,6 are of higher value compared to the other polymers used to make carpet, so there are significant financial incentives to produce their monomers cheaper than current production prices. Depolymerization of the nylon in carpet waste is a potential route for recovering these monomers (caprolactam from nylon 6; adipic acid and hexamethylene diamine from nylon 6,6).

2.2. Depolymerization

Many methods for the depolymerization of nylons have been developed since the 1940's; they normally fall into four categories: ammonolysis, hydrolysis, phase transfer catalysis and pyrolysis. To catalyze these reactions, acids, bases, or salts are used. (Recent reviews on the methods used to depolymerize nylons can be found in references [4] and [1].)

2.2.1 Ammonolysis

In ammonolysis, nylon-containing material is heated in the presence of ammonia with temperature and pressure ranging from 300-350°C and 500-2500 psig, respectively [6]. For each mole of amide group, at least one mole of ammonia should be present in the batch or continuous reactor [6]. The highest reported monomer yield was 81%; water production and the reaction equilibrium inhibited a higher conversion [6]. By-products from this process include: 5-cyanovaleramide, adiponitrile, 6-aminocaproamide and aminocapronitrile [6]. Even though these by-products can be further reacted to give monomers, their separation is very difficult, which is a significant disadvantage for this process.

A two-step amide/ammonolysis depolymerization process for nylon 6, 6 has been used by Bordero et al. [4, 7]. In the first step, nylon 6,6 is treated by n-butylamine at 300°C and 45 atm. From this step, hexamethylene diamine (HMDA) and NN-dibutyladipamide are generated. In the second step, the NN-dibutyladipamide from the first step is ammonolyzed at 285°C and 50 atm to produce adiponitrile. At optimum conditions for this process, the estimated yield is 48% for adiponitrile and 100% for HMDA [4, 7]. Even though the yield of HMDA was good, the yield of the adiponitrile (which can be sold as is or converted to adipic acid or caprolactam) is low which means that there is significant material loss during the process.

A process more selective than traditional ammonolysis was patented by Hendrix et al. [8]. In this process, nitrogen-containing compounds such as amines and ammonia with boiling points lower than 267°C (the boiling point of caprolactam) are used to depolymerize nylon 6. Lewis acids (such as Al_2O_3) and Brønsted acids (such as H_3PO_4)

are used as catalyst. The reaction takes place at temperature and pressure of 250-350°C and 0.9-3 atm, respectively. To prevent the formation of nitriles, the reaction is recommended to take place in the presence of water, unlike traditional ammonolysis processes. Even though the reaction can take place in water, in the examples provided, there were nitriles present in the product. These nitriles represent a burden in purification.

2.2.2 Hydrolysis

Hydrolysis is a decomposition process involving the splitting of a bond in a compound and the addition of hydrogen cations and hydroxide anions from water. For nylon depolymerization, hydrolysis has been done with and without acid and base catalysts. High pressure/superheated steam is normally used in un-catalyzed hydrolysis [9-11]. The highest yield reported was 98% of caprolactam, but the purity wasn't noted [4]. With lower reported yields, the reported purity was only 94.4%, which may limit the ability to give high conversion during re-polymerization [10]. Although the yield from this process is high, non-nylon components were not included in the reactor. The presence of non-nylon components in the reactor may cause a yield reduction. If this method is used industrially, further purification will have to be done which would increase both capital and operating costs.

Acid hydrolysis (also known as the Zimmer AG process) of nylons involves the use of acid in the presence of water (in most cases superheated steam) to decompose a substance [4, 12-21]. Typically in acid hydrolysis, 5-35 weight percent of mineral acids in the presence of superheated steam is used to produce aminocaproic acid, a precursor for caprolactam. Acid hydrolysis is typically a continuous process with an operating

temperature range of 250-400°C. The highest reported yield was 96.4% of caprolactam and 90.7% of adipic acid [1, 4, 17]. The main disadvantage is the numerous purification steps required to recover pure monomers.

Another disadvantage of acid hydrolysis is that it cannot be used with non-mixed polyamide materials [22], so using it with carpet waste would require near perfect separation of the nylon fibers. Also, the CaCO_3 from the backing of the carpet will consume some of the acid used [1].

Basic hydrolysis of nylon to recover the monomers is not as popular as acid hydrolysis. The bases typically used are alkali/alkaline earth oxides, hydroxide and carbonates, as well as, sodium and potassium amino caproates [23-25]. Reactions are typically done between 180-300°C and 0.5-2.2 MPa. The highest reported yield was 92% adipic acid and 98% caprolactam. The main problems with this method are the waste salts generated while recovering adipic acid, and the large amount of base-catalyst used is not reusable. Also, no examples with non-nylon components were provided, which might change the dynamics of the reaction.

2.2.3 Phase Transfer Catalysis

C. Won was able to recover yields as high as 85% of adipic acid and 93% of HMDA from nylon 6,6 with aqueous HCl and benzytrimethylammonium bromide under reflux for 24 hrs [25, 26]. However, under similar conditions, only oligomers were recovered when aqueous NaOH was used. Despite the reasonable yields, the length of the reaction might be too long for industrial applications.

2.2.4 Pyrolysis

Pyrolysis is the decomposition of a substance by simply heating the substance. Only caprolactam was reported as the product from non-catalyzed pyrolysis of nylon 6 between 350-500°C, but the yield and purity wasn't recorded [24]. (It was found that when caprolactam is formed at the end of a chain, the reaction is much faster than when it is formed in the middle of a chain.) Higher temperature pyrolysis of nylon 6 and 6,6 was done at 800°C, and the main products were found to be caprolactam and cyclopentanone, respectively [23].

With the aid of bases, pyrolysis has become a very promising method for depolymerizing nylons. Mukherjee et al. used solid NaOH in a batch reactor for four and a half hours to obtain 90.5% yield of caprolactam from nylon 6 [27]. To shift the equilibrium to the right and obtain the caprolactam, a vacuum was used to pull the caprolactam off. By increasing the catalyst concentration, the yield of caprolactam increased, then started decreasing, and eventually reached an asymptote. By increasing the temperature, there was a three-fold increase in yield between 240 and 250°C. However, by increasing the temperature from 250 to 270°C, there was no appreciable increase in yield. As would be expected according to Le Chatlier's Principle, by increasing the pressure, the yield of caprolactam decreases. Based on these findings, they concluded optimum conditions were: 250°C, 3 mmHg and 1% NaOH. Although the 4½ hours might not seem like a long time, it would not be favorable since other methods have been shown to give higher conversions in less time.

Bayer AG has patented a method in which they used potassium carbonate (0.5-2.5 wt %) as a catalyst to depolymerize nylon 6 [28]. In a stirred tank with an inert atmosphere

and temperature range of 270-300°C, 95% of very pure caprolactam was recovered. It was also found that potassium carbonate increases the rate of depolymerization as compared to that of sodium carbonate. To receive the purity obtained, two distillations were done. No reactions were done with non-nylon components present that might affect the purity of the product.

Czernik et al. from the National Renewable Energy Laboratory (NREL) investigated the catalytic pyrolysis of nylon 6 waste using α -alumina supported KOH (5% w/w) as the catalyst and both a micro-scale reactor/molecular-beam mass-spectrometer system and a fluidized bed [29]. The reaction was carried out in an inert atmosphere and the caprolactam was trapped using a condenser, an electrostatic precipitator, a cold trap and a glass wool filter. At 330-360°C, the rate of the reaction and selectivity were high. In 60 minutes at 360°C, an 85% yield of caprolactam was obtained. The caprolactam collected was less than 90% pure and the major by-products were 2- ω -aminopentylazacyclohept-1-ene and a dimer of caprolactam.

Bockhorn et al. did comparative studies of the depolymerization of pure nylon 6 and nylon 6 from carpet recycling (the only non-nylon 6 component present was 30% polypropylene) with phosphoric acid hydrolysis, non-catalyzed pyrolysis and eutectic NaOH/KOH (60/40 mol %) catalyzed pyrolysis [30, 31]. However, according to several published works (references [32-35]), a true eutectic mixture of NaOH and KOH is 51 and 49 mole% , respectively, and it's melting point is 170°C not 185°C as reported by Bockhorn et al. Nonetheless, at the temperatures used in their works, according to the phase diagram, the catalyst mixture should be all liquid. According to them, since the catalyst is liquid when the polymers are molten, this would prevent phase transfer

limitations. However, phase limitations still exist because the organic liquid of the polymer is not necessarily miscible with the non-organic catalyst. The real advantage of using a liquid catalyst is that with adequate mixing, there would potentially be more dispersion than with the catalyst being solid.

To get dynamic measurements, Bockhorn et al. used a coupled thermogravimetry/mass spectrometry, while to get isothermal measurements they used a closed loop-type reactor. To validate their results, a cycled spheres reactor was utilized. Under purge gas, it was found that the eutectic NaOH/KOH was the most efficient of the methods considered. With the eutectic NaOH/KOH, caprolactam with a purity above 99% was recovered at 290°C from a 5 hour run. Unfortunately, even though the rate increases at higher temperatures, undesired by-products are formed. It was found that while water increased the rate of depolymerization with the acid catalyzed reaction, water impeded the base catalyzed reaction. However, the way in which their kinetic data was attained is questionable and will be discussed later in Chapter 2.

2.2.5 Depolymerization summary

Of the four methods of depolymerization, the base-catalyzed pyrolysis method has been shown to give both high monomer yield and purity. Since in most of the published works, the reactions were done with pure material or brand-new carpet, the effects of the contaminants in PCC were not investigated. Also, direct comparisons of all the catalysts have not been done. So the aim of this work was to efficiently recover both monomers and catalyst from PCC with minimal separation.

2.3 Catalysts Characterization

In the base catalyzed pyrolysis literature, several different bases have been used which show promising results for the recovery of monomers from nylons. However, the equipment and/or the conditions in/under which these catalysts were tested varied significantly from author to author. To test these catalysts under the same condition, a technique call thermogravimetry can be employed.

2.3.1 Thermogravimetry

“Thermogravimetry (TG) is the study of the relationship between a sample’s mass and its temperature” [36]. Typically, as the temperature is increased, the mass decreases because of degradation. This thermal degradation is not only a function of temperature, but also a function of the amount and nature of the decomposition process that proceeded it [37]. There are several ways in which TG is done and they are [36]:

- Dynamic or linear rising temperature
- Isothermal
- Step-wise isothermal
- Sample controlled
- Constrained rate or high resolution
- Constant rate of mass change

In dynamic TG, the sample is heated at a constant rate to a set temperature. As the name suggests, in isothermal TG, the sample is heated to a set temperature and held at that temperature for a predetermined time. A major drawback of isothermal measurement is that they are time-consuming and it is impossible to bring the sample up to the required

temperature without some decomposition at lower temperatures [36]. Step-wise isothermal TG is done by alternating between linear heating at a constant rate and isothermal segments [36]. Unlike step-wise isothermal TG, in sample-controlled TG, the rate of temperature rise is slowed or suspended when a preprogrammed rate of mass is detected and isn't resumed until no further change of mass is sensed [36, 38]. In constrained rate or high resolution TG, as the rate of mass loss increases, the rate of temperature change is slowly reduced from the initial rate [36]. In the final method, as the name suggests, the rate of mass change is set constant and a feedback loop controls the temperature [36]. A nearly quantitative yield of the monomers is usually obtained from TG in an inert atmosphere [36]. The products from polymers with nitrogen usually contain ammonia and or hydrogen cyanide [36].

2.3.1.1 Kinetics from TG

The purpose of doing kinetics studies is to obtain parameters that will be used to predict reaction speed. In order to find out what these parameters are, knowledge of the mechanism of the reaction is needed. However, in heterogeneous kinetics, mechanism determination is very difficult, so reaction models are used to guess/rule out the “mechanism(s)” [39]. There are several ways to use TG to obtain kinetic data and the most popular methods are derived from dynamic, isothermal and modulated TG. Figure 2.1 shows some (of many) different types of computational methods that are used in determining kinetic parameters using isothermal and dynamic methods. Usually with model free methods, only the activation energy is reported while with the model fitting, the pre-exponential term can also be found [39]. Model free methods are sometimes

referred to as isoconversional, but not all model-free methods are isoconversional; for instance, the Kissinger method is not isoconversional, but is model-free [39]. The model is usually chosen by using statistical fits of the data. Because of this, researchers support their models by using other techniques such as microscopy, spectroscopy, X-ray diffraction, and product/evolved gas analysis [39].

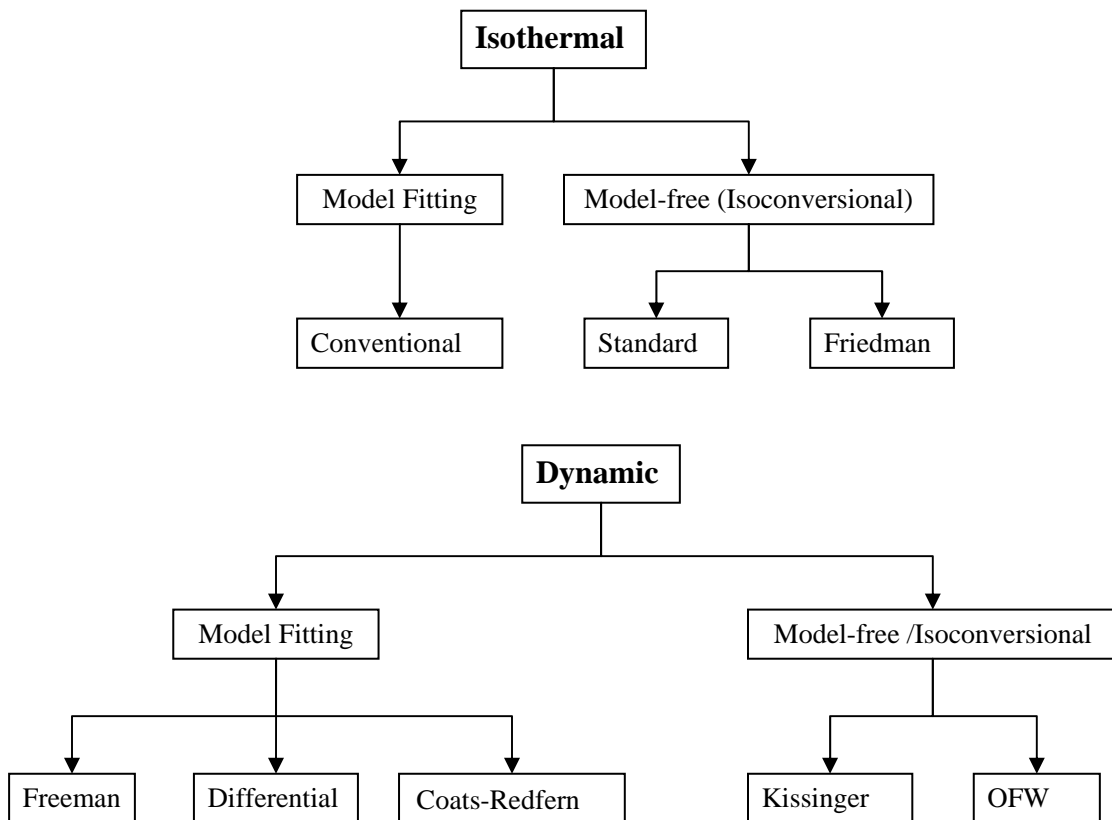


Figure 2.3: Different types of computational methods used in determining kinetic parameters from isothermal and dynamic TG data (OFW=Ozawa-Flynn-Wall) [39]

Since the samples in polymer decompositions are usually solid/molten, the catalysts solids and the products gases, the decompositions are considered heterogeneous

reactions [36]. The rate equation below is normally used to determine the kinetic parameters (Arrhenius-like) [40]:

$$\frac{d\alpha}{dt} = kf(\alpha) \quad 2.1$$

where, α is the conversion fraction, t is time, $f(\alpha)$ is the differential reaction model and

$$k = A \exp(-E_a / RT) \quad 2.2$$

where, R is the universal gas constant, T is the temperature, E_a provides a measure of the magnitude of the energy barrier to reaction while A measures the frequency of the conditions that may lead to a reaction [36]. However, there is controversy in the scientific community on the validity of using these Arrhenius parameters which have no theoretical basis in heterogeneous reaction [40]. Nevertheless, these kinetic constants when derived for heterogeneous reactions can be treated as “procedural parameters” as long as their limitations are acknowledged [40].

With the differential reaction model of Equation 2.1 there naturally exists the integral reaction model which is [39]:

$$g(\alpha) = \int \frac{d\alpha}{f(\alpha)} \quad 2.3$$

After integration and substitution of equation 2.1 , then the integral reaction model becomes:

$$g(\alpha) = A \exp\left(-\frac{E_a}{RT}\right)t \quad 2.4$$

Equations 2.1 and 2.4 are only applicable when isothermal conditions are used; they can be changed to non-isothermal/dynamic by substituting equation 2.5 into equation 2.1 to obtain the differential reaction model ($f(\alpha)$ - equation 2.7) and then integrating to give the respective integral reaction model ($g(\alpha)$ – equation 2.8).

$$\frac{d\alpha}{dT} = \frac{d\alpha}{dt} * \frac{dt}{dT} \quad 2.5$$

By defining,

$$\beta = \frac{dT}{dt} \quad 2.6$$

Then equation 2.5 becomes

$$\frac{d\alpha}{dT} = \frac{1}{\beta} kf(\alpha) \quad 2.7$$

By rearranging equation 2.7 and substituting it into equation 2.3 and then integrating, the following equation for the non-isothermal integral reaction model is derived:

$$g(\alpha) = \frac{A}{\beta} \int_0^T e^{-\frac{E_a}{RT}} dT \quad 2.8$$

The general relationship of the differential reaction model is normally shown in the Ng equation (equation 2.9) [36].

$$\frac{d\alpha}{dt} = k\alpha^m(1-\alpha)^n \quad 2.9$$

By changing the values of m and n other subclasses such as: reaction order decay, nucleation and growth, geometric contraction, diffusion are derived (see Table 2.1) [36, 39]. (If the reader is interested, an excellent review of these different models can be found in reference [39].)

Table 2.1 below contains kinetics models based on physical-geometrical assumptions of regularly shaped bodies [40]. (The designation of constant, sigmoidal, acceleration, or deceleration come from plotting α versus t [39, 41]). These models relate nucleation and nuclei growth to the kinetics of phase transformations and decompositions [40]. Before using these models, one must keep in mind the boundaries that apply to these models. It has been shown that the physico-geometric kinetic model is dependent on the shape of the crucible and the arrangement of the powder [42]. Additionally, under different settings, the sample compound may fit different $f(\alpha)$ functions [42]. Furthermore, even though there is a lack of meaning of n in some models, data may fit well with reaction orders of 0, $\frac{1}{2}$, $\frac{2}{3}$, or 1 [42].

The power law models are derived from geometric models of advancing interface [43]. For the power law model, n is defined as:

$$n = \eta + \lambda \quad 2.10$$

where, η is the number of steps involved in the formation of the reacting nucleus. (If nucleation continues during the reaction, the acceleratory character of the reaction increases.) λ is the number of dimensions in which the nuclei grow. These acceleratory

equations are only applicable to the early stage of reaction when the assumption of unrestricted nucleus growth is acceptable [43]. For the power law models, the value for n can only be whole numbers; hence, the different models are referred to as $P1$, $P2$, etc. depending on the value of n . For the base catalyzed pyrolysis of nylon, the growth of nuclei is unrestricted therefore, the power law models maybe applicable.

Table 2.1: Commonly used kinetic models of solid state reactions [39, 41, 42, 44]

Symbol	Model	$f(\alpha)$	$g(\alpha)$
Constant			
F0/R1	zero order	1	α
Sigmoidal Curves			
JMA	Nucleation and growth ($n= 0.5, 1, 1.5, 2, 2.5, 3, 4$)	$n(1-\alpha)[-ln(1-\alpha)]^{1-1/n}$	$[-ln(1-\alpha)]^{1/n}$
Deceleration Curves			
Rn	Phase boundary controlled reaction (Geometrical Contraction) ($n=0, 1/2, 2/3$)	$(1-\alpha)^n$	$[1-(1-\alpha)^{1-n}]/1-n$
D1	1D-diffusion	$1/2\alpha$	α^2
D2	2D-diffusion	$-1/ln(1-\alpha)$	$\alpha+(1-\alpha)ln(1-\alpha)$
D3	3D-diffusion (Jander equation)	$[3(1-\alpha)^{2/3}]/[2(1-(1-\alpha)^{1/3})]$	$[1-(1-\alpha)^{1/3}]^2$
D4	3D-diffusion (Ginstling-Brounshtein equation)	$3/2[(1-\alpha)^{-1/3}-1]$	$1-2a/3-(1-a)^{2/3}$
F1	First-order	$(1-\alpha)$	$-ln(1-\alpha)$
F2	Second- order	$(1-\alpha)^2$	$(1-\alpha)^{-1}-1$
F3	Third-order	$(1-\alpha)^3$	$0.5((1-\alpha)^{-2}-1)$
Acceleration Curves			
Pn	Power law	$n\alpha^{(n-1)/n}$	$\alpha^{1/n}$

The JMA models, also known as the Avrami-Erofeev models, have been developed from two different approaches which yielded the same results [43]. One approach is based on the probability of the reaction steps occurring in a particular time interval while the other approach was derived from the power law model with the 3D

growth of randomly-distributed nuclei on large crystals [43]. The meaning on n for the JMA models depends on the nucleation rate law, whether it be power, linear, exponential, or instantaneous [43]. The short form nomenclature for the JMA model is similar to the power law, where the value of n is attached to a letter as in $A2$ where A is the symbolic representation for the JMA models. The $A2$ model was developed for flat nuclei while the $A3$ model is for reactions that proceed through the development of cylindrical nuclei which are initiated at the edges or surface cracks in the reactant solid [43]. The $A1$ model is the same as the $F1$ model which is applicable to fine powders when the particle nucleation occurs randomly and the growth doesn't advance beyond the individual crystallite that was nucleated [43]. Since the development of the nuclei in the based catalyzed depolymerization of nylon cannot be discerned, the JMA models may be applicable.

The geometric contraction models, Rn 's, are applicable when there is a rapid development of a large number of closely spaced growing nuclei [43]. This occurs because the Gibbs energy for nucleus formation is comparable to that of the subsequent growth or the development of the nuclei is anisotropic [43]. As a result, the maximum rate of reaction occurs at low α ; hence, these curves are deceleratory [43]. When $n=2$ ($R2$), nucleation occurs only on certain crystal surfaces and then proceed inwards from the edges of only a disc or plate-like particle hence, only the area is contracting [43]. $R3$ is known as the contracting volume model, and like $R2$, proceeds from the surface inwards, but occurs in a 3D manner [43]. $R1$ is the same as the $F0$ model which applies to reactions that proceeds at constant rate, i.e. linear advancement of reaction at a constant rate [43]. As with the JMA models, the development of the nuclei in the based catalyzed

depolymerization of nylon cannot be discerned so the geometric contraction models may be applicable to the base catalyzed depolymerization of nylon.

The diffusion models, as the name suggests have to do with the diffusion of both products and reactants. The *D1* model is valid for reactions where there is a constant reaction zone area and the rate of product formation decreases in direct proportion to the thickness of the product barrier layer [43]. *D2* is applicable for diffusion controlled reactions in 2D as in a cylindrical particle [43]. *D3* was derived from a combination of *D1* with *R3*, i.e. diffusion in 3D with a constant reaction zone volume [43]. *D4*, even though a 3D model, is applicable when the ratio of the molar volume of the reaction and product approaches 1, in which case *D3* is simplified to *D4* [43]. Because of the size of the nylon chain, there may be some diffusion limitations in the depolymerization, so the diffusion models maybe probable.

Even though determining which form to use can be done by using isothermal TG, the process is not very straightforward [36]. Also, one has to be careful when interpreting the data at different temperatures because the mechanism may change at higher temperatures [36].

2.3.1.1.1 Isothermal TG: Model-Fitting Method

In the conventional isothermal curve fitting method, the first step is to determine $g(\alpha)$ for each isotherm by taking several α values from 0.01 to 0.99 and substitute them in the model functions shown in Table 2.1 for $g(\alpha)$ [39]. Next, each $g(\alpha)$ is plotted against the corresponding time for the selected α 's. At this point, the model that fits best can be determined by using equation 2.1; i.e. a linear regression is done of the data and from which the highest coefficient of determination (R^2) is obtained - which should be the

closest to 1. The slope of this linear fit is equivalent to the rate constant, k , in equation 2.1.

A second fit is then needed to determine the A and E_a from the natural logarithm of equation 2.1. This is done by plotting the natural logarithm of k versus the inverse temperature from the different isotherms. The slope of each fit will correspond to $-E_a/R$ for each model and the intercept will be equal to A . The authors of reference [39] pointed out that for all the models, the values of E_a was similar, which usually doesn't happen with homogenous reactions, but a complete explanation of why this occurs has not yet been presented.

2.3.1.1.2 Isothermal TG: Model-free/Isoconventional Methods

2.3.1.1.2.1 Standard / Flynn Technique

If the natural logarithm is taken of equation 2.4, the resulting equation would be [39, 45]:

$$\ln(g(\alpha)) = \ln(A) - \frac{E_a}{RT} + \ln(t) \quad 2.11$$

By rearranging the above equation, a plot of $-\ln t$ versus $1/T$ for each α can be made. From this, and E_a for each α can be obtained. It should be noted that in past observations with isothermal heating, E_a decreases with increasing weight loss, whereas with dynamic heating, E_a increases with increasing in weight loss [45].

2.3.1.1.2.2 Friedman's Isoconversional Method

The Friedman method utilizes the proportionality of the conversion rate and the rate constant for a given conversion to get the E_a over different temperatures [42]. If equation

2.2 is substituted into equation 2.1 and the natural logarithm is taken, then the resulting equation is [39, 42, 45]:

$$\ln \frac{d\alpha}{dt} = \ln(Af(\alpha)) - \frac{E_a}{RT} \quad 2.12$$

Regardless of the model used from Table 2.1, the slope of a plot of $\ln(d\alpha/dt)$ versus $1/T$ will yield E_a for each α [39].

2.3.1.1.3 Dynamic TG: Model-Fitting Methods

2.3.1.1.3.1 Masterplots

One way to determine which kinetic model best describes the experimental data is to fit the data to theoretical curves or masterplots [42]. The most distinct masterplot is that of $f(\alpha)g(\alpha)$ versus α [42]. For the theoretical curves, E_a is not required, just α from the experiments can be substituted in the equations in the Table 2.1. For the experimental plot, a known value of E_a is needed to calculate $g(\alpha)$ (equation 2.13) in the $f(\alpha)g(\alpha)$ expression. The dynamic $g(\alpha)$ is calculated from the following equation (its derivation is discussed in reference [42]):

$$\ln g(\alpha) = \ln \frac{AE_a}{\beta R} - 5.33 - 1.05 \frac{E_a}{RT} \quad 2.13$$

The curve that the experimental plot fits is indicative of the kinetic method that best describes the process.

2.3.1.1.3.2 Direct Differential Method

Another way to obtain kinetics from dynamic TG is to use the direct differential method. In this method, the natural logarithm of the differential form of the rate law is used. The resulting equation is [39]:

$$\ln \frac{d\alpha / dT}{f(\alpha)} = \ln \frac{A}{\beta} - \frac{E_a}{RT} \quad 2.14$$

From the slope and intercept of plotting $\ln \frac{d\alpha / dT}{f(\alpha)}$ versus $1/T$, E_a and A can be calculated respectively.

2.3.1.1.3.3 Coats and Redfern Method

The Coats and Redfern method is an integral method (which uses Taylor's expansion in order to do the integral) which has been shown to have small experimental errors [40, 44]. From the integral form of the rate law and the Taylor's expansion one obtains [39, 41, 44]:

$$\ln \frac{g(\alpha)}{T^2} = \ln \left(\frac{AE_a}{R\beta} \left[1 - \left\{ \frac{2RT_{\text{exp}}}{E_a} \right\} \right] \right) - \frac{E_a}{RT} \quad 2.15$$

where T_{exp} is the mean experimental temperature. By plotting $\ln(g(\alpha)/T^2)$ vs $1/T$, the E_a can be calculated from the slope. The model that is chosen from this method is that one that gives the best linear fit.

2.3.1.1.3.4 Freeman and Carroll

The original method of Freeman and Carroll is very popular and it assumes that the kinetic law follows [42]:

$$\frac{d \ln(d\alpha / dt)}{d \ln(1-\alpha)} = n - \frac{E_a}{R} \frac{d(1/T)}{\ln(1-\alpha)} \quad 2.16$$

Like other methods, E_a can be obtained from the slope of a plot of:

$$\frac{d \ln(d\alpha / dt)}{d \ln(1-\alpha)} \text{ vs } \frac{d(1/T)}{\ln(1-\alpha)}$$

The reaction order can be obtained from the intercept and the A can be obtained by using the equation from the Friedman technique [46]. However, it suffers from not being able to correctly describe the type of reaction that takes place, whether nucleation or diffusion, etc. [42]. To compensate for this and to make it more wide-ranging to see which method fits best, a more general approach is to take the natural logarithm of the differential form of the rate law, then take the incremental differences of the variables and rearrange to obtain [39]:

$$\frac{\Delta \ln \frac{d\alpha}{dt}}{\Delta \ln f(\alpha)} = - \frac{E_a}{R} \frac{\Delta 1/T}{\Delta \ln f(\alpha)} \quad 2.17$$

After plotting $\frac{\Delta \ln \frac{d\alpha}{dt}}{\Delta \ln f(\alpha)}$ versus $\frac{\Delta 1/T}{\Delta \ln f(\alpha)}$, E_a can be attained from the slope [39].

2.3.1.1.3.5 Direct Least Square Method

Another approach for model fitting proposed by Bockhorn et al. is to use a Direct Least Square method for finding the kinetic parameters [47]. They assumed that:

$$f(\alpha) = (1 - \alpha)^n \quad 2.18$$

They then proceeded to describe a method that involves using least squares between the experimental α 's and the calculated α 's. A major flaw with their method is that to get the calculated α 's, they used the "kinetic compensation effect" that was described by Criado and Gonzalez [48]. The "kinetic compensation effect" is when there is a linear relationship between the activation energy and the pre-exponential factor in the Arrhenius equation. Bockhorn et al. did not describe how they accounted for this effect since they were simultaneously calculating n , A and E_a . If one assumes that they used the coefficients in the Criado and Gonzalez paper to find the relationship between A and E_a , then they are using the wrong coefficients since the three parameters compensation effect relationship that was described by Criado and Gonzalez were for carbonates of cadmium (Cd), manganese (Mn) and lead (Pb); all of which had different linear coefficients to relate A and E_a . Hence, the kinetic parameters that they found in references [30, 31] for nylon 6 and carpet are questionable.

2.3.1.1.4 Dynamic TG: Model-free/Isoconventional Methods

Isoconventional methods are called model-free methods because they allow for the calculation of E_a without having to assume a kinetic model [42]. An advantage of isoconventional methods is that one can test if the kinetic parameters remain constant for

the entire conversion [42]. Included in this category are the methods of Kissinger, Friedman, and Flynn-Wall-Ozawa.

2.3.1.1.4.1 Kissinger Method

The Kissinger method involves using the temperature at the maximum rate of conversion [42]. However, it has been shown that this method is applicable to all conversions [42]. In the Kissinger method, $f(\alpha)$ is taken as [39]:

$$f(\alpha) = (1 - \alpha)^n \quad 2.19$$

As indicated by Kissinger, the maximum reaction rate takes place when the second temperature derivative of α is zero [42]. If equation 2.19 is then substituted into equation 2.1, then the second temperature derivative of α is taken and set to zero, the resulting equation would be a function of the peak (maximum) temperature and the equivalent α [39, 41]. By taking the natural log of this resulting equation, one obtains [41]:

$$\ln \frac{\beta}{T_p^2} = \ln \frac{AR}{E_a} + \ln [n(1 - \alpha_p)^{n-1}] - \frac{E_a}{RT_p} \quad 2.20$$

Through plotting $\ln (\beta/T_p^2)$ vs $1/T$, the E_a can be obtained. (A more generalized Kissinger method can be done with the $f(\alpha)$'s listed in Table 2.1 [39].)

2.3.1.1.4.2 Ozawa-Flynn-Wall (OFW)

The most popular method for determining degradation kinetics, OFW, comes from the independently done work of Ozawa and Flynn, and Wall. Their works have been incorporated into the ASTM standard [36, 49-51]. In the ASTM standard, the degradation is assumed to be first order and TG is done for at least three different heating rates [36]. The temperature at which set percentages of mass loss is noted and plotted against the heating rate to give linear plots whose slopes and intercepts are used to determine E_a and A [36]. To use the OFW with any model not just first order, used for the right hand side of equation 2.13 for the dynamic $g(\alpha)$. With some rearrangement and taking the common log of the resulting equation the subsequent equation is acquired [39, 41, 42]:

$$\log \beta = \log \frac{AE_a}{g(\alpha)R} - 2.315 - 0.457 \frac{E_a}{RT} \quad 2.21$$

The slope of a plot of $\log \beta$ versus $1/T$ generates E_a .

2.3.1.1.4.3 Distributed Activated Energy (DAE) Model

Another approach to determining kinetics from dynamic TG was done by Scott et al. [52]. In their approach, they utilized the distributed activated energy (DAE) model, which was used previously by other authors, to identify and characterize the core distribution of a finite number of reactions that occur during devolatilizations without using a step function approximation. One of the major assumptions made is that the reactions occur sequentially in order of increasing activation energy. It is assumed that

these activation energies do not overlap even though in reality the reactions maybe occurring in parallel [52]. Under these circumstances, for a given conversion, one single reaction will dominate no matter what the conversion may be [52]. For this method, data from at least two TG runs at constant but different heating rates are used. One of the assumptions in this method is that there is a complex mixture of components in the sample that decomposes with first order kinetics [52]. According to the authors, the data may deviate from first order kinetics because of either a distribution of activation energy or a gradual spread of the reacting front through the sample.

From the inversion of the DAE, one is able to identify a set of possible reactions and to calculate the corresponding E_a , A , and the fraction of the original sample that follows that pair of kinetic constants. It turns out that A increases monotonically with E_a because of the compensation effect due to changes in the entropy. However, even though A was found for all conversions, the value of A is not accurate for each conversion because it was evaluated for conversion, $\alpha = 1 - e^{-1} = 0.368$ [52]. This value corresponds to the maximum rate of degradation for a single first order reaction [52].

2.3.1.1.5 Modulated (MTG)

The use of modulated thermogravimetry (MTG) is a relatively new and model-free method for obtaining TG kinetics. In MTG, an oscillatory temperature program is used to linearly ramp the temperature [36]. This induces an oscillatory mass flow which is proportional to the physical properties of the polymer specimen being used [36]. The activation energy of a decomposition reaction may be calculated using Equation 2.22 [36].

$$E_a = \frac{R[T_{av}^2 - (0.5T_{amp})^2]L}{T_{amp}} \quad 2.22$$

where R is the universal gas constant, T_{av} is the average thermodynamic temperature, T_{amp} is the amplitude of the temperature modulation and L is the logarithm of the amplitude of the rate of mass loss over one modulation.

2.3.1.1.6 TG Kinetics Drawbacks

Before techniques such as TG, the analysis of heterogeneous reactions to obtain the activation energy was studied by using isothermal conditions but this method is burdensome and tedious [40]. As a result, 90% of kinetics studies in recent papers present results from conventional dynamic TG method [40]. However, there are groups of scientists that question the reliability of these methods. Many say that the physical meaning of these kinetic constants is murky and these constants are only applicable to the experimental conditions from which they were derived [40].

Conventional TG failures arise from the influence of experimental factors such as the grain size and shape, the composition of the gas atmosphere and the heating rate [40]. While maintaining a constant heating rate when the sample size is increased, the TG curve moves towards higher temperatures [40]. Similarly, when the pumping rate is decreased and the sample size and heating rates are held constant the curves move towards higher temperatures [40]. This has led to lack of agreement and reproducibility of data. Some interpret this as a mass transport effect [40].

The concept of reaction order and the application of the Arrhenius equation are borrowed from homogenous kinetics and are usually applied to condensed phase reactions. Because of this, there is a misconception of the theoretical basis for the equation [40]. It should also be noted that in solid and liquid state reactions, there may be an infinite number of elementary processes and none will be rate limiting and so the specific Arrhenius parameters will not be the only significant ones [40]. Hence, some say that activation energy has no relevance in condensed phase reactions [40]. Others have found a strong mutual correlation between E_a and A , in which A increases as E_a increases; this is known as the kinetic compensation effect [40]. Some say this is an artifact from using the Arrhenius equation, but no one has been able to present any physical meaning for the kinetic compensation effect [40].

2.3.2 Differential Thermogravimetry (DTG)

Differential thermogravimetry or derivative thermogravimetry (DTG) is similar to TG except that the output is the mass rate loss versus time or temperature [37]. In a plot of the rate loss (dm/dt) versus temperature, the area under the curve is equal to the mass-change and the height of the peak at any temperature gives the rate of the mass-change at that temperature [53].

DTG is useful in determining mechanism because it can be used to show the various stages of thermal decomposition by the peaks [37]. By using the minimum in the DTG curve, one may be able to approximately determine where the different reaction starts or at what temperature range is that one dominant [53]. If there are overlapping

reactions occurring, it may be difficult to locate a clear-cut point on the TG curve where one reaction ends and the other starts [53].

2.3.3 Differential Scanning Calorimeter (DSC) and Differential Thermal Analysis (DTA)

Either differential scanning calorimeter (DSC) or differential thermal analysis (DTA) is used in the characterization of polymers by analysis of thermal transitions [54]. In DSC, there are two chambers: a reference and a sample chamber. The reference contains an empty pan while the sample is in a similar pan but with the material whose thermal characteristic is to be determined. In a DSC, the sample and reference are provided with separate heaters while in the DTA they are not [54]. When the DSC is being run, the temperature of both chambers is monitored and if their temperatures differ, heat or coolant is used to make the temperatures equal to the programmed temperature [55]. The temperature is usually ramped at a controlled rate to follow the program temperature [54]. The heat capacity of the sample is thus measured because it is proportional to the difference in energy to the two chambers per unit time [55]. By using high heating rates, the thermal spectra become more sensitive, but have a lower resolution for the transition temperature [54]. A plot of the heat flux versus temperature is the output from the DSC [54]. By dividing the heat flux by the heating rate, then the heat capacity, C_p , can be obtained [54].

There is always an instrumental lag time with scanning thermal analysis which can cause the observed transitions to be “smeared” [54]. To account for the lag time, the onset of melting is used as the melting point rather than the peak value, but typically the

peak is reported as the melting points [54]. In polymers, the melting peak is usually broad (up to 50°C) [54]. The instrumental error for DSC is typically $\pm 1^\circ\text{C}$ [54].

DTA analysis is complicated and is often viewed as a crude sibling of DSC [54]. In DTA, both cells are heated with a constant heat flux and the difference in temperature is observed [54]. If the temperature difference between the sample and reference is negative, this is indicated by an endotherm [54]. The only difference between the output for the DTA and the DSC is that the DTA output is the heat flux versus the temperature difference of the sample and reference unlike the DSC which is just the temperature [54]. In DTA, a constant heat flow is sent to the reference and sample and the difference in temperature is measured which gives a good measure of the heat capacity [55].

In general, the sample holder and materials are assumed not to have any temperature gradients; however, this assumption is only valid for stirred samples, which the DTA samples are not [56]. The heat transfer to the sample and the rate of generation and absorption of heat by the sample as it undergoes a physical change will have an effect on the shape of the DTA curve [56]. When a decomposition is endothermic in DTA, the sample temperature will lag behind the reference material, whilst the opposite is true for exothermic DTA in which the temperature of the sample will be more than that of the reference [37].

Melting and crystallization are considered first order transitions and in DSC, they appear as peaks or spikes [55]. The area under these peaks is a measure of the heat evolved or absorbed in that transition [55]. The melting point of crystalline materials are usually depressed by the presence of miscible, non-crystallizing components [54].

The onset and peak temperatures of transitions are sensitive to the rate of heating or cooling [55]. By increasing the heating rate, these temperatures may also increase [55]. The end temperature of the transition would be the most logical to report since at that temperature all the crystals have disappeared or formed, but it is the least to be reported [55].

Some polymers can form more than one type of crystal, so it is possible to have different melting points and the DSC trace can have multiple peaks [55]. The percent crystallinity can also be measured from the area under the melting transition [55]. The higher the cooling rate, the amount of crystallization is reduced as indicated by the reduced area under the peak and also it is more likely to have a lower T_c [55]. Care must also be taken to have a small sample since the peak temperature increases with increasing sample size [56].

DTA can be used to measure the heat of a reaction. The area under the peak in the reaction zone is usually considered as the heat of the reaction; however, reference [56] has shown that this area is proportional to the heat of the reaction as well as the density while inversely proportional to the thermal conductivity of the material. This leads to the following equation that should be used to derive the heat of reaction from DTA measurements:

$$H_{rxn} = \frac{A_p k_{smp}}{Gm} \quad 2.23$$

where A_p is the area under the peak, k_{smp} is the thermal conductivity of the sample, G is the calibration factor and m is the mass of the sample.

If the peak area is calculated from a graph of ΔT versus time, then the area is independent of the heating rate; however, if it is measured versus sample temperature, then the area is proportional to the heating rate [56].

2.4 Probable Mechanisms

As stated earlier, in heterogeneous kinetics, mechanism determination is very difficult, so reaction models are used to guess/rule out the “mechanism(s)” [39]. However, basic chemistry can be used to propose possible mechanisms that may occur. There are six mechanisms that are used to describe the routes in which polymers degrade and they are [36]:

1. depolymerization
2. main-chain scission
3. side group scission
4. elimination
5. cyclization and
6. crosslinking

Both cyclization and crosslinking are usually not detected by TG unless they occur in conjunction with the other mechanisms [36].

Some of the proposed mechanisms for the depolymerization and degradation of nylon 6 via pyrolysis are shown in Figure 2.4 to Figure 2.12. From these proposed mechanisms, some of the compounds and class of compounds from these reactions include: alkene, ammonia, caprolactam, nitrile, tertiary amide (crosslinked), and water.

One of the major impurities that was found by NREL was 2-(5-aminopentyl)-4,5,6,7-tetrahydro-3H-azepine hereafter referred to as an imine [57]. The formation of this imine is postulated to occur through base-catalyzed Claisen-type condensation reaction of two caprolactam molecule [58]. This mechanism was verified by NREL, by reacting pure caprolactam with KOH at reaction at a given temperature; the resulting analysis of the result indicated the formation of this imine [57]. In this work, the goal is to have the reactions producing caprolactam whose probable mechanism shown in Figures 2.6, 2.10, 2.11 and 2.12 to be dominant.

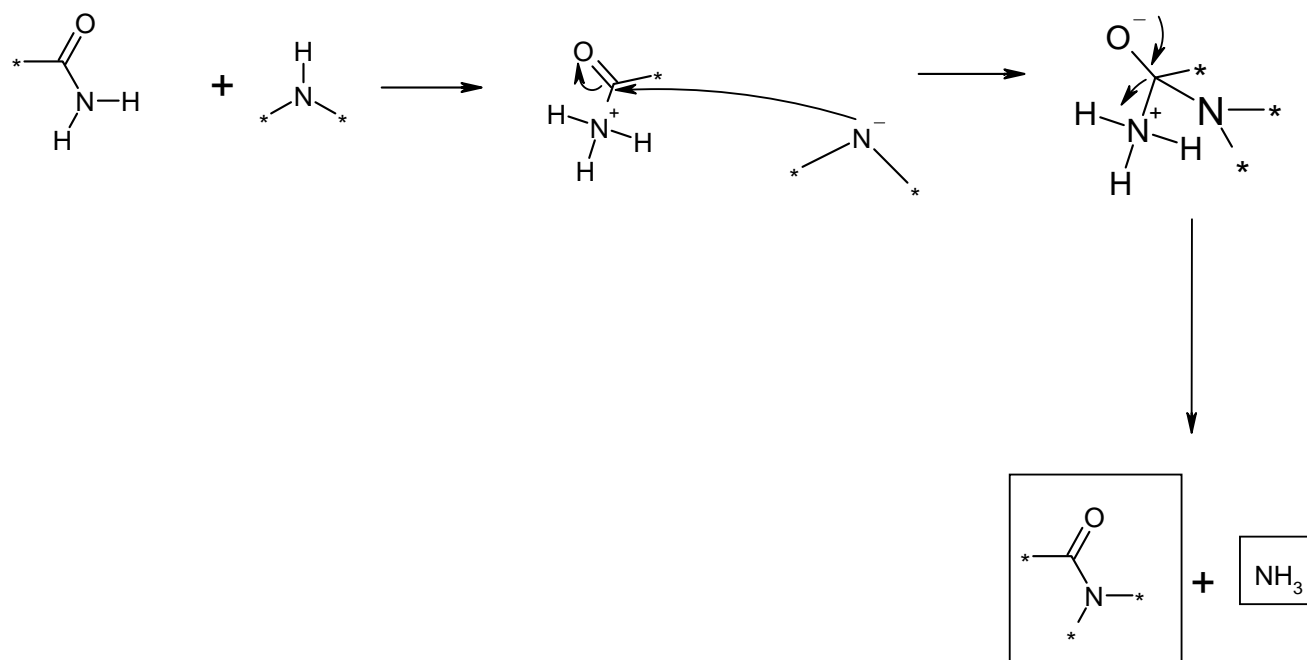


Figure 2.4: Proposed crosslinking mechanism 1 for nylon 6 [59, 60]

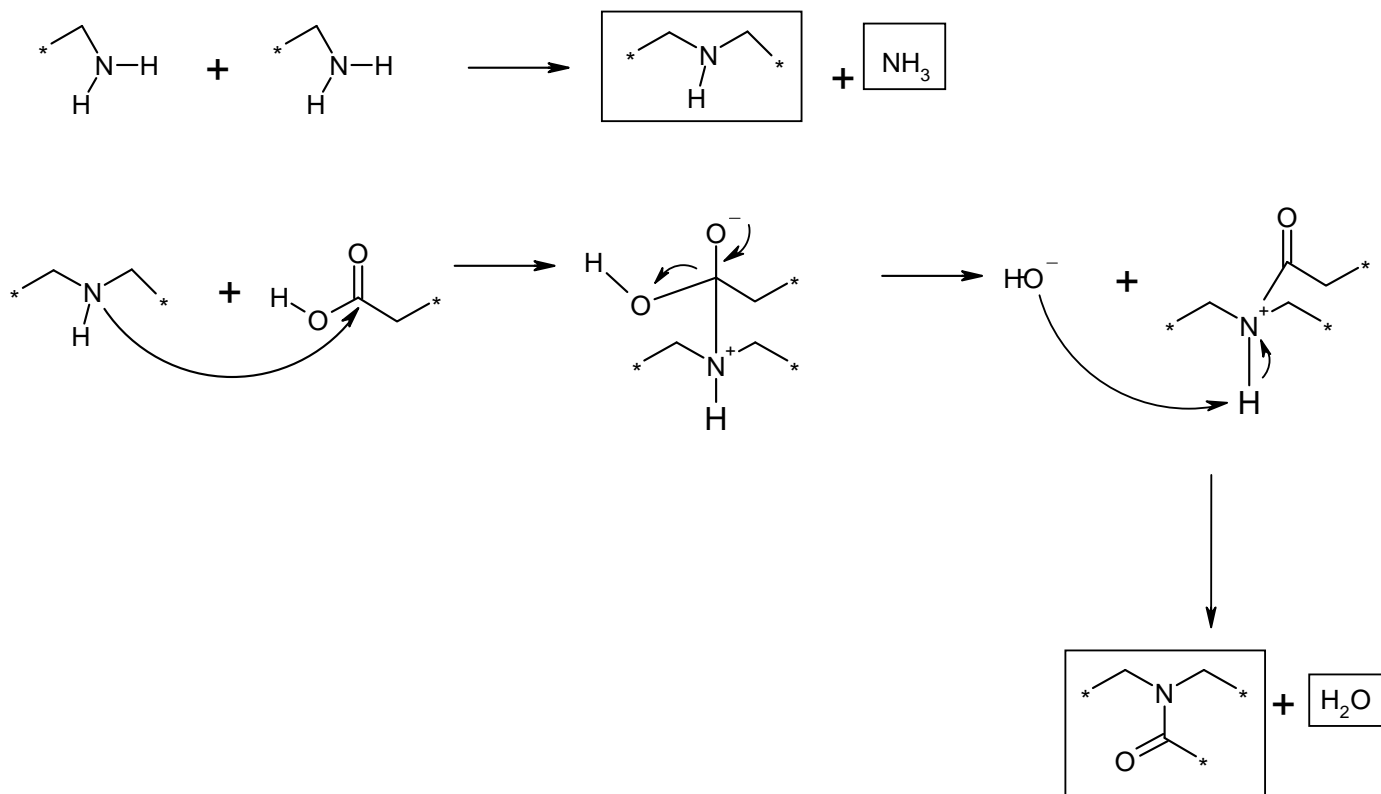


Figure 2.5: Proposed crosslinking mechanism 2 for nylon 6 [59, 61]

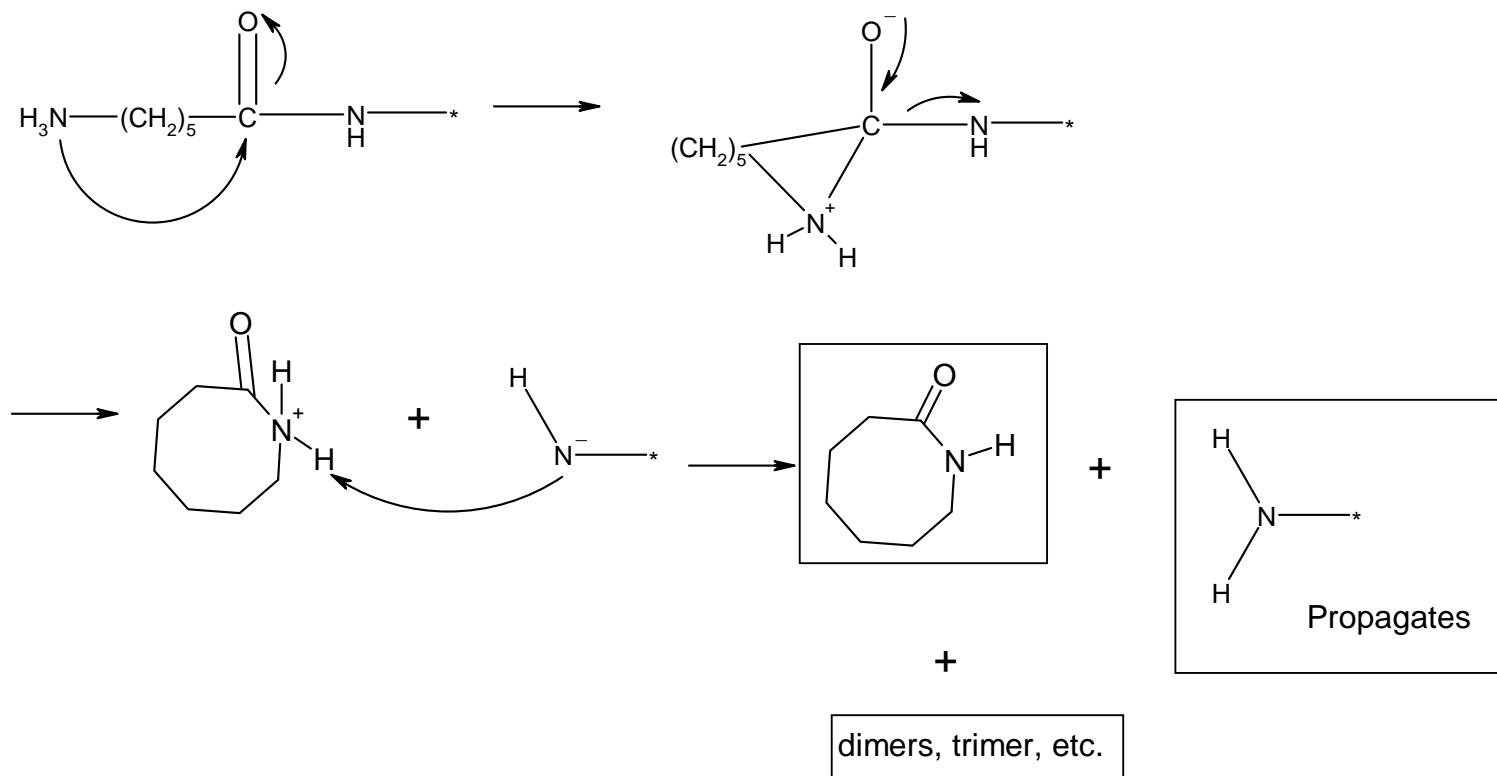
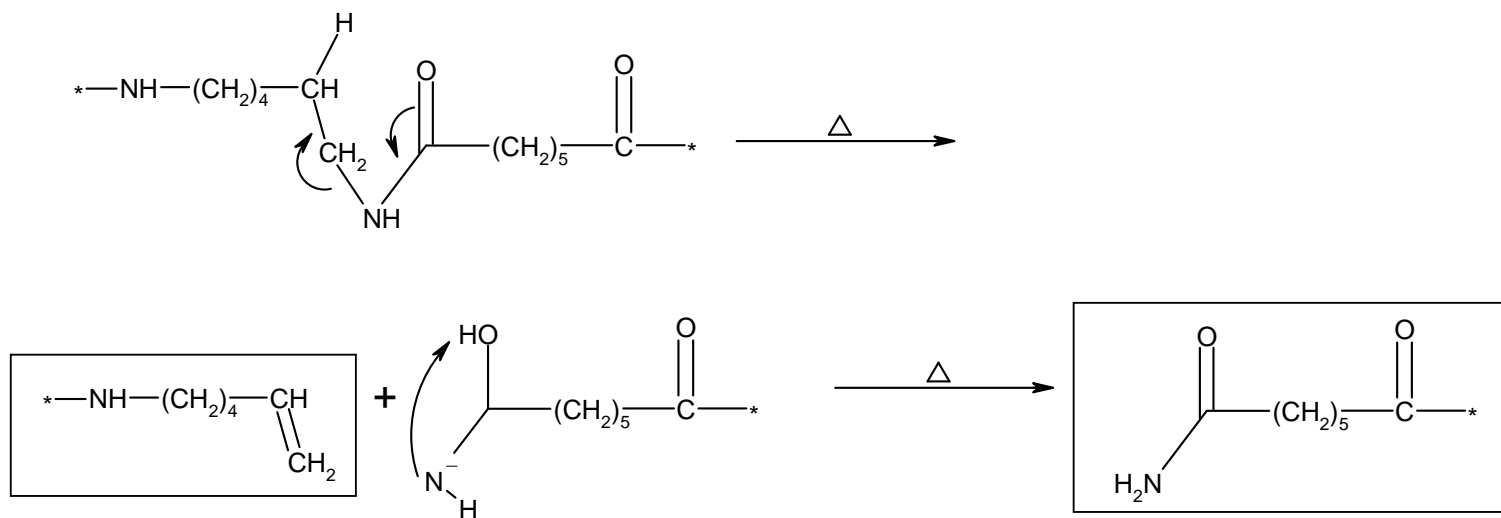


Figure 2.6: Proposed intramolecular backbiting mechanism for nylon 6 [59]



Plus combinations of these end groups of different chain lengths

Figure 2.7: Proposed mechanism for neighboring H abstraction/ β-C-N hydrogen transfer for nylon 6 [59]

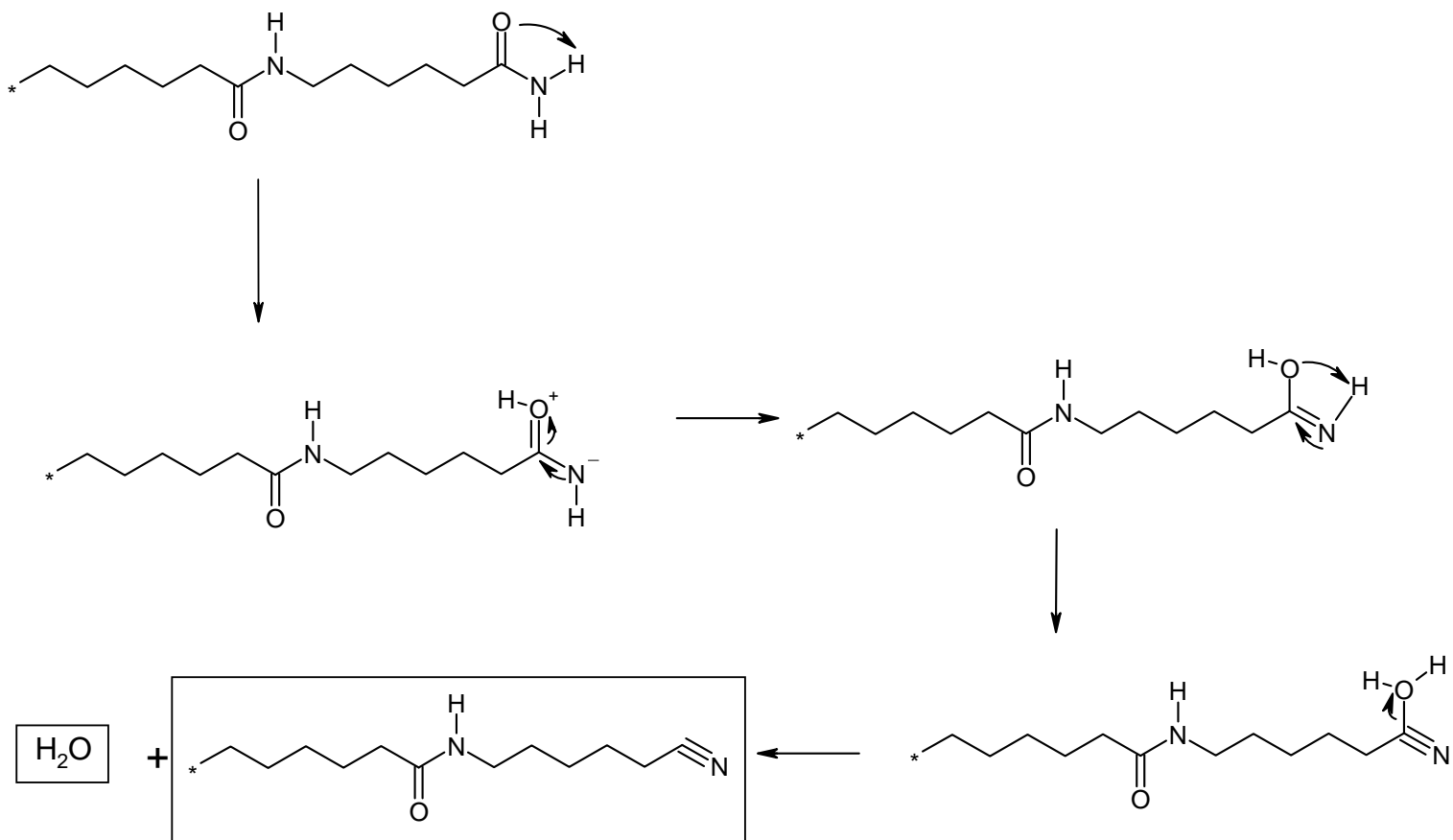


Figure 2.8: Proposed mechanism for end group nitrile formation for nylon 6 [62]

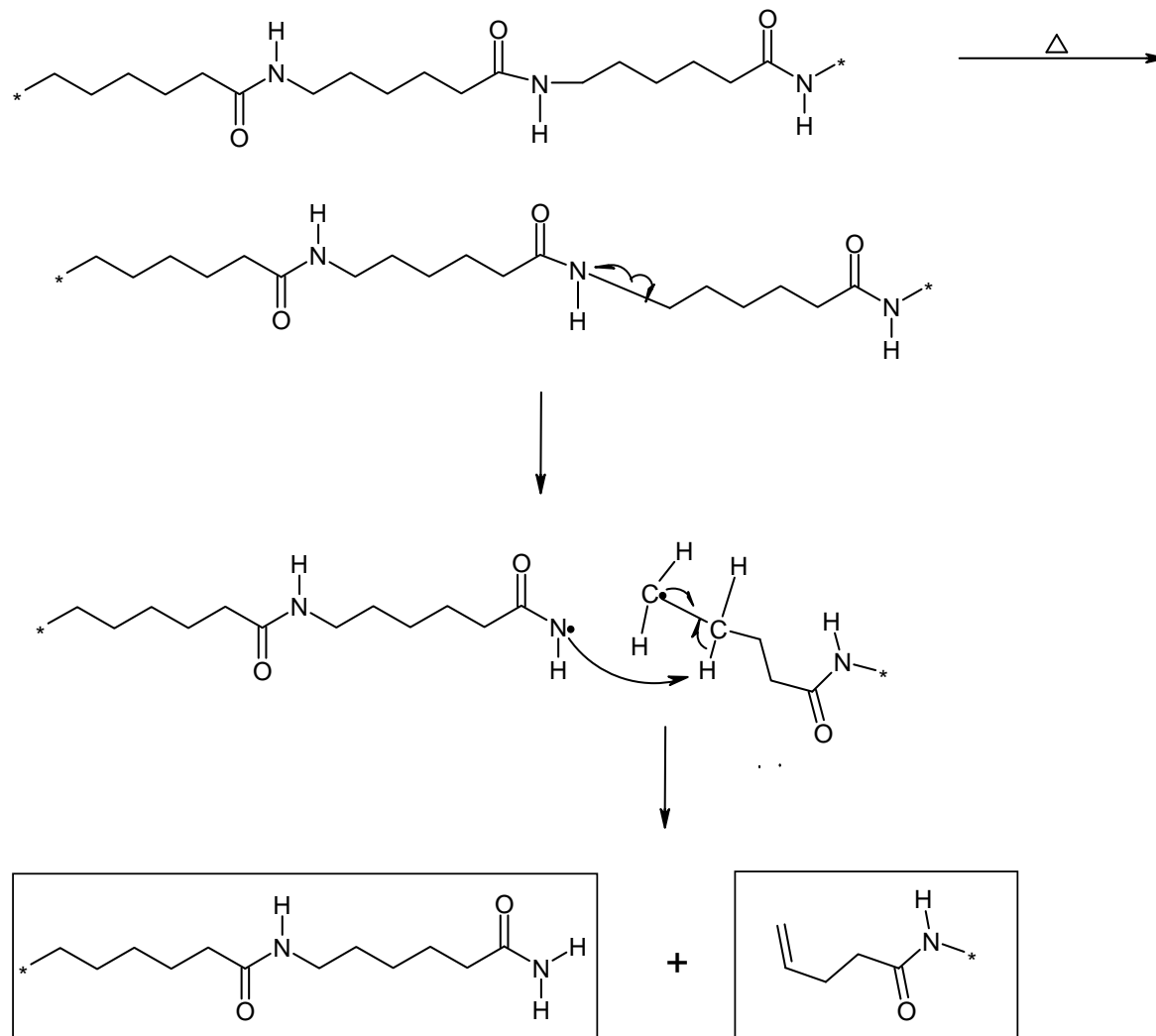


Figure 2.9: Proposed mechanism for single site scission of nylon 6 [62]

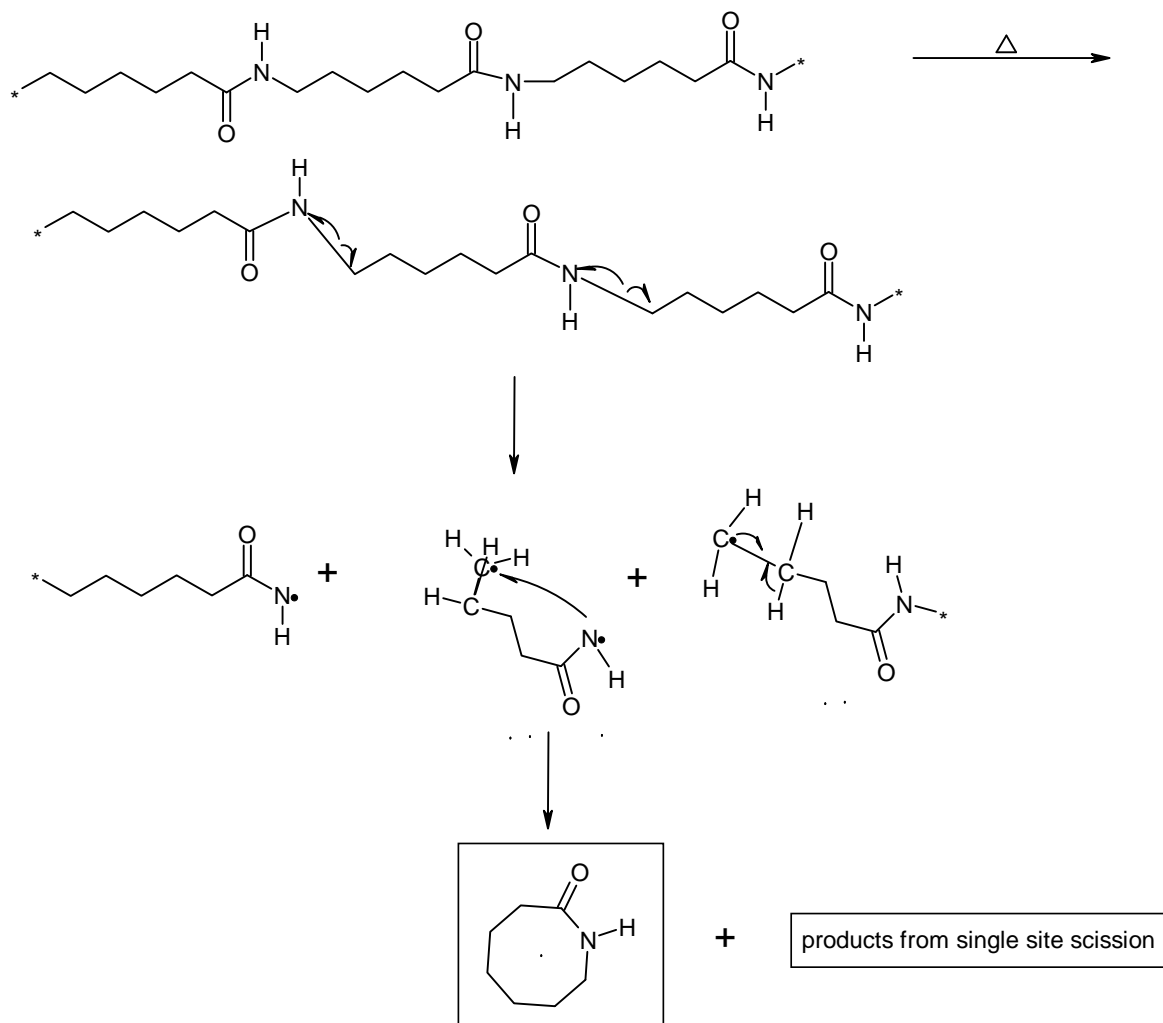


Figure 2.10: Proposed mechanism for single site scission of nylon 6 [62]

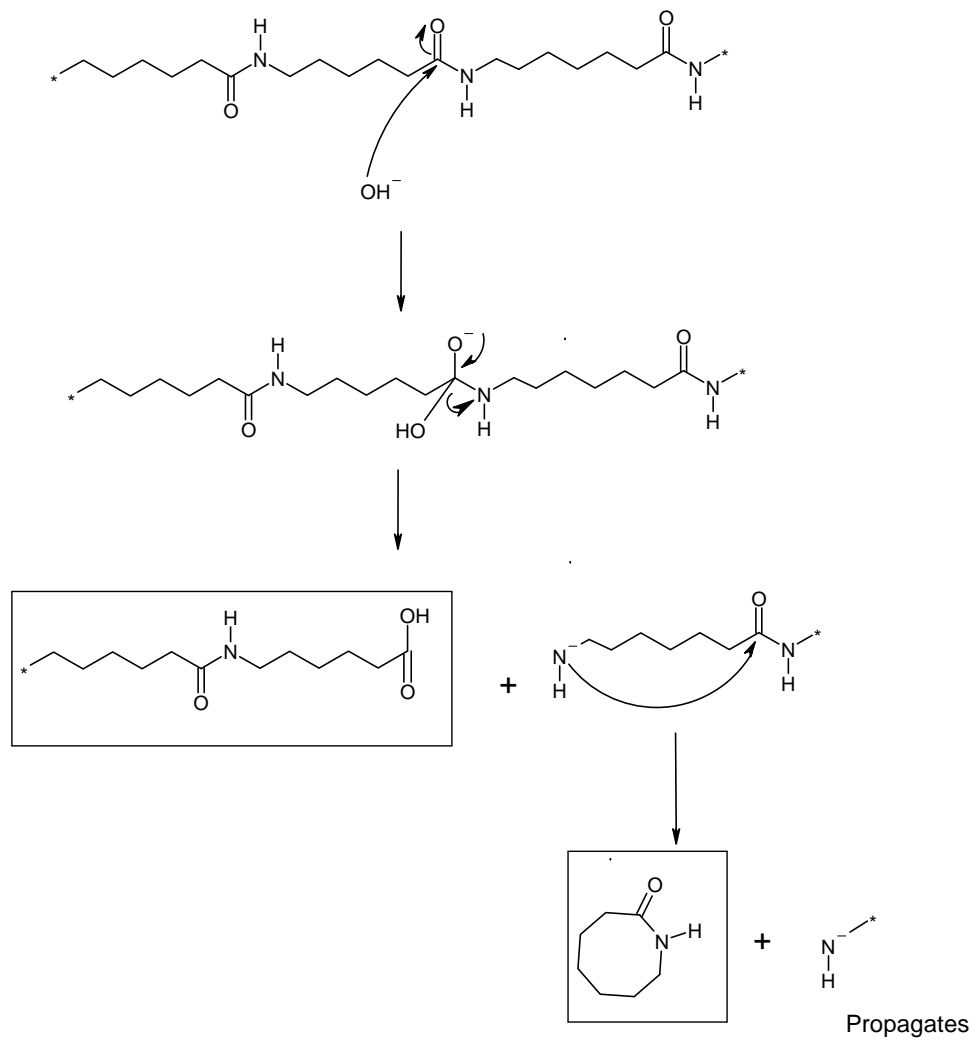


Figure 2.11: Proposed mechanism for single site KOH attack on nylon 6

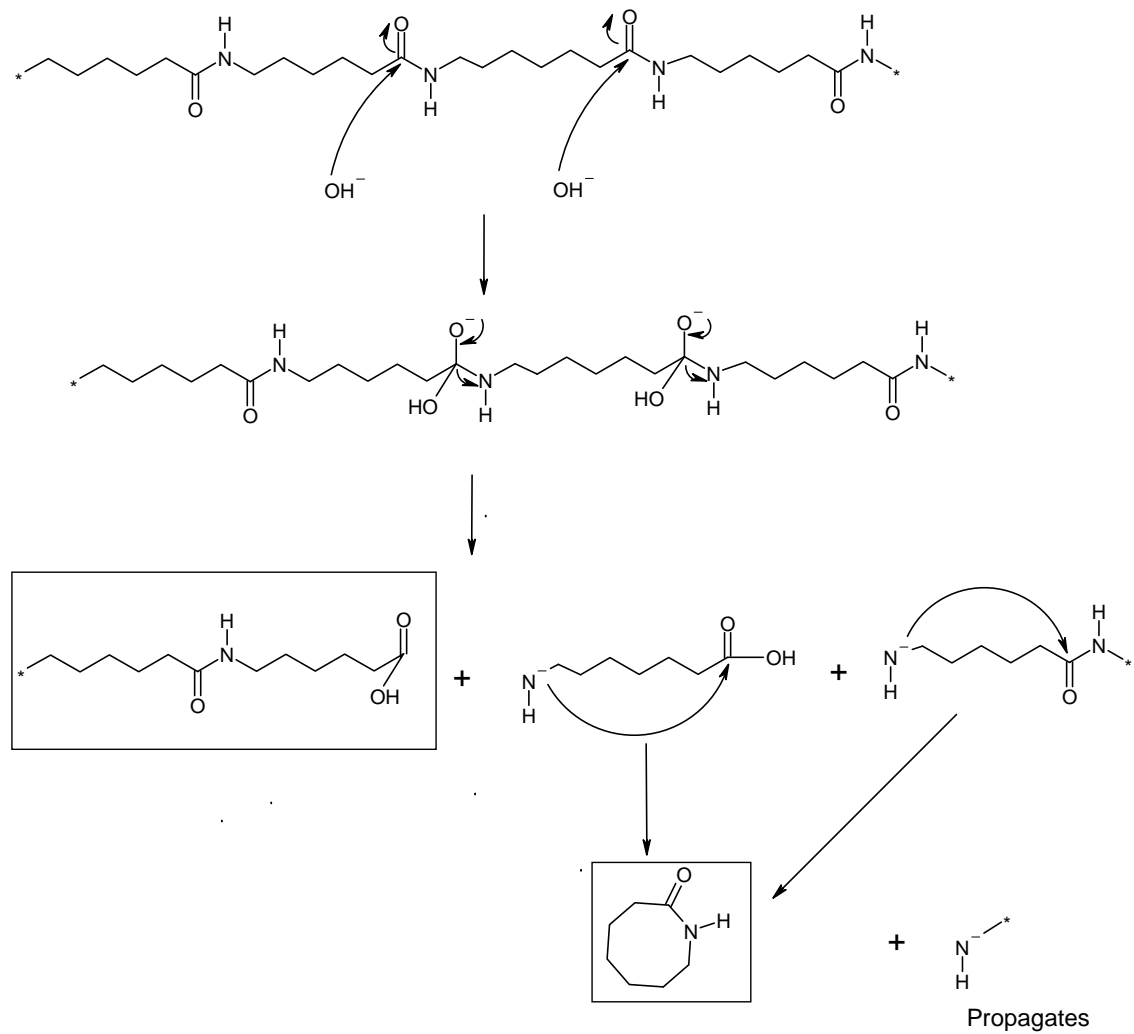


Figure 2.12: Proposed mechanism for neighboring site KOH attack on nylon 6

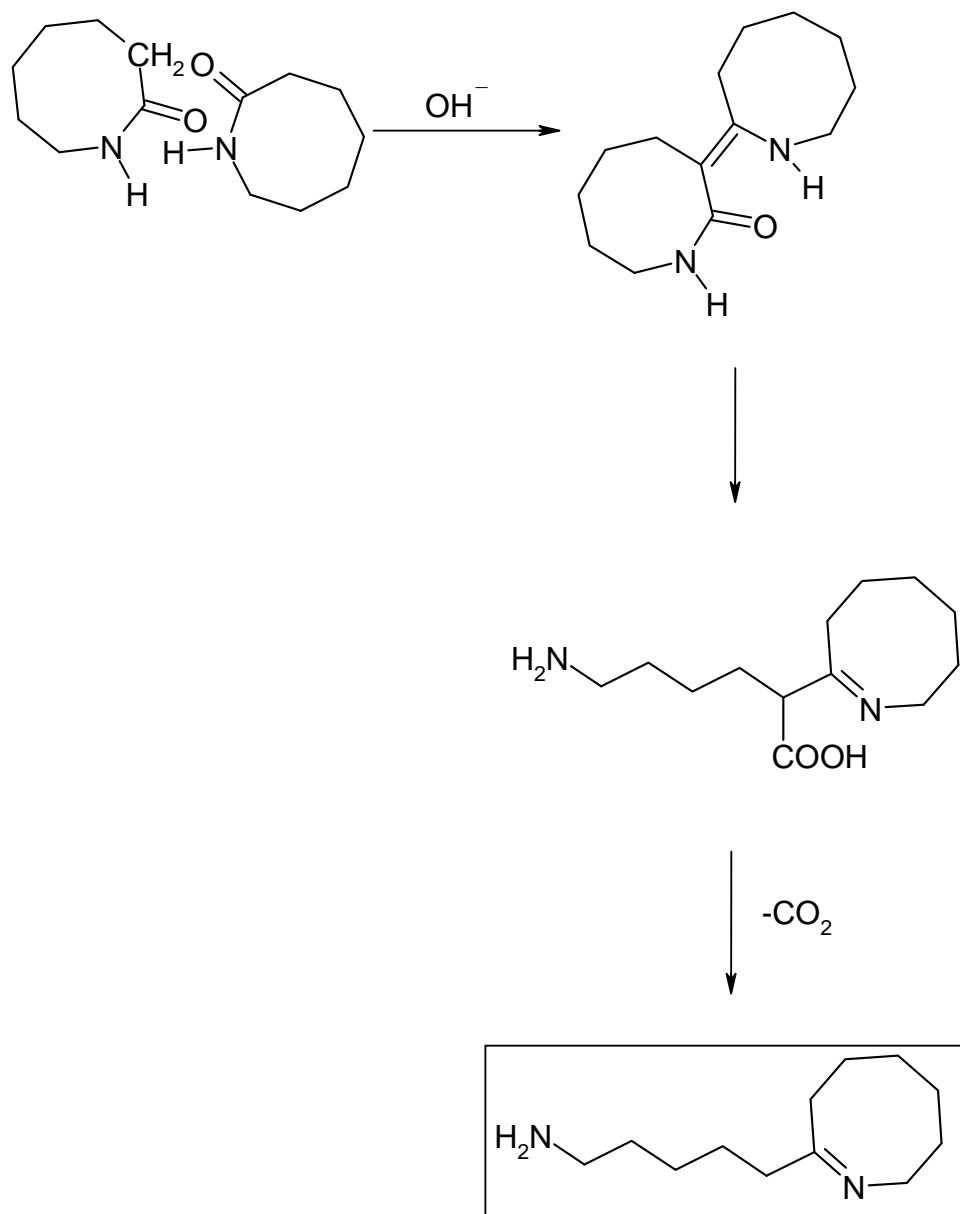


Figure 2.13: Formation of imine impurity through a base-catalyzed Claisen-type condensation reaction [57, 58]

CHAPTER 3

EXPERIMENTAL METHODS

3.1 *Catalyst Screening*

3.1.1 Materials

To determine the best catalysts that can be used to recover the nylon monomers from carpet, different base catalysts were mixed with pure nylons and then thermogravimetric analysis (TGA) was done to these samples. Nylon 6 (Capron[®] 8200 NL-BPL) was obtained from Honeywell polymers before they were acquired by BASF while the nylon 6,6 (48BX) was obtained from Solutia, Inc. Both the nylon 6 and 66 post consumer carpet was provided by Wellman Inc. (Wellamid[®] N6 PCR and N66 PCR). The bases considered were: potassium hydroxide (KOH), sodium hydroxide (NaOH), cesium hydroxide (CsOH), potassium carbonate (K₂CO₃), sodium carbonate (Na₂CO₃) and cesium carbonate (Cs₂CO₃); all of which was purchased from Fisher Scientific. A combination of 60 mol % NaOH and 40 mol % KOH was made into a “eutectic” mixture to simulate the results obtained by reference [31]. Since it wasn't feasible to make the eutectic mixture from the pure molten state as described by reference [32]; i.e. melting at 673 K under a stream of dry nitrogen during at least 12 hours. Instead, the same mole ratios (or mass ratio of 1g NaOH:1.07g KOH) were mixed in distilled water and heated at 200 °C for 24 hours, then rapidly cooled.

3.1.2 Mixing

Prior to mixing, the nylon and catalyst were dried in a vacuum oven for 24 hours before weighing. For each sample, 30 grams of dried nylon mixed with a respective ratio of different catalysts. (For the initial screening, 3 grams of each base; i.e. 10 wt% of the nylon or 10:1 nylon to catalyst ratio was used.) Melt mixing of the nylon with the bases was done in a Haake® Rheomix 600 for 5 minutes under a nitrogen atmosphere at 240°C for nylon 6 and at 270°C for nylon 6,6. The samples were removed promptly after mixing and allowed to air cool. After cooling, they were ground in a Standard Model No. 3 Wiley Mill from Arthur H. Thomas Co. in Philadelphia using the 1 mm screen.

3.1.3 Scanning Electron Microscope (SEM)

To determine if the catalyst was thoroughly distributed throughout the polymer matrix, samples were scanned using a high resolution (2 nm) field emission Hitachi S4100 scanning electron microscope with Noran thin window light element X-ray Spectrometer. [The X-ray Spectrometer facilitates doing energy-dispersive x-ray (EDX) analysis which gives a spectrum of the elements that are present in a targeted area of the sample.] The samples were mounted to SEM aluminum stub using double sided carbon tape. For all the samples, except those containing cesium, a 10 keV primary acceleration voltage was used; for cesium containing samples, 15 keV was used. For all samples, bulk analysis was done followed by individual particles to show statistical variability.

3.1.4 Differential Scanning Calorimeter (DSC)

A TA Instruments DSC 2920 was used in DSC studies to determine the effect that the catalysts had on the thermal properties of nylon 6 during the 5 min mixing in a Haake® Rheomix 600 at 240°C under nitrogen atmosphere. For all DSC runs, a sample of around 6-8 mg was first heated at 10 degrees per min to 240 °C and held at that temperature for 5 minutes. After that, each sample was cooled at 3 degree per minute to 25 °C, and then heated to 300 °C at 3 degrees per minute.

3.1.5 Thermogravimetry Analysis (TGA), Differential Thermal Analysis (DTA) and Differential Thermogravimetry (DTG)

Each grounded sample was heated from room temperature to 500°C at 10 degrees per min using a Seiko TG/DTA 320. The time, temperature, mass, differential thermal analysis (DTA), and Differential thermogravimetry (DTG) are recorded during each run. From the mass, the weight loss fraction or conversion at a particular time or temperature, α , is found using the following equation.

$$\alpha = \frac{m_0 - m}{m_0 - m_\infty} \quad 3.1$$

where, m_0 is the initial mass of the sample, m is the mass at a given time or temperature and m_∞ is the mass of the char which should be equivalent to the amount of catalyst.

Comparative plots of the weight loss fraction versus temperature for each sample were then made to determine which catalyst(s) started and completed the degradation process fastest. Lower percentages of the better performing catalysts were mixed with the

nylons to see the effect of catalyst concentration. The amount of char remaining after each TG run was also used to determine how well distributed the catalyst is after mixing. For a selected few, comparison of having similar molar ratio of different catalysts was also explored. Also, isothermal runs were done at four different temperature in the range in which the catalyst was found to be effective.

3.2 Kinetic Determination

After the initial catalyst screening to see which catalysts were the most effective, determination of the kinetic parameters was done. As discussed in Chapter 2, there are several different techniques/methods in which kinetic constants can be attained from TG data. Of the methods discussed, five were selected to carryout the kinetic analysis. The five that were chosen are:

- Isothermal TG: Model-Fitting Method
- Isothermal TG: Standard Isoconversional Method (Flynn technique)
- Dynamic TG: Model-Fitting Direct differential method
- Dynamic TG: ASTM/Ozawa-Flynn-Wall (OFW)
- Dynamic TG: Distributed activated energy (DAE) model

Since some dynamic methods (as discussed in Chapter 2) involved multiple heating rates for a specific nylon/catalyst ratio, the same method described above was used but with different heating rates (typically 5, 7.5, 10, and 15 degrees per minute; a few 2 and 20 degrees per minute were done for comparison).

CHAPTER 4

EXPERIMENTAL RESULTS AND DISCUSSION

4.1 *Dispersion of Catalysts in Nylon Mixture*

4.1.1 **Scanning Electron Microscope / Energy-Dispersive Spectrometry (SEM/EDS)**

After mixing pure nylon 6 (N6) with the respective catalysts, SEM analysis was done on a few samples to determine how well mixed the nylon and the catalysts were. Figure 4.1 shows a snap shot of a 10:1 ratio mixture of N6:KOH. From this Figure, one can see that the KOH crystals are dispersed in the nylon 6 matrix, but the dispersion is uneven.

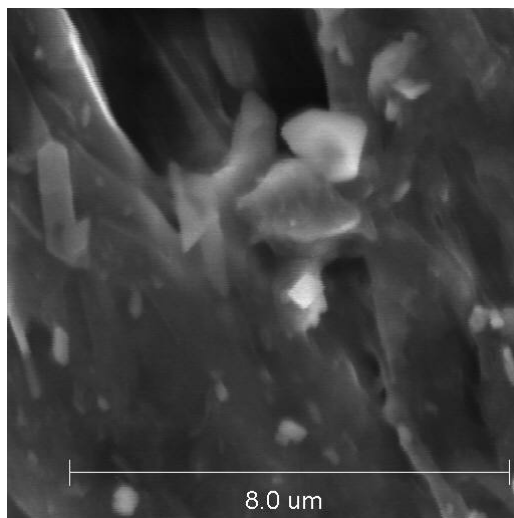


Figure 4.1: Scanning Electron Microscope image of a sample of 10:1 ratio of N6:KOH

Since other samples showed similar distribution of catalyst in the nylon, energy-dispersive x-ray (EDX) or energy-dispersive spectrometry (EDS) analysis was then

performed to see the ratio of the metal count from each catalyst to the nitrogen count from the nylon. Figure 4.2 shows EDS spectrum of 10:1 ratio of N6:KOH. On the vertical axis is the number of count of X-rays plotted against the energy on the horizontal axis. The peaks in the spectrum correspond to the elements present as identified by reference tables or databases. (The peak for carbon is very intense since, in addition to the carbon from the nylon, there was carbon from the tape that was used to hold the sample.) The X-ray intensity from the sample was then compared to a standard of known composition and with correction for background and instrument effects, then the composition of the analysed volume was estimated [63]. The correction method used in this work is the ZAF, which corrects for number (Z), absorption (A) and fluorescence (F) effects. With the correction, the ratio of the weight percentages of the metal to the nitrogen were determined. From this, the ratio of catalyst to nylon was determined with the contribution of the end groups of the nylon being ignored (i.e. an H from the amine side and an OH from the acid side on each chain). By ignoring the mass of the end groups in the analysis, there is a small percent error in the results, but it is a good approximation instead of doing rigorous lab work and calculations.

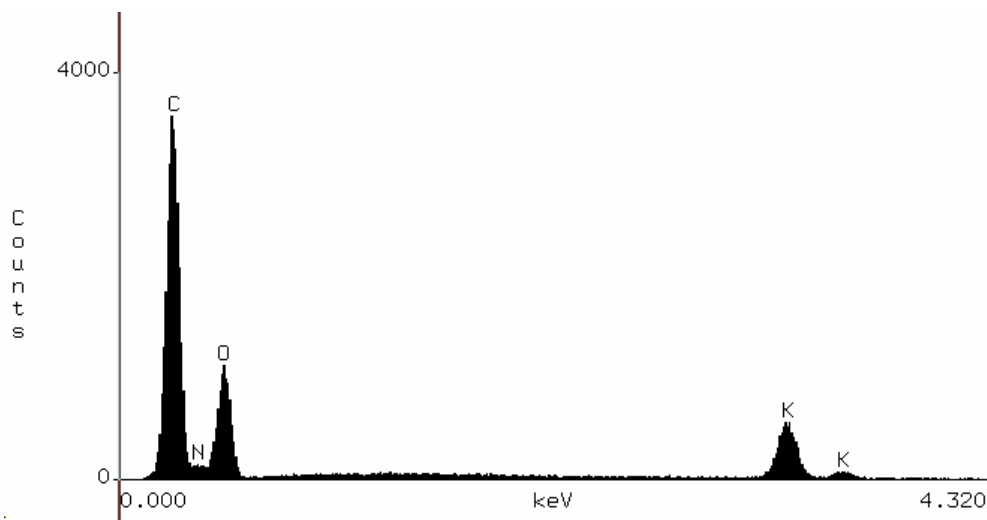


Figure 4.2: Spectrum of a 10:1 ratio of N6:KOH using energy-dispersive spectrometry showing the peaks at energies of characteristic elements present

Table 4.1 covers the results from the EDS analysis as well as shows a comparison to the theoretical compositions of selected samples. Bearing in mind that the end groups were not accounted for in the calculations, the EDS results were overall in agreement with the theoretical compositions if the standard deviation is considered as well. Hence, the mixing procedure, including the mixing time in the Rheomix ®, is considered to be sufficient.

Table 4.1: Comparison of the composition of different catalyst in nylon 6 after mixing using energy-dispersive spectrometry (EDS) [cr means carpet ratio]

Catalyst	Theoretical ratio of nylon 6 (N6) to catalyst	EDS determined ratio of N6 to catalyst	% error (EDS measured to theoretical)
KOH	10:1	13 ±7: 1	20
K ₂ CO ₃	10:1	13±2:1	30
Cs ₂ CO ₃	10:1	9±2:1	8
K ₂ CO ₃	100:1	83±2:1	17
KOH	200:1	239±135:1	9
CaCO ₃	1.8:1 (cr)	2±0:1	5

4.1.2 Percent Char from TG runs

Another way to determine how dispersed the catalysts are in the nylon mixtures is to look at the percent char from dynamic TG runs.

Table 4.2 shows a comparison of the average percent char obtained from using different heating rate in dynamic TG to that of the premixed ratio of nylon 6 to catalyst. For most of the samples shown, the dispersion is very good. The highest difference between the averages and the predicted percent is 7.1. The percent difference between the TG char percent and the premixed percent are much lower than the errors found in EDS. This was expected because of the assumptions made when doing the EDS calculations and because the % char calculation is more direct.

Table 4.2: Percent char from dynamic TG with heating to 500°C for different catalyst in nylon 6 (cr means carpet ratio)

catalyst	Ratio of nylon 6 to catalyst	% char expected	TG %char		% error (TG measured to theoretical)
			average	standard deviation	
CaCO ₃ (cr)	1.8:1	34.41	35.00	0.41	1.7
Cs ₂ CO ₃	10:1	9.09	8.61	0.38	5.3
K ₂ CO ₃	10:1	9.09	8.44	0.28	7.1
KOH	10:1	9.09	9.68	0.15	6.4
Na ₂ CO ₃	10:1	9.09	9.04	0.12	0.5

4.2 Catalyst Effect on Thermal Properties of Nylon 6

DSC studies were done to determine the effect that the catalysts had on the thermal properties of nylon 6 during the 5 minute mixing in a Haake® Rheomix 600 at 240°C under nitrogen atmosphere. Figure 4.3 shows the complete DSC cycle for pure nylon 6 (N6). After heating the sample to 240°C at 10°C/min and then holding it at that temperature for 5 minutes, the sample was cooled at 3°C/min to 25°C, and then heated to 300°C at 3°C/min. The first heating in the cycle was used to remove the thermal history of the material; only the cooling and the second heating curves are used in the ensuing analysis. The magnitude of the second heating curve is smaller than that of the first heating curve because with smaller heating rate was used in the second heating cycle.

For pure nylon 6, the thermal transitions data are shown in Table 4.3. These values will be used to examine if the mixing process affects the thermal properties that will influence the kinetics obtained by TGA. One of the indicators of the property change

in the polymer is to look at the shift in the temperature of the melting curve minimum point and crystallization curve maximum.

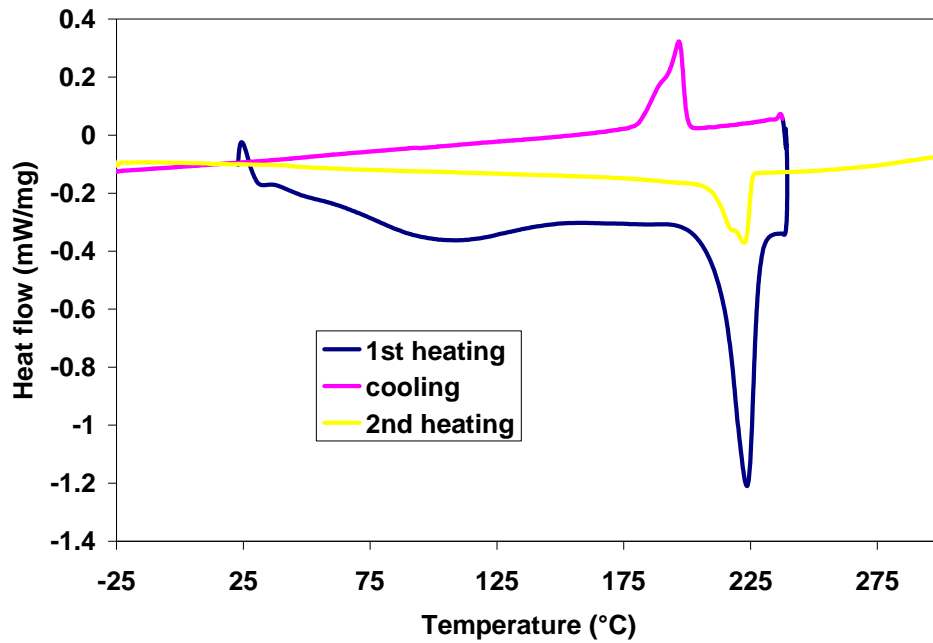


Figure 4.3: DSC curve for pure nylon 6 (1st heating at 10°C/min, 2nd heating and cooling at 3°C/min)

Table 4.3: Thermal transitions of pure nylon 6

Property	Heating	Cooling
Onset Temperature (°C)	208	200
Latent heat (J/g)	77	58
max/min peak/dip Temperature (°C)	222	197

Table 4.4 provides a summary of the temperature corresponding to the melting curve minimum point for different amounts of catalysts in nylon 6 while Table 4.5

contains the crystallization peaks summary. As shown in Table 4.4, with 10:1 N6:catalyst, all the catalysts lowered the temperature of the melting curve minimum point of nylon 6, but NaOH gave the greatest difference. (Also as seen in Table 4.5, NaOH crystallized at lower temperature for all the ratios shown; it is over 40°C lower than the pure N6 for the 10:1 ratio.) While the melting temperature for pure N6 was 222°C, that of the 10:1 ratio of N6:NaOH was 187°C; a difference of over 35°C. The other catalysts lowered the melting point of nylon by a range of 4-11°C. Of the 20:1 catalysts, again NaOH was the lowest melting catalyst polymer mixture. However, 100:1 Cs₂CO₃ melts the polymer at a lower temperature while the NaOH is the highest melting mixture, but it was still lower than that of pure nylon by 6°C. These melting points don't seem to indicate whether the polymer will degrade the nylon faster, since from dynamic TG results (discussed later), at 10:1 KOH and K₂CO₃ started to degrade much faster than their NaOH and Na₂CO₃ counterparts.

The presence of the carpet components slightly decreased the melting temperature of nylon, which is similar to catalysts loadings of 100:1. The decrease in the melting temperature may have occurred because the presence of these N6 insoluble catalysts. For some catalysts mixtures (namely KOH and NaOH), the more insoluble present, the lower the melting and crystallizing temperatures; whereas, for others like K₂CO₃, there isn't a noticeable difference with composition. This may suggest that the presence of the hydroxide bases not only alter the melting point of the N6, but may have changed its chemical structure during mixing.

Table 4.4: Melting temperature for different catalyst mass ratios of nylon 6:catalyst

Temperature of the melting curve minimum point (°C)							
10:1 nylon 6:catalyst		20:1 nylon 6:catalyst		100:1 nylon 6:catalyst		carpet ratio of nylon 6 to components	
NaOH	187	NaOH	206	Cs ₂ CO ₃	216	Finished latex (5.4:1)	217
KOH	198	KOH	211	Na ₂ CO ₃	216	CaCO ₃ (1.8:1)	217
Cs ₂ CO ₃	212	Cs ₂ CO ₃	212	KOH	217	Filler (1.8:1)	218
Na ₂ CO ₃	217	Na ₂ CO ₃	217	CaO	217	PP (7.6:1)	218
K ₂ CO ₃	217	K ₂ CO ₃	217	K ₂ CO ₃	217	Pure	222
CaCO ₃	217	CaO	217	NaOH	219		
CaO	218	Pure	222	Pure	222		
Pure	222						

Table 4.5: Crystallization peak temperature of different ratios of nylon 6:catalyst

Peak Temperature of cooling curve (°C)							
10:1 nylon 6:catalyst		20:1 nylon 6:catalyst		100:1 nylon 6:catalyst		carpet ratio of nylon 6 to components	
NaOH	154	NaOH	178	NaOH	195	Finished latex	196
KOH	164	KOH	187	K ₂ CO ₃	196	PP	196
Cs ₂ CO ₃	193	Cs ₂ CO ₃	193	Cs ₂ CO ₃	196	CaCO ₃	196
CaCO ₃	197	K ₂ CO ₃	197	CaO	197	Pure	197
Pure	197	CaO	197	Pure	197	Filler	197
K ₂ CO ₃	197	Pure	197	KOH	197		
CaO	197	Na ₂ CO ₃	198	Na ₂ CO ₃	198		

Since the amount of base sites that would react is different in the mass ratios, comparing of equivalent moles ratio was done to determine how the number of base groups affects the thermal properties. Table 4.6 and Table 4.7 summarize the shift in the melting and crystallization temperature for the different catalysts at various mole catalyst

to nylon mass ratio. At the highest ratio (0.1 mol catalyst to 30 grams nylon 6), NaOH has the lowest melting temperature with a significant difference between that and pure N6 of 28° C while all the others lowered the melting temperature by approximately 6°C. When cooling, the difference between the crystallization peak temperature for the pure and the lowest crystallizing sample (which contained NaOH) was 33°C.

At a 0.05 mol loading, KOH has the lowest melt temperature, but only around 1 degree lower than NaOH. The difference between the highest and lowest melt temperatures was around 16°C. Similarly with crystallization, 0.05 mol KOH and NaOH reduced the crystallization temperature by over 16°C. There doesn't seem to be any correlation between melting temperatures and crystallization temperatures. There is no noticeable difference between the 0.05 mol and the 0.25 mol temperatures for both melting and crystallization.

Table 4.6: Melting temperature for different catalyst mole ratios to 30 grams of nylon 6

Melting peak Temperature (°C)					
0.1mol catalyst : 30g nylon6		0.05mol catalyst : 30g nylon6		0.025mol catalyst : 30g nylon6	
NaOH	194	KOH	206	Cs ₂ CO ₃	212
K ₂ CO ₃	217	NaOH	208	K ₂ CO ₃	217
CaCO ₃	217	Cs ₂ CO ₃	212	Na ₂ CO ₃	217
CaO	218	K ₂ CO ₃	217	Pure	222
Pure	222	Na ₂ CO ₃	217		
		CaCO ₃	218		
		CaO	218		
		Pure	222		

Table 4.7: Crystallization peak temperature for different catalyst mole ratios to 30 grams of nylon 6

Crystallization peak Temperature (°C)					
0.1mol catalyst : 30g nylon6		0.05mol catalyst : 30g nylon6		0.025mol catalyst : 30g nylon6	
NaOH	165	KOH	177	Cs ₂ CO ₃	193
K ₂ CO ₃	196	NaOH	180	Na ₂ CO ₃	196
CaCO ₃	197	Cs ₂ CO ₃	192	K ₂ CO ₃	196
Pure	197	Na ₂ CO ₃	196	Pure	197
CaO	198	K ₂ CO ₃	196		
		Pure	197		
		CaCO ₃	197		
		CaO	198		

Since there was so much variation in the melting temperature of polymer/catalyst mixtures, a comparison of the trend with respect to different loadings of the same catalyst might indicate the catalyst strength in degradation. Table 4.8 provides such a summary. Figure 4.4 through to Figure 4.19 (which can be found within pages 64 through 77) give a pictorial view of these results.

Table 4.8: Comparison of melting temperatures for each catalyst loading in Nylon 6

Melting peak Temperature (°C)					
KOH		NaOH		Cs ₂ CO ₃	
Quantity of Catalyst	(°C)	Quantity of Catalyst	(°C)	Quantity of Catalyst	(°C)
10:1	198	10:1	187	10:1	212
10.7:1 (0.05 mol)	206	7.5:1 (0.1 mol)	194	20:1	212
20:1	211	20:1	206	1.8:1 (0.05 mol)	212
100:1	217	15:1 (0.05 mol)	208	3.68:1 (0.025 mol)	213
Pure	222	100:1	219	100:1	216
		Pure	222	Pure	222
K ₂ CO ₃		Na ₂ CO ₃		CaCO ₃	
Quantity of Catalyst	(°C)	Quantity of Catalyst	(°C)	Quantity of Catalyst	(°C)
20:1	217	100:1	216	1.8:1 (carpet ratio)	217
4.3:1 (0.05 mol)	217	10:1	217	3:1 (0.1 mol)	217
8.7:1 (0.025 mol)	217	20:1	217	10:1	217
2.2:1 (0.1 mol)	217	11.3:1 (0.025 mol)	217	6:1 (0.05 mol)	218
10:1	217	5.7:1 (0.05 mol)	217	Pure	222
100:1	217	Pure	222		
Pure	222				

4.2.1 KOH

Generally for KOH (as shown in Table 4.8 and Figure 4.4), the higher the amount of catalyst, the lower the melt temperature. Initial comparison shows that the sample with 10:1 N6: KOH ratio has the lowest melting temperature followed by the 10.7:1 ratio. During the crystallization of the KOH mixtures, one of the mixtures had 2 peaks (Figure 4.5). The only composition with the two peaks is the 10:1 ratio. The 10:1 ratio had a noticeably wider crystallization range than the others, but that may correspond to the small peak around 260°C in the melting curve which might be indicative of caprolactam. This would suggest that at the 240°C mixing temperature, the KOH has already started to degrade the nylon 6.

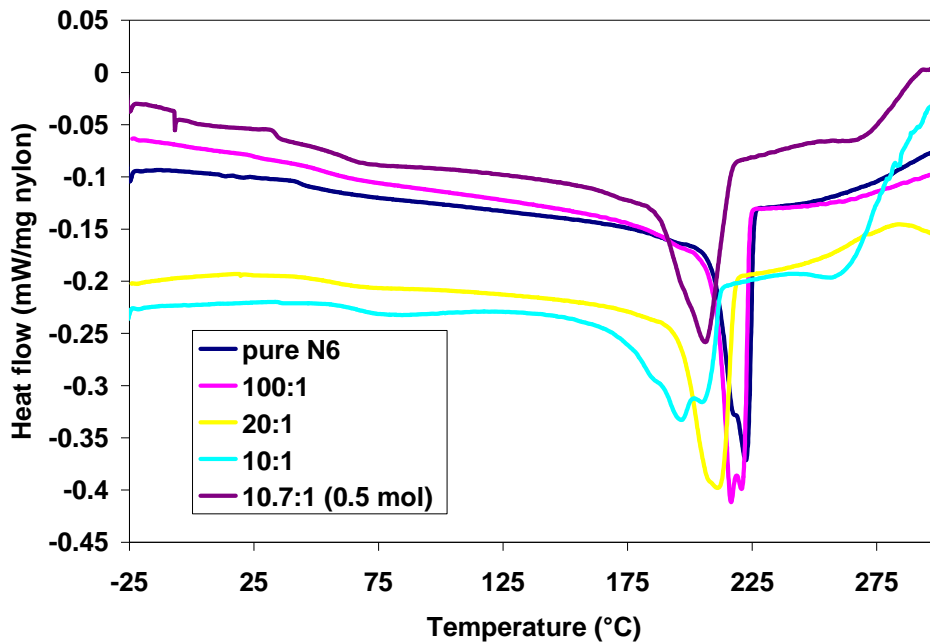


Figure 4.4: Second heating curves for different nylon 6:KOH ratios (heating at 3°C per min)

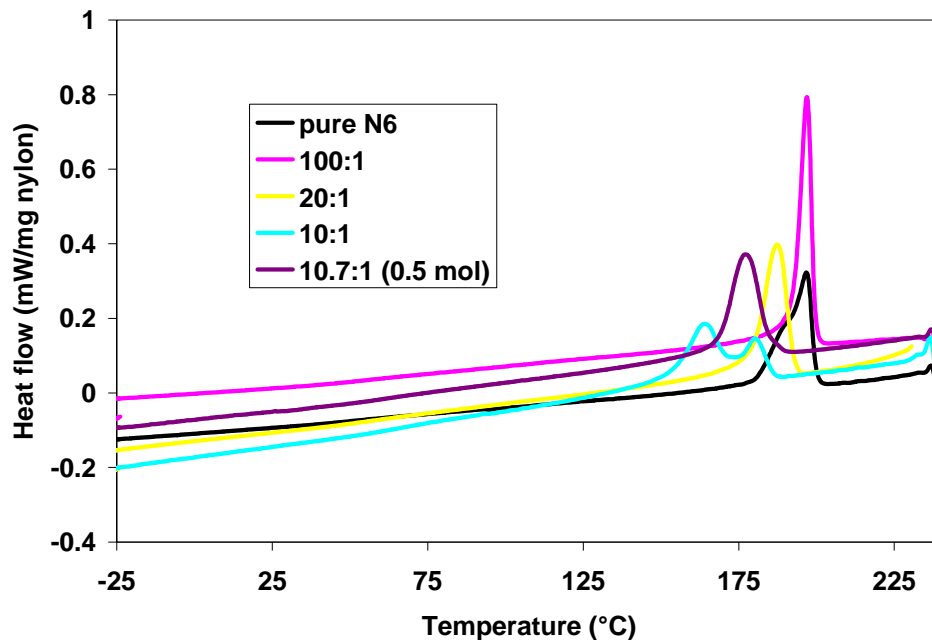


Figure 4.5: Cooling curves for different nylon 6:KOH ratios (cooling at 3°C per min)

Since some of the samples indicated that mixing the catalyst and N6 changed the thermal properties of the N6, KOH were extracted from two samples using deionized water until a neutral pH was obtained. Before that, the sample was washed in methanol to remove any caprolactam or methanol soluble compound that may have been formed/trapped during mixing. Figure 4.6 and Figure 4.7 show a comparison of the second heating curve and cooling curves respectively for different nylon 6:KOH ratios and their residue after catalyst extraction. In both Figures, the extracted samples melted and crystallized around the same temperature range as pure N6. However, there is a significant difference between the un-extracted 10:1 and the extracted. A possible explanation for this is may have been the melting temperature depression discussed earlier. The slight difference between the extracted curves and the pure N6 might be from

embedded unextracted catalyst or may indicate that the N6 has had a minor change, i.e. some degradation has occurred.

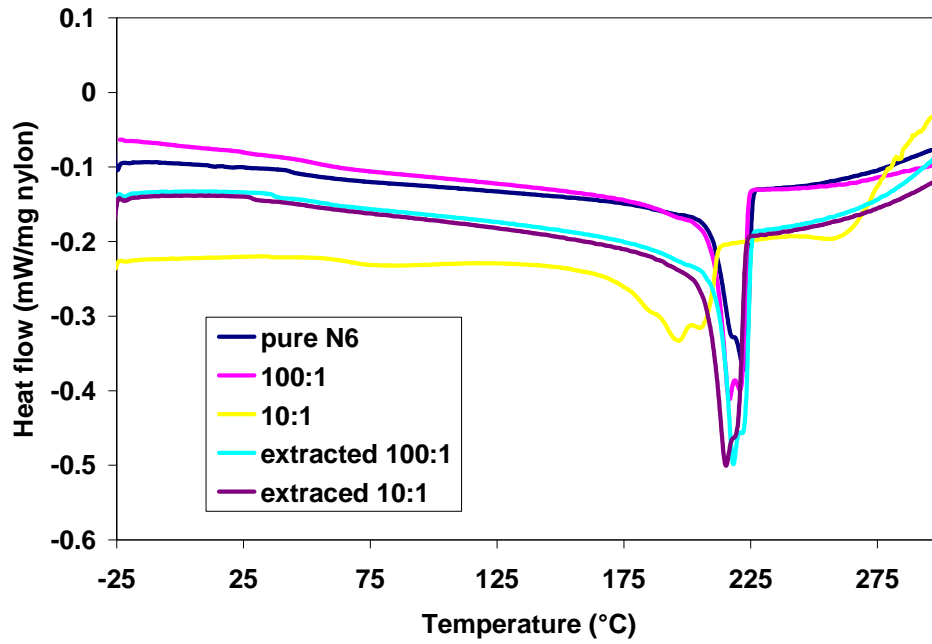


Figure 4.6: Comparison of the second heating curves for different nylon 6:KOH ratios and their residues after catalyst extraction (heating at 3°C per min)

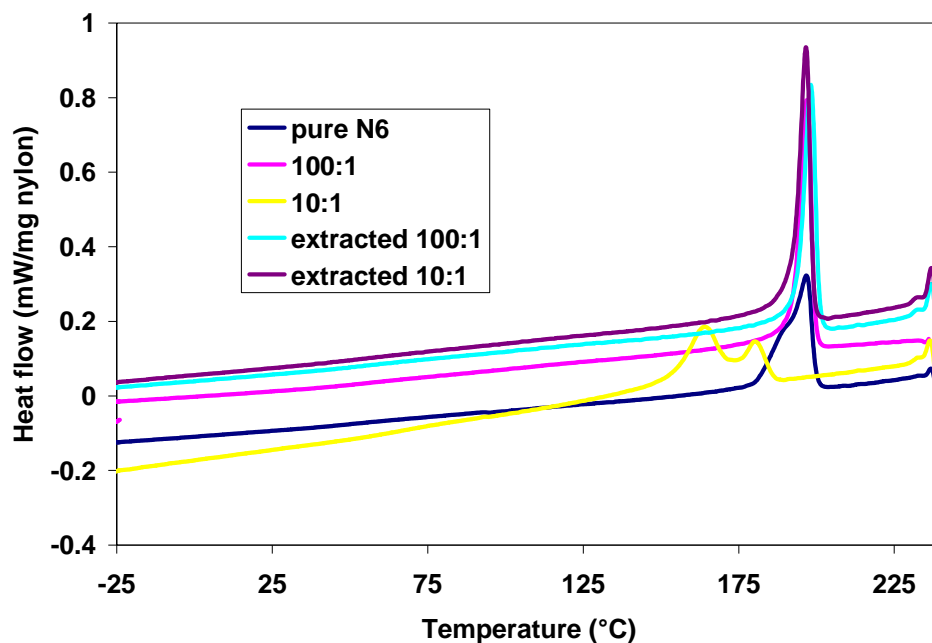


Figure 4.7: Comparison of the cooling curves for different nylon 6:KOH ratios and their residues after catalyst extraction (cooling at 3°C per min)

4.2.2 K₂CO₃

With K₂CO₃, as shown in Figure 4.8, in addition to the melting transition of nylon, two other transitions can be seen between 20 and 85°C. The first transition that is visible is the glass transition (which was only slightly visible with KOH). The other transition seems to be that of melting caprolactam since the melting temperature of caprolactam is 69°C [64]. This would suggest that at the 240°C mixing temperature, the K₂CO₃ has already started to degrade the nylon 6, even with the 100:1 ratio which shows a slight caprolactam peak. However, there was no caprolactam peak in the cooling curve (Figure 4.9). Also in Figure 4.8, above 275°C, there seems to be a downward shift in the curve for most of the K₂CO₃ samples except for the 100:1 ratio. This would indicate that significant degradation starts to occur below 300°C. It should also be noted that the

K_2CO_3 samples melt around $6^\circ C$ lower than the pure nylon and the composition doesn't affect the melting temperature. Also, the crystallization of the K_2CO_3 samples was uniform and narrower than the pure nylon (Figure 4.9 and Table 4.8).

Since there were the lower transitions seen the K_2CO_3 samples, the 10:1 N6: K_2CO_3 ratio was extracted the same way as the KOH was done and a comparison of the second heating curve of the pre- extraction and post-extractions are shown in Figure 4.10. The melting transitions of the two are almost equivalent, but there is no lower temperature transition noted in the extracted sample. This suggests that the component that showed up in the pre-extraction sample is soluble in methanol and/or water. Since N6 does not melt at this temperature, the most probable compound that melts at that temperature is caprolactam.

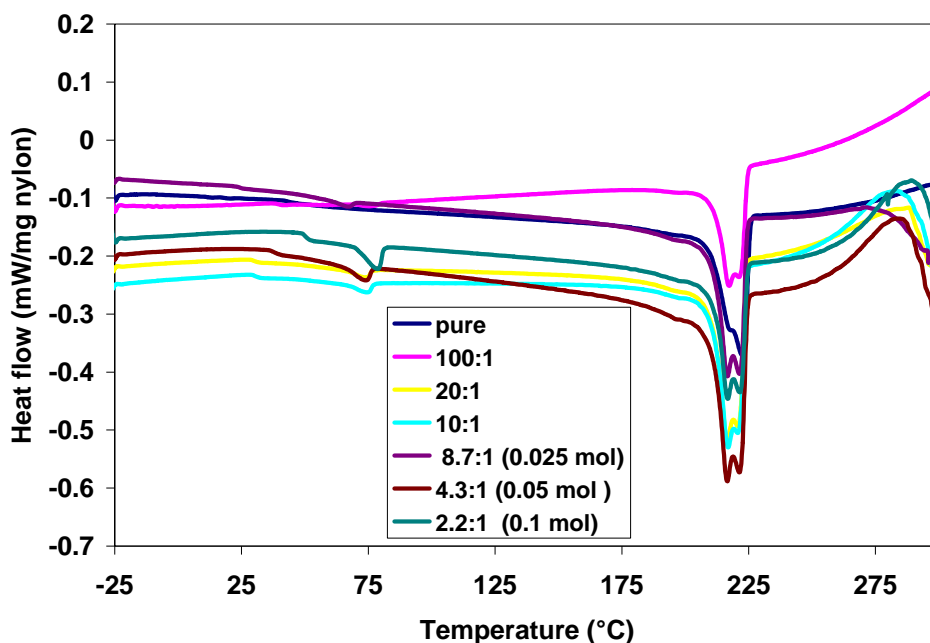


Figure 4.8: Second heating curves for different N6: K_2CO_3 ratios (heating at $3^\circ C$ per min)

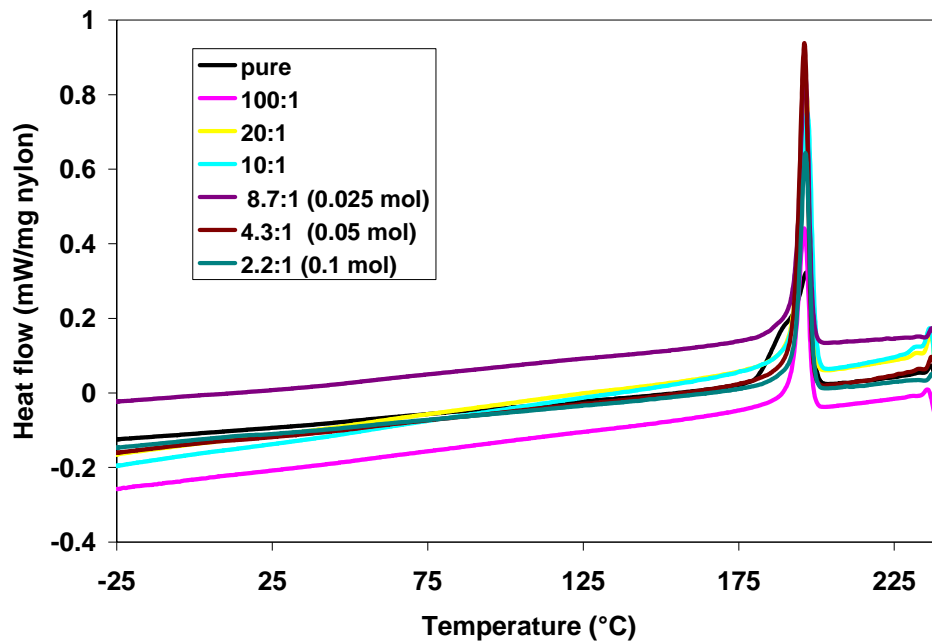


Figure 4.9: Cooling curves for different N6:K₂CO₃ ratios (cooling at 3°C per min)

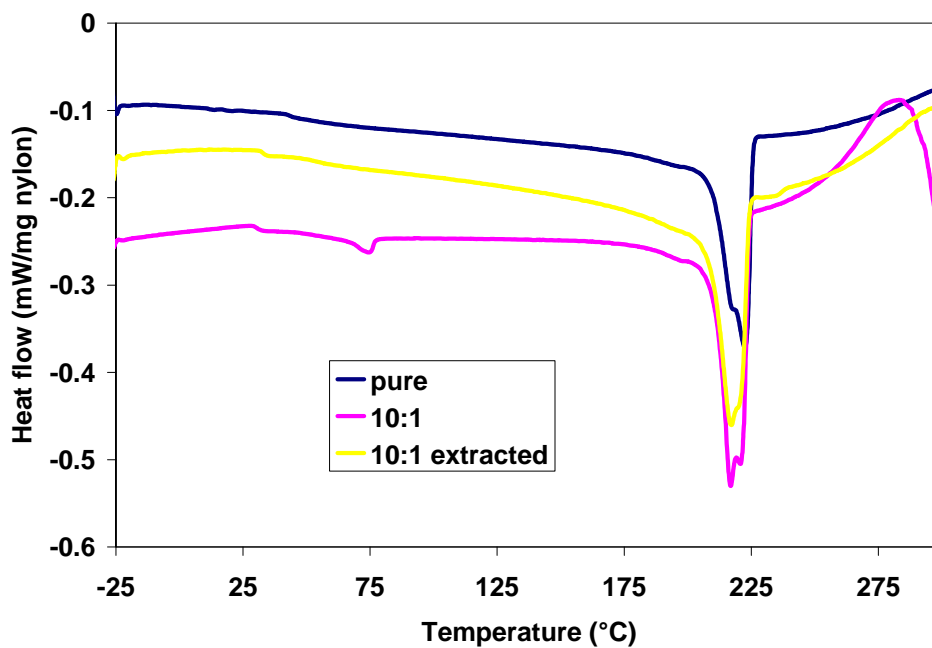


Figure 4.10: Comparison of the second heating curves for 10:1 N6:K₂CO₃ ratio and its residue after catalyst extraction (heating at 3°C per min)

4.2.3 NaOH

Similar to K_2CO_3 , for NaOH the amount of catalyst present does not indicate a trend in the melting temperature of the mixture (see Figure 4.11). However, the heating and cooling curves for NaOH are much more interesting than those of the previously mentioned bases. In the cooling curves for these samples (Figure 4.12), the 0.1 mol ratio and 10:1 ratio have a second crystallization peak around between 112-125°C and 100 - 120°C, respectively. In the heating curves for these samples (Figure 4.11), the transition of the melting of the nylon is not as smooth as the others. The transitions of the NaOH mixtures occur over a wide region as with the KOH (unlike K_2CO_3). But the temperatures at which they occur do not correspond to any trend with respect to their catalyst concentration.

Figure 4.13 and Figure 4.14 shows a comparison of the second heating curve and cooling curves respectively for the 10:1 N6:NaOH ratio and their residue after catalyst extraction. In both Figures, the extracted samples melted/crystallized around the same range as pure N6. However, there is a significant difference between the un-extracted 10:1 ratio and the extracted ratio. A possible explanation for this difference may be due to melting temperature depression as discussed earlier. The slight difference between the extracted curves and the pure N6 might be from embedded unextracted catalyst or may indicate that the N6 has had a minor change, i.e. some degradation has occurred.

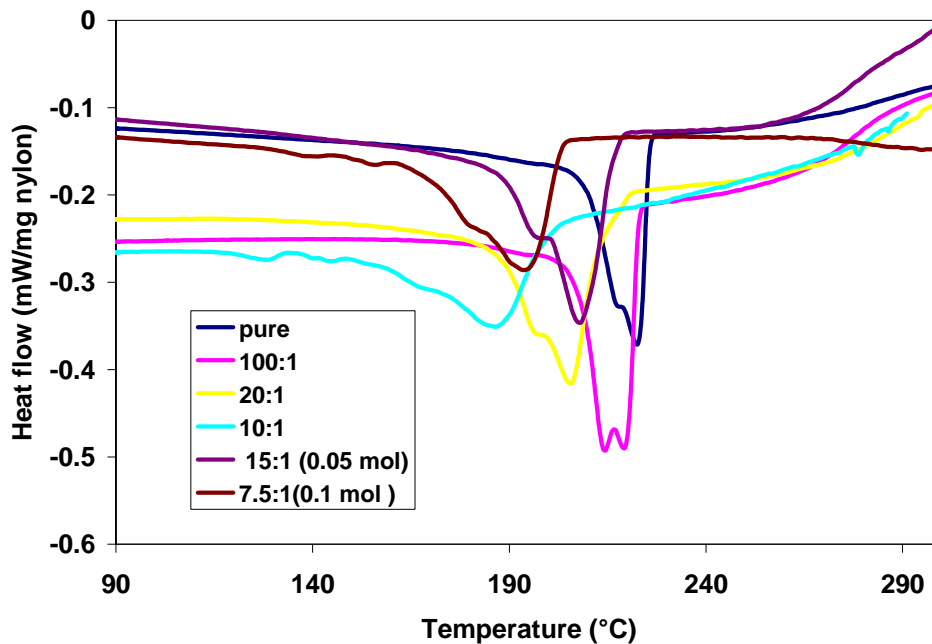


Figure 4.11: Second heating curves for different N6:NaOH ratios (heating at 3°C per min)

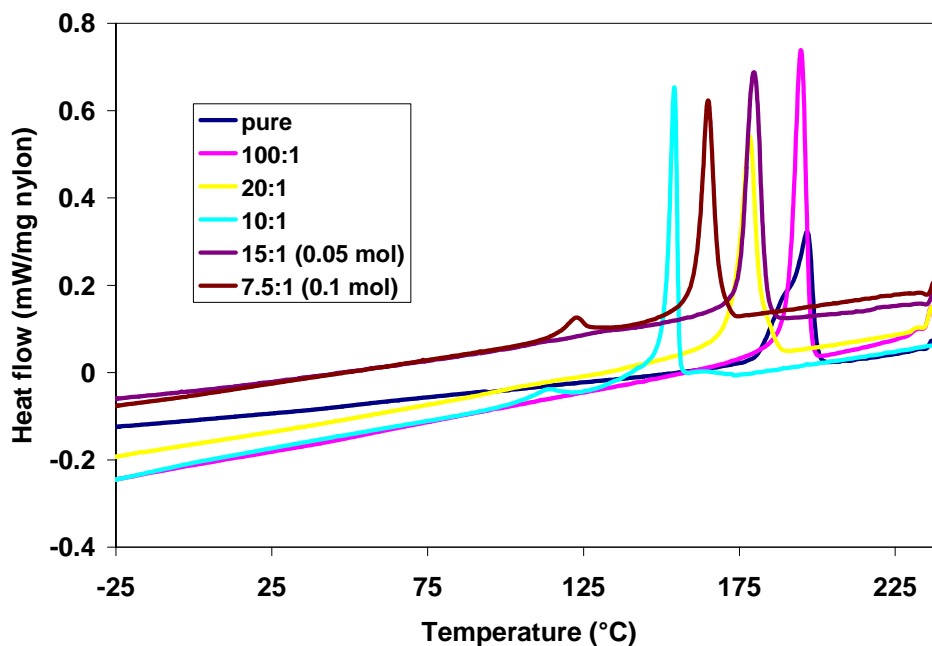


Figure 4.12: Cooling curves for different N6:NaOH ratios (cooling at 3°C per min)

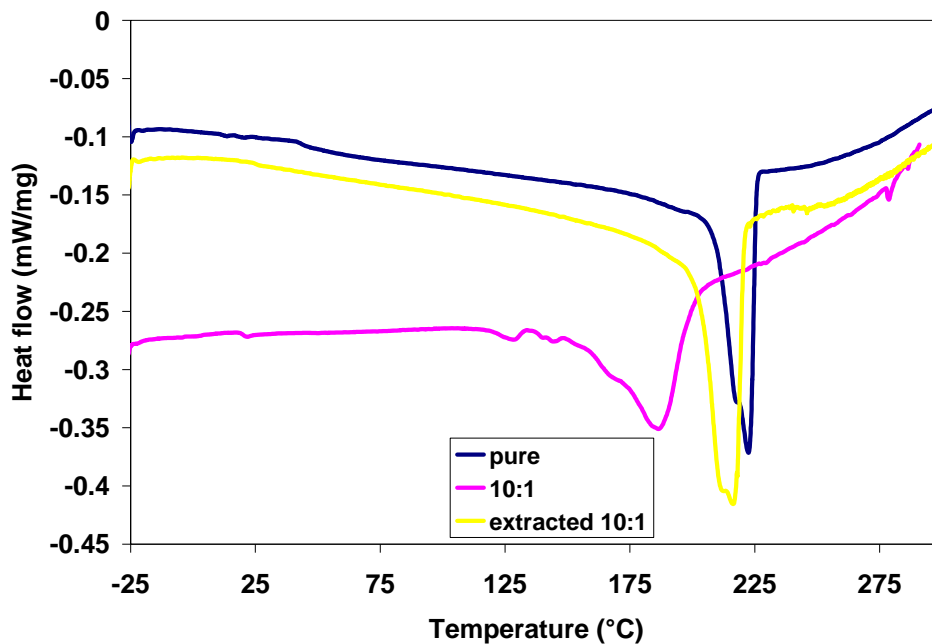


Figure 4.13: Comparison of the second heating curves for 10:1 N6:NaOH and its residue after catalyst extraction (heating at 3°C per min)

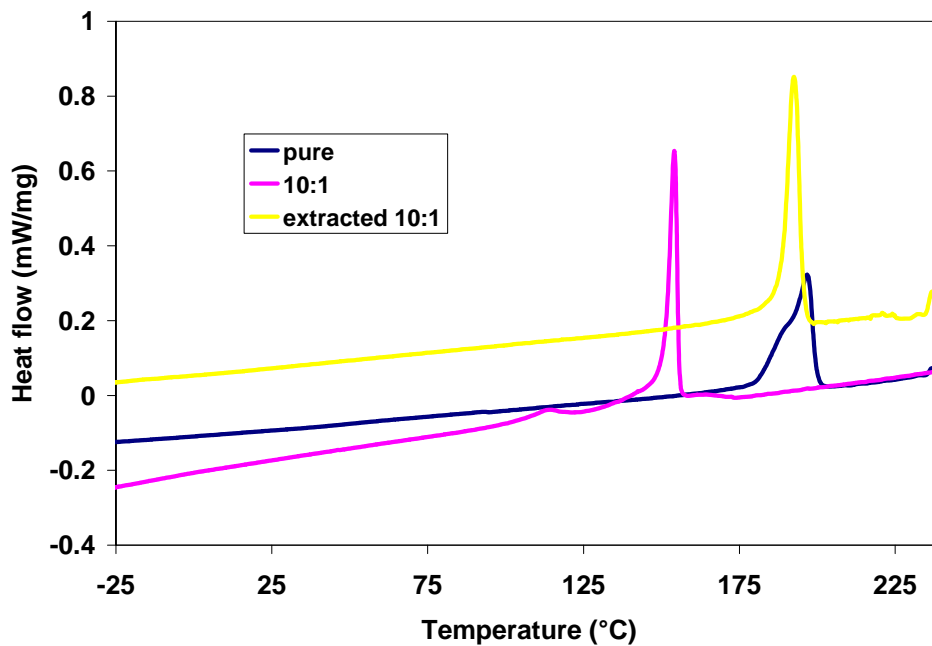


Figure 4.14: Comparison of the cooling curves 10:1 N6:NaOH and their its after catalyst extraction (cooling at 3°C per min)

4.2.4 Na₂CO₃

With Na₂CO₃, the melting and crystallization transitions are similar in nature to K₂CO₃, i.e. little variation of transition temperature and narrow transitions (see Figure 4.8, Figure 4.9, Figure 4.15 and Figure 4.16). However, unlike the K₂CO₃, there is no downward slope near 300°C in the heating curve which would have suggested degradation starting below 300°C.

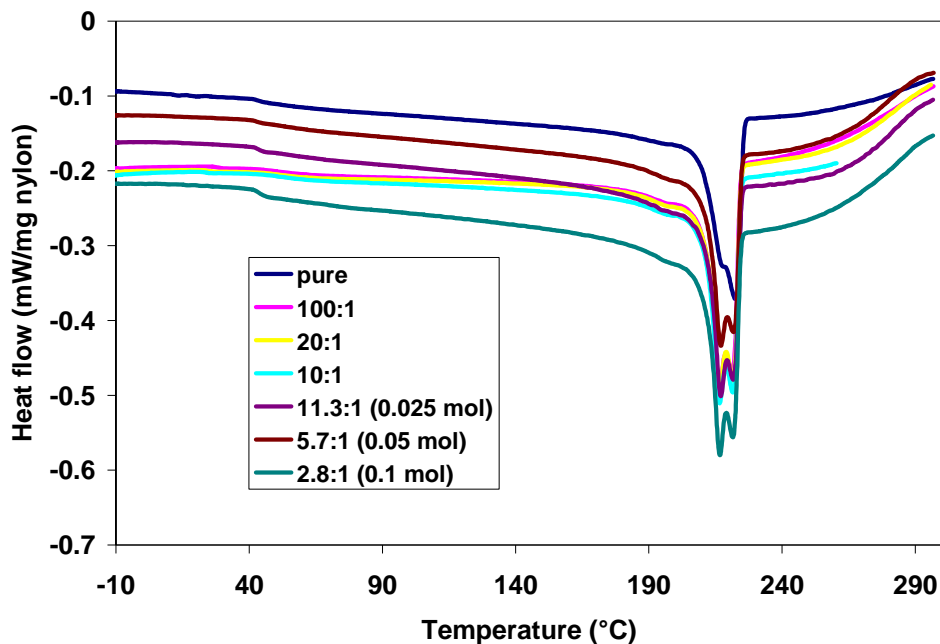


Figure 4.15: Second heating curves for different N6:Na₂CO₃ ratios (heating at 3°C per min)

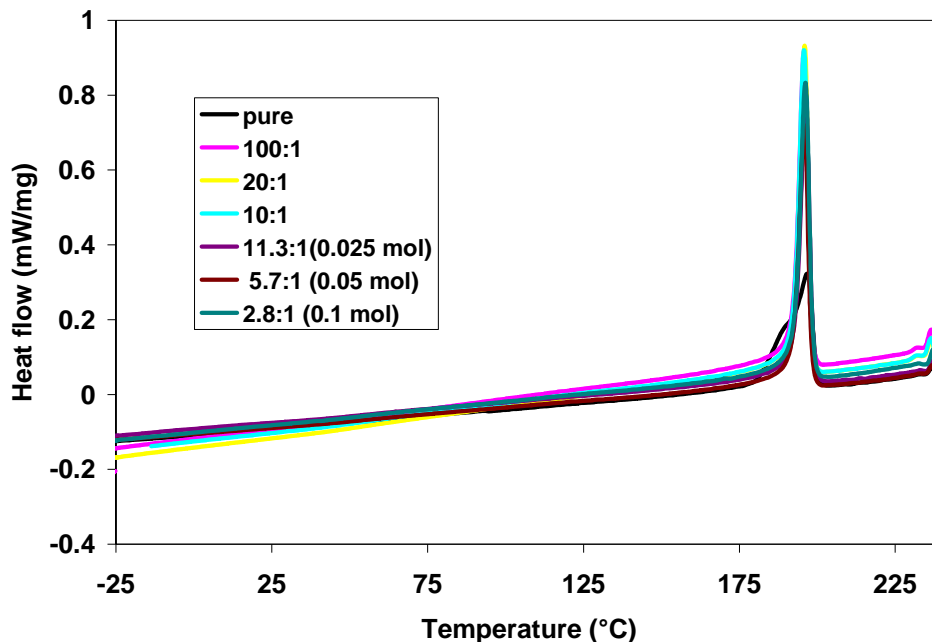


Figure 4.16: Cooling curves for different N6:Na₂CO₃ ratios (cooling at 3°C per min)

4.2.5 Cs₂CO₃

The pattern described above for the carbonates (K⁺ and Na⁺), does not hold for Cs₂CO₃. With Cs₂CO₃, there is only a slight variation of transition temperature with respect to concentration (see Table 4.8, Figure 4.17 and Figure 4.18). The melting temperatures with Cs₂CO₃ are approximately 10°C lower than the pure nylon 6. Similar to K₂CO₃ (after the melting transition), most of the Cs₂CO₃ mixture (except 100:1 ratio) shows another transition occurring around 300°C, perhaps degradation (Figure 4.17). The earliest transition starts around 255°C for the second highest loading of Cs₂CO₃, 0.025 mol ratio.

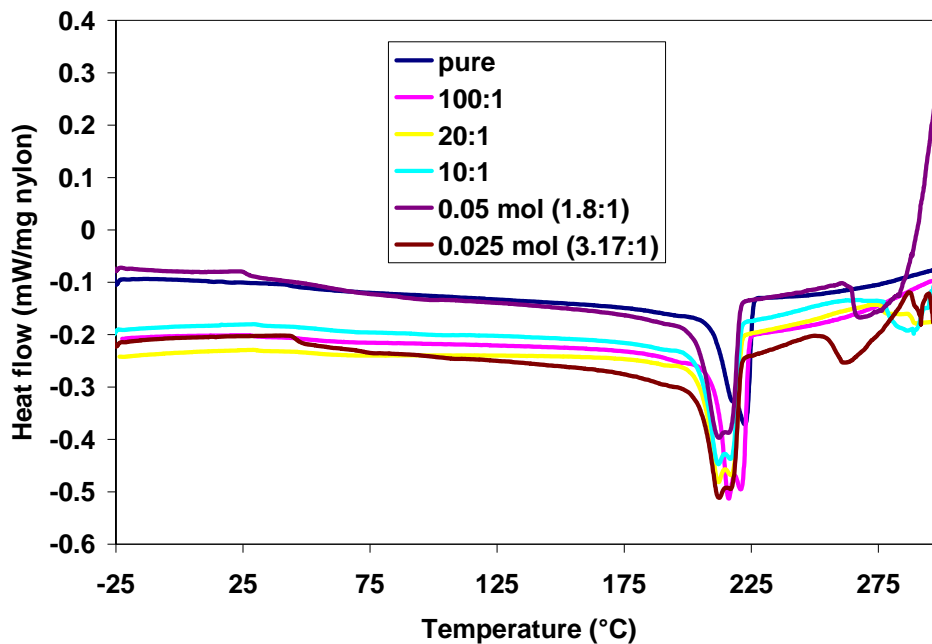


Figure 4.17: Second heating curves for different N6:Cs₂CO₃ ratios (heating at 3°C per min)

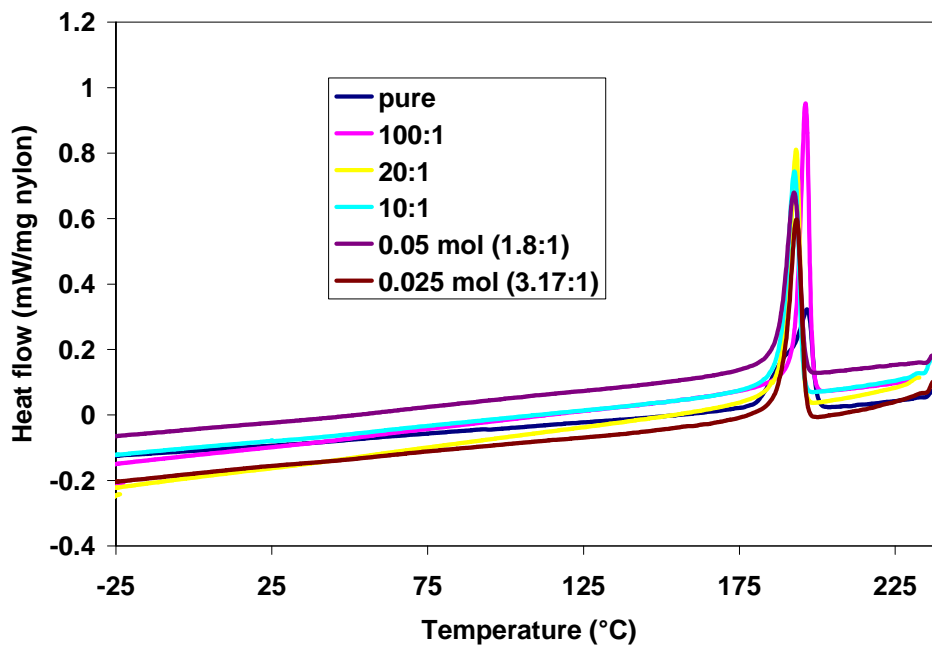


Figure 4.18: Cooling curves for different N6:Cs₂CO₃ ratios (cooling at 3°C per min)

4.2.6 CaCO₃

Similar to the K₂CO₃ and Na₂CO₃, CaCO₃ leads to little variation of transition temperatures and narrow transitions (Figure 4.8, Figure 4.9, Figure 4.15, Figure 4.16, Figure 4.19 and Figure 4.20). However, unlike the K₂CO₃ there is no downward slope near 300°C in the heating curve, which would have suggested degradation starting below 300°C.

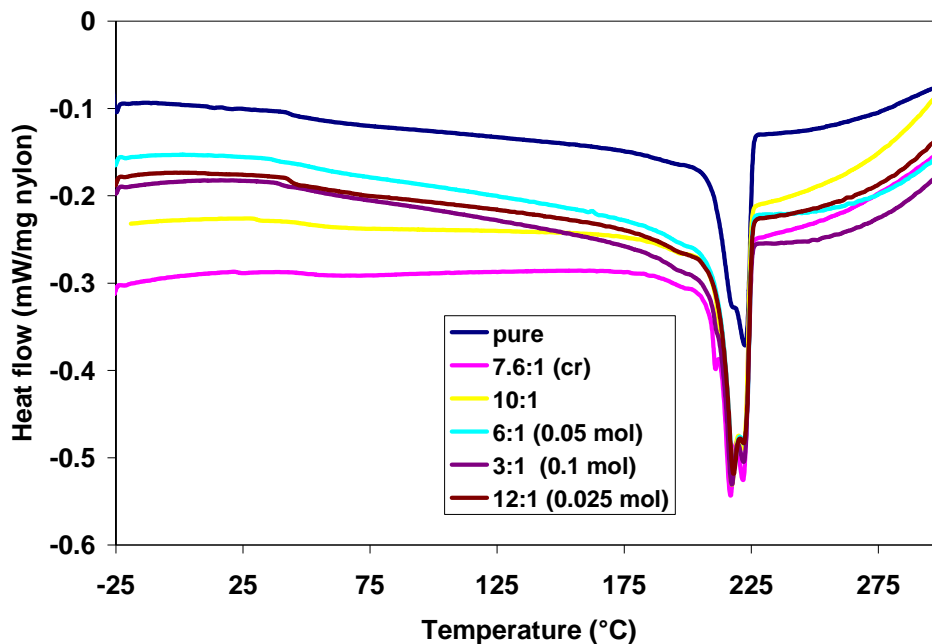


Figure 4.19: Second heating curves for different N6:CaCO₃ ratios (heating at 3°C per min)

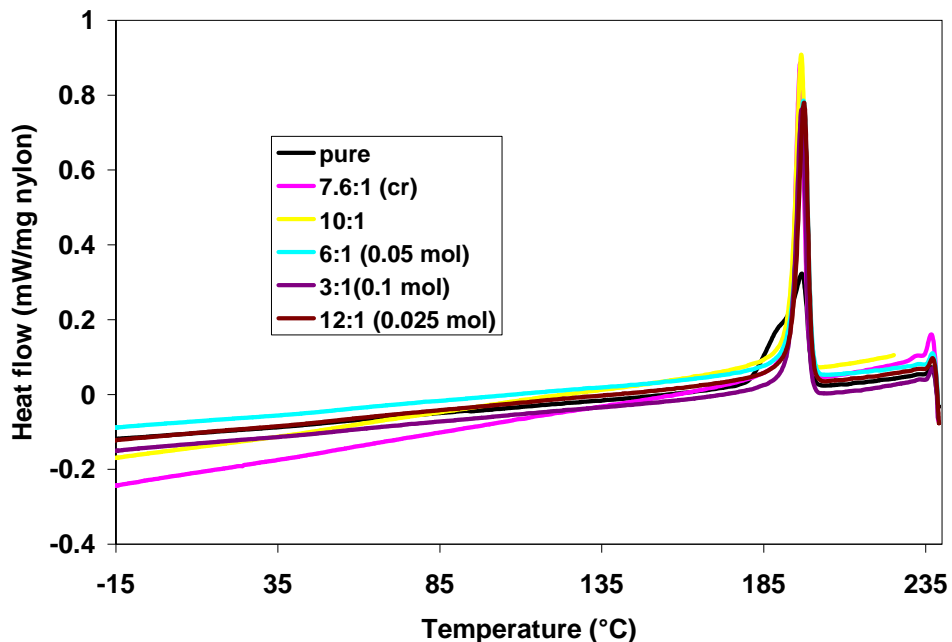


Figure 4.20: Cooling curves for different N6:CaCO₃ ratios (cooling at 3°C per min)

4.2.7 DSC Results Summary

The carbonates generally decrease the melting point of nylon 6 by around 6°C, except Cs₂CO₃ which decreases it by 10°C. The hydroxides had boarder melting transitions for the different catalyst concentrations, unlike the carbonates. However, no trend could be seen with respect to the catalyst loading and that of the temperature at which these transitions occurs. Some K₂CO₃ and NaOH samples had a transition peak below that of pure nylon 6, which might be caprolactam; indicating that some degradation might occur at 240°C. The 10:1 ratio of KOH had two cooling peaks, which didn't occur in any other KOH sample. The heating curves also suggest that some K₂CO₃ and Cs₂CO₃ start to degrade below 300°C. Since the results from the DSC indicate that

some degradation occurred during mixing, the kinetics obtained from TG may be misleading.

4.2.8 Extracted components from N6 catalyst mixtures

As mentioned above, since some of the samples indicated that mixing the catalyst and N6 changed the thermal properties of the N6, some samples were washed in methanol to remove any caprolactam or methanol soluble compound that may have been formed/trapped during mixing. The wash was then analyzed using GC-MS (Electron Impact). For 100:1 ratio of N6 to K_2CO_3 , the GC of the methanol wash is shown in Figure 4.21. As can be seen, there are five significant peaks in the GC results, all with retention times less than 10 mins. The first peak that occurs around 2 minutes is that of the methanol. The mass spectra scan of the second peak, which has a retention time of around 3.5 minutes, is shown in Figure 4.22. In Figure 4.22, there are no spectral lines around 113, which is the molecular weight of caprolactam. There are however lines around 105 and 207. The compound(s) which these lines may indicate has yet to be determined. For a retention time of around 5 minutes, shown in Figure 4.23, the 207 peak is more noticeable. In addition to the 207 line, for retention time of about 7 minutes (Figure 4.24), there are also lines around 281 and 251. Like the 207 line, these compounds have yet to be identified. Similar trends were seen for the other catalysts.

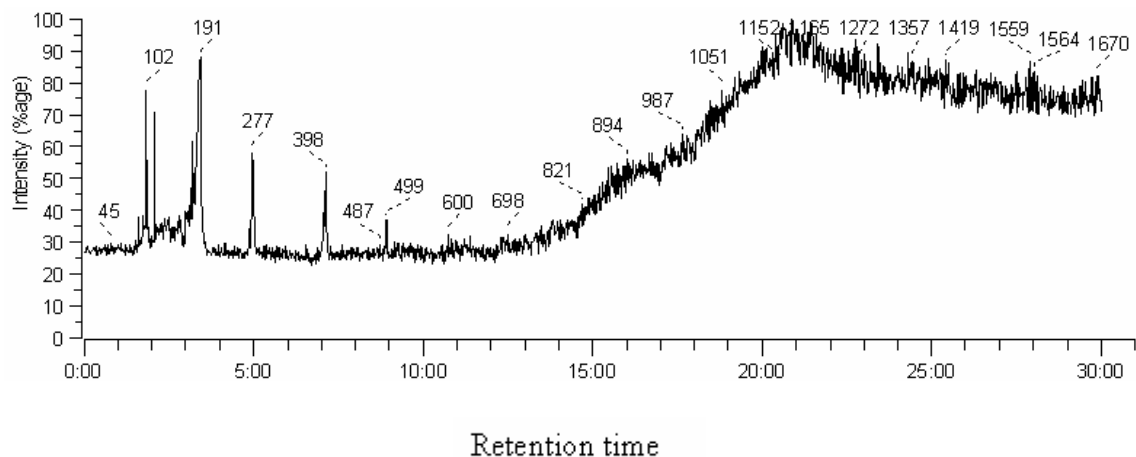


Figure 4.21: GC of the methanol wash extract from a 100:1 ratio of N6 to K₂CO₃ mixture

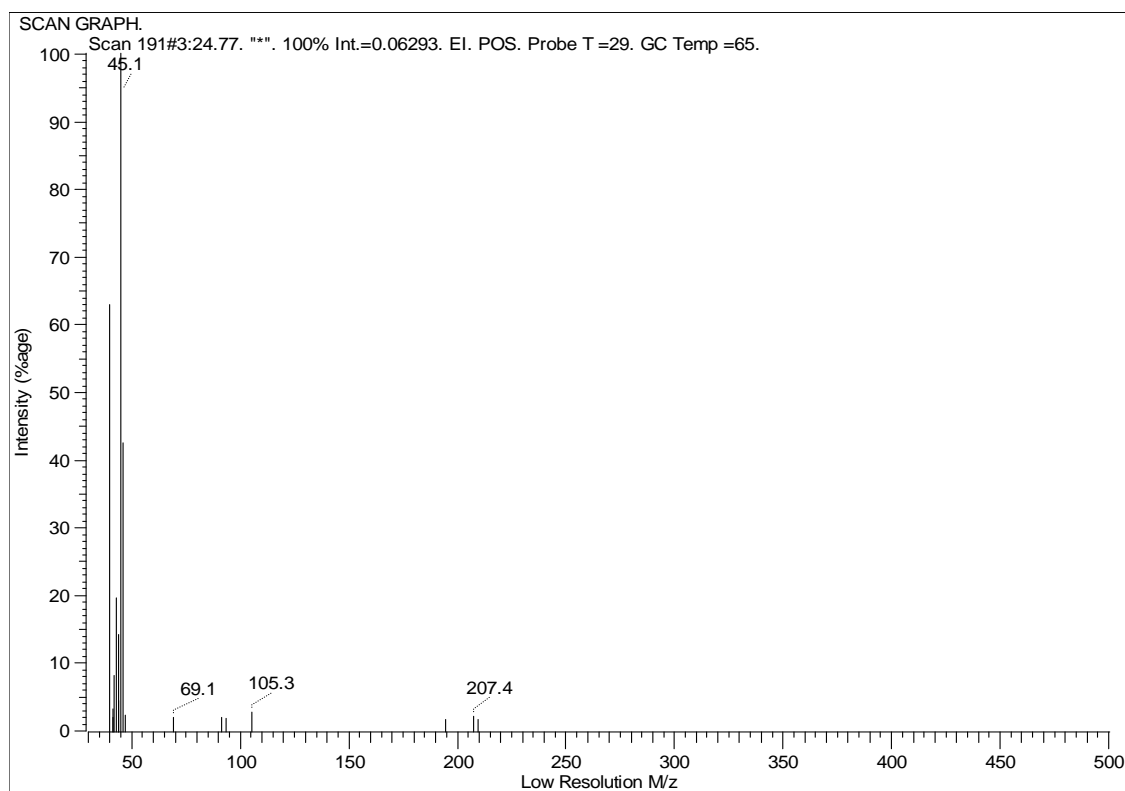


Figure 4.22: Mass spectrum scan of the second peak, which has a retention time of around 3.5 minutes, from the GC of a 100:1 ratio of N6 to K₂CO₃ mixture

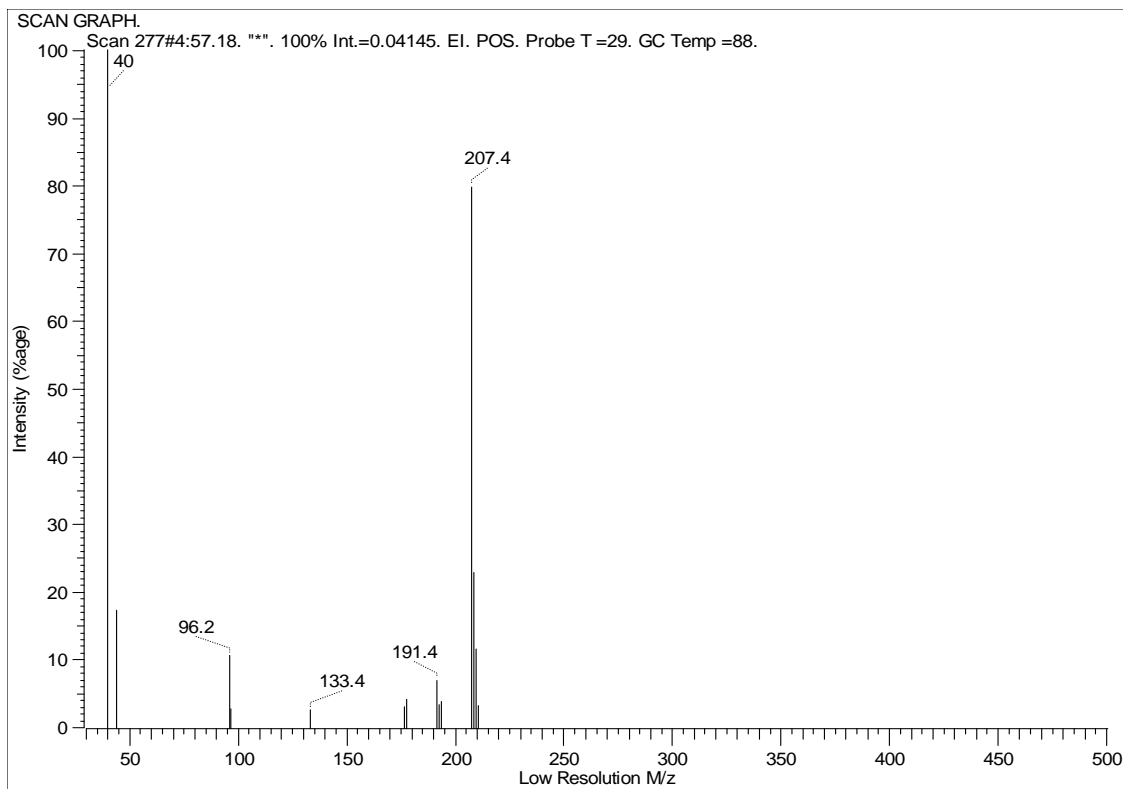


Figure 4.23: Mass spectrum scan of the third peak, which has a retention time of around 5 minutes, from the GC of a 100:1 ratio of N6 to K_2CO_3 mixture

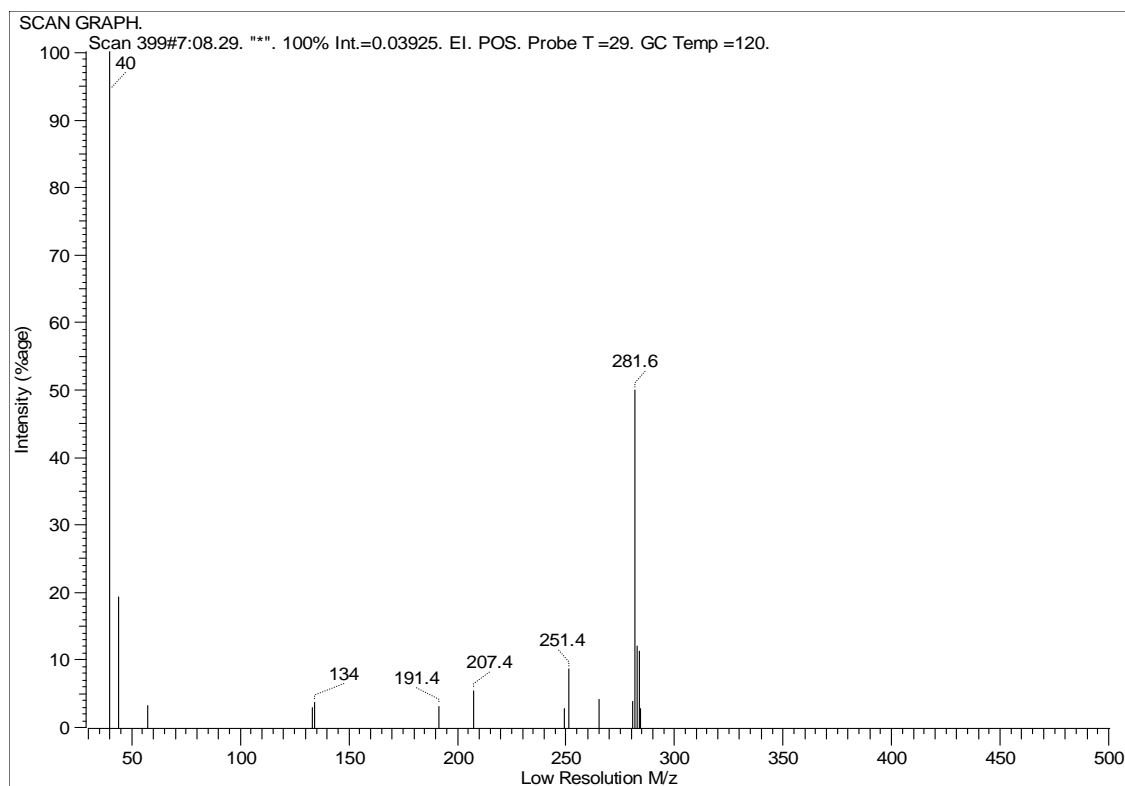


Figure 4.24: Mass spectrum scan of the fourth peak, which has a retention time of around 7 minutes, from the GC of a 100:1 ratio of N6 to K_2CO_3 mixture

4.3 Catalyst Screening: Degradation Onset

From the mass as a function of temperature obtained by doing TG, the weight loss fraction, α , was found using equation 3.1. Comparative plots of the weight loss fraction versus temperature for each sample were then made to determine which catalyst(s) started and completed the degradation process fastest.

4.3.1 Nylon 6

Figure 4.25 shows a comparison of the different hydroxides mixed at 10:1 ratio nylon 6 to catalyst that were considered to aid in the depolymerization of N6. One can

observe that pure nylon 6 starts to degrade around 400 °C while with catalyst, degradation starts between 250-300°C. This is over a 100° C difference. As can be seen, KOH & CsOH are the most effective catalysts. All the metallic portions of the catalysts considered are in Group I of the periodic table, and as the atomic number increases in Group I metal, so does its reactivity. Hence, true to form, CsOH is the better catalyst of its fellow Group I hydroxides. But since CsOH is more expensive than KOH, and CsOH gave no significant decrease in degradation onset over KOH, the most reasonable choice would be to use KOH.

A eutectic mixture of NaOH and KOH was also tested to see if that combination would be more effective than each of those components separately. This was done because the eutectic mixture, which melts at 185 °C (according to reference [31]) is supposed to be easier to mix in the nylon and provide more surface area; hence, enhancing the reaction. In Figure 4.25, the eutectic mixture did not perform as expected. Its performance was between its respective components' performance.

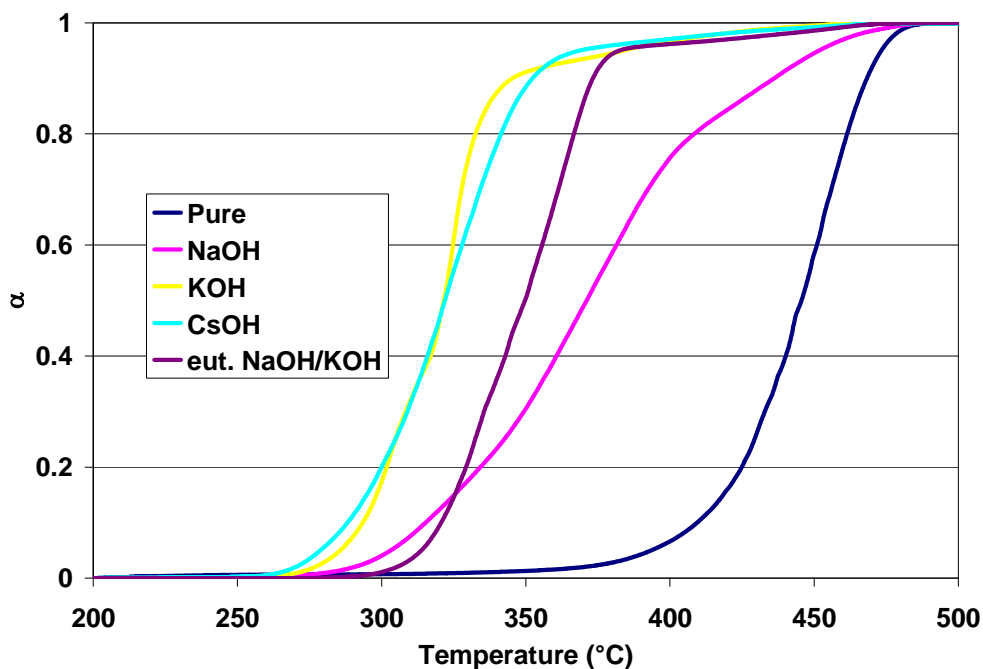


Figure 4.25: Comparison of 10:1 ratios of pure nylon 6 to that of hydroxides catalysts; eut. means eutectic

Figure 4.26 shows a comparison of the different carbonates considered to assist in the depolymerization of N6. Analogous to the hydroxides, the best performing carbonate catalyst contains Cs as its metallic constituent. This is followed by the corresponding K then Na carbonates from Group I of the periodic table. Even though CaCO_3 had a higher percentage within its sample than the carbonates with Group I metals, it was the least effective catalyst. This was expected because Ca is in Group II of the periodic table and Group I metals compounds with the same anion are generally more reactive than those from Group II. However, since the carpet ratio (cr) of CaCO_3 decreases the degradation onset, it may be helpful to reduce the amount of the other catalysts to depolymerize the nylon portion of the carpet.

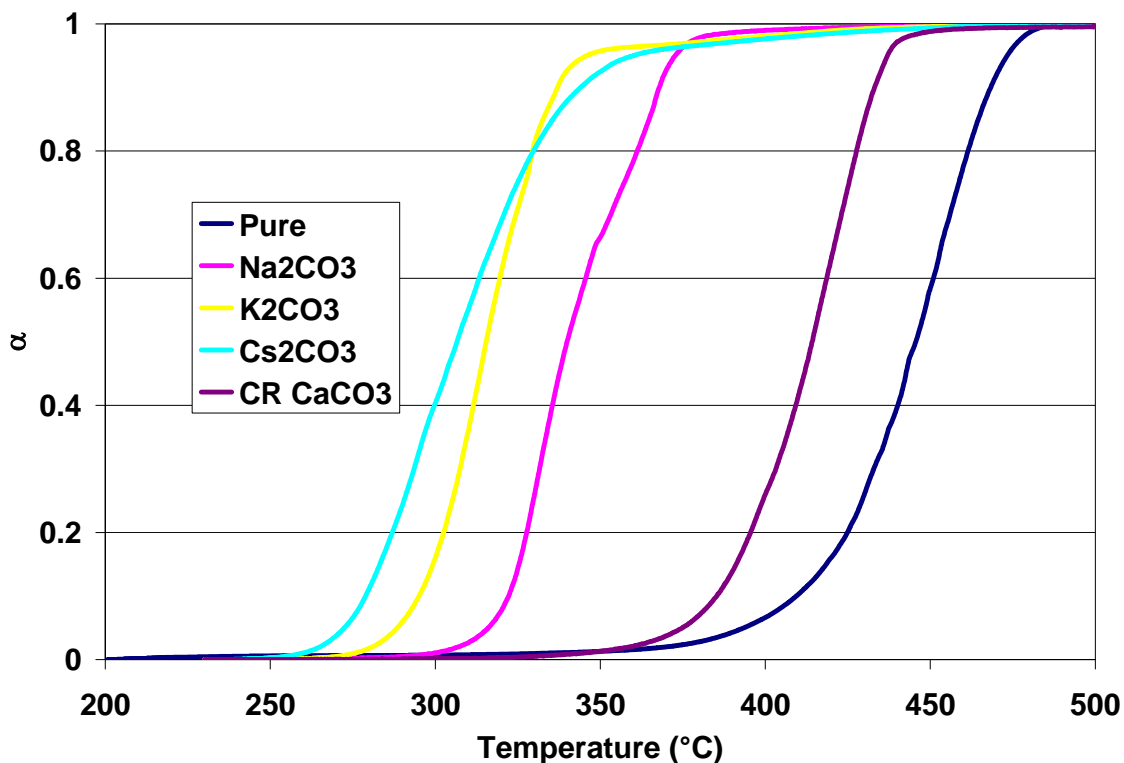


Figure 4.26: Comparison of 10:1 ratios of pure nylon 6 to that of carbonates catalysts (cr means carpet ratio)

Since Cs⁺ bases are more expensive than K⁺ bases, and there is no significant decrease in onset degradation temperature, the catalysts of choice are KOH and K₂CO₃. Both 10:1 ratio of N6 to KOH and K₂CO₃ have similar onset temperatures, but since a 10:1 ratio of N6 to catalysts would increase production costs, smaller amounts of catalysts were also tested. Figure 4.27 shows a comparison of 10:1 and 100:1 ratios mixtures of N6 to these catalysts. From this Figure, one can see that the 100:1 ratio of N6:KOH has a similar onset temperature as the 10:1 ratio of N6:KOH. The 100:1 ratio of N6:K₂CO₃ has a higher onset temperature than its 10:1 ratio

counterpart; however, the performance of the 100:1 N6:K₂CO₃ is still better than just pure N6.

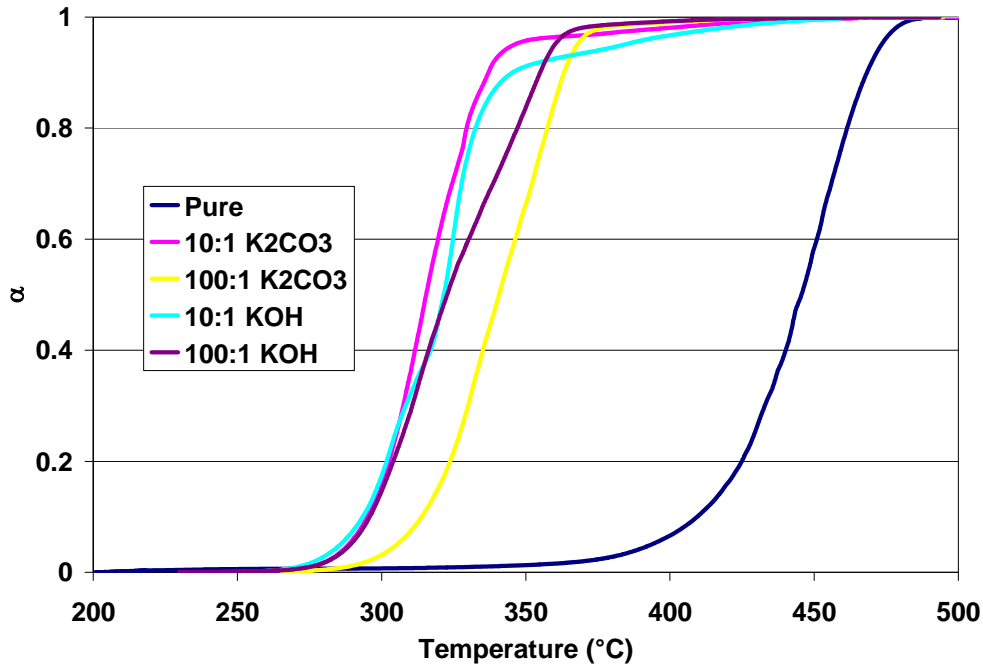


Figure 4.27: Comparison of 10:1 and 100:1 ratios of nylon 6 to KOH and K₂CO₃ catalysts

Since the 100:1 ratio catalysts performance was exceptional, 200:1 ratios of each catalysts were also tested and the results are shown in Figure 4.28. The following observations can be made from this Figure:

- With a 200:1 ratio of N6:KOH, onset degradation temperature was the same as the 100:1 ratio N6:K₂CO₃
- With a 200:1 ratio of N6:K₂CO₃, starts degrading above 300°C, but it still degrades at much lower temperatures than just pure N6.

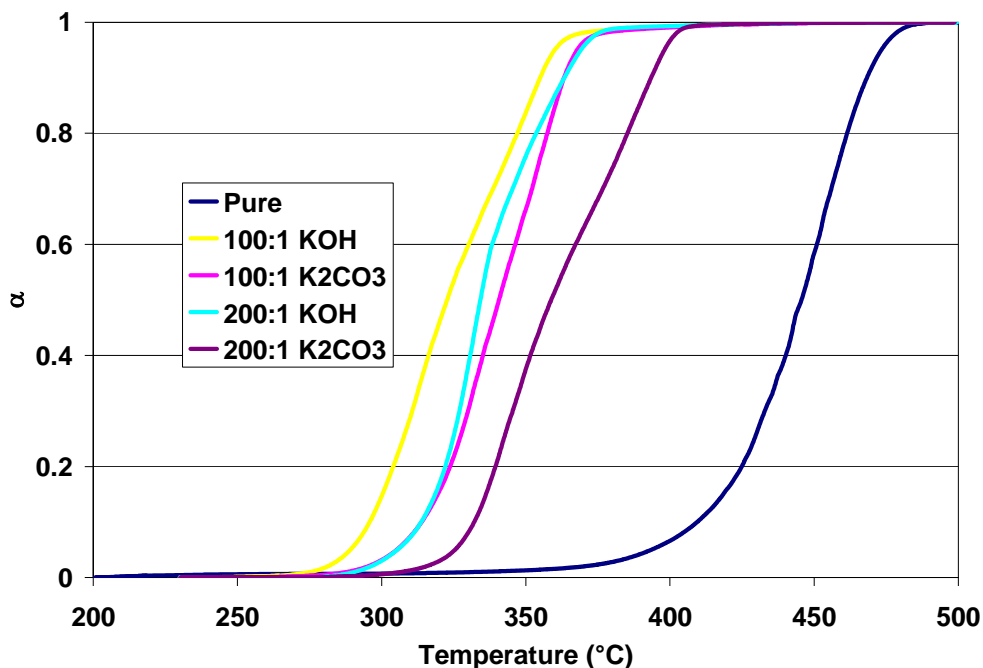


Figure 4.28: Comparison of 200:1 ratios of N6 to KOH and K₂CO₃ catalysts

4.3.2 Nylon 6,6

Figure 4.29 shows a comparison of the different hydroxides and carbonates mixed at 10:1 ratio of nylon 6,6 (N66) to catalyst that were considered to aid in the depolymerization of N66. Of the four catalysts shown, their performances were similar; they all started to degrade at a lower temperature than pure N66. Surprisingly, NaOH started the degradation process at the lowest temperature, but later, it had similar conversion at higher temperatures to KOH. Even though the Cs₂CO₃ started degradation before its carbonate counterpart K₂CO₃, K₂CO₃ achieved 90% conversion at a lower temperature than the Cs₂CO₃.

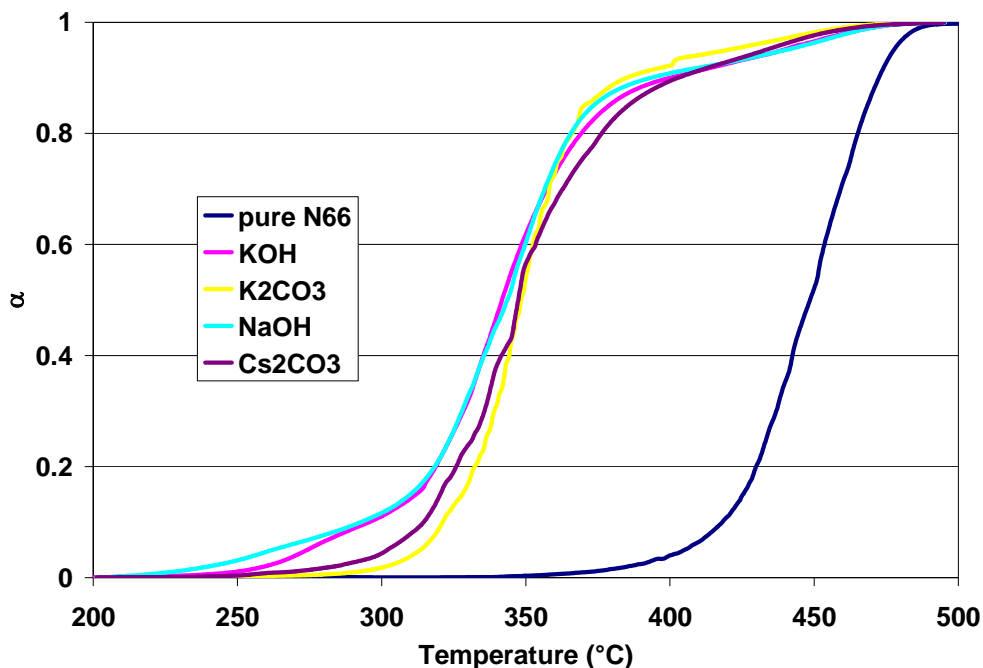


Figure 4.29: Comparison of 10:1 ratio of pure nylon 6, 6 to hydroxides and carbonates catalysts

Since the 10:1 ratio of pure nylon 6, 6 to catalysts were so effective lower quantities were also tested. Figure 4.30 and Figure 4.31 shows a comparison of the 10:1 and 100:1 ratios counterparts (the carpet ratio of CaCO_3 is also included for comparison). With the 100:1 ratio of N66 to NaOH and KOH, the degradation onset started around the same temperature, but compared to their 10:1 ratio counterparts the onset degradation temperature increased by approximately 50°C . However, at 90% conversion, 100:1 N6:NaOH was at the same temperature as that of the 10:1 N6:catalyst.

With the carbonates at 100:1 ratios, the degradation onset started at a higher temperature than their 10:1 counterparts. With 100:1 ratios, these catalysts still performed better than a carpet ratio of CaCO_3 , which like with N6, helped to degrade N66 faster than just pure N66.

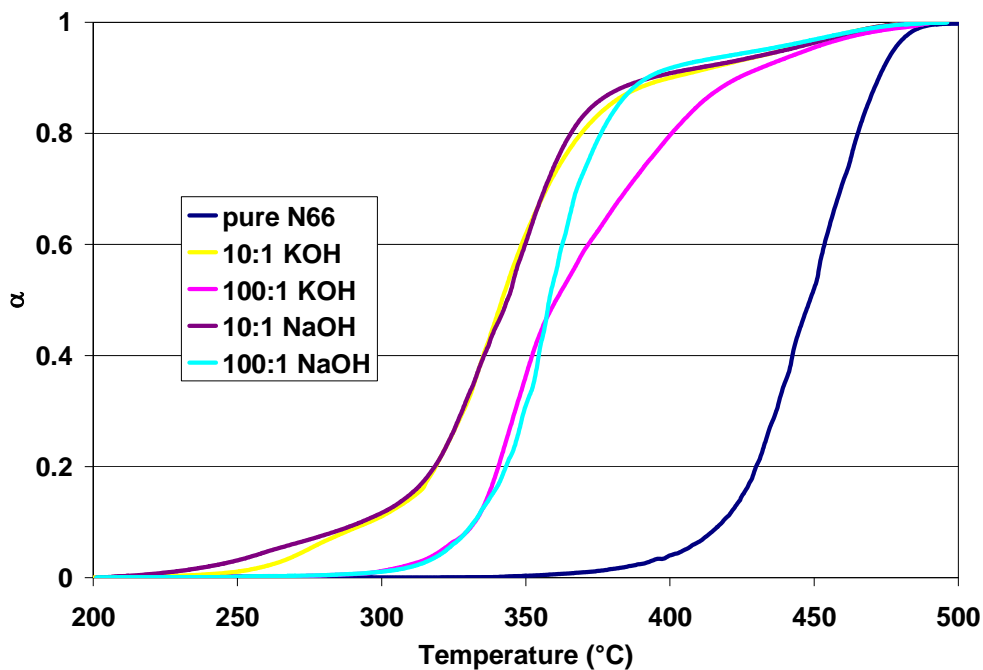


Figure 4.30: Comparison of 10:1 and 100:1 ratios of Nylon 66 to hydroxide catalysts

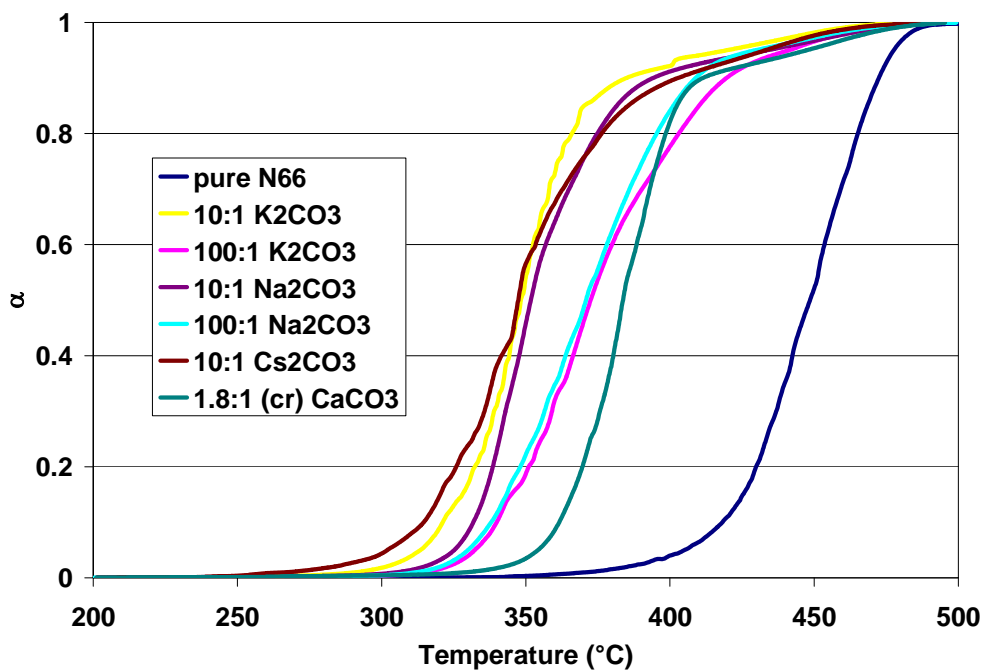


Figure 4.31: Comparison of different ratios of nylon 66 to carbonate catalysts (cr means carpet ratio)

4.3.3 Catalyst degradation onset summary

From TG measurements, it has been shown that both metallic hydroxides and carbonates decreased the onset degradation temperature of both nylon 6 and nylon 6,6. It was also determined that small amounts of these bases significantly lowered the onset degradation temperature when compared to the pure polymers. For some catalysts, degradation onset for 10:1 and 100:1 ratios of nylon to catalysts were around the same temperature. For N6, the most effective and the same time economical catalysts were KOH and K_2CO_3 , while for N66, they were NaOH and KOH.

4.4 Kinetics Results

Several of the computational methods that are used in determining kinetic parameters for isothermal and dynamic data highlighted in Chapter 2 were used to model the degradation of the un-catalyzed and catalyzed nylon 6. After finding the kinetic parameters for each model, a simulation was made to imitate the experimental conditions.

4.4.1 Pure N6

4.4.1.1 Pure N6 Isothermal TG: Model-Fitting Method

With isothermal model-fitting of pure nylon 6, for each of the four temperatures considered, a different model was found to be the best fit for each (see Table 4.9). This might indicate that there are different mechanism/reactions occurring at these different temperatures. The models shown in Table 4.9 are of the deceleration type, except for F0

which is constant. As stated before, with deceleration type reactions, the maximum rate of reaction occurs at low α .

Table 4.9: Coefficient of determination (R^2) and model for nylon 6 with different temperatures from using isothermal data (*See Table 2.1 for model expressions)

	R^2's in Calculating k			
Temperature ($^{\circ}\text{C}$)	333	365	382	423
Maximum R^2	0.9952	0.9982	0.9986	0.9702
Model* corresponding maximum R^2	F0	R2	R3	D3

Since there wasn't an unambiguous model fit, step two was proceeded with by using the best model fits. From the four best model fits for the k 's, E_a and A were found. Of these four, the best fit was also found as shown in the latter part of Table 4.10. According to this method, the best fit was model D3, the 3D diffusion model. Even though there might be diffusion limitation in the exiting of the product, D3 cannot be justifiably chosen as the correct model because it was the best fitting model at the highest temperature and this is counterintuitive.(One would expect that has the temperature increases, the diffusion limitations would decrease.)

Table 4.10: Determination of E_a and A from the best fitting model from using isothermal data for pure N6; *See Table 2.1 for model expressions

<i>Maximum R^2</i>	0.9958
<i>Model* w/ max</i>	D3
<i>E_a (kJ/mol)</i>	58
<i>A (min^{-1})</i>	167

4.4.1.2 Pure N6 Isothermal TG: Standard Isoconversional Method (Flynn technique)

The Flynn technique (section 2.3.1.1.2.1)[39, 45] was applied to the isothermal data, it was found that as the conversion increases, the E_a decreases. Since this decrease in E_a has no theoretical basis, this technique was deemed flawed.

4.4.1.3 Pure N6 Dynamic TG: Model-Fitting Direct Differential Method

This method is presented in section 2.3.1.1.3.2. For pure N6, four different heating rates were used as shown in Table 4.11. Of the four, three were found to follow the trend of the D3 model found above in isothermal model fit. Unfortunately, for each heating rate, different values of E_a and A were obtained. Therefore, application of this model is not very practical.

Table 4.11: Models and kinetics parameters for different heating rate of pure N6;
*See Table 2.1 for model expressions

Heating rate (degrees per minute)	Model* fit	E_a (kJ/mol)	A (min ⁻¹)	R ²
5	D3	412	5E+28	0.98854
10	D3	448	1.2E+31	0.97234
15	D3	451	1.2E+31	0.98132
20	F2	449	1.9E+32	0.9759

4.4.1.4 Pure N6 Dynamic TG: ASTM/Ozawa-Flynn-Wall (OFW)

This model is presented in section 2.3.1.1.4.2. The ASTM E 1641 – 99 standard [49] was used. This method assumes 1st order decomposition. The kinetic parameters derived using this method are shown in Table 4.12. When used to simulate different

heating rates, these parameters gave a very good fit over all the conversion values. An example of this can be seen for the 5 and 10 degrees per minute of pure nylon 6 as shown in Figure 4.32.

Table 4.12: Kinetic parameters found by using the ASTM standard for pure n6

Kinetic constant	Average	Standard Deviation
E_a (kJ/mol)	203	6
A (min^{-1})	2.00E+14	1.33E+14

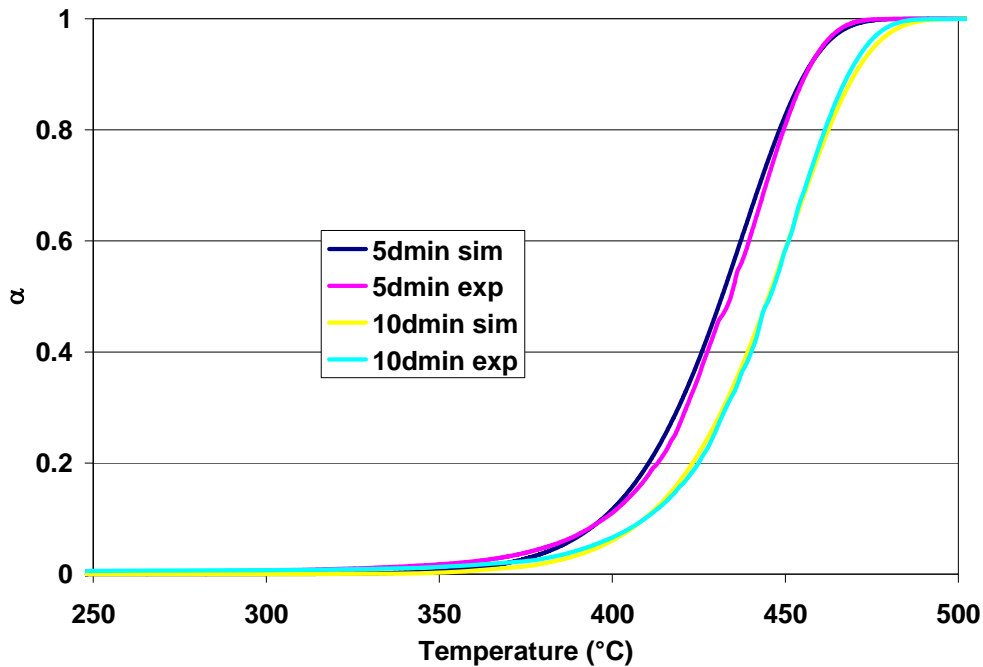


Figure 4.32: Simulated and experimental conversion curves for dynamic heating of pure N6 using the kinetic parameters found by using the ASTM method.

4.4.1.5 Dynamic TG: Distributed activated energy model (DAE)

The final method that was used to try to ascertain kinetic parameters for pure N6 using dynamic TG data was the Distributed activated energy model (DAE). This method is presented in section 2.3.1.1.4.3. Figure 4.33 shows the E_a/R , A and Fraction allocated

for the 50 possible reactions against the normalized mass of the sample. For pure N6, the E_a/R didn't vary much, and neither did the A calculated. However, six dominant reactions were found as indicated by the fraction contributions. The corresponding temperatures, E_a and A for these fractions were found as shown in Table 4.13. Even though first order reactions were assumed in this model, all of the E_a 's and A 's, except for one set, are higher than that found using the ASTM standard. Using the E_a 's and A 's, a comparative plot of simulated and experimental data was made of the normalized mass remaining (which is equivalent to $1-\alpha$) and is shown in Figure 4.34. Like the ASTM, the simulated results from DAE model were comparable to the experimental.

Table 4.13: Corresponding temperatures for the E_a , A and Fractions found for pure N6 using DAE model

Temperature (°C)	E_a (kJ/mol)	A (1/min)	Fraction
284.85	247	3.06E+17	0.67
287.88	248	3.52E+17	0.05
357.58	250	1.05E+18	0.19
409.09	233	1.08E+17	0.07
493.94	166	9.54E+12	0.02
500.00	254	7.15E+21	9.34E-05

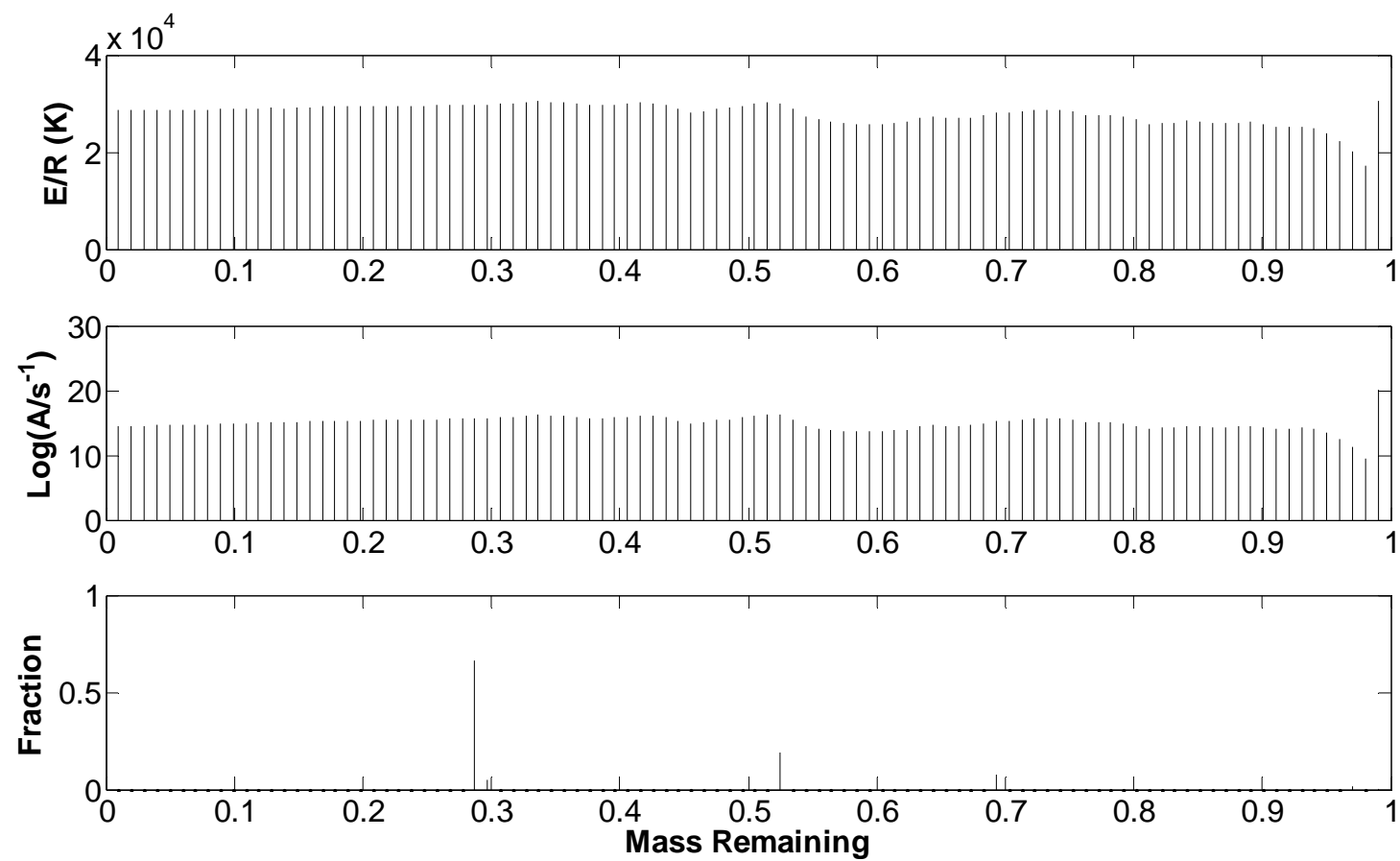


Figure 4.33: E_a/R , A and Fraction allocated for the 50 possible reactions against the normalized mass of the pure N6.

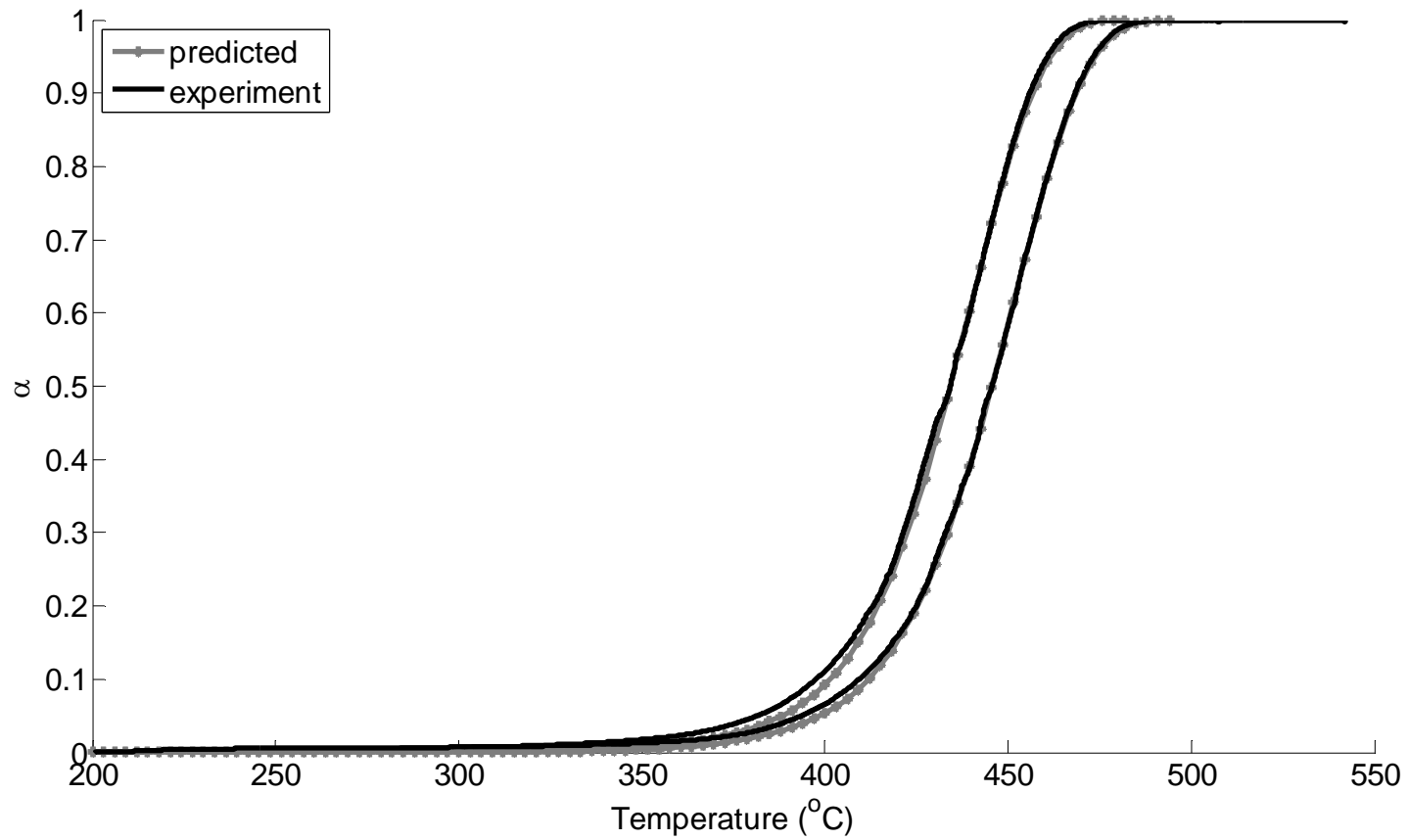


Figure 4.34: The normalized mass remaining for heating at 5 and 10 degrees per minute using the kinetic parameters from the DAE method for pure N6.

4.4.1.6 Pure N6 conclusion

By comparing all of the above methods for determining the model/kinetics that best describe the decomposition of pure nylon, the kinetic parameters obtained from using the ASTM method, are chosen as the best set because it gave a good fit over the entire temperature range whereas with the DAE method, the kinetic parameters have to be reported with the temperature range for which they are applicable.

4.4.2 Nylon 6 Kinetics summary

Similar analysis for kinetic parameters was done for N6 with catalysts using all the different model determining methods. For all these catalyzed systems, the ASTM method gave the best results. Table 4.14 shows a summary of the kinetic parameters for different catalysts and catalyst contents in pure N6. The highest E_a and A were for pure N6 without any catalyst, while the lowest combination belonged to the ratio of 10:1 N6:KOH. With 10:1 ratios of N6 to KOH and K_2CO_3 , both activation energies were less than their corresponding activation energies for 100:1 ratios. Even though the 10:1 ratio of N6:KOH had lower activation energy than 10:1 ratio of N6: K_2CO_3 , with their 100:1 counterparts, the opposite was true. It should be noted that A for the 100:1 ratio of N6:KOH was higher by a order of magnitude. However, because of the “kinetic compensation effect” (see page 27), to get a better comparison of the kinetics of these catalyst, it is best to look at their conversion times. Table 4.15 contains the time to get 90% conversion for these catalyst. Clearly, the best catalyst of those shown is 100:1 N6:KOH.

Table 4.14: Summary of E_a and A for different catalysts amounts in pure N6

Catalyst	Ratio N6:catalyst	E_a (kJ/mol)		A (min ⁻¹)	
		Average	Standard Deviation	Average	Standard Deviation
None	n/a	203	6	2.00E+14	1.33E+14
KOH	10:1	99	1	5.06E+07	1.49E+07
K ₂ CO ₃	10:1	123	0	1.08E+10	3.27E+09
KOH	100:1	131	2	9.68E+10	1.19E+11
K ₂ CO ₃	100:1	129	1	1.01E+10	2.63E+09
CaCO ₃	1.8:1	158	15	5.36E+11	5.41E+11

Table 4.15: Summary of time to get 90% conversion for some catalyst combinations of N6

Temperature (°C)	Time to get 90 % conversion (min)				
	Pure N6	10:1 N6:K ₂ CO ₃	100:1 N6:K ₂ CO ₃	100:1 N6:KOH	1.8:1(carpet ratio) N6: CaCO ₃
300	36212	35	139	22	1002
325	6105	12	45	7	251
350	1187	4	16	2	70
400	65	1	2	0.4	7

4.4.2.1 KOH N6 Dynamic TG: ASTM/Ozawa-Flynn-Wall (OFW)

The use of the ASTM standard on the dynamic TG data yielded the kinetic parameters for the 100:1 ratio N6:KOH and the 10:1 ratio N6:KOH shown in Table 4.16 and Table 4.17 respectively. When these parameters used to simulate the conversion curves for 5 and 10 degrees per minute, the 100:1 ratio of N6:KOH gave decent predictions while the 10:1 ratio of N6:KOH gave mediocre simulated results (see Figure 4.35 and Figure 4.36, respectively). The results for the 10:1 N6:KOH is contrary to the results using the ASTM method from the pure N6 which gave more or less a perfect fit.

Considering that the ASTM method uses only conversion values less than 20%, it gives fairly good prediction over the entire conversion range.

Table 4.16: Kinetic parameters found by using the ASTM standard with the 100:1 ratio of N6:KOH

Kinetic constant	Average	Standard Deviation
E_a (kJ/mol)	131	2
$A(\text{min}^{-1})$	$9.68\text{E}+10$	$1.19\text{E}+11$

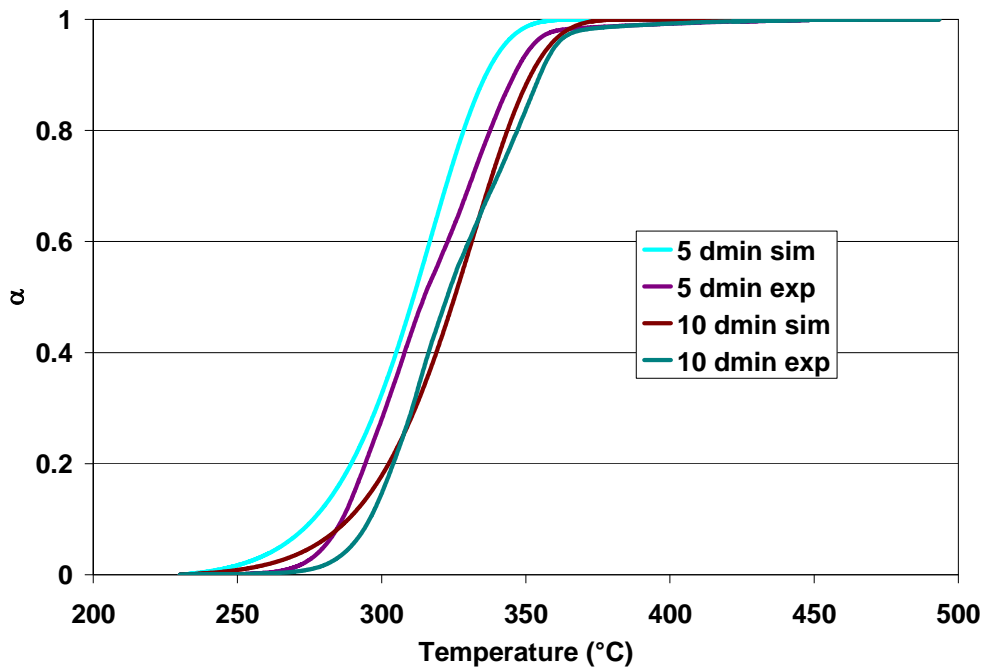


Figure 4.35: Simulated and experimental conversion curves for dynamic heating of 100:1 ratio of N6:KOH using the kinetic parameters found by using the ASTM method

Table 4.17: Kinetic parameters found by using the ASTM standard for 10:1 ratio of N6:KOH

Kinetic constant	Average	Standard Deviation
E_a (kJ/mol)	98	1
A (min ⁻¹)	5.06E+07	1.49E+07

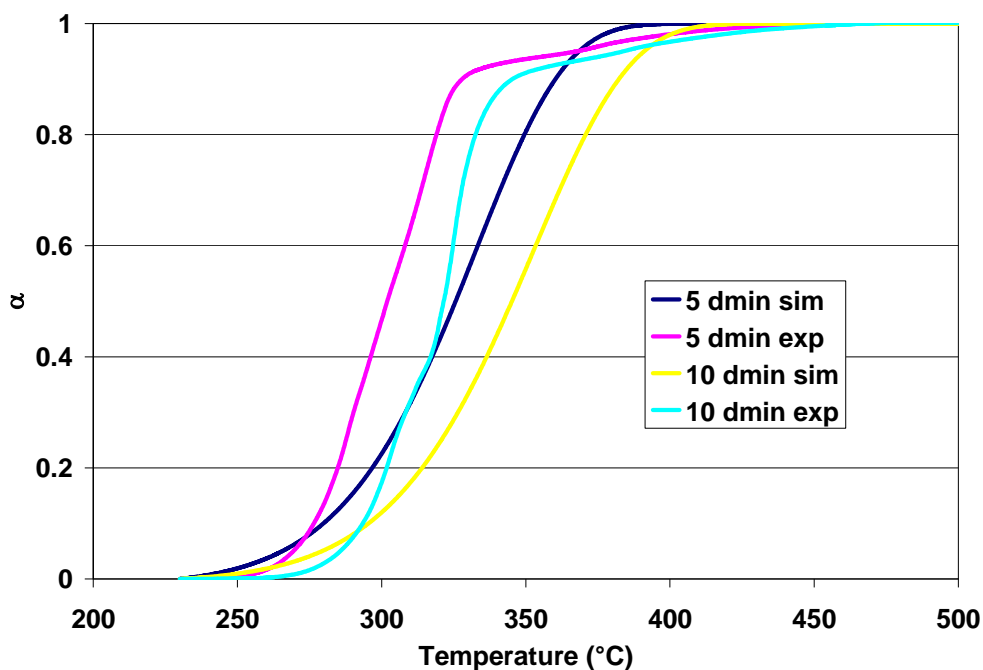


Figure 4.36: Simulated and experimental conversion curves for dynamic heating of 10:1 ratio of N6:KOH using the kinetic parameters found by using the ASTM method

4.4.2.2 K_2CO_3 N6 Dynamic TG: ASTM/Ozawa-Flynn-Wall (OFW)

By applying the ASTM method to the dynamic TG data for 100:1 N6: K_2CO_3 and 10:1 N6: K_2CO_3 , the kinetic parameters obtained are shown in Table 4.14. These constants were used to simulate the heating of their respective samples at 5 and 10 degrees per minute, as shown in Figure 4.37 and Figure 4.38. The simulated results do not follow the experimental data as well as pure N6 (Figure 4.38); however, they are

within close proximity and can be used to give a decent estimate of the rate of conversion. The time to get 90 % conversion for each of these samples is shown in Table 4.15. As anticipated, the 10:1 ratio of N6:K₂CO₃ proceeded faster than the 100:1 N6:K₂CO₃ ratio. However, as predicted by the catalyst screening, the 100:1 N6:K₂CO₃ reaction was slower than the 100:1 N6:KOH while being faster than just pure N6.

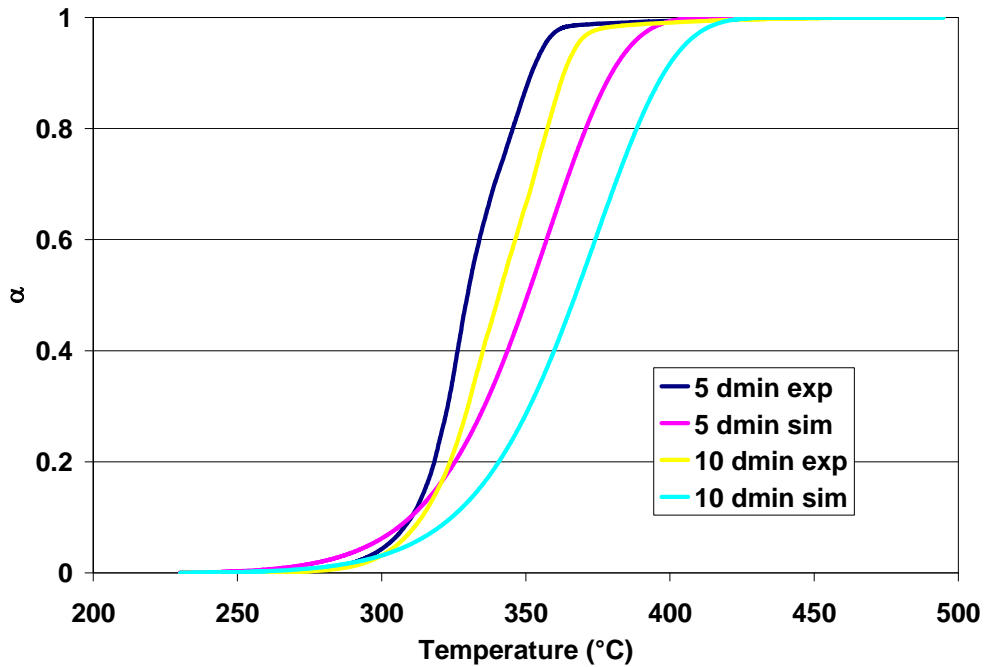


Figure 4.37: Simulated and experimental conversion curves for dynamic heating of 100:1 N6:K₂CO₃ using the kinetic parameters found by using the ASTM method

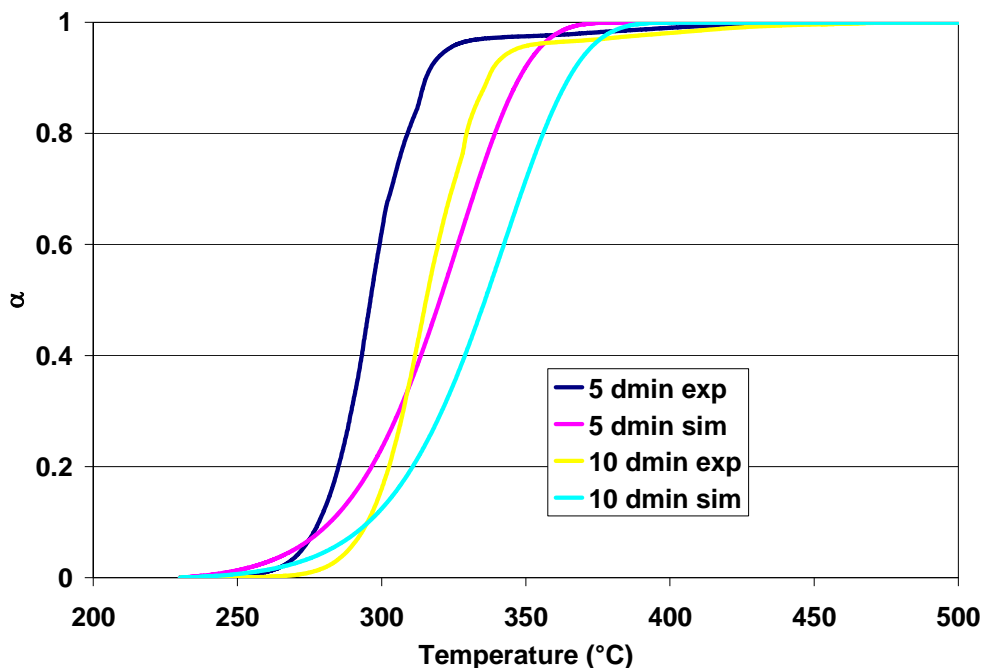


Figure 4.38: Simulated and experimental conversion curves for dynamic heating of 10:1 N6:K₂CO₃ using the kinetic parameters found by using the ASTM method

4.4.2.3 CaCO₃ N6 Dynamic TG: ASTM/Ozawa-Flynn-Wall (OFW)

The ASTM method was also applied to the TG data for carpet ratio mix of CaCO₃ with N6. The kinetic parameters obtained are in Table 4.14. Using these parameters, simulated data for heating at 5 and 10 degrees per minute were plotted and are shown in comparison to the experimental data in Figure 4.39. The simulated data seem to underestimate the conversion at a given temperature. Since the simulated curves are underestimates of the actual conversion, the times to get 90% conversion at various temperatures shown in Table 4.15 are the worst case limits.

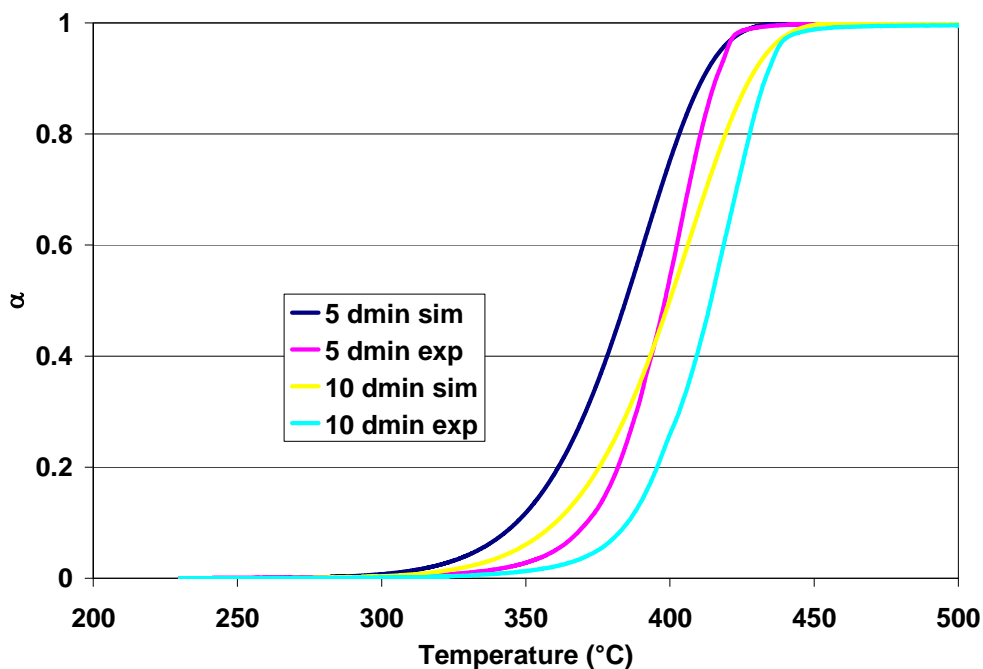


Figure 4.39: Simulated and experimental conversion curves for dynamic heating of carpet ratio (1.8:1) N6:CaCO₃ using the kinetic parameters found by using the ASTM method.

4.4.3 Nylon 66 Kinetics Summary

Table 4.18 shows a summary of the kinetic parameters for different catalysts in pure N66. As expected the pure N66 without any catalyst had the highest activation energy followed by the mixture containing CaCO₃. Using these parameters, simulated data for heating at 5 and 10 degrees per minute were plotted and are shown in comparison to the experimental data in Figure 4.40 to Figure 4.45. For all these plots the simulated data was not a perfect match for the experimental data; however, they were in close proximity. Therefore, these parameters can be used as a good estimate of how the reaction would proceed. Considering that the ASTM method uses only conversion values

less than 20%, it gives a fairly good prediction over the entire conversion range. To get a better understanding of how these catalysts work, a comparison of how long it would take to get 90% conversion at various temperatures was done and is shown in Table 4.19.

While some catalyst did perform better at lower temperatures than others, their advantage was significantly decreased at the higher temperature.

Table 4.18: Summary of E_a and A for different catalyst ratios to N66

Catalyst	Ratio N66:catalyst	E_a (kJ/mol)		A (min ⁻¹)	
		Average	Standard Deviation	Average	Standard Deviation
No catalyst	n/a	157	2	3.95E+10	1.82E+10
NaOH	100:1	117	6	7.11E+08	4.79E+08
KOH	10:1	116	10	5.04E+08	3.35E+08
KOH	100:1	139	1	6.65E+10	3.28E+10
K ₂ CO ₃	10:1	136	15	1.35E+11	8.99E+10
CaCO ₃	1.8:1	151	9	4.53E+11	6.43E+11

Table 4.19: Summary of time to get 90% conversion for some catalyst ratios with N66 using ASTM kinetic parameters

Temperature (°C)	Time to get 90 % conversion (min)					
	Pure N66	100:1 N66:KOH	10:1 N66:KOH	10:1 N66:K ₂ CO ₃	100:1 N6:NaOH	Carpet ratio CaCO ₃
300	13047	171	155	45	140	282
325	3279	50	56	14	50	75
350	921	16	22	5	20	22
400	96	2	4	1	4	3

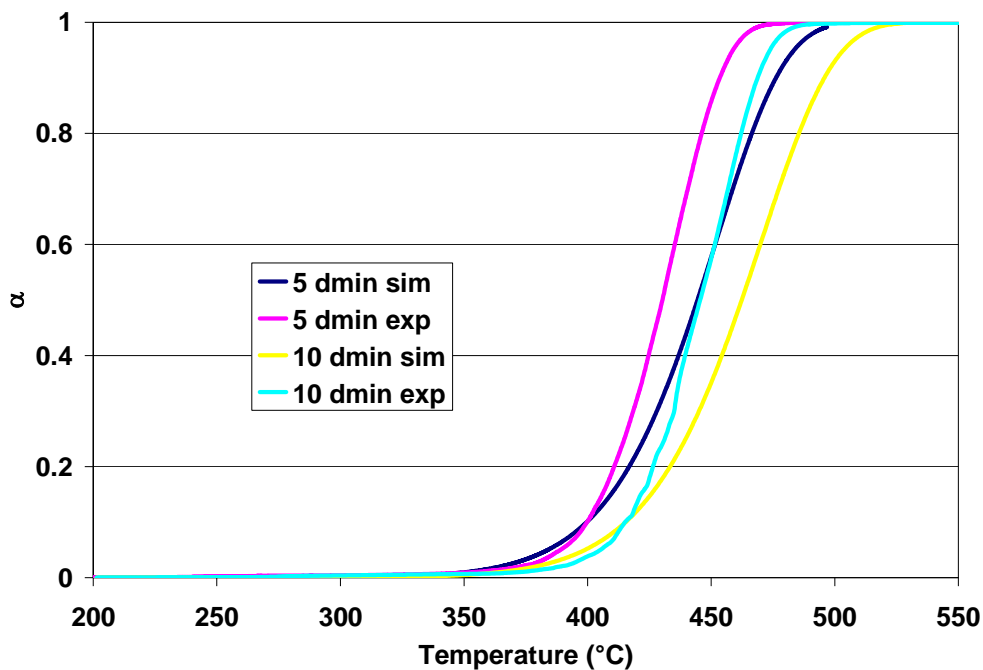


Figure 4.40: Simulated and experimental conversion curves for dynamic heating of Pure N66 using the kinetic parameters found by using the ASTM method

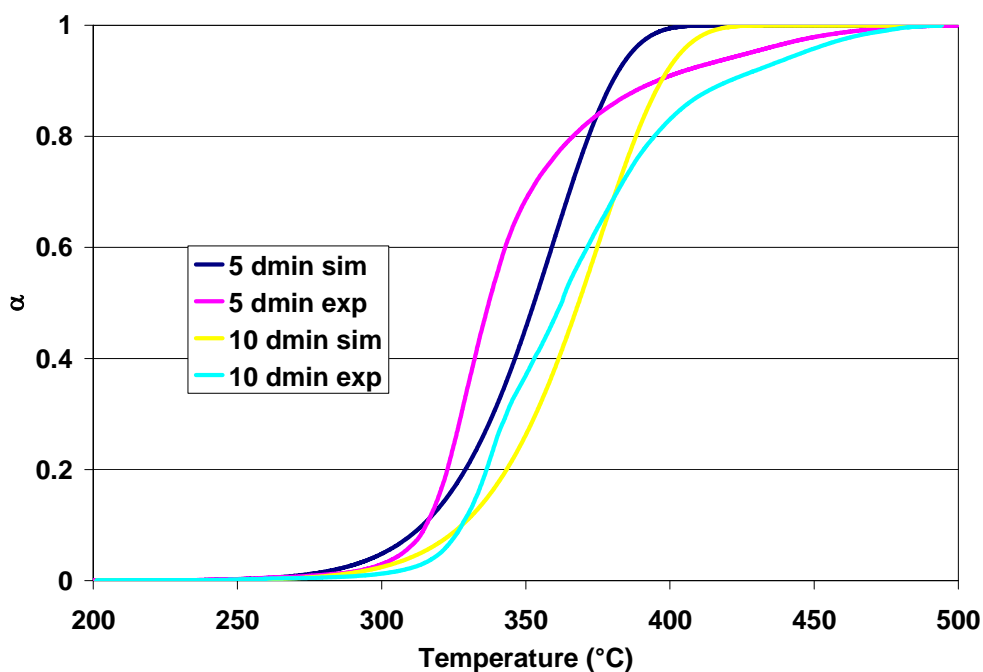


Figure 4.41: Simulated and experimental conversion curves for dynamic heating of 100:1 N66:KOH using the kinetic parameters found by using the ASTM method

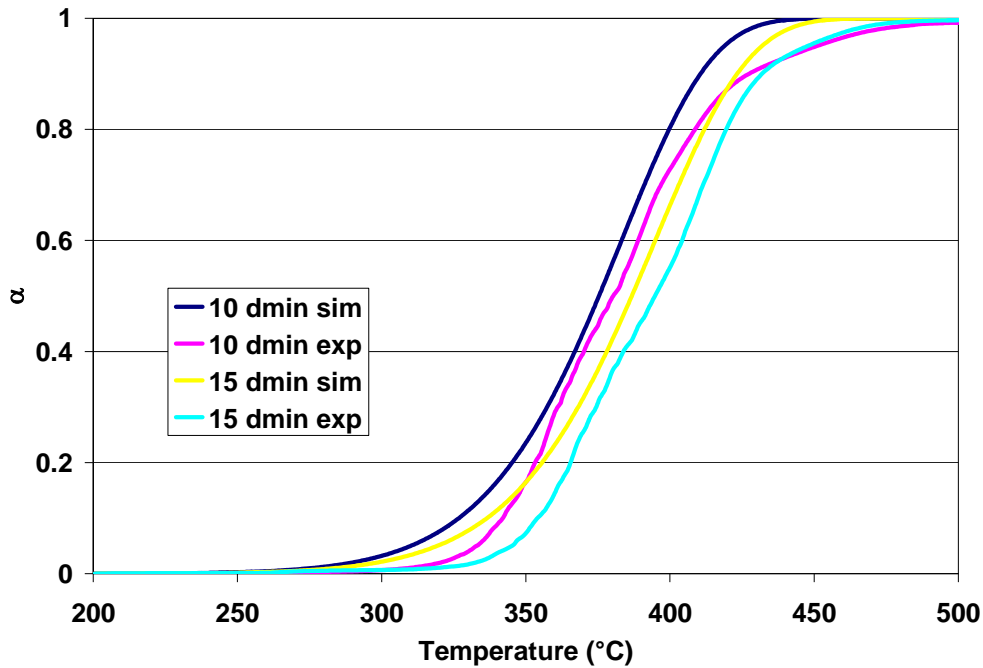


Figure 4.42: Simulated and experimental conversion curves for dynamic heating of 10:1 N66:KOH using the kinetic parameters found by using the ASTM method

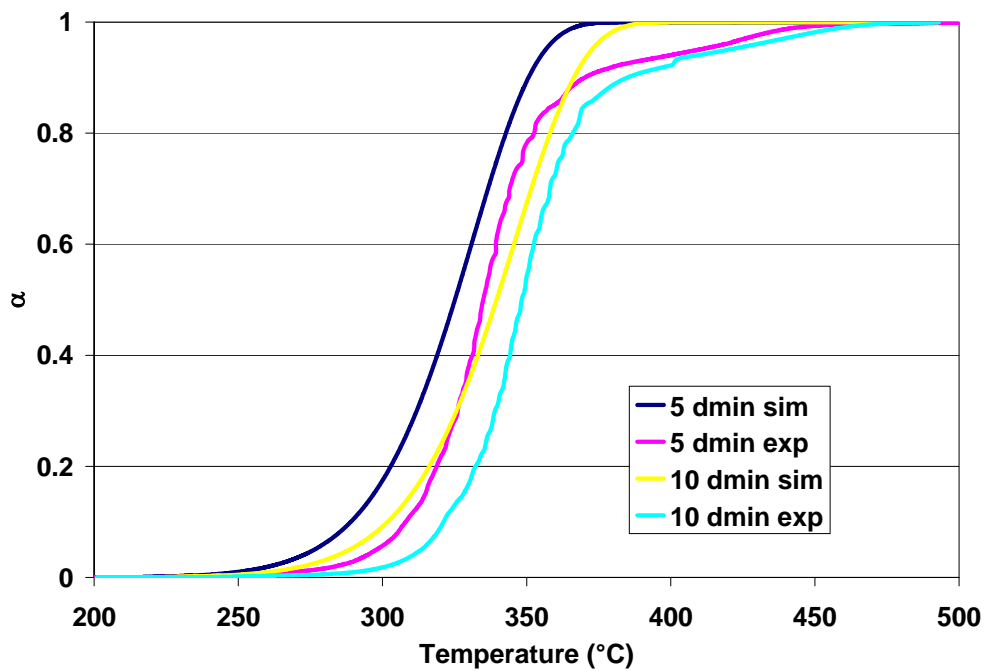


Figure 4.43: Simulated and experimental conversion curves for dynamic heating of 10:1 N6:K₂CO₃ using the kinetic parameters found by using the ASTM method

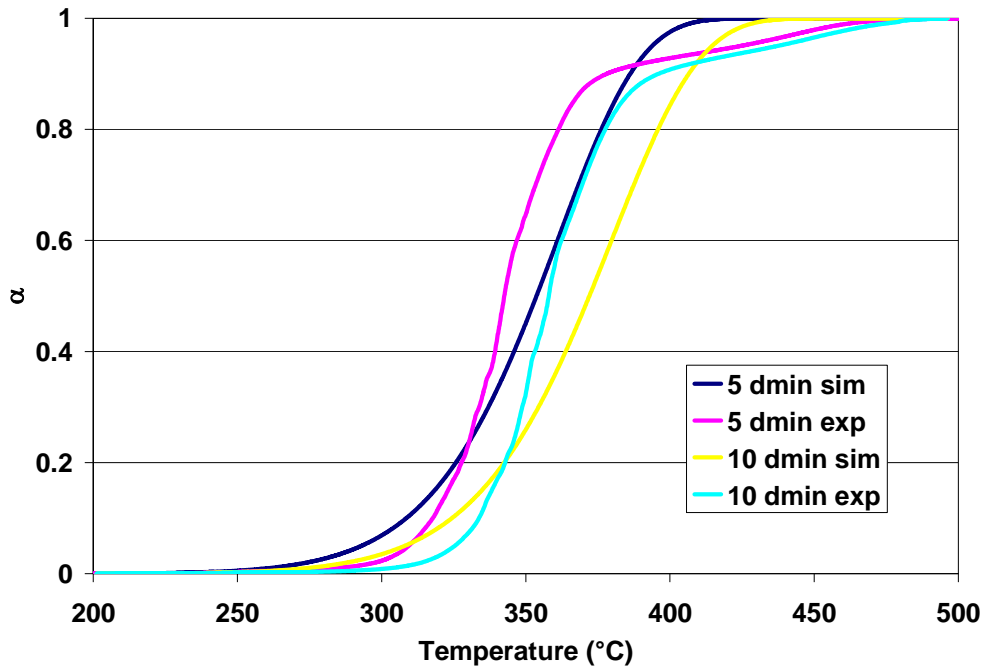


Figure 4.44: Simulated and experimental conversion curves for dynamic heating of 100:1 N66:NaOH using the kinetic parameters found by using the ASTM method

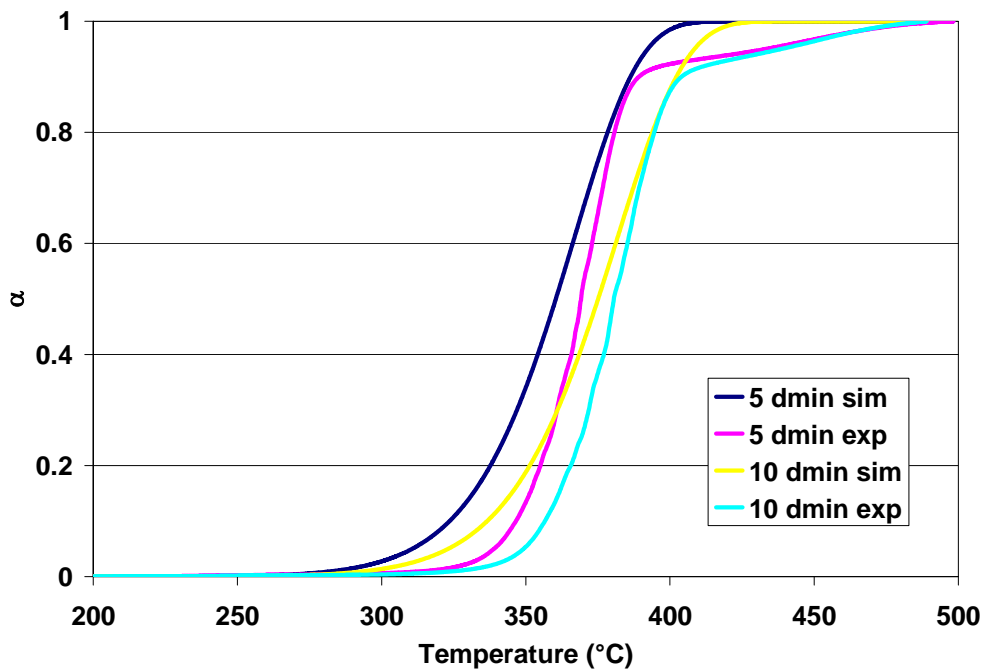


Figure 4.45: Simulated and experimental conversion curves for dynamic heating of carpet ratio (1.8:1) N66:CaCO₃ using the kinetic parameters found by using the ASTM method

4.4.4 Carpet N6

4.4.4.1 Carpet N6 Dynamic TG: ASTM/Ozawa-Flynn-Wall (OFW)

When the ASTM method was applied to the TG data for carpet ratio mix of CaCO_3 and pure N6, the kinetic parameters that were obtained can be found in Table 4.20. Using these parameters, simulated data for heating at 5 and 10 degrees per minute were plotted and are shown in comparison to the experimental data in Figure 4.46. Like the previous samples discussed, the prediction is not very accurate, but gives an idea of what the conversion should be with a given heating rate at a certain temperature.

Table 4.20: Kinetic parameters found by using the ASTM standard for carpet N6

E_a	142	kJ/mol
A	2.01E+10	min ⁻¹

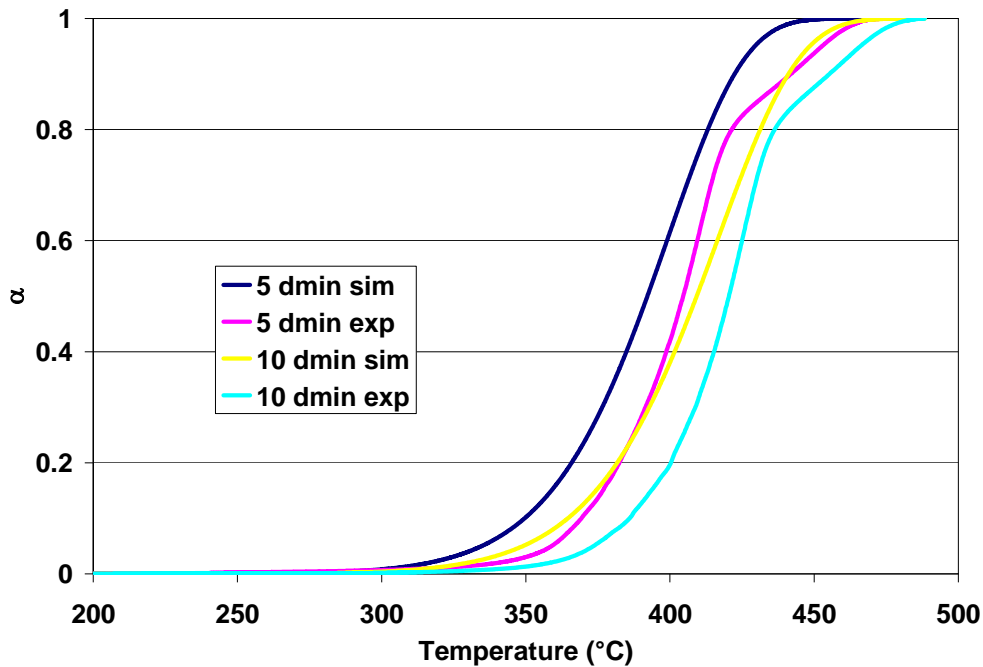


Figure 4.46: Simulated and experimental conversion curves for dynamic heating of carpet N6 using the kinetic parameters found by using the ASTM method.

Table 4.21 shows the time to get to 90% conversion of pure N6, N6 carpet, and carpet ratio of CaCO₃ and N6. Worth noting is that the pure N6 does take a longer time to degrade than its carpet counter part because the carpet contains CaCO₃. A comparison of the time to get 90% conversion at various temperatures shows that the kinetics parameters obtained for N6 carpet resulted in a longer reaction time than the pure N6 with an equivalent carpet ratio of CaCO₃. This is because some of the CaCO₃ is removed during pelletization of the carpet. To enhance the reactivity, care should be taken not to remove any of the CaCO₃ from the carpet during melting, compaction and pelletization of the carpet.

Table 4.21: Comparison of time to get 90% conversion for some catalyst combinations of N6 and carpet N6

Temperature (°C)	<i>Time to get 90 % conversion (min)</i>		
	Pure N6	N6 carpet	carpet ratio CaCO ₃
300	36212	994	1002
325	6105	286	251
350	1187	91	70
400	65	12	7

4.5 Differential Thermogravimetry (DTG)

As stated in Chapter 2, DTG can be useful in determining mechanism because it can be used to show the various stages of thermal decomposition by the peaks [37]. By using the minimum of peaks on the DTG curve, one may be able to

approximately determine where the different reaction starts or at what temperature range is that one dominant [53].

4.5.1 N6

Figure 4.47 through Figure 4.50 show the DTG curves obtained for samples containing pure N6 with different amounts of various catalysts when TG was performed at heating rates of 5 and 10 degrees per minute. With pure N6, on the low temperature side of the peaks there were a few irregularities to the curve which may indicate a different mechanisms. If one recalls from Chapter 2, there may be at least four different reactions competing in the thermal degradation of nylon 6. Among the many products from these reactions are water, ammonia and caprolactam; all of these compounds' boiling points are below that of the peak of this reaction. Therefore, they will be expelled as gaseous products. The expulsion of these from the TG crucible all affect the rate of weight loss. Since the rate at which these compounds are produced and expelled differ, this causes the departure from a smooth DTG curve if only one product was being expelled or if they all had the same reaction and evaporation rate. From the DTG curve, it is very difficult to say exactly which temperature range each mechanism may be occurring since there may be some overlap within the temperature range. Another possible explanation for the irregularity in the peak could come from gas building up in the sample that is foaming and at one instant a few bubbles burst and so significant gas was expelled from the sample and caused the significant change in the rate of weight lost. This is the most probable case since the general shape of the curve has only one distinct peak. This indicates that there is probably one main mechanism.

For 10:1 and 100:1 ratios of N6:KOH at both heating rates there were two distinct peaks in the DTG curve as can be seen in Figure 4.47 and Figure 4.49. These two peaks are clearly separated by a minimum which may indicate two distinct mechanisms with the KOH. In the TG curves, this apparent change in mechanism is seen above 90% conversion and is indicated by a very small slope in the TG curve shown earlier. This may be an indication of diffusion limitation; i.e. the remaining polymer can't get to the catalyst, or there is remnant cross-linked polymer that get burnt off during the final stages of the dynamic TG.

Figure 4.47 and Figure 4.49 also contain the DTG curves for the carpet ratio of nylon 6 to that of CaCO_3 . Like pure N6, for both heating rates, there are irregularities on both sides of the peak DTG value. However, by looking at the TG curve, these are not recognizable. So since there is no distinct minimum in these curves, the only conclusion is that there is one dominating mechanism.

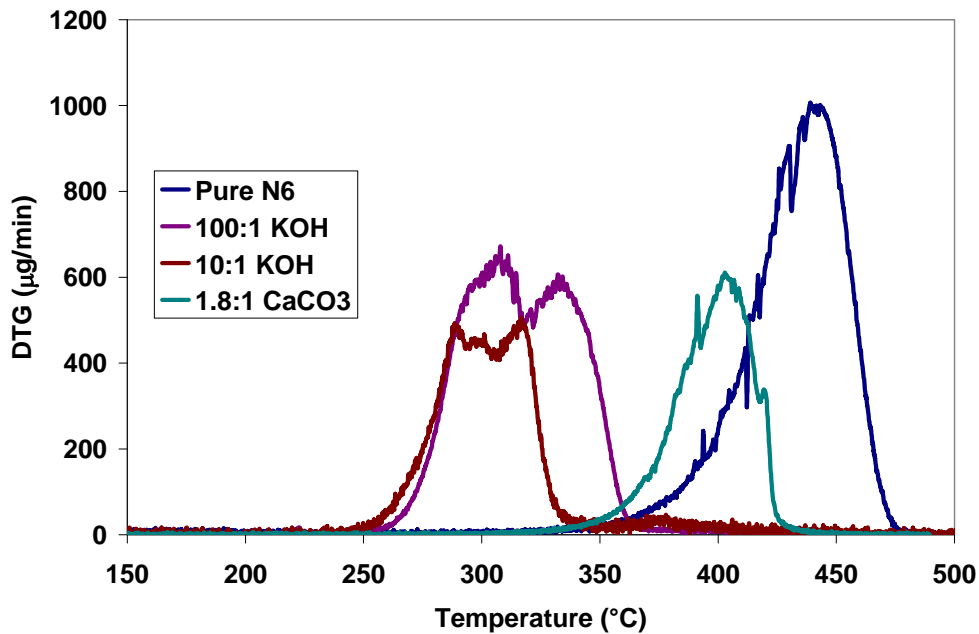


Figure 4.47: DTG of pure N6 with a heating rate of 5 degrees per minute with KOH and CaCO₃ in different ratios

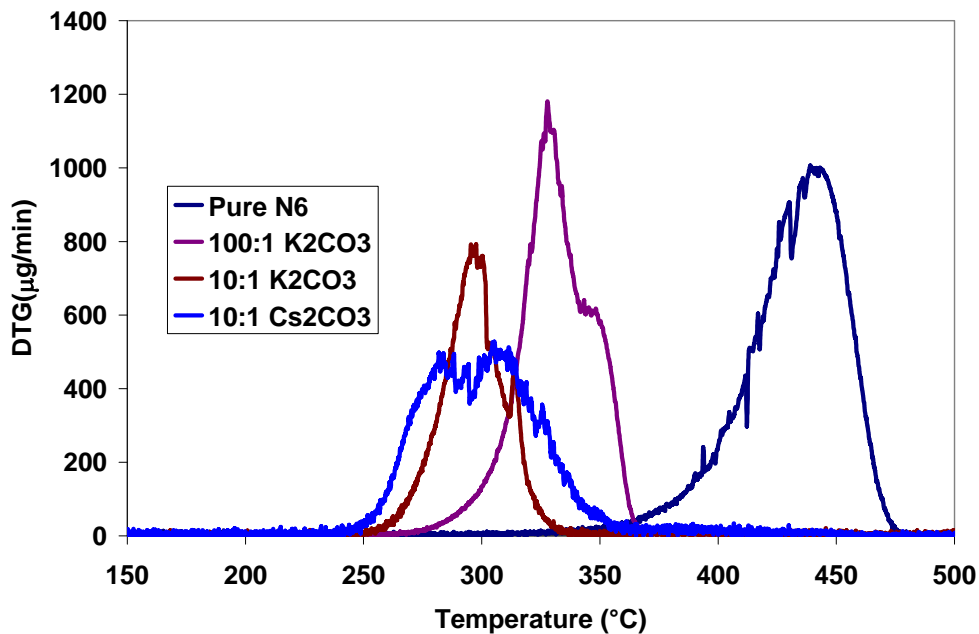


Figure 4.48: DTG of pure N6 with a heating rate of 5 degrees per minute with different ratios of K₂CO₃ and Cs₂CO₃

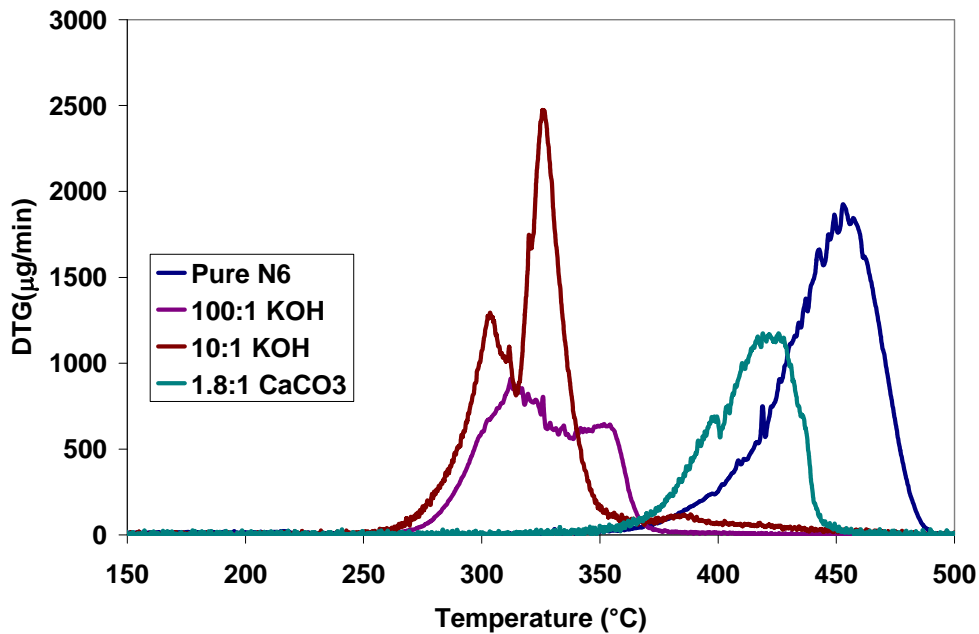


Figure 4.49: DTG of pure N6 with heating rate of 10 degrees per minute with different ratios of KOH and CaCO₃

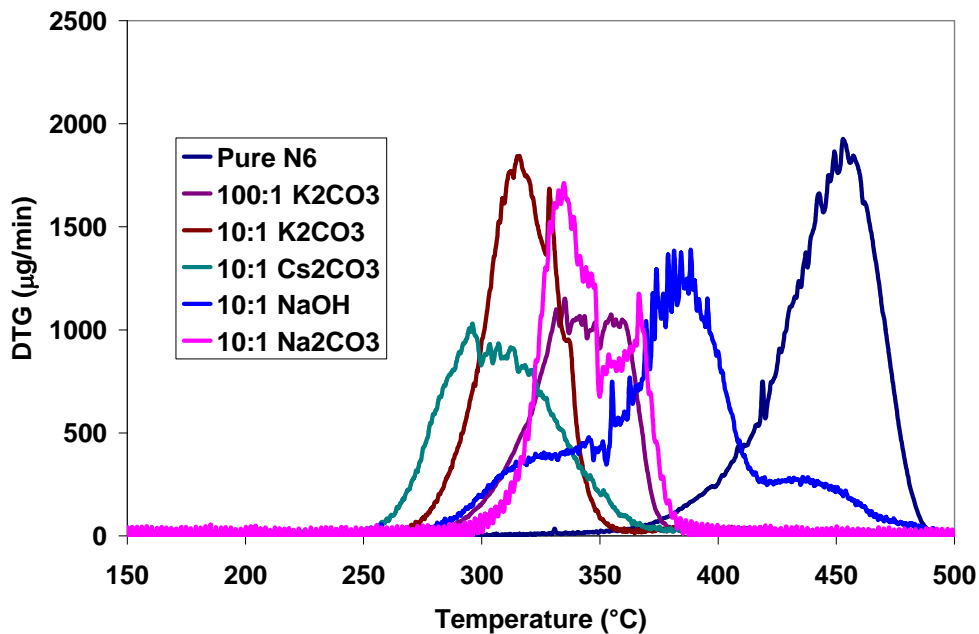


Figure 4.50: DTG of pure N6 with a heating rate of 10 degrees per minute with different ratio of K₂CO₃, Cs₂CO₃ NOH and Na₂CO₃

The results from the DTG curves of K_2CO_3 in pure N6 were mixed. For both 10:1 and 100:1 ratios of N6: K_2CO_3 heating at 5 degrees per minute, the shape of the curves were similar as presented in Figure 4.48. They both had an asymmetrical “bump” on the right side of DTG peak, which allowed the peak to broaden. On the other hand, when heated at 10 degrees per minute, as can be observed in Figure 4.50, the shapes of both curves are different and they do not have the same asymmetry. The 10:1 sample did have a second peak, but it was very narrow whereas the 100:1 sample didn't have a distinct peak, but several small peaks in a somewhat plateau shape. Since there isn't a clear-cut minimum in these four DTG curves for K_2CO_3 , it is difficult to say that there are multiple mechanisms at play. It is worth noting that in the TG curves for K_2CO_3 , there is a portion of the curve after 90% conversion in which the slope of the curve was very small, similar to the KOH samples.

The DTG curves of 10:1 N6: CS_2CO_3 for both 5 and 10 degrees per minute heating rate contain many small peaks making up the curve (Figure 4.48 and Figure 4.50, respectively). This may or may not indicate several complicated separate reactions. Figure 4.50 also contains the DTG curve for 10:1 N6:NaOH and 10:1 N6: Na_2CO_3 when heated at 10 degrees per minute. From these curves one can clearly see that the NaOH has at least 3 distinct mechanisms and the Na_2CO_3 has at least 2. Since there were a lot of peaks and valleys in these curves, the exact amount of different reactions occurring cannot be discerned from the DTG curves.

4.5.2 N6 carpet

Figure 4.51 contains the DTG curve for N6 carpet and N6 carpet containing 100:1 N6:KOH heating at 5 degrees per minute. In both samples there are at least two distinct mechanisms; one for the degradation of N6 and the other for the degradation of PP. Moreover, the carpet contains some CaCO_3 which, as shown in Figure 4.47. The CaCO_3 causes degradation of N6 at a lower temperature.

With 100:1 N6:KOH in the carpet, there is only one peak for the degradation of the N6. This is unlike the two peaks seen for the degradation of pure N6 with KOH above. One of the possible reasons for this is the contaminants that are present in the carpet that might have reacted with the catalyst and causes it to function differently in this reaction.

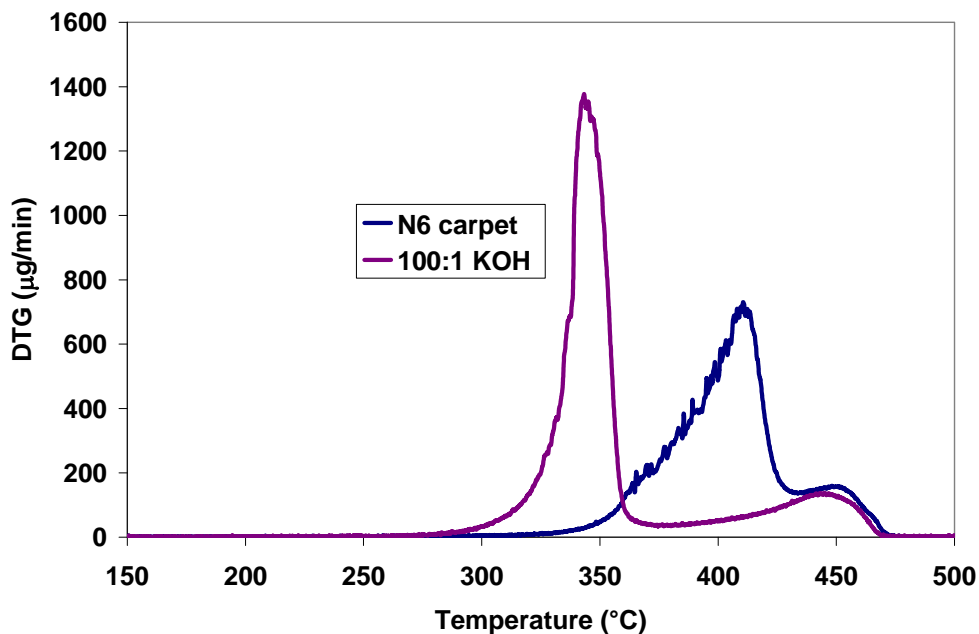


Figure 4.51: DTG of N6 carpet with a heating rate of 5 degrees per minute 100:1 N6:KOH

4.5.3 N66

Figure 4.52 through Figure 4.54 show the DTG curves obtained for samples containing pure N66 with different amounts of various catalysts. For pure N66 heating at 5 degrees per minute, the DTG curve in Figure 4.52 is very smooth relative to that of its 10 degrees per minute counterpart in Figure 4.55. With 10:1 N66:K₂CO₃, for both the heating rates shown, there are a lot of peaks and this ever occurs when there is not significant reaction occurring, i.e. at low temperatures and higher temperatures (see Figure 4.52 and Figure 4.54). If less data points were considered, the shape of the 10:1 N66:K₂CO₃ DTG may have been smoother and would follow the trend of the 100:1 N66:K₂CO₃ DTG. With 100:1 N66:K₂CO₃, there are fewer peaks, put there is an indication that multiple reactions may be occurring.

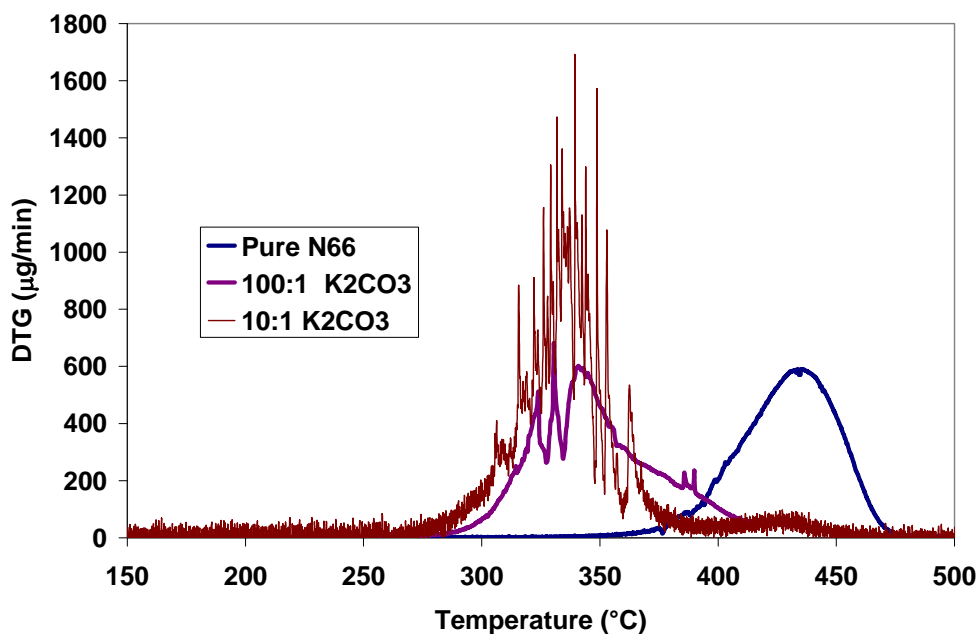


Figure 4.52: DTG of pure N66 with a heating rate of 5 degrees per minute with different ratios of K₂CO₃

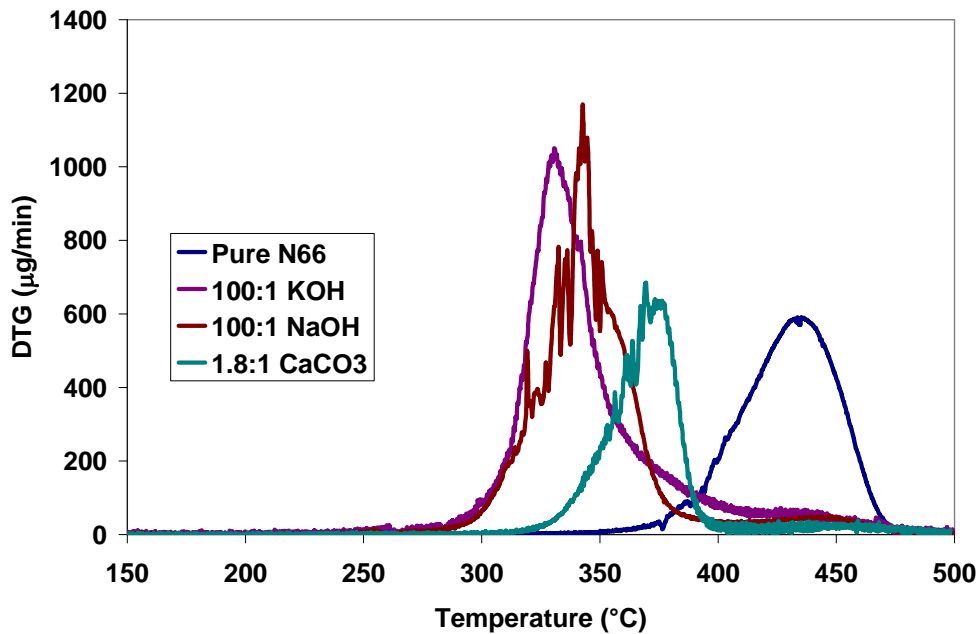


Figure 4.53: DTG of pure N66 with a heating rate of 5 degrees per minute with different ratios of KOH, NaOH and CaCO₃

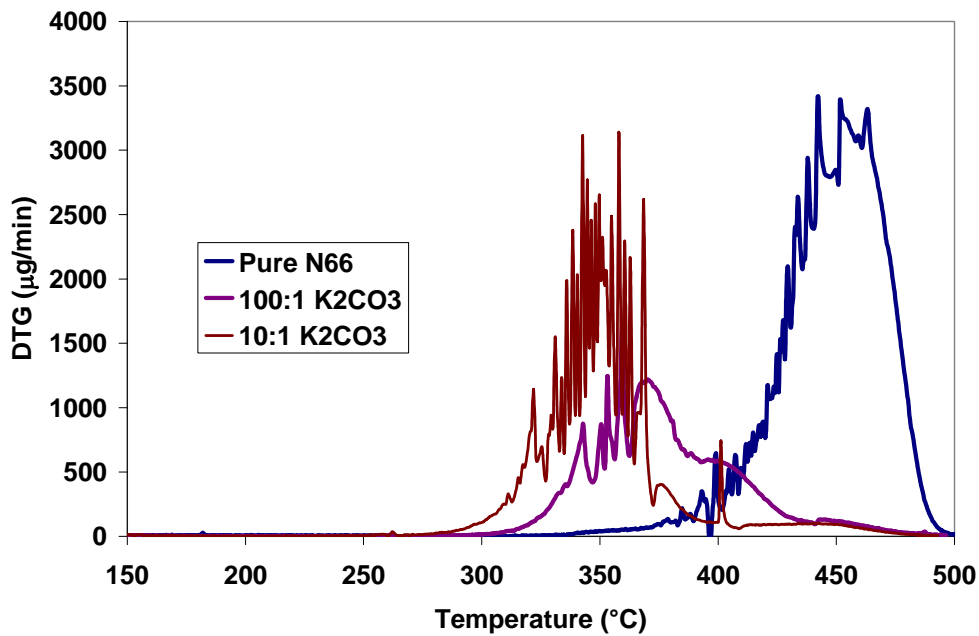


Figure 4.54: DTG of pure N66 with a heating rate of 10 degrees per minute with different ratios of K₂CO₃

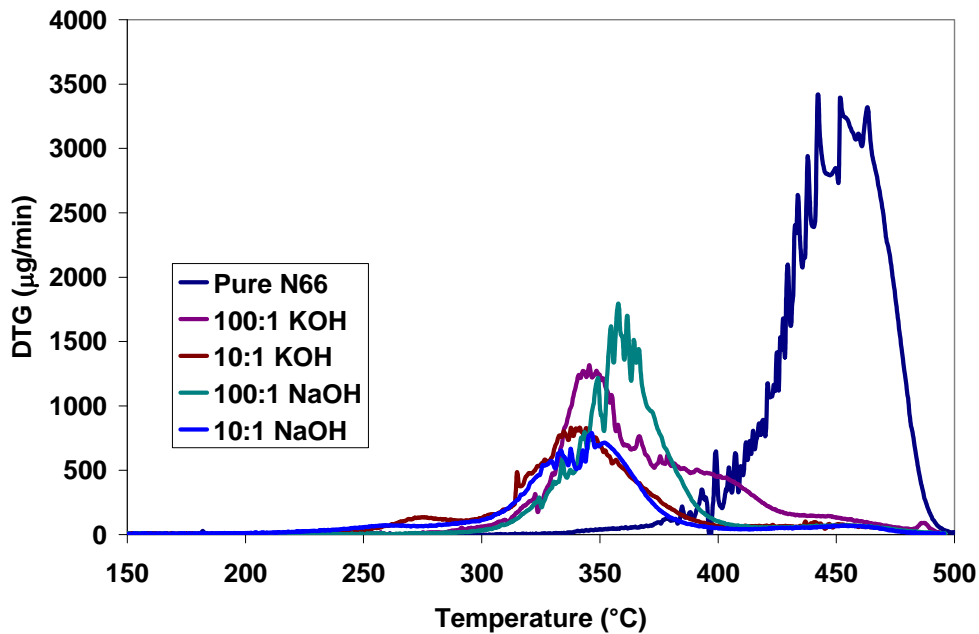


Figure 4.55: DTG of pure N66 with a heating rate of 10 degrees per minute with different ratios of KOH and NaOH

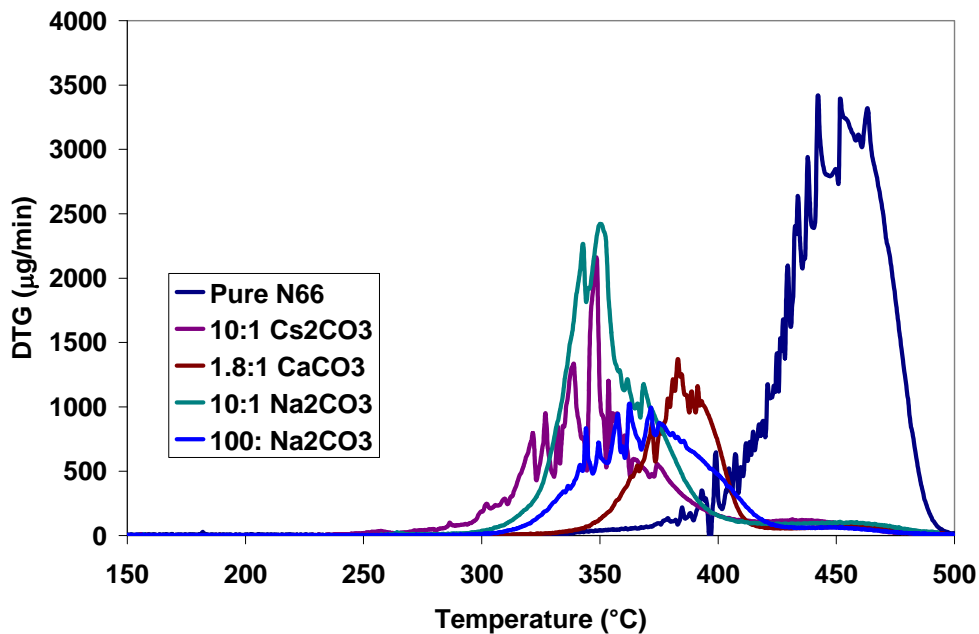


Figure 4.56: DTG of pure N66 with a heating rate of 10 degrees per minute with different ratios of Cs₂CO₃, CaCO₃, and Na₂CO₃

Similar to pure N66, the DTG curve of 100:1 N66:KOH is very smooth for 5 degrees per minute heating (Figure 4.53), but has jagged points in the 10 degrees per minute heating (Figure 4.55). As with the other catalysts with KOH in N66, there is indication that there maybe multiple competing reactions. For samples of NaOH, Na₂CO₃, CaCO₃, and Cs₂CO₃ their DTG curves are shown in Figure 4.53 and Figure 4.56. These DTG curves do not have a single dominant peak, so this may indicate multiple mechanisms or the bursting of foaming bubbles discussed earlier.

4.5.4 N66 carpet

Figure 4.57 contains the DTG curve for N66 carpet and N66 carpet containing 100:1 N66: KOH heating at 5 degrees per minute. As with their N6 equivalent, in both samples there are at least two distinct mechanisms; one for the degradation of N66 and the other for the degradation of PP. To the left of the N66 peak of both samples, the curves are somewhat jagged, but there is not a broad range in their jaggedness so there doesn't appear to be any real competing mechanism to the most dominant mechanism that is seen in the general shape of the curve.

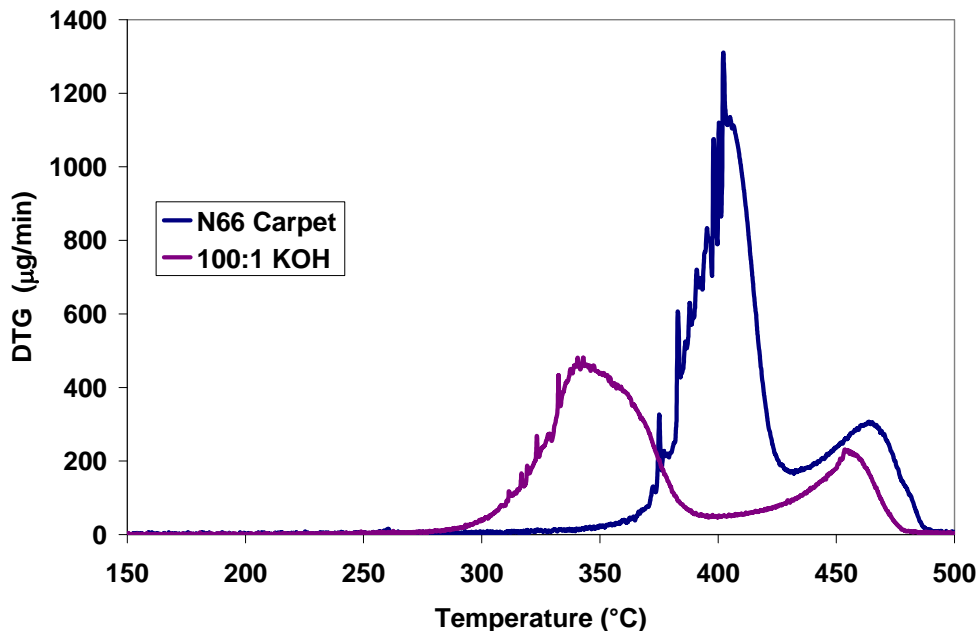


Figure 4.57: DTG of N66 carpet with a heating rate of 5 degrees per minute 100:1 N66:KOH

4.5.6 DTG summary

For all the samples considered, there were irregularities in their DTG curves. Some have indication of a single dominating reaction while others suggest that there may be competing reactions occurring. It is very difficult to distinctly say what exactly which temperature range each mechanism may be occurring; in fact there may be some overlap in temperature ranges. Another possible explanation for the irregularity in the peak could come from gas building up in the sample that is foaming and at one instant a bubble burst and so significant gas was expelled from the sample and caused the significant change in the rate of weight lost. The use of a TG in tandem with a Mass Spec and/or FTIR is needed to determine which mechanisms are occurring.

4.6 Differential Thermal Analysis (DTA)

4.6.1 N6

Figure 4.58 through Figure 4.61 show the DTA curves obtained for samples containing pure N6 with different amounts of various catalysts. DTA is measured concurrently with TG. The first endotherm in each curve occurs around 220°C indicating the melting of N6. The only exception to this is the sample containing 10:1 N6 to NaOH and KOH which seem to start melting at an earlier temperature when heated at 10 degrees per minute. As discussed earlier from the DSC results, this trend confirms that the nylon had partially degraded while mixing in these 10:1 cases.

The second endotherm is for the endothermic degradation or depolymerization of the N6 portion of each sample. As expected, these second endotherms occur at different temperatures and correspond to the effectiveness of the catalyst present in the sample as shown in the TG section of this report. The shape of each endotherm is more or less unique to each individual sample. The magnitudes of these endotherms are discussed later.

With pure N6, the irregularities in the DTA curves seem to correspond to those of the DTG curves indicating the possibility of multiple mechanisms or heat lost due to sudden evaporation when bubbles burst. Similarly, for both percentages of KOH in the two heating rates presented, there is a maximum in their respective endotherms indicating two distinct mechanisms with the KOH as indicated in the DTG section.

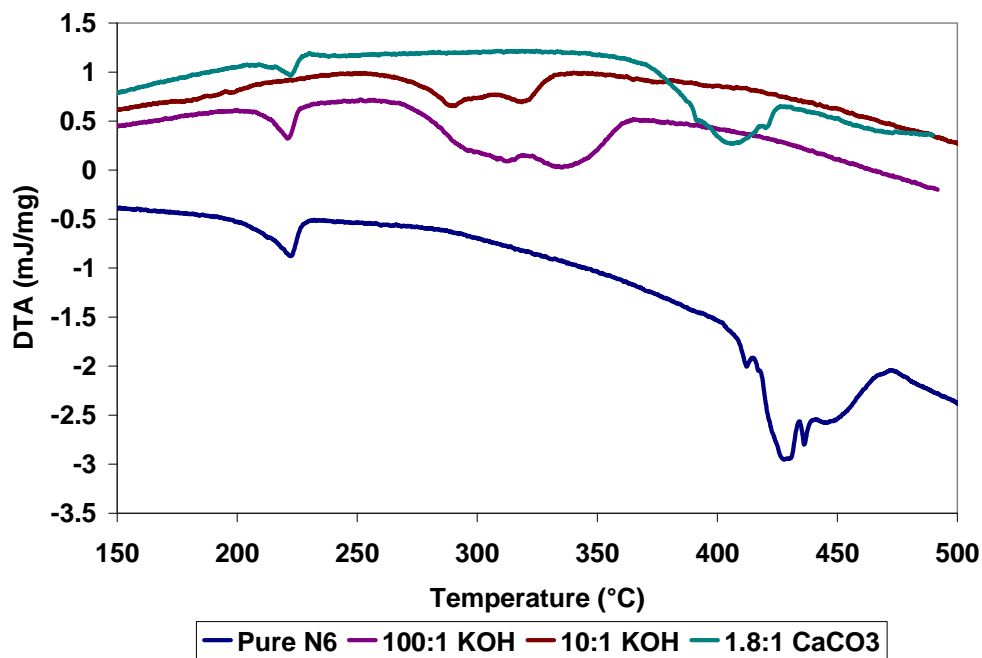


Figure 4.58: DTA of pure N6 with a heating rate of 5 degrees per minute with different ratios of KOH and CaCO₃

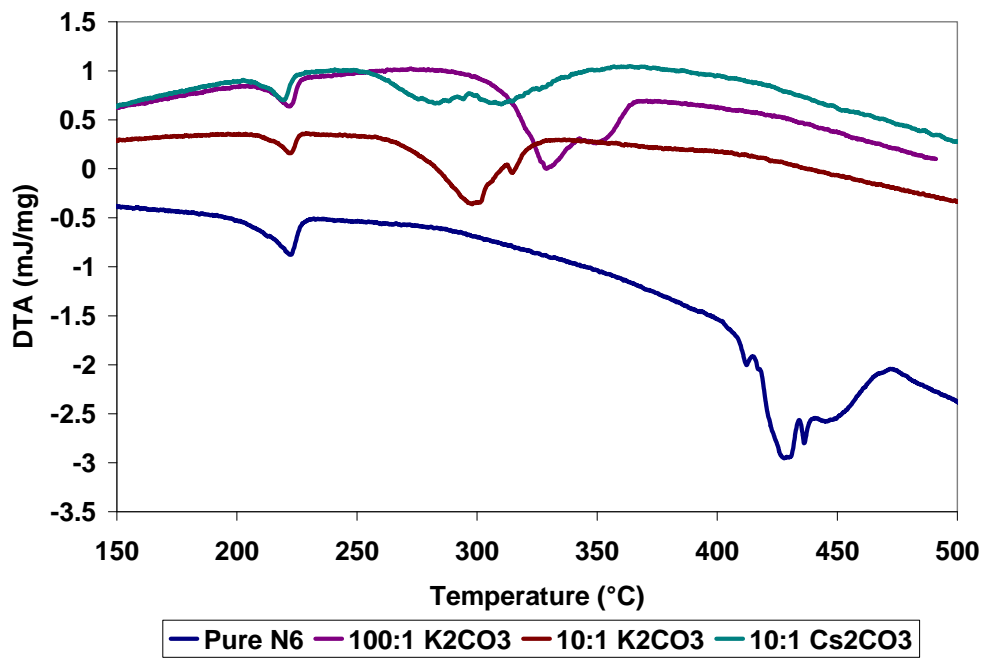


Figure 4.59: DTA of pure N6 with a heating rate of 5 degrees per minute with different ratios of K₂CO₃ and Cs₂CO₃

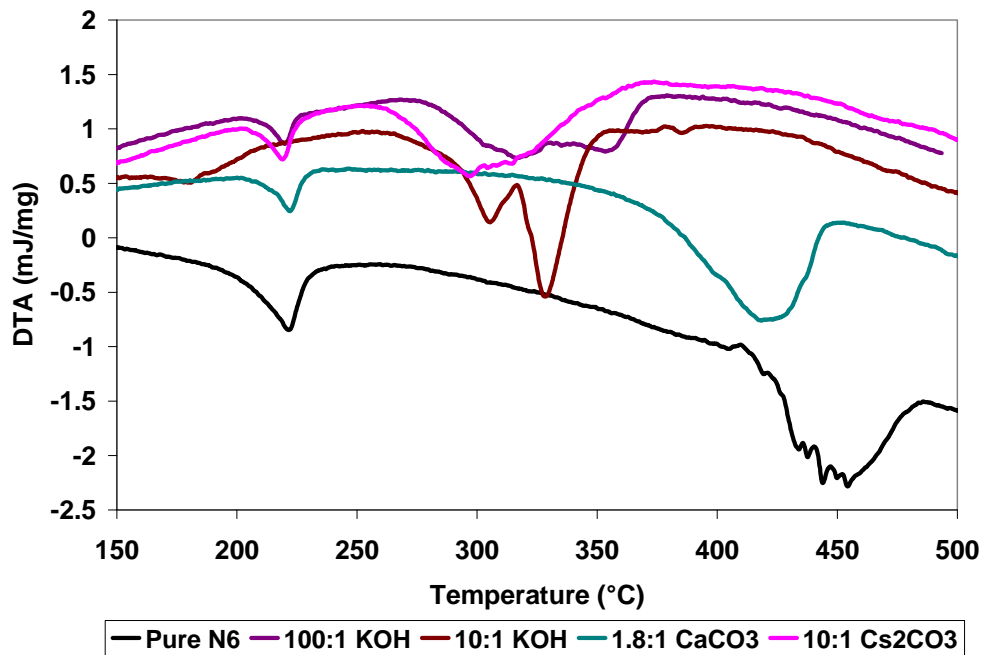


Figure 4.60: DTA of pure N6 with a heating rate of 10 degrees per minute with different ratios of KOH, CaCO₃ and Cs₂CO₃

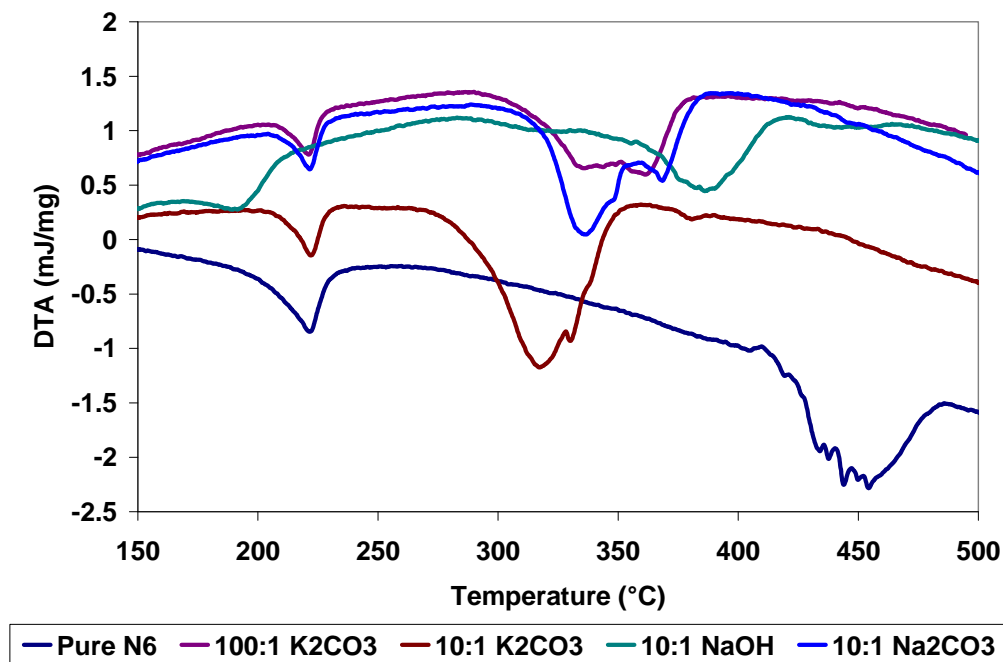


Figure 4.61: DTA of pure N6 with a heating rate of 10 degrees per minute with different ratios of K₂CO₃, NaOH and Na₂CO₃

The asymmetrical “bumps” on the right side of DTG peak curves of K_2CO_3 in pure N6 are more discernable in the DTA curve of Figure 4.59 and Figure 4.61. This may be indicative of multiple reactions occurring in the degradation process. As mentioned in the DTG section, when compared to the TG curves for K_2CO_3 , there is a portion of the curve after 90% conversion in which the slope of the curve was very small, similar to the KOH results.

The DTA curves for 10:1 N6: CS_2CO_3 show a maximum in its endotherms indicating at least two possible mechanisms. The DTA curve is less sensitive than the DTG curve so it doesn't show as much irregularities. The DTA curve of Na_2CO_3 points to at least two different mechanisms as pointed out earlier from the DTG curve.

4.6.2 N6 carpet

Figure 4.62 contains the DTA curve for N6 carpet and N6 carpet containing 100:1 N6:KOH heating at 5 degrees per minute. Unlike the DTG curve, the degradation of the N6 apart from the PP is not easily differentiated in this Figure. While both show the melting of PP around 150°C and N6 around 220°C, there is only a relatively tiny endotherm (compared to the N6) with the plain carpet; with the KOH, an endotherm began after the degradation of the N6, but never recovered before the temperature limit was reached.

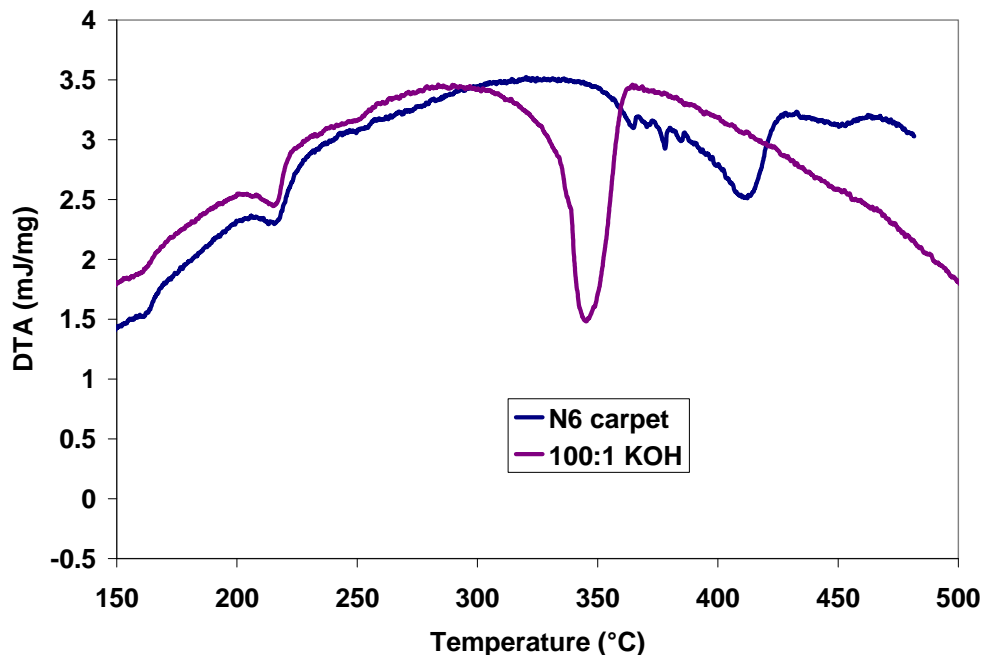


Figure 4.62: DTA of N6 carpet with a heating rate of 5 degrees per minute 100:1 N6:KOH

4.6.3 N66

Figure 4.63 through Figure 4.67 show the DTA curves obtained for samples containing pure N66 with different amounts of various catalysts when TG was performed at heating rates of 5 and 10 degrees per minute. On each curve, the first endotherm occurs around 260°C indicating the melting of N66. The second endotherm is for the endothermic degradation or depolymerization of the N66 portion of each sample. As with N6, these second endotherms in the N66 DTA occur at different temperatures. These endotherms correspond to the effectiveness of the catalyst present in the sample as shown in the TG section of this report. The shape of each endotherm is more or less unique to the individual samples. Due to some irregularities, the endotherms for Pure N66, CaCO₃, NaOH, KOH when heated at 5 degrees per minute (see Figure 4.63) indicate a multiple

mechanism for the degradation. Likewise, when heated at 10 degrees per minute, their DTA curves are complicated.

With K_2CO_3 , for both the heating rates shown, DTA curves were not as erratic as the DTG curves, but nonetheless, they indicate that multiple mechanisms may be at play in its reaction. Similar to K_2CO_3 , the DTA curves of Na_2CO_3 and Cs_2CO_3 may indicate multiple mechanisms taking place during these reactions.

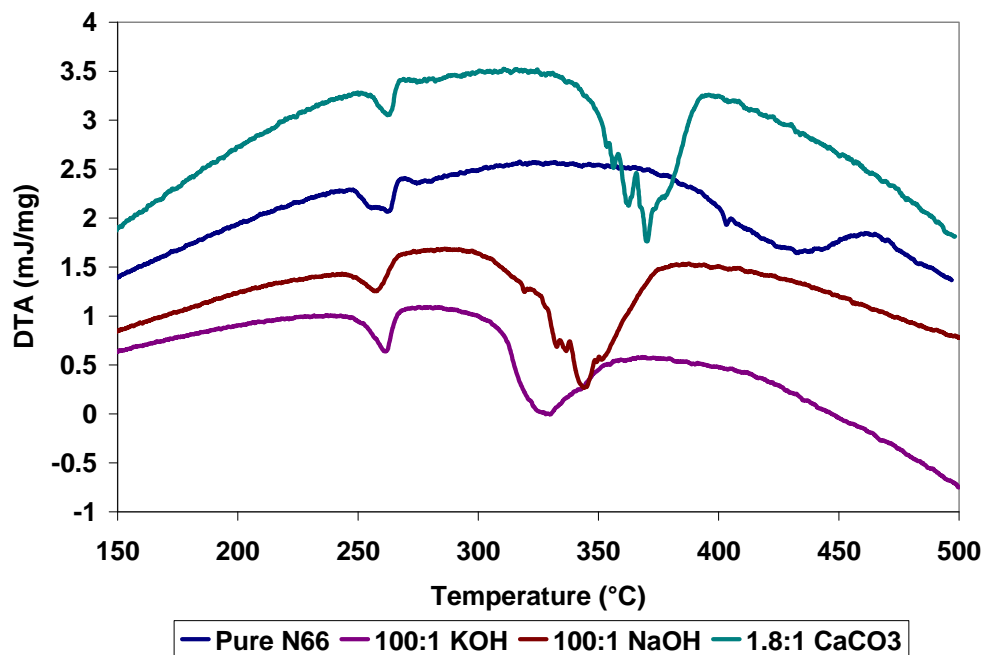


Figure 4.63: DTA of pure N66 with a heating rate of 5 degrees per minute with different ratios of KOH, NaOH, and $CaCO_3$

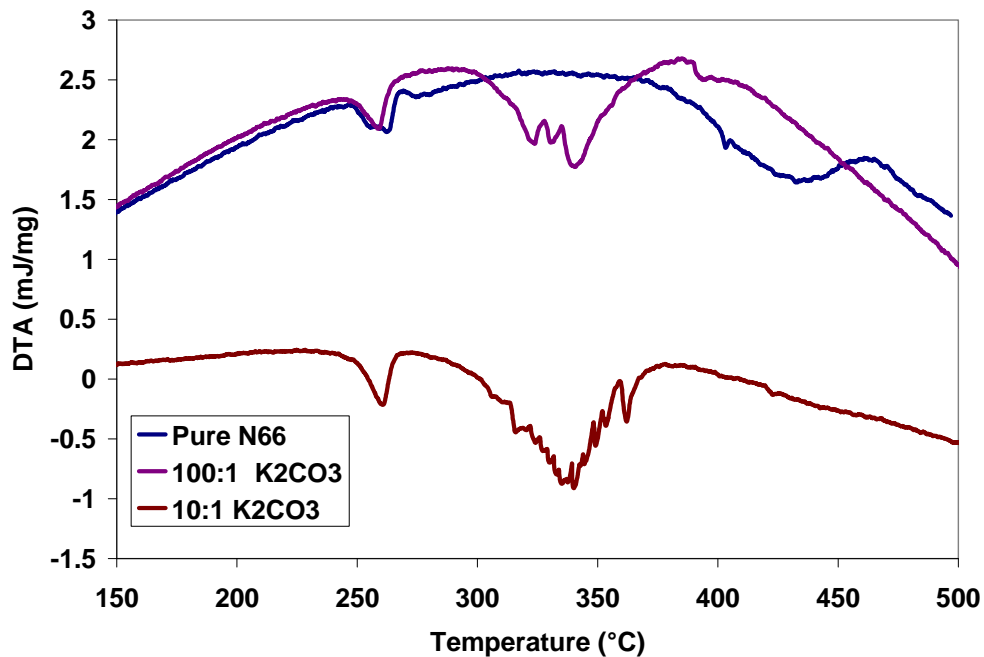


Figure 4.64: DTA of pure N66 with a heating rate of 5 degrees per minute with different ratios of K₂CO₃

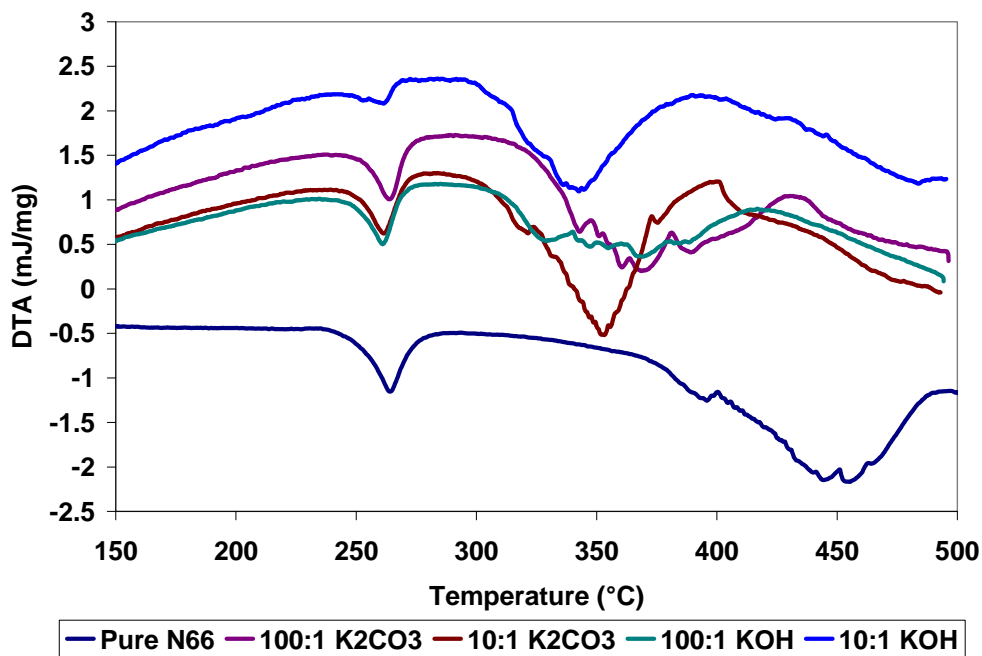


Figure 4.65: DTA of pure N66 with a heating rate of 10 degrees per minute with different ratios of K₂CO₃ and KOH

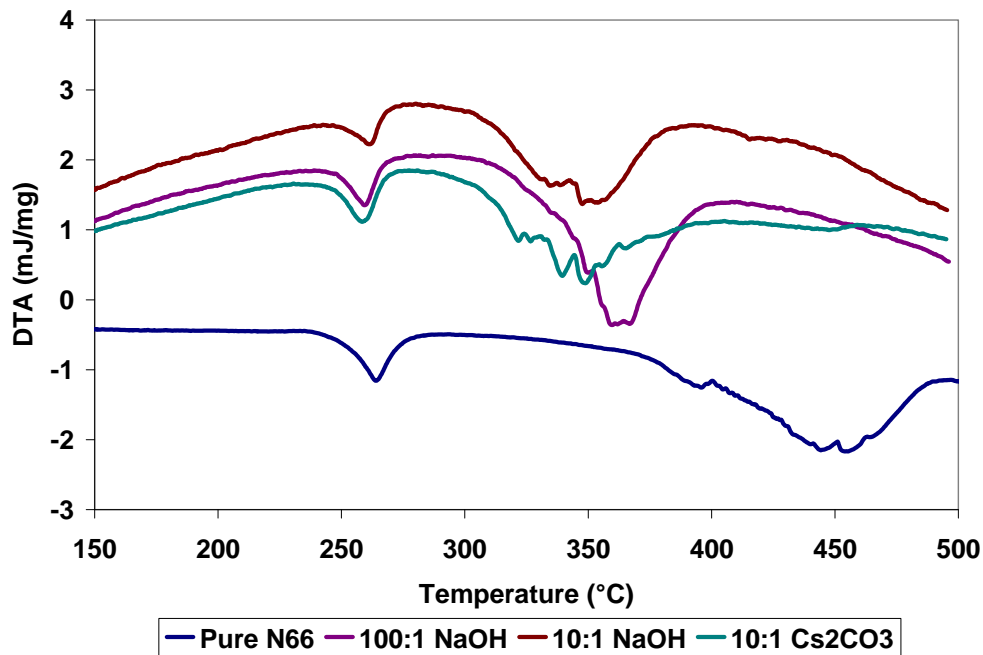


Figure 4.66: DTA of pure N66 with a heating rate of 10 degrees per minute with different ratios of NaOH and Cs₂CO₃

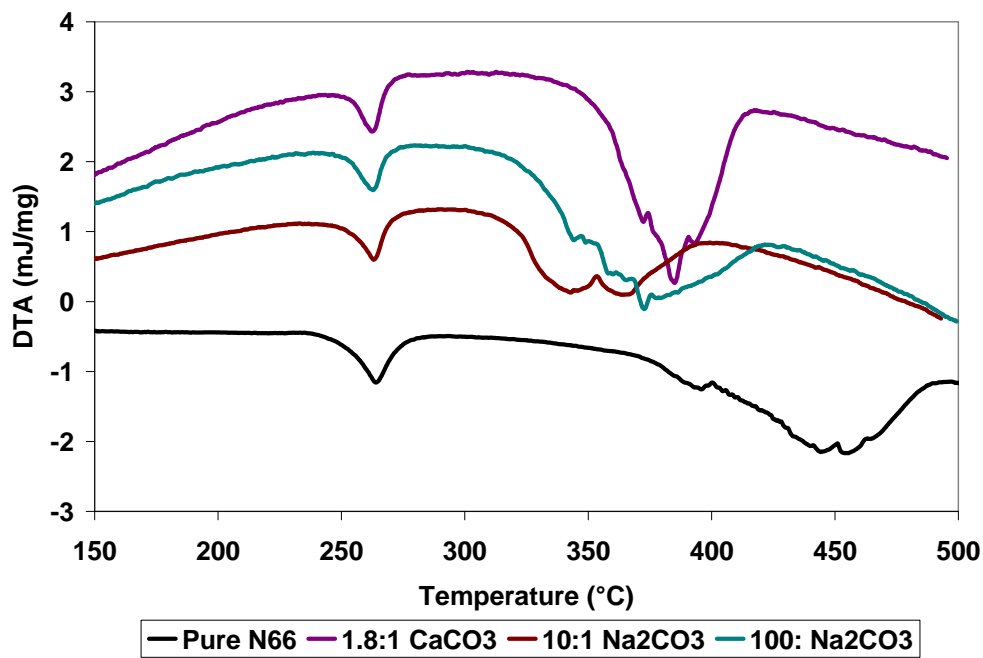


Figure 4.67: DTA of pure N66 with a heating rate of 10 degrees per minute with different ratios of CaCO₃ and Na₂CO₃

4.6.4 N66 carpet

Figure 4.68 contains the DTA curve for N66 carpet and N66 carpet containing 100:1 N66:KOH heating at 5 degrees per minute. Similar to the N6 carpet DTA curve, the DTA curve of N66 carpet has the melting of PP around 150°C and N66 around 260°C. As expected, the endotherm for the KOH sample occurred at a lower temperature than that of the N6 in the carpet. Like the N6 carpet, the endotherm for the PP is not easily discerned here.

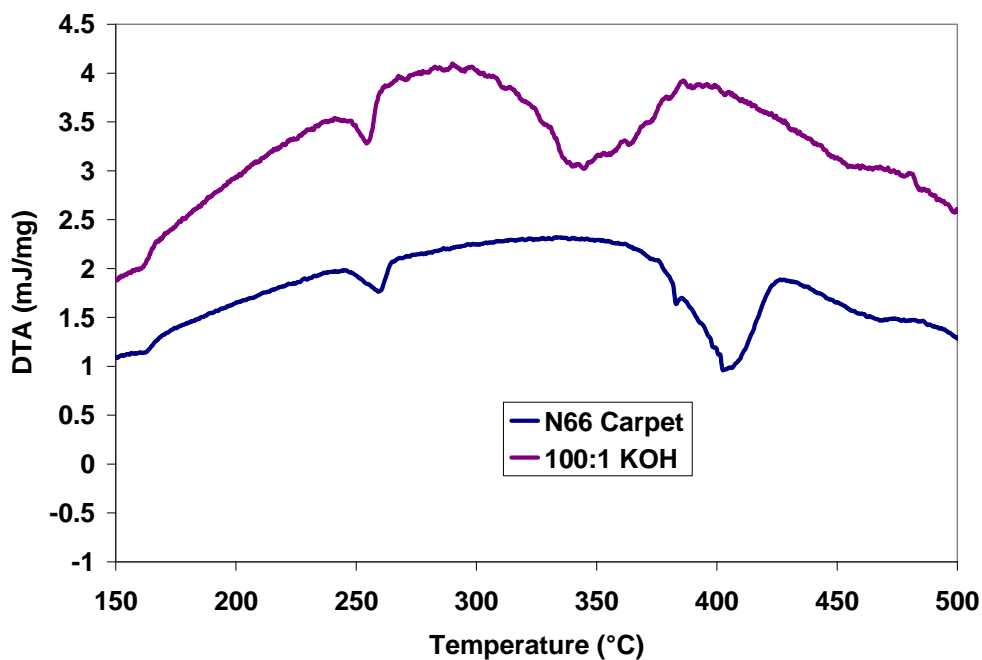


Figure 4.68: DTA of N66 carpet with a heating rate of 5 degrees per minute and 100:1 N66:KOH

4.6.5 DTA summary

The first endotherm in each curve indicates the melting of the respective nylon. The second endotherm is for the endothermic degradation or depolymerization of the respective nylon portion of each sample. As expected, these second endotherms occur at different temperatures and correspond to the effectiveness of the catalyst present in the sample as shown in the TG section of this report. The shape of each endotherm is more or less unique to each individual sample.

4.7 Heat of Reaction

The heat of a reaction is the amount of energy absorbed during a reaction. In the degradation or depolymerization of N6 and N66, heat is normally absorbed making the process endothermic as indicated in Figure 4.58 to Figure 4.68. The heat of reaction can be calculated from the area of the endotherm for the entire reaction temperature range as discussed in of Chapter 2. It should be noted that the DTA endotherm for each reaction occurred at different temperature ranges for each sample and all the peaks in the range were used in the calculations. Additionally, the range of the integration is prone to human error, since the person has to guess at what temperature to start and stop integrating. These results are normalized to the mass of the nylon in the sample; hence there is a inherent error since the energy used to heat the catalyst during this temperature range is not removed from the data. Nevertheless, this is to be used as an estimate to to the heat of reaction.

4.7.1 N6

According to the Polymer Handbook, the exothermic heat of polymerization for nylon 6 at 250 °C is -16.5 kJ/mol [65]. After multiplying this value by 113, the molecular weight of caprolactam, the specific heat of polymerization is -146 J/g. Therefore, the theoretical heat of depolymerization of nylon 6 at 250 °C is 146 J/g since depolymerization is endothermic and therefore is the additive inverse of the heat of polymerization.

Table 4.22 contains the average heat of reaction for samples of pure N6 with different concentrations of various catalysts. These values are higher than the theoretical heat of depolymerization listed above because the values contain the heat of reaction lumped together with the heat of vaporization. Another reason they are higher is that the reactions take place above the boiling point of caprolactam (267 °C); normally, the heat of vaporization decreases with increasing temperature from those in literature at the boiling point. Hence, this varying heat of vaporization for different catalyst mixtures reacting at several temperatures causes the values in Table 4.22 to be higher and different for each mixture listed. With pure N6, the heat of reaction is around 212 J/g. The low standard deviation shows consistency with the statement present in reference [56] that if the peak area is calculated from a graph of ΔT versus time, then the area is independent of the heating rate.

Table 4.22: Calculated heat of reaction in J/g for pure N6 with various concentration of several catalysts at different heating rates

Catalyst	Ratio N6:catalyst	Average	Standard Deviation
none	n/a	212	2
KOH	100:1	337	21
KOH	10:1	238	15
K ₂ CO ₃	100:1	325	13
K ₂ CO ₃	10:1	337	10
Cs ₂ CO ₃	10:1	276	20
NaOH	100:1	224	6
NaOH	10:1	221	6
Na ₂ CO ₃	10:1	324	3

Part II:

Reactive Extrusion

CHAPTER 5

EXTRUSION THEORY

The reasons why a specific type of extruder was chosen as a viable reactor for the depolymerization of nylon is explained in this chapter. Then, the different elements and processes within the extruder are examined to determine the effect on the outcome of the reaction.

5.1 Extruders

The extruder can be considered as a slightly back-mixed plug flow reactor [66]. There are several economic advantages for using an extruder as a reactor, including: reductions in real estate charges and the elimination of solvent purchases and recovery costs [66]. Some of the technical advantages of using an extruder includes [66]:

- easy feed melting
- superb dispersive and distributive mixing
- good temperature control
- control of the residence time distribution
- can attain high pressures
- provision to process continuously
- accessibility to and from different stages
- relatively easy removal of volatiles.

5.1.1 Types of extruders

There are several different classifications of extruders. The two most common types are single-screw and twin-screw. In a twin screw extruder, the arrangement of the two screws and the direction of their rotation provide another subset classification of twin-screw extruders as shown in Figure 5.1 and Figure 5.2. The performance and operation of single- and non-intermeshing twin-screws extruders are similar, so some of the basic principles developed for single screws will be applicable for twin-screws [67]. Since non-intermeshing screws have greater sensitivity to pressure flow, there is an increase axial flow for distributive mixing [66]. With non-intermeshing screws, the screw profile is somewhat free from geometrical constraints [67]. Because of this, the melting, mixing and pumping mechanisms are predominantly dependent on the viscous drag of the polymer [67].

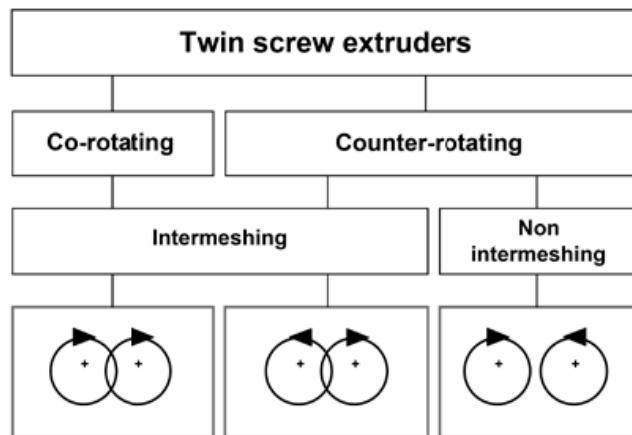


Figure 5.1: Classification of twin screw extruders [3]



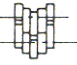

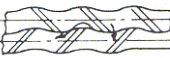




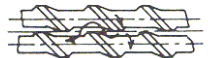
SCREW ENGAGEMENT		SYSTEM	COUNTER-ROTATING	CO-ROTATING	
INTERMESHING	FULLY INTERMESHING	LENGTHWISE AND CROSSWISE CLOSED	1 	2 THEORETICALLY NOT POSSIBLE	
		LENGTHWISE OPEN AND CROSSWISE CLOSED	3 THEORETICALLY NOT POSSIBLE	4 	
		LENGTHWISE AND CROSSWISE OPEN	5 THEORETICALLY POSSIBLE BUT PRACTICALLY NOT REALIZED	6 	
	PARTIALLY INTERMESHING	LENGTHWISE OPEN AND CROSSWISE CLOSED	7 	8 THEORETICALLY NOT POSSIBLE	
		LENGTHWISE AND CROSSWISE OPEN	9A 	10A 	
			9B 	10B 	
	NOT INTERMESHING	NOT INTERMESHING	LENGTHWISE AND CROSSWISE OPEN	11 	12 

Figure 5.2: Arrangements of different twin screws [68]

Another categorization of non-intermeshing extruders is whether the screws are separated or tangential as shown in Figure 5.3. With a tangential extruder there is no limit to the barrel length and there are units in operation that have a length to diameter ratio, L/D , of 100 [66, 69]. (The overall length of the extruder is determined by: melting of feed; incorporation of reactants; the reaction; devolatilization (DV); and pressure development [66].) The type of extruder that is used in this undertaking is a tangential, counter-rotating nonintermeshing twin-screw extruder (CRNI). In CRNI, the transport of the molten polymer is by drag flow similar to that of single screw extruder except that the open area of the apex adds an additional pressure flow [70].

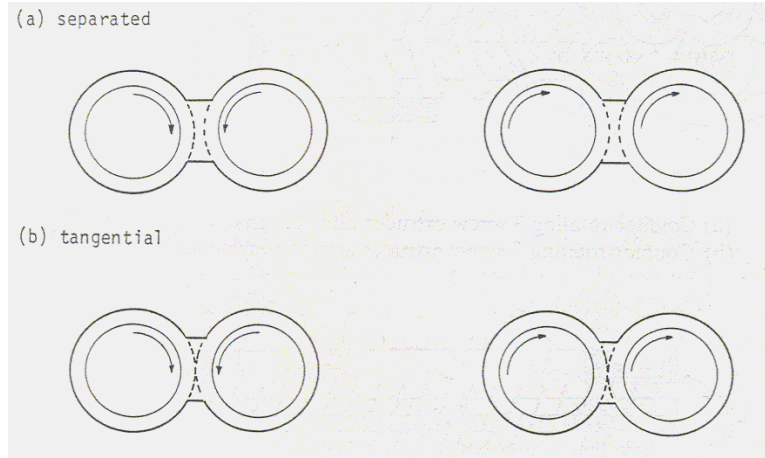


Figure 5.3: Contact types in twin screw extruders; left column - counter rotating; right column - co-rotating [69]

A characteristic design of CRNI is to have screws with different lengths as shown in Figure 5.4 [70]. The advantage of configuring one of the screws longer than the other is that there is an improvement in the pumping characteristics [66, 70]. This configuration leaves thrust load on one screw only, thus the thrust on the short screw will be a small value which greatly facilitates the thrust bearing design [67, 71]. In other words, the major thrust is only on one screw in the gearbox [66].

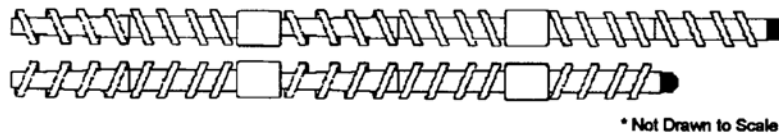


Figure 5.4: CRNI showing different screw lengths [72]

5.1.2 Screw elements characteristics

The screws are one of the most important parts of extruders. Knowing screw design is critical in understanding the performance of an extruder. Figure 5.5 shows the important geometric factors of an extruder screw. Sometimes, the screw root is curved and the flights are not necessarily perpendicular to the screw root even though they are to the axis of the screw [69].

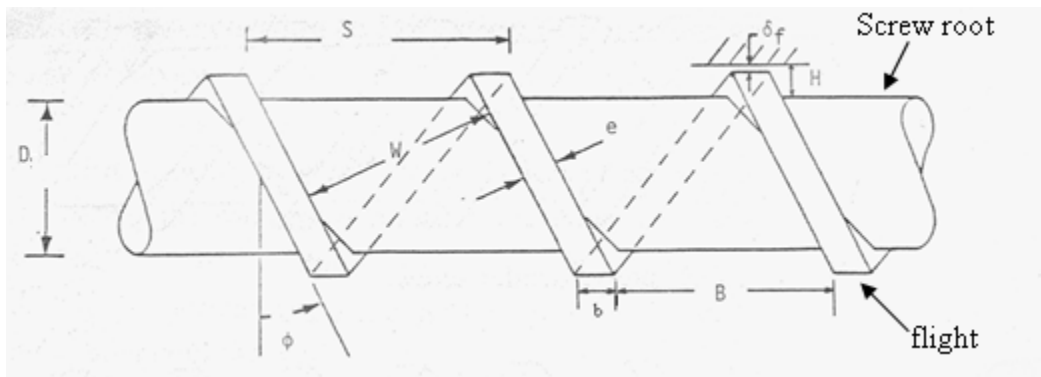


Figure 5.5: Illustration of a screw with its important geometry shown [69]

Where, D is the diameter of the screw; S is the pitch; δ_f is the radial clearance between the screw flight and the barrel; H is the channel depth which is the distance between the root of the screw and the internal barrel surface; W is the channel width; ϕ is the screw helix angle; e is the perpendicular width of the flights; b is width of the screw flights in the axial direction; B is the axial distance between the flights [69].

For an extruder, the geometric factors either [66, 69, 73]:

- Stay constant (e.g. S , B , e , δ_f , D_b , where D_b is the barrel diameter). However, δ_f and D_b may change due to wear over time.
- Vary in the axial direction (e.g. H in tapered sections; sometimes S and B); H can vary with position between flights

- Vary in the radial direction (e.g. W, ϕ, B, b); W may increase with increasing flight altitude; ϕ may vary with radius.

Some of the relationships between screw geometry are:

barrel helix angle, θ_b , is defined as:

$$\theta_b = \tan^{-1} \frac{S}{\pi D_b} \quad 5.1$$

$$W_b = B \cos \theta_b \quad 5.2$$

$$W = S * \cos(\phi) - e \quad 5.3$$

$$\tan \phi = \frac{S}{\pi D_s} \quad 5.4$$

$$z_b = L / \sin \phi \quad 5.5$$

z_b is the helicoidal length at the barrel surface.

If the channel depth is too large, the lead length of H/Z would be undesirable because there is the possibility of stagnant flow in the root of the channel [66]. It should be pointed out that the screws should be replaced when the clearances reaches 15% of channel depth due to wear [73].

A lot of extruders are multi-flighted (see Figure 5.6) so fluid can simultaneously travel along two or more parallel flights [69].

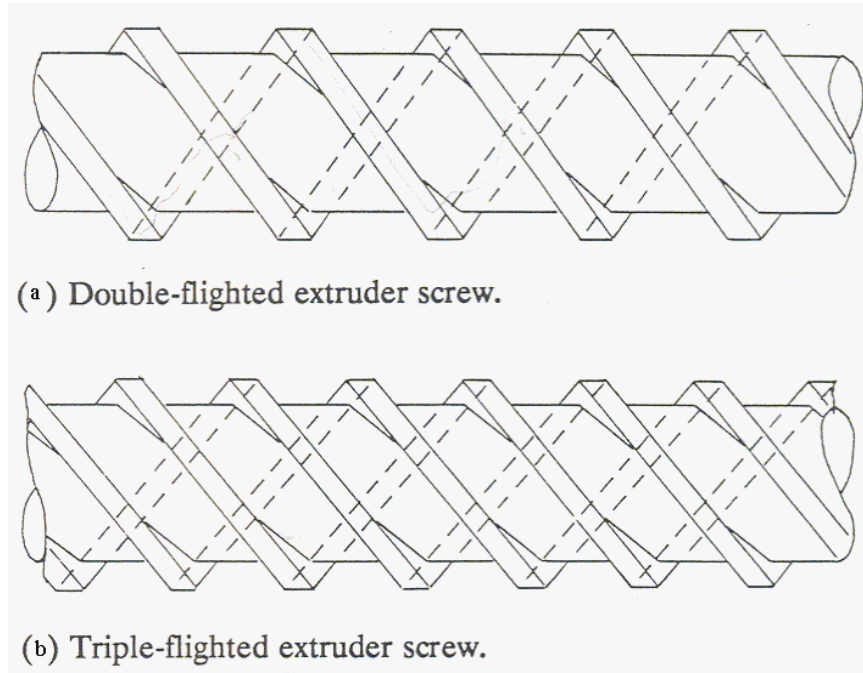


Figure 5.6: Examples of multi-flighted screws [69]

The screw elements can be either right-handed or left handed and when rotated clockwise will either be forward or backward pumping [69]. With backward pumping screws elements, the helix angle and pitch are negative [69]. Backward pumping screw elements reduce the pressure and also change the direction of leakage flow. As a consequence, leakage flow between screws is dominant in backward pumping screws while in forward pumping screws, the forward drag flow is dominant over the backward leakage flow [69]. CRNI extruders must have a right-handed screw and a left-handed screw, such that, as the name suggests, must rotate in opposite directions [67, 69]. Left-handed helix that causes flow from right to left, has the side nearest to the reader moving down the page while a right handed helix has to rotate in the opposite direction to cause the same flow [67].

Extruders sometimes have elements on the “screw” that are not true screw elements such as discs and other rotors that are used for kneading, mixing, and increasing pressure [69]. Commonly utilized screw elements are: square pitch, single flight conveying screws; long pitch, multi-flighted screws for vent zones; and cylindrical or reverse flight compounders or seal sections [70]. In CRNI the most common seals are cylindrical compounders. By increasing the diameter of these cylinders, the temperature rise and pressure drop can increase exponentially [70].

5.1.3 Modes of operation

Twin-screw extruders are normally operated in starvation mode. Among the advantages of starved feeding is that there is greater control of the extrusion process in which either the screw speed or throughput can be held constant while varying the other [71]. To successfully starve feed, the extruder has to be 30D or longer, else its not beneficial to get complete melting and mixing of the polymer [71]. To vary the degree of fill, one might put flow path elements that are not designed primarily to convey, or one that is completely neutral, or other mixing devices that may be made “partial conveyors” by incorporating a moving surface with an appropriate forward pitch [66]. Behind these restrictive elements, the screw channel is filled to a certain length that has sufficient pressure to keep the melt conveying in the extruder the same as the feed rate [74]. However, if these restrictions are too great, the screw can completely fill and then limit the extruder’s capacity [74]. Likewise, if the screw fill is too small, then the residence time will be low and so the extruder will not provide adequate mixing or reaction time [74].

When the pressure falls to zero in the middle of the extruder, this is representative of starvation [69]. This is usually determined by using the flow equation and specifying the die pressure and then back calculating to get the pressure profile along the axis of the screw [69]. If the pressure rises from the feed section to the die, the pressure will cause backflow [67]. Starvation continues until an element (usually a backward pumping element) that has decreasing pressure in the flow direction is reached [69]. As the degree of filling increases, the shear stresses and shear rates become nearly equal and so the pumping efficiency increases [67]. Leakage flow occurs only in fully-filled sections, not starved sections [69].

In all twin-screws extruders, the screws can either be configured as matched or staggered as shown in Figure 5.7. With a matched flight configuration, the melting mechanism is similar to single screws where there is a melt pool on the leading side of the flight [69]. But with staggered flights, no melt pool is formed and the pellets are scattered in the melt matrix [69].

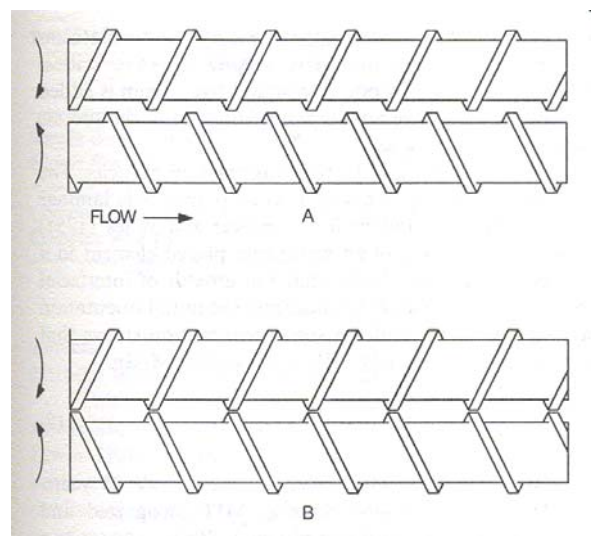


Figure 5.7: (A) Staggered screw flights; (B) Matched screw flights [70]

For simple screw assemblies of tangential CRNI, matched flight configurations have better pumping characteristics than the staggered flight machines [69, 75]. With modular screws in tangential CRNI, for both matched and staggered configurations with backward pumping screw elements, there is less pressure development than with forward pumping screw elements [69, 75]. When staggered, there is more interchange between the screws, which is beneficial in reorientation the polymer flow [66]. Staggered arrangement causes a unique pressure distribution that establishes the flow of material back and forth from one screw channel to the opposing screw [70]. The mean residence time is longer for staggered compared to matched configurations because the drag flow of staggered screws is 70% of the drag flow for the matched configuration [69, 74].

5.1.4 Sections of an extruder

Within a typical extrusion process, there are usually three different zones. In zone I, polymer pellets (solid) are either metered in or flood-fed and are conveyed towards zone II. In zone II, melting occurs and in the final zone, melt pumping of the polymer occurs. In order to have a stable extrusion process, the volumetric flow rate of the solids, Q_s , has to be greater than that of the melt, Q_m , which in turn must be greater than that of the melting pumping zone, Q_p . In other words, $Q_s \geq Q_m \geq Q_p$ [67]. For a stable process the drag in the solid zone must be at a higher rate than the melting zone [67].

5.2 *Reactive Extrusion*

Reactive extrusion is considered as the deliberate performance of chemical reaction during continuous extrusion of polymer and/or polymerizable monomers [66]. Reactive extrusion is sometimes referred to as “reactive compounding” or “reactive processing”, even though those can incorporate other processes [66]. Reactive extrusion is usually performed in twin screw extruders, however, little is known about the stability of these processes [76]. The extruder is effectively a stirred reaction vessel. The motion of the screws make the extruder essentially a ‘scraped’ heat exchanger, however, there is limited cooling because of shear heating [67]. Some of the processes that are normally carried out in reactive extrusion include: bulk polymerization, graft reaction, inter-chain copolymerization, coupling/cross-linking reaction, functionalization, and controlled degradation/depolymerization [66, 76]. Because polymeric materials have viscosities that range from 10-10,000 Pa s, it is not generally possible to carry out these reactions in conventional reactors [66].

Some of the characteristics of extruders that makes them advantageous as a reactor are that they: are able to run continuously at constant throughput; provide stable pumping for the highly viscous polymer; are adjustable for optimum reaction conditions by changing the screw design for mixing; have a relative ease for devolatilization; provide good melting of polymers; facilitate good control over residence time distribution and temperature; and give excellent dispersive and distributive mixing [66, 76].

Amongst the restrictions for using reactive extrusion are that the process: can be relatively expensive; the residence time may be short, so the kinetics have to be fast [76]. So a major limitation is the high cost for long reaction times [66]. To be economical, the

residence time of extruders should range between a few seconds to around 20 minutes [66]. As with other systems, the reaction time may differ in the extruder from batch data, so they should be verified in the continuous equipment [66]. For example, a reaction which takes 4 hours to complete in a batch reactor may get a similar conversion in a twin-screw extruder with residence time of 10 minutes [66].

Another disadvantage of using extruders as reactors is scaling up because the possibilities for heat and mass transfer are limited in larger equipment, which can cause significantly different temperature gradients and diffusion limitations [76]. However, the advantages of using an extruder as a reactor far out weigh the few limitations.

5.2.1 Residence time distribution (RTD)

The measurement of the RTD allows for the characterization of the mixing behavior compared to ideal reactors models [70]. CRNI closest model fit the Pinto and Tadmor model that was derived for single screw extruders [70, 77]. This model shows that the CRNI performance is between the upper limit of a plug flow and the lower limits of a CSTR [70]. Lu *et al.* have shown that by reversing one of the screw segments, the CRNI behaves more like a CSTR [70, 78]. (The CRNI used in this thesis has the option to use a reverse screw element.)

The volume available for reaction is dependent on the barrel diameter and flight depth (the helix angle is not essential to determine the volume) [66]. The volume required for reaction is [66]:

$$V = \frac{MR_t}{\rho f_v} \quad 5.6$$

where M is the mass flow rate, R_t is the residence time required, ρ is the melt density and the f_v is the volumetric fraction full and is defined as:

$$f_v = Q_p / Q_d \quad 5.7$$

where Q_d is the volumetric flow rate due to drag.

The definition of the maximum residence time is the available volume divided by the volumetric output [66]. But in starve feeding, the residence time, which is independent of the degree of fill, can be approximated by [66]:

$$R_t = 2L_b / ZN \quad 5.8$$

where, L_b is the barrel length, Z is the lead length of the screw and N is the screw speed. The value of Z is typically $0.25-1.5D$ [66]. Small residence time distribution is favorable because it leads to more uniform product [76]. Increasing the screw speed or throughput decreases the average residence time [76]. Because of the change in viscosity in reactive extrusion, there is a strong asymmetry in the residence time distribution [76]. Hence, it is not a good idea to model reactive extrusion with residence times obtained from non-reactive experiments [76].

5.3 Solid Conveying

Understanding of the solid conveying and melting performance of an extruder is central in determining if the extrudate will exhibit steady flow and/or will be completely melted [67]. Two of the most important aspects of solids conveying with respect to the

performance of the extruder are the filling of the screw channel from the feed throat and the transport of the solids by the screw [67]. (If the process is flood-fed then the gravity in the hopper will also be important.) Usually, the feed opening is offset or tangential to the screw [67]. It is also vital that the feed throat have good cooling to prevent the polymer from sticking and affect the flow stability [67].

Simulation of flow in extrusion utilizes the conservation of mass and balances of forces [69]. In solid conveying experimental studies done by Darnell and Mol, the pellets appear to move through the barrel as a solid plug [69, 79]. In their work, they modeled the bed of pellets as a continuum that is dragged forward by the motion of the screw [69]. Assumptions made when determining the solid conveying flow rate are [67]:

- The solid acts like a elastic continuum with no internal deformation that has a plug flow velocity
- The channel is full of polymer; [not valid for metered starved fed mode]
- There is constant channel depth
- There is no backwards flow through the mechanical gap between screw and barrel
- The density and the friction coefficient are independent of pressure and temperature
- The pressure varies only in the down channel direction and
- The barrel is moving whilst the screw is stationary.

The assumptions that the barrel is moving and screw is not will change the effects of the inertia forces on the polymer but the error it produces is small [67].

After applying the above assumptions and multiplying the velocity by the cross sectional area, the solids flow rate for a flooded extruder is [73]:

$$Q_s = \pi^2 N D_b (D_b - H) \frac{\tan \phi_p \tan \theta_b}{\tan \phi_p + \tan \theta_b} \left(\frac{\bar{W}}{\bar{W} + e} \right) \quad 5.9$$

where, ϕ_p is the angle between the direction of the moving solid plug relative to the barrel and

$$\bar{W} = \frac{\pi}{p} (D_b - H) \sin \bar{\theta} - e \quad 5.10$$

where, the bar on top of the variables means the average; θ_b is the barrel helix angle; and p is the number of flights in parallel.

After doing a force balance on the plug, the pressure profile for solid conveying zone is [73]:

$$P = P_1 \exp \left[\left(\frac{B_1 - A_1 K_d}{B_2 + A_2 K_d} \right) z_b \right] \quad 5.11$$

where,

$$A_1 = f_b W_b \sin \phi_p + 2 H f_s \sin \theta_b + W f_s \sin \theta_b \quad 5.12$$

$$A_2 = H \bar{W} \sin \bar{\theta} \quad 5.13$$

$$B_1 = f_b W_b \cos \phi_\rho - 2Hf_s \sin \theta_b \cot an\bar{\theta} \frac{\bar{D}}{D_b} - W_s f_s \sin \theta_b \cot an\phi_s \frac{D_s}{D_b} \quad 5.14$$

$$B_2 = H\bar{W} \cos \bar{\theta} \frac{\bar{D}}{D_b} \quad 5.15$$

$$K_d = \frac{\bar{D} \sin \bar{\theta} + f_s \cos \bar{\theta}}{D_b \cos \bar{\theta} - f_s \sin \bar{\theta}} \quad 5.16$$

$$z_b = \frac{l}{\sin \theta_b} \quad 5.17$$

P_l is the pressure at the entrance; f is the coefficient of friction; subscript s means of screw and b means of barrel; l is the axial distance.

As one can see, friction forces between solid polymer and the barrel and screw surfaces play a crucial roll in the solids conveying mechanism [73]. When one body slides over another, the tangential resistance is called friction. For ideal plastic material f is 0.2 [73]. An estimate for Nylon-6 is 0.6 while those reported are between 0.04 and 0.8 [73]. On a clean surface, for Nylon-6, f is 0.05 and increased to 0.42 after 10,000 cycles of rubbing polymer on the surface [73]. Irregularities that are usually observed when a new extruder is started up might be explained by the low coefficient of friction on its clean surfaces [73]. To get the maximum flow rate, one can polish or coat the screws to minimize the friction of the screw surface [73]. If the barrel and screw coefficient of frictions are almost equal, the output is small [67]. However, if f_b is slightly increased,

there is a significant increase in the output [67]. Surprisingly, when $f_b \gg f_s$, the output increases [67].

Flood feeding may be detrimental to the mixing capability of an extruder since the high pressure that it creates tends to agglomerate ingredients [71]. For this reason, twin-screw extruders are usually starve-fed, and so one has control of the screw speed and mixing independently of the feed rate [66]. In metered starved fed extrusion, the polymeric particulates (pellets) fed do not generate a lot of pressure in the screw channel [71]. This prevents the compaction of the pellets that forms the solid bed (which is typical in flooded fed extrusion) that moves down the screw channel in plug flow [71]. Instead, the channel will only be partially filled with polymeric particles and this type of flow is known as “Archimedean transport” [71]. In starved feeding, the first few screw turns are partially filled; when the screw channel becomes filled, the pressure then starts to build up [71]. Because of the delay in filling, starve feeding decreases the effective length of the extruder [71].

5.4 *Plasticating/Melting*

The single-screw extruder is an Archimedean screw or ‘drag’ pump, which conveys solid particles and generates pressure in the solid [67]. This conveying causes shearing and with the heat conducted from the barrel, generates heat and causes the solid to melt [67]. For CRNI matched screw flights, the melting behavior is similar to that of a single screw extruder in which there is a melting pool on the leading flight [69]. Whereas, with staggered screws, there is no melt pool formed but the pellets are scattered in the melt matrix [69].

Melting in twin screw extruders occurs by dispersed solids melting (DSM) [71]. DSM is when the individual solid particles are suspended in the melt matrix and their sizes reduce with the progression of melting [71]. Another melting mechanism is contiguous solids melting (CSM), which is more likely to occur in single screws [71]. CSM occurs when pellets are compacted into a dense, continuous solid bed that forms a helical ribbon (around the screws) that reduces in size as melting progresses [71]. Typical melting length in CSM is 10-15D while that of DSM is 2-3D [71]. From this, it is obvious that DSM is more efficient in melting than CSM. It has also been found that DSM reduces the power consumed by the screws by as much as 30% and that the temperature is more uniform and lower [71].

In order to know how much length is required for melting and how much unmelted polymer is present at any point in the extruder, one needs to use a model for melting. The model for DSM will not be discussed because it can only be applied after half the solid has melted; if the reader is interested, the derivation can be found in reference [71]. The CSM model is an idealized melting mechanism known as the Maddock or Tadmor mechanism. It is the most popular and is often used in software packages [67, 71]. When modeling melting, the existence of steady state is assumed; i.e. the velocity distribution at the cross section, the temperature distribution and the boundaries of the solid bed do not change with time [73]. Also, the interface boundaries are assumed to be sharp. In this mechanism, if a particular point in the extruder, the barrel temperature is held constant with time at T_b , this temperature causes a polymer melt thin film to be formed at the barrel surface, see Figure 5.8 [73]. Heat then is conducted from the barrel surface through a thin film of melt to the interface with the solid bed. Heat is

generated by viscous dissipation because of the relative motion of the barrel velocity and the solid bed, which causes the film of melt to be under constant shear [73]. At times, the temperature of the film may be higher than that of the barrel if the heat generated by viscous dissipation is large [73].

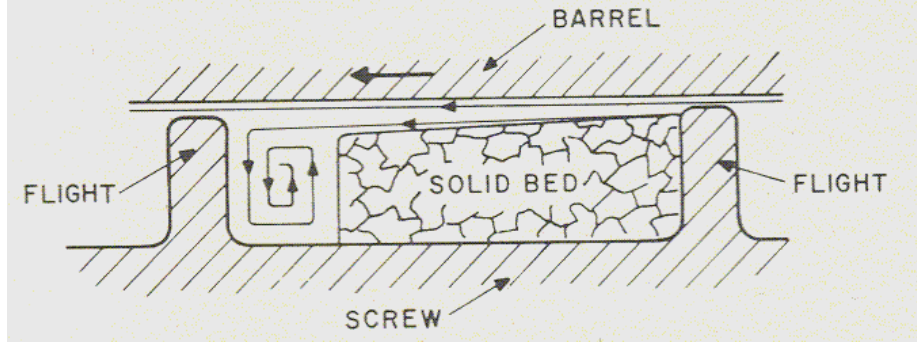


Figure 5.8: Idealized cross section of a channel showing the grow of the film and the direction of flow [73]

The heat flux at the melt interface (see Figure 5.9) is given by:

$$-q_{y=0} = k_m \left(\frac{dT}{dy} \right)_{y=0} = \frac{k_m}{\delta_t} (T_b - T_m) + \frac{\mu V_j^2}{2\delta_t} \quad 5.18$$

where, k_m is the thermal conductivity of the melt, δ_t is the thickness of the melt film

between barrel and solid bed, T_m is the melting temperature, μ is the viscosity,

$$V_j = \left\{ V_b^2 - V_{sz}^2 - 2V_b V_{sz} \cos \theta_b \right\}^{1/2} \quad 5.19$$

where, V_{sz} is the velocity of the solid bed in the down channel direction (see Figure 5.10)

in the melting zone. Some of the heat going in will be used to heat the solid bed up and

the rest to melt it. Since the thermal diffusivity of polymers is usually very low, in heat

transfer calculations, the solid bed is assumed to have an infinite depth [73]. This

assumption is further justified since the continual movement of the solid bed into the interface causes the temperature inside the solid bed to drop drastically from that of the melting point at the interface [73].

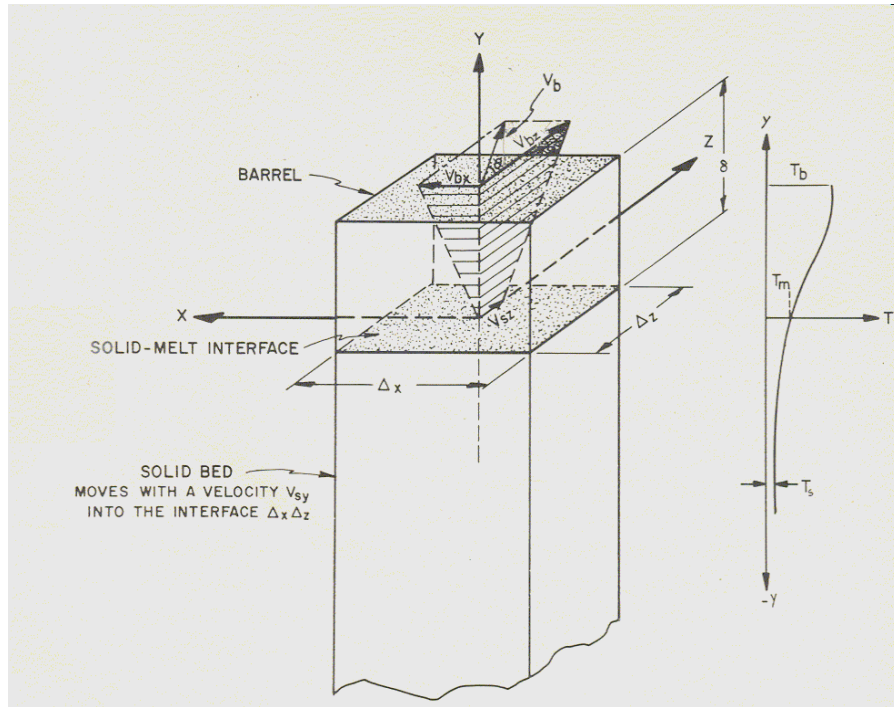


Figure 5.9: Profiles of the temperature and velocity of the differential volume which is perpendicular to the solid melt interface [73]

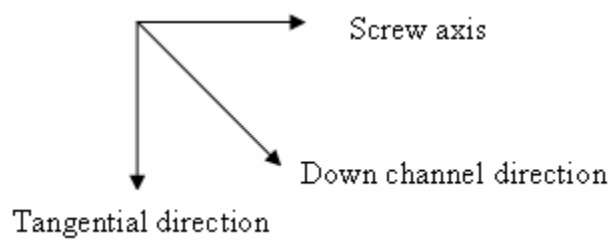


Figure 5.10: Vector directions used in describing flow in the extruder.

Assuming a constant Newtonian viscosity which is independent of temperature, the temperature profile in the melt film T_f is:

$$\frac{T_f - T_m}{T_b - T_m} = \frac{\mu V_j^2}{2k_m(T_b - T_m)} \frac{y}{\delta} \left(1 - \frac{y}{\delta}\right) + \frac{y}{\delta} \quad 5.20$$

y is the direction from the screw to the barrel; δ is the thickness of the film between barrel and solid bed; k_m is thermal conductivity of the melt; and T_m is temperature at the melt interface .

The term $\mu V_j^2 / k_m (T_b - T_m)$ is a dimensionless group referred to as the “Brinkman number” which measures the magnitude of the viscous heat generation to the heat conduction from the imposed temperature difference. When the Brinkman number is greater than 2, a maximum temperature exists between the barrel and the solid-melt interface.

The average film temperature is [67]:

$$T_{AV} = \frac{T_f + T_m}{2} + \frac{\mu V_j^2}{12k_m} \quad 5.21$$

The temperature of the solid inside the solid bed, T_{ss} , is:

$$\frac{T_{ss} - T_s}{T_m - T_s} = \exp\left(\frac{V_{sy} y}{\alpha_s}\right) \quad 5.22$$

where

$$\alpha_s = \frac{k_s}{\rho_s c_s} \quad 5.23$$

k_s, ρ_s, c_s are the thermal conductivity, density and specific heat of the solid bed, respectively; V_{sy} is the velocity of the solid bed in the barrel depth direction in the melting zone.

The width of the solid bed profile, X , is [73]:

$$\frac{X}{W} = \left(1 - \frac{\psi}{2H} z\right)^2 \quad 5.24$$

$$\psi = \frac{\Phi W^{1/2}}{M / H_0} \quad 5.25$$

where, z is the length in the down channel direction; M is the mass flow rate and is given by: $M = V_{sz} H W \rho_s$; λ is the heat of fusion of the polymer and

$$\Phi = \left\{ \frac{V_{bx} \rho \left[k_m (T_b - T_m) + \frac{\mu}{2} V_j^2 \right]}{2 [c_s (T_m - T_s) + \lambda]} \right\}^{1/2} \quad 5.26$$

The above equation is a measure of the rate of melting; i.e. the numerator is proportional to the rate at which heat is supplied for melting and the denominator is proportional to the heat required to change the solid temperature from T_s to T_m .

The film thickness, δ , is found by [73]:

$$\delta = \left\{ \frac{[2k_m(T_b - T_m) + \mu V_j^2]X}{V_{bx}\rho_m[c_s(T_m - T_s) + \lambda]} \right\}^{\frac{1}{2}} \quad 5.27$$

The length of melting, z_T , is therefore:

$$z_T = \frac{2M}{\Phi W^{\frac{1}{2}}} \frac{H}{H_0} \quad 5.28$$

The above equation means that the length of the melting zone is directly proportional to the throughput and inversely proportional to the rate of melting [73].

There are two main sources of errors involved in using the Newtonian model. The first error is that the amount of heat needed to bring the temperature of the newly melted polymer to the average temperature of the film was not included [73]. To include this, the heat of fusion is replaced by:

$$\lambda^* = \lambda + c_m(T'_{AV} - T_m) \quad 5.29$$

where c_m is the specific heat of the melt and

$$T'_{AV} = \frac{2T_b + T_m}{3} + \frac{\mu V_j^2}{12\lambda_m} \quad 5.30$$

$$V_j = Vb - V_{sz} \quad 5.31$$

$$V_{sz} = pND_s \cos \phi_p \quad 5.32$$

The second source of error in is that the Newtonian model assumes that the viscosity does not change with the temperature [73]. To eliminate this, non-Newtonian models that account for the viscosity changing with temperature and shear rate should be used. Since these results are really complicated and difficult to solve, they will not be used in the modeling of this work.

5.4.1 Effect of screw geometry on melting

Based on the model equation for melting, the following observations were made:

- A small flight clearance increases the rate of melting [73]. If the channel depth is large, the effect of the channel curvature should not be neglected [73].
- If the channel depth is decreased, the velocity of the solid bed will increase which would decrease the velocity difference between the barrel and solid bed, which would in turn decrease the amount of heat generated and results in slower melting [73]. If the viscous heat generation is small, this effect is not very strong. The shallower the channel depth, the greater the delay in melting will be [73].
- The helix angle has a similar effect to that of channel depth with some added complexity during melting [73]. By decreasing the helix angle, the helical length is increased, which allows more time for melting and decreases the amount of the extruder length for melting. Decreased helix angle also decreases the channel depth, which decreases the amount of heat generation [73].
- Increasing the flow rate and keeping all the other variables constant will increase the melting zone length [73]. If the extruder is not long enough, incomplete melting will result and the product will not be homogenous [73]. Also, the increased flow rate will increase the delay in the start of melting which also increases the end point of melting [73].
- Unlike the linear effect of flow rate on melting length, the effect of screw speed is complex. With all other variables held constant, by increasing the screw speed, the amount of viscous dissipation increases in the melt, which is proportional to N^2 [73]. The rate at which the melt is removed from the film and deposited in the

melt pool is also increased, proportional to N [73]. Since the increase in screw speed increases the rate of melting, it therefore shortens the melting zone of the extruder [73].

- By increasing the barrel temperature: the heat transfer increases from barrel to polymer which causes a higher average melt film temperature; thereby, reducing the viscosity in the film, which in turn lowers the amount of heat generated by viscous dissipation which causes a reduction in the rate of melting [73].

Because of these effects, an optimal barrel temperature is usually found [73]. This is dependent on the relative importance of heat transfer and heat generation. To have faster melting, one should preheat the solid pellets before feeding them into the extruder [71].

5.4.2 Effect of tapered screw on melting

By tapering, one can generally accelerate melting because the tapered screw roots reduces the cross section of the channel, which causes the solid bed to be more exposed to the hot barrel [73]. For a tapered channel where the channel depth is given by $H=H_1-Gz$, the channel bed profile is [73]:

$$\frac{X}{W} = \left(\frac{\psi}{G} - \left[\frac{\psi}{G} - 1 \right] \left[\frac{H_1}{H_1 - Gz} \right]^{\frac{1}{2}} \right)^2 \quad 5.33$$

where H_0 is the channel depth where melting starts; H_1 is the channel depth at the end of tapered section; G is the slope of tapered section. The term:

$$\psi = \frac{\Phi W^{\frac{1}{2}}}{M / H_0} \quad 5.34$$

is dimensionless and is a ratio of the rate of melting down the channel distance to the rate of mass flow of the solids per unit channel depth.

For tapered screws, the total length for melting is:

$$z_T = \frac{H_1}{\psi} \left(2 - \frac{G}{\psi} \right) \quad 5.35$$

5.5 Metering/Melt Pumping

In melt conveying or melt pumping, the rotation of the screws drags the melt along the barrel surface down the channels of the screws [74]. Pressure that opposes this drag flow comes from restrictive elements used for mixing and also from the die. In addition, leakage flow also reduces the total flow of the extruder [74]. The melt pumping region is often called the ‘metering’ section because mass flow in this region is usually the limiting flow rate in the extruder design [67]. Efforts to understand the flow in non-intermeshing counter-rotating twin screw extruders are relatively sparse. The first model was made by Kaplan and Tadmor [69, 80]. They used a 3-plate model and assumed the screw was stationary and the barrel moves. However, they neglected the leakage flow between screws. Nichols and Yao then accounted for flow in the apex area [69, 81]. Other models that have been developed include: the lubrication theory and finite element model that are very complex and will not be discussed here, they are detailed by White [69].

A first approximation for a non-intermeshing extruder is to view it as two parallel single-screw extruders [76]. However, because of the apex, the open area that connects the two barrel halves, the throughput is less than two single-screws because the two screws interact with each other [76]. In the modeling of extruders, the root of the extruder is flattened out and the coordinate system is based off the flat screw. Shearing by the flight walls are considered a secondary effect and are usually neglected in some analysis [69]. But, like the screws, the polymer melt will stick to the flights as well. The flights also cause a pressure differences in the adjacent channels, which leads to backwards leakage flow over the clearance [69].

In most of the models, a three plate model is used where the outside plates represent the screws, the middle plate is considered to have zero thickness and is representative of the barrel (see Figure 5.11) [76]. The middle plate has parallel slots, which represents the apex openings [76]. For the two results that will be presented below, the model plate is assume to have a thickness of W_a which is equal to the apex width as shown in Figure 5.12.

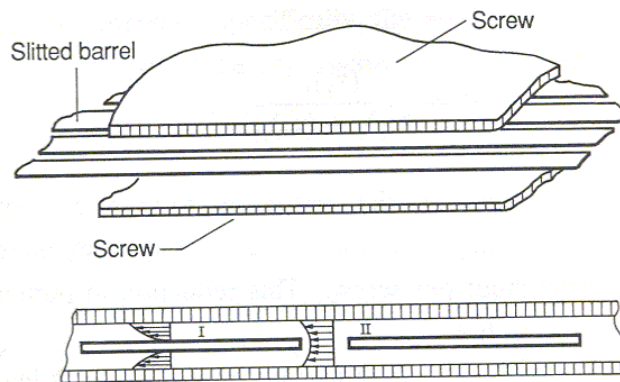


Figure 5.11: Three plate model used for flow in a CRNI extruder [69]

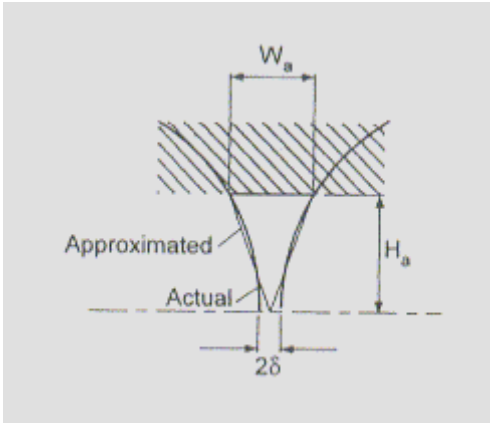


Figure 5.12: Apex area of a CRNI extruder [71]

Typical assumptions when modeling melt flow are [67, 71]:

- continuous steady state
- polymer is fully melted and is homogeneous
- polymer sticks (no slip) to screw and barrel surfaces but not to the front and back of the flights. (The flow becomes indeterminate if the polymer does not adhere to the barrel and screw.)
- curvature of helix is neglected; hence, neglecting inertia terms which will imply that the mean channel velocities are overestimated.
- channel depth is very small in comparison to barrel inner diameter
- Viscosity is not a function of shear rate or time, but is a function of temperature.

(Drag flow is independent of the pseudo-plastic behavior of polymer melts since it is independent of viscosity, by increasing screw speed the drag flow is unaffected [67]. But by increasing the screw speed, the back flow due to pressure is increased because of the increase in shear rates and a reduction of the viscosity[67]. The

lower the viscosity in a pseudo-plastic fluid, the lower the output. For a non-Newtonian fluid, the viscosity will vary across the channel and the integration of the Navier-Stokes equation becomes complex and has to be solved numerically.)

- Isothermal flow:
- Body and inertia forces are negligible; gravity is neglected
- Constant depth screw
- Channel width is considered infinite.

For modeling, a rectangular coordinate system is assumed in which the effect of screw curvature is negligible because the channel is wound off the cylindrical screw [73]. As with the solid conveying model, the barrel instead of the screw is modeled as rotating. This is done because the shear stress distribution is identical in both cases; however, the radial pressure distribution is different [73]. With the outer cylinder rotating, a more stabilized flow is produced which can sustain a laminar flow up to higher Reynolds numbers [73]. In extruders, polymer flow is slow (in the laminar region); therefore, the centrifugal forces produced has a small effect and this coordinate system can be used because it does not distort the problem [73].

Another is the lubrication assumption [73]. In the lubrication assumption, the convection in the tangential direction of the surfaces of a small gap and also the velocity component in the normal direction are neglected [73]. It has been shown that the lubrication assumption is valid for even non-Newtonian fluids if the local angle between the surfaces is less than 10° [73]. The lubrication assumption is reasonable since in CRNI, the interaction of the converging and diverging flow streams between the screws, prevents the occurrence of fully developed flow [70]. These simplified mathematical

formulae obtained by using these assumptions are used to give the trends in operation and can be compensated for by using correction factors [67].

The net flow rate, Q , in the melt conveying of a CRNI is the sum of the drag flow, Q_d , pressure flow, Q_p , apex flow, Q_a , and flight leakage, Q_l [74]:

$$Q = Q_d - Q_p - Q_a - Q_l \quad 5.36$$

for matched CRNI extruders with a correction factor for non-Newtonian behavior, the drag flow is defined as [74]:

$$Q_d = \pi D N W H f \cos \phi (4 + n) / 5 \quad 5.37$$

where f the factor that accounts for the fact that the barrel is closed over 85% of each screw circumference; n is the power law index. It was determined experimentally that for staggered screws, the drag flow is 70% of the matched screws [74]. The pressure flow in the channel for matched and staggered screws are treated the same and is defined as [74]:

$$Q_p = 2 W H^3 f \sin \phi \Delta P / L / (4 \mu) / (1 + 2n) \quad 5.38$$

where P is the backpressure, L is the screw channel fill length and μ is the viscosity at the temperature and shear rate in the channel. The pressure data should form a straight line and decrease to zero where the filled length ends with a maximum at the seal. The apex flow is a pressure flow and is modeled as flow through a rectangular opening that is formed by twice the apex height, h_a , and the average apex width, w_a and is given by [74]:

$$Q_a = W_a^3 H_a \Delta P / L / (42 \mu) \quad 5.39$$

the leakage flow is small and is modeled as the down channel pressure leakage between the flights and the barrel and is defined as [74]:

$$Q_l = 2\pi^2 D^2 \delta^3 \cos^2 \phi \Delta P / L / (12W\mu_{cl}) \quad 5.40$$

The derivation of the output equations are discussed in reference [71] and others. The output per screw for staggered screw configuration is [71]:

$$Q_p = \frac{1}{2} f_u WHV_{bz} - \frac{WH^3 g_z}{12\mu} - \dot{V}_{11} - \dot{V}_{1d} - \dot{V}_{1p} \quad 5.41$$

where,

$$\dot{V}_{11} = \frac{\pi D \delta_f^3 \cos \phi}{12\mu_{cl} e} \left(\frac{\pi D g_z \cos \phi}{p} - \frac{6\mu V_{bx} W}{H^2} \right) + \frac{pe \delta_f^3}{12\mu_{cl}} g_z \quad 5.42$$

$$\dot{V}_{1d} = \frac{1}{2} (1 - f_u) \pi D (H + 0.5W_a) V_b \sin \phi \quad 5.43$$

$$\dot{V}_{1p} = \frac{0.5\pi D(1-f_u)(H+0.5W_a)^3 g_a}{12\mu} \quad 5.44$$

$$W_a = D(1 - \cos \alpha_a) + 2\delta \quad 5.45$$

$$f_u = \frac{\alpha_a}{\pi} \quad 5.46$$

$$V_{bz} = pND_b \cos(\theta_b) \quad 5.47$$

$$V_{bx} = pND_b \sin(\theta_b) \quad 5.48$$

$$g_z = \frac{\partial P}{\partial z} \quad 5.49$$

$$g_a = \frac{g_z}{\sin \phi} \quad 5.50$$

α_a is the apex angle; V_{bz} is the velocity in the down channel direction; f_u = the ratio of the uninterrupted barrel circumference with to that of the total barrel circumference; g_z is the pressure gradient; P is pressure; z is direction of flow; μ is the average viscosity; D is screw diameter; δ_f is flight clearance; μ_{cl} is the viscosity over the flight clearance; p is the number of flights in parallel; V_b is the velocity in the cross channel direction; V_b =velocity of screw barrel (actually the screw, but in model, barrel is moving not screw), W_a is the height of the approximated apex triangle Figure 5.12; and g_a is the axial pressure gradient

For matched screw configuration, the output per screw can be approximated by [71]:

$$Q_p = \frac{1}{2} f_u WHV_{bz} - \frac{WH^3 g_z}{12\mu} - \dot{V}_{11} - \dot{V}_{12} \quad 5.51$$

where,

$$\dot{V}_{12} = 0.017(H_a - 0.61W_a)W_a^3 \left(\frac{g_a S}{\mu p e} \right) \quad 5.52$$

$$H_a = \frac{1}{2} D \sin \alpha_a \quad 5.53$$

In the design of twin screw extruders, there is a single screw pumping section next to the die. To model the extruder, an equation for the flow (Newtonian) in single screws is needed. The flow through single screw extruder can be determined by [76]:

$$Q_{SE} = \frac{WH}{2} \pi ND \cos \phi \left(1 - 0.57 \frac{H}{W} \right) - \frac{WH^3}{12\mu} \frac{dP}{dz} \left(1 - 0.62 \frac{H}{W} \right) \quad 5.54$$

For the compounding cylinders, the relationships between the flow and the pressure is [82]:

$$\Delta P = \frac{L_{cl} Q_p \mu}{\xi + \beta} \quad 5.55$$

where,

$$\beta = \frac{189\left(\frac{w_a}{2H_a}\right)^5 + 35\left(\frac{w_a}{2H_a}\right)^2}{2475\left(\frac{w_a}{2H_a}\right)^4 + 1710\left(\frac{w_a}{2H_a}\right)^2 + 135} \quad 5.56$$

$$\xi = \pi R^4 \left(1 - \left(\frac{D_{cl}}{D_b}\right)^4 + \frac{\left(\frac{D_{cl}}{D_b}\right)^4 - 2\left(\frac{D_{cl}}{D_b}\right)^2 + 1}{\ln\left(\frac{D_{cl}}{D_b}\right)} \right) \quad 5.57$$

Dimensionless output is a ratio of the actual flow to the theoretical and is defined as [67]:

$$\frac{Q}{V_{bz}BH} \quad 5.58$$

When less than 0.5 the pressure gradient is small, but when greater the pressure gradient is negative [67]. If it tends to zero then the pressure gradient is large [67]. For simplified calculation, if the feed port and the die are used as reference points the pressure difference will be close to zero [76].

5.5.5 Degree of fill in melt pumping

In order to determine the degree of fill inside the extruder, one has to work backwards from the die pressure. The pressure drop across the die can be found by

$$\Delta P_{die} = \frac{8Q_p L_d}{\pi R_d^4} \quad 5.59$$

where, R_d is the radius of the die and L_d is the length of the die.

After determining the pressure drop of the die, the fill length of each screw section from the die back towards the hopper is determined depending on the screw section type that is used. Below, one will find the necessary equation to find the fill length from different screw elements.

5.5.5.1 Fill of matched screw in front of a cylindrical element

The fill length prior to the cylinder in matched screw configuration is given by [82]:

$$\Delta L = \frac{k_p \Delta P}{\mu(k_N N - Q_p)} \quad 5.60$$

where,

$$k_p = k_{ch} + k_a + k_{c12} \quad 5.61$$

$$k_{ch} = \frac{WH^3}{6} \quad 5.62$$

$$k_a = 2 \frac{7 \left(\frac{W_a}{2H_a} \right)^3 H_a^4 \left[2 \left(\frac{W_a}{2H_a} \right)^4 + 5 \right]}{90 \left[55 \left(\frac{W_a}{2H_a} \right)^4 + 38 \left(\frac{W_a}{2H_a} \right)^2 + 3 \right]} \quad 5.63$$

$$k_{c12} = \frac{\pi^2 D^3 \delta^3 \cos^2 \phi}{6ep} + \frac{pe\delta^3}{6} \quad 5.64$$

$$k_N = fWH\pi D \cos \phi - \frac{\pi D \delta^3 \cos \phi \pi D W \sin \phi}{eH^2} \quad 5.65$$

5.5.5.3 Fill of reverse pumping elements

For reverse pumping elements, the filled length can be estimated from (the upper case K 's indicate reverse pumping.) [82]:

$$L_F = L_R \frac{K_{P_F}}{K_{P_R}} \left[\frac{K_{N_F} + Q/N}{K_{N_R} + Q/N} \right] \quad 5.66$$

The reverse pumping elements produces backpressure, so in the pressure-throughput equation it has the same form as the forward pumping but the signs are reversed [82].

5.5.5.4 Using Fill to determine residence time

The average residence time and is defined as [82]:

$$t_{av} = \frac{V_f + V_u + V_c}{Q} \quad 5.67$$

where:

V_f is the volume of fluid in the fully filled section and is defined as [82]:

$$V_f = 4\pi H^2 \frac{360 - 45}{360} L \quad 5.68$$

V_c is volume of material around the cylinder and can be found thusly [82]:

$$V_c = L_{cl} \left(\frac{\pi}{4} D_b^2 + W_a H_a + \frac{\pi}{4} d_{cl}^2 \right) \quad 5.69$$

V_u is the unfilled volume in the partially filled area; with constant depth, V_u is defined as [82]:

$$V_u = (100 - D_{\%}) 4\pi H^2 \frac{360 - 45}{360} L \quad 5.70$$

where, $D_{\%}$ is the percent drag flow which is better measurement of the extruder condition than Q/N [82]. It can be found by [82]:

$$D_{\%} = \frac{Q/N}{K_N} \quad 5.71$$

5.6 *Mixing*

In any reactor, there should be sufficient mixing to ensure that the distance between the reacting components is small enough so that diffusion can provide complete homogenization or good stoichiometry so that the reaction can be completed in a characteristic time [76]. When there are multi-components in a reactions, often the compounds can be immiscible and so the reaction occurs mainly at the interface between the compounds [76]. Because of this, micromixing plays an important part because this type of reaction may be diffusion limited [76]. (Temperature and macro mixing also affect the reaction [76].)

The ultimate mechanism for mixing the molecular participants in a reaction is diffusion [66]. Therefore, promoting convection and assisting the diffusion process by reducing diffusion length and/or increasing interfacial area is key [66]. The Fourier number, Fo , is used to determined if diffusion can allow for homogenization within a reasonable time and is defined as [76]:

$$Fo = \frac{\Gamma t}{r_s^2} > 1 \quad 5.72$$

where Γ is the diffusion coefficient, t is the available time and r_s is the characteristic size of inhomogeneities [76].

5.6.1 *Mixing modes*

The mixing actions that depend on the compatibility of the components are dispersive, distributive and longitudinal mixing [76]. In dispersive mixing, the components are thermodynamically incompatible so two phases exist [76]. To overcome the interfacial forces, significant shear force is needed to provide good mixing; therefore,

high viscosity matrix favors good dispersive mixing [76]. Dispersive mixing is the breaking up of agglomerates of solid in a fluid matrix [69].

Conversely, in distributive mixing, the components are thermodynamically miscible, and there are no interfacial forces, but the shear rate is important for homogenization [76]. To put it more simply, distributive mixing is the continual rearrangement of the compounds present to diminish non-uniformities [69]. When the molecules are small, compatibility is better entropically [76]. But when they are alike, compatibility is reached enthalpically [76]. The solubility parameter, δ , is used to determine if the components are compatible or not. The closer the solubility parameters are, the more compatible are the components [76]. The criterion for solubility is [76]:

$$|\delta_1 - \delta_2| < 3.5E10^3 \text{ (J/m}^3\text{)}^{1/2} \quad 5.73$$

If the components can be mixed distributively then [76],

$$|\delta_1 - \delta_2| < 1.3E10^3 \text{ (J/m}^3\text{)}^{1/2} \quad 5.74$$

The solubility parameters can be attained from the cohesive energy density, CED [76].

$$\delta = \sqrt{CED} \quad 5.75$$

where,

$$CED = \frac{\Delta h_{vap} - RT}{V_0} \quad 5.76$$

Δh_{vap} is the theoretical/hypothetical heat of vaporization, V_0 is the molar volume which by definition is molecular weight divided by density.

Another approach to derive the CED is from the Flory-Huggins equation [76]:

$$\frac{\Delta G_m}{RT} = \phi_1 \ln \phi_{1+} + \frac{\phi_2}{x_n} \ln \phi_2 + g_i \phi_1 \phi_2 \quad 5.77$$

where ϕ_i is the volume fraction, ΔG_m is the free energy of the mixture, x_n is the degree of polymerization, g is the interaction parameter.

$$g = \frac{V_0}{RT} (\delta_1 - \delta_2) \quad 5.78$$

Unlike the previous mixing actions, longitudinal mixing is associated with the residence time distribution, which reduces the inhomogeneity from the feed as one proceeds down the extruder [76].

5.6.2 Mixing in extruders

Single screw extruders have low dispersive and distributive mixing because of their continuous channel, (no velocity rearrangement occur) [76]. However, in the counter-rotating extruder, the shearing forces and elongation forces are extremely large in the gap, but the shear levels are low in the chambers because of the deep channel when at low screw speed [76]. In reactive extrusion, the lack of isoviscous material affect the filled length of the extruder significantly [76]. Low viscosity material affects the working of the zone in which it is in [76]. When low viscosity material is in a partially filled zone, the material is likely to not being dragged properly down the channel of the screw and will build up in the bottom of the extruder and be influenced more by gravity than with viscous forces [76]. The Jeffrey's dimensionless number, Je , relates the gravity and

viscous forces (the ratio between the Reynolds and Froude numbers) and is defined as [76]:

$$Je = \frac{\rho g D}{\mu N} \quad 5.79$$

where, g is the gravitational acceleration; D is screw diameter; ρ is melt density; N is screw speed; and μ is viscosity. With high Jeffreys number and low degree of fill, the material remains at the bottom of the channel and does not go over the screws [76]. With low Jeffreys number and low degree of fill, the material collects at the pushing flight [76]. However, when there is high degree of fill, the material will stick to both flights [76].

Mixing is enhanced in staggered configuration even though the pressure build up is low; but with the match configuration, a better pressure build up is attained, but the mixing ability is diminished [76].

5.7 Energy Balance

Sources of energy input into the extruder are from [67, 73]:

- enthalpy of the feed, I_{in}
- mechanical energy from screw rotation which is measured at the drive motor output, E . The majority of the mechanical energy is converted by viscous dissipation into thermal energy, while the remaining causes an increase in pressure and kinetic energy of the melt.
- energy from heaters, Q_w

In comparison, the sources for energy output of are [67]:

- enthalpy of the products (sum), I_{out} and
- losses of the extruder through transmission belts or gears and in the bearings, S_L .

Generally, 61% of energy put into process is used to melt the polymer [83].

The components in the overall energy balance of an extruder reactor are [76]:

- Mechanical energy supplied by the screw rotating (power provided by the drive unit), E , which is used for
 - Pressure generation, $Q_p \Delta P$ (where Q_p is the volumetric throughput)
 - Heat generation by internal friction used to heat up the materials, $Q_p \rho C_p \Delta T$, and to melt the polymer, $Q_p \rho H_m$
- Heat flow through the walls, Q_w and
- Heat of reaction, H_r

Using the above the macroscopic energy balance for an endothermic reaction can be written as [76]:

$$E + Q_w = Q_p (\Delta P + \rho C_p \Delta T + \rho H_m + \rho H_r) \quad 5.80$$

The total power from the screw is the sum of the power used for: melting, increasing the pressure of the melt, viscous heat dissipation in the melt pool, viscous heat dissipation in the flight clearance, and in solid conveying (see Figure 5.13) [73]. There are two sources of energy used in melting in an extruder: conductive and mechanical. 80-90% (or more) of the energy is supplied by the screw [71].

POWER

$$\underbrace{(\text{Shear Rate})(\text{Viscosity})}_{\text{Shear Stress}} \underbrace{(\text{Shear Area})(\text{Radius})}_{\text{Force}} (\text{Speed}) = \text{Power}$$

$$\underbrace{\hspace{10em}}_{\text{Torque}}$$

Power

$$\left(\frac{\pi DN}{t}\right)(\eta)(\pi DL)\left(\frac{D}{2}\right)(N)$$

if $t \ll D$

$$\text{Power} \propto \eta D^2 L N^2$$

Figure 5.13: Elements that consumes power in an extruder [66]

Heat flows in the melt pumping sections [67]:

- Radial heat transfer through outer barrel diameter by heaters or coolant
- Radial conduction in barrel wall
- Radial heat transfer from inner barrel and screw to/from the polymer
- Radial and helical conduction in polymer
- Axial conduction in barrel wall
- Axial and radial conduction in screw flight
- Local axial conduction in screw between the flights and channel root.
- Axial conduction in screw root
- Shear heating of polymer
- Radial mixing as a result of transverse circulation
- Conduction along the helix of the flight
- Shear heating in flight clearances

From the above, one can see that extrusion can never to be considered as an isothermal process because of the rotation of the screws that causes shearing that leads to the irreversible conversion of mechanical energy into internal energy or heat [73]. Non-uniform temperature distributions in the extruder occur in the radial and down channel direction. In the radial direction there is a temperature difference between the screws and barrel, while in the down stream direction, the contribution of the radial temperature distribution and the amount of heat generated by viscous dissipation causes the temperature differential [73].

As a result of the temperature distribution in the radial direction a viscosity distribution also occurs in the radial direction [73]. If a linear relationship is assumed for the viscosity distribution then the distribution can be written as [73]:

$$\mu = \mu_s \left[1 - (1 - r_\mu) \frac{y}{H} \right] \quad 5. 81$$

$$r_\mu = \frac{\mu_b}{\mu_s} \quad 5. 82$$

where, the subscripts *s* and *b* represent that of the screw and barrel respectively, and *y* is the distance from the screw going towards the barrel.

The heat transfer in the radial direction is also important. Models have been made for the unsteady state heat transfer from a constant temperature barrel surface to the molten polymer in the channel [73, 84]. In the model, subsequent to the flight sweeping over a point on the barrel, the constant temperature barrel surface is cooled with a film created by the existence of the flight clearance. [However, if a large amount of heat is generated in the flight clearance, the temperature of the film will be higher than the barrel's so this analysis cannot be used.]

The heat transfer in reactive extrusion is important because [66]:

- Selectivity and extent of reaction kinetics may be sensitive to temperature
- Heat transfer effects have to be considered during scale-up
- A stable temperature may be needed to maintain good product uniformity.

Low heat transfer can lead to the polymer solidifying and causing the extruder to stop [76]. The heat transfer coefficient of the extruder is dependent on the screw speed, flight clearance, and polymer properties. The heat transfer in an extruder is often modeled as concentric layers of cylinders, which is usually valid for single screws, but dubious for twin-screws [66]. However, when finite element calculations were done for twin screws, the results were less than 10% off; so using concentric layers of cylinders to calculate heat transfer will give a good approximation [66].

The most common type of barrel design is the jacketed type shown in Figure 5.14 [66].

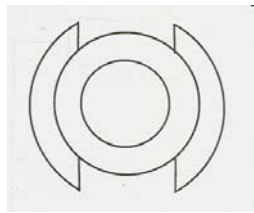


Figure 5.14: Jacketed barrel

The local heat transfer is given by [76]:

$$Q_w = UA(T_p - T_w) \quad 5.83$$

where U is the overall heat transfer coefficient, A is the heat transfer area, T_p is the temperature of the polymer and T_w is the temperature of the barrel wall.

There are limited models available for the poor heat transfer that occurs in polymer processing. If heat exchange mediums such as cooling water are ignored, the overall heat transfer coefficient can be approximated by [76]:

$$U = \frac{1}{\frac{R_i \ln\left(\frac{R_o}{R_i}\right)}{\lambda_m} + \frac{1}{\alpha_i}} \quad 5.84$$

where R_o and R_i are the outer and inner radius of the barrel, respectively; R_i for twin screw extruders is approximated as shown in Figure 5.15 [76]. λ_m is the heat conductivity of the metal and α_i is the heat transfer coefficient of the polymer and barrel wall. The heat transfer coefficient can vary between 400-600W/m²K [76].

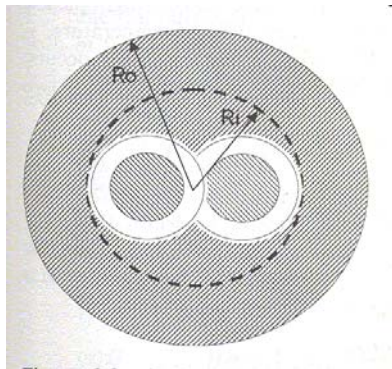


Figure 5.15: Approximation of the inner diameter for twin screw extruders [76]

In the oldest model for heat resistance that occurs between the polymer and the barrel wall, the extruder is treated as a scraped heat exchanger where the screw flight is considered a scraper as it passes the barrel [76]. The heat transfer coefficient derived based on experiments and is [76]:

$$\alpha_i = 0.94 \frac{\lambda_c}{D} \left(\frac{\rho N D^2}{\mu} \right)^{0.28} \left(\frac{C_p \mu}{\lambda_c} \right)^{0.33} \quad 5.85$$

where, λ_c is the heat conductivity of the polymer.

It should be noted that heat transfer coefficient is particular for the machine/process in question.

Heat transferred by melt during one revolution per unit barrel areas is:

$$q_T = \rho c_m H (\bar{T} - T_i) = U (T_b - T_i) / N \quad 5.86$$

In an extruder, the performance lies between an isothermal and an adiabatic process [73]. To get a useful representation of the axial temperature distribution, adiabatic extrusion can be used as a limiting case [73]. Adiabatic operation is a good approximation for high screw speeds. By considering the adiabatic case one can get an estimate of the maximum temperature that can be reached [73].

The three dimensionless groups that are used in estimating the temperature rise are [76]:

- The Damköhler IV number, Da_{IV} , is the ratio between the heat absorbed/released by the reaction and the heat added/removed by the walls through conduction –

$$Da_{IV} = \frac{\rho H_r Q}{\lambda \Delta T D} \quad 5.87$$

(where λ is heat conductivity of the wall, D is the screw diameter)

- The Brinkmann number, Br , is the ratio between the heat released by viscous dissipation and the heat removed by conduction at the walls –

$$Br = \frac{\mu N^2 D^2}{\lambda \Delta T} \quad 5.88$$

(where μ is the viscosity)

- The Graetz number, Gz , is the ratio between the heat removed by conduction and that transported by convection. –

$$Gz = \frac{aL}{Q} \quad 5.89$$

(where a is the thermal diffusivity of the material, L is the extruder/screw length)

For exothermic reactions, if $Da_{IV} / Br \gg 1$, the heat released by viscous dissipation can be neglected with respect to the heat of reaction [76]. In larger extruders, $Gz \ll 1$ because the convective heat flow dominates the conductive heat transfer through the wall, so the process moves toward an adiabatic process [76].

The polymer film heat transfer coefficient is usually $170\text{-}567 \text{ Wm}^{-2} \text{ K}^{-1}$, but should be determined empirically for the system being considered [66]. The barrel metals of small extruder usually have much smaller thermal resistance than the polymer, but with large machines and with corrosion, the resistances are comparable [66]. Standard practice is to use tight clearances where better heat transfer is desired [66].

5.7.1 Calculation of E, Energy input from extruder drive

Equations have been derived that can be used to determine the amount of energy consumed in different sections of the reactor.

The power consumed by solid conveying is [67]:

$$E_w = \pi ND(\cos \theta_c) f_b W_b Z_b (P_2 - P_1) / \ln(P_2 / P_1) \quad 5.90$$

where,

$$\theta_c = 90 - \phi \quad 5.91$$

P_2 is the pressure at the end of the zone and P_1 is the pressure at the beginning of the zone.

The power turned into heat in the solid conveying zone is [67]:

$$E_h = \pi ND f_b W_b Z_b \frac{\sin \phi_b}{\sin(\phi_b - \theta_c)} \frac{(P_2 - P_1)}{\ln(P_2 / P_1)} \quad 5.92$$

(the definition of these variables can be found on pages 137 and 152)

The power absorbed in the melt pumping section of length dz is:

$$E_{dz} = \frac{\mu V_{bx}^2 B dz}{H} \left[4 \left(1 + \tan^2 \phi - \frac{6\dot{V}}{V_{bx} BH} \right) \right] + \frac{\mu V_{bx}^2 e dz}{\delta_f \cos \phi} \quad 5.93$$

The Power consumed in each melt pumping zone is given by [66]:

$$P_c = \frac{2\pi D^3 N^2 L \mu}{2(D_b - F_d)} \quad 5.94$$

where F_d is the diameter of the screw root plus the flight.

Viscous heat generation, \dot{E}_d , is defined as [71]:

$$\dot{E}_d = m \dot{\gamma}^{n+1} \quad 5.95$$

where m is the consistency index, n is the power law index, and $\dot{\gamma}$ is the shear rate.

The shear rate can be found by using [83]:

$$\dot{\gamma} = \frac{\pi DN}{H} \quad 5.96$$

The power (E) needed to drive the screw can be found using the following equations obtained from references [66], [69], [73] and [76] and multiplying the results by 2 (because of 2 screws).

$$E = p\mu N^2 (\pi D_b)^2 \frac{W}{H} \frac{L}{\sin \theta_b} f_g \quad 5.97$$

$$f_g = 4 - 3 \cos^2 \theta \left(\frac{Q_p}{Q_d} \right) + \frac{\mu_f}{\mu} \frac{H}{W} \frac{e}{\delta_f} \quad 5.98$$

$$Q_d = \frac{pV_{bz}WH}{2} \left(1 - \frac{\delta_f}{H} \right)^2 \quad 5.99$$

$$V_{bz} = pND_b \cos(\theta_b) \quad 5.100$$

where, p is the number of flights in parallel; μ is the viscosity; N is the Screw speed (RPM); D_b is the inside barrel diameter; W is the channel width; H is the channel depth; L is the length of the screw (axial distance); θ_b is the barrel helix angle; f_g is a geometrically determined factor; Q_p is the volumetric throughput; Q_d is the volumetric drag flow; μ_f is the average viscosity in the flight clearance; e is the width of the flight; δ_f is the flight clearance; and V_{bz} is the velocity in the down channel direction.

5.8 *Devolatilization*

Devolatilization (DV) is a thermodynamically driven process in which volatile material is separated from a less volatile material [70]. The dominant factors in DV are pressure, temperature and free volume available for separation. In DV, distributive mixing is essential to the success of the process while obviously, dispersive mixing is not critical to the process success [70]. Because most devolatilization processes only last a finite time, equilibrium is usually never reached and the final concentration of the volatiles will be greater than the equilibrium concentration in the melt [70].

In many polymer DV, the process is diffusion controlled because the diffusional mass flow rate (small diffusional constants) is usually lower than the convective mass flow rate [71]. In concentrated polymer solutions, the diffusion coefficients range from 10^{-8} to 10^{-12} m²/sec [70]. To increase the diffusivity of volatiles as its concentration gets low, one can add an inert substance, such as water, to reduce the weight fraction of the polymer [70].

When the volatile concentration is large, the mass transport of the volatile component will often occur by bubble transport because the viscosity of the liquid is relatively low [71]. This form of devolatilization is known as foam devolatilization. Foaming occurs at high levels of volatiles, while molecular diffusion occurs at lower level of volatiles [71].

Most devolatilization processes occur through a foaming mechanism [70]. Foaming in molten polymer usually occurs when the pressure is reduced or by purging with inert gas. Foaming is an essential part of DV since it increases the interfacial mass transfer area and so increases the separation efficiency [71]. The stages of removing

components from polymer melts are: foam formation, foam growth and rupture into a contiguous gas phase [71]. After nucleation reaches a threshold, vigorous foaming occurs, which may last from a few seconds to a few minutes. The inertial forces from screw rotation usually restrict the bubble growth and terminate the bubbles. “Flash” separation is usually observed with vacuum DV; hence, the RPM has a prominent effect on the DV process [71]. High RPM increases the internal pressure of the bubble and slows down bubble growth [71].

Another technique is that of flash DV in which the mixture is delivered to a flash point at high pressure and temperatures about the boiling point of the volatile component and then expanded through a nozzle [71]. Even though large amounts of volatiles are removed by this process, a second step, called a conventional melt film DV, is necessary [71]. In this step, the material in the film is continuously renewed. For this process, the rate of volatiles evaporation, \dot{E} , is expressed as [71]:

$$\dot{E} = X_e \dot{V}_f (C_o - C_e) \quad 5. 101$$

$$X = 1 - \frac{8}{\pi^2} \exp\left(-\frac{\pi^2 \lambda_f}{4\lambda_D}\right) \quad 5. 102$$

$$\lambda_f = \frac{t_f A_f}{\dot{V}_f} \quad 5. 103$$

$$\lambda_D = \frac{t_f^2}{D} \quad 5. 104$$

Where, V_f is the volumetric flow rate of the film; C_o is the initial volatile component concentration; C_e is the equilibrium volatile component concentration; X_e is the stage efficiency; λ_f is the exposure time; λ_D is the characteristic time for diffusion; t_f is the

thickness of the film; A_f is the surface area of the film; and D' is the molecular diffusivity of the volatile component.

5.8.1 Bubble nucleation (BN)

Bubbles are known to be the key active loci in foam DV; hence, it is good to have an understanding of bubble formation [70]. An essential step in DV is bubble nucleation, which occurs when the polymer melt is saturated with volatiles [70]. When another phase is generated in a meta-stable single phase, this occurrence is known as bubble nucleation. Bubble nucleation can either be homogenous or heterogeneous [70]. Homogenous BN happens when the dispersed gas is generated in the polymer matrix while heterogeneous BN takes place when a bubble nucleates at the interface of two different phases [70]. There exist relationships for rates of nucleation for both phases. However, the heterogeneous model contains several parameters that have to be determined experimentally for carpet, which of itself could be another dissertation topic. With that said, the homogenous model will be used as an approximation. The rate of homogeneous nucleation, J , is [70]:

$$J = N_d \frac{\sigma}{\eta} \left(\frac{\sigma}{kT} \right)^{1/2} \left(1 - \frac{P_L}{P_1} \right) \exp \left(\frac{-16\pi\sigma^3}{3kT(P_v - P_L)^2} \right) \quad 5. 105$$

where N_d is the number density of molecules the liquid, k is Boltzmann's constant, P_v is the vapor pressure, P_L is the pressure in the liquid, P_1 is defined as [70]:

$$P_1 = P_L + \frac{2\sigma}{r_c} \quad 5. 106$$

where σ is the surface tension and r_c is the critical radius. The surface tension is approximated by [70]:

$$\sigma = 5.2E10 - 8\delta^{4/3} \quad 5. 107$$

To find the pressure, the Flory-Huggins relationship for polymer-solvent mixtures can be used and it is described [71]:

$$\ln \frac{\bar{P}}{P_0} = \ln(1 - V_p) + \left(1 - \frac{1}{x_n}\right)V_p + \chi V_p^2 \quad 5. 108$$

where \bar{P} is the effective partial pressure of the volatile component; P_0 is the vapor pressure of the pure volatile component ; x_n is the degree of polymerization; V_p is the volume fraction of the polymer; and χ is the interaction parameter. An estimation for χ is [70]:

$$\chi = 0.35 + \frac{\tilde{V}_1}{RT} (\delta_1 - \delta_2)^2 \quad 5. 109$$

where \tilde{V}_1 is the solvent molar volume and subscript, 1, is for the solvent. High values of χ represents very poor compatibility while negative values shows strong affinity of the polymer for the volatile compounds [70]. If the solvent and polymer is chemically similar then χ is between 0.3 and 0.5, if fully miscible then χ is 0.4 and if not fully miscible χ is 0.5 [71].

5.8.1 Bubble growth

Crucial to the DV process is the growth of bubbles containing vapor of the volatile material. During DV, the rate of bubble growth depends on the rate at which the volatiles can diffuse from the bulk to the surface and the resistance of the polymer to the displacement of the growing bubble [70]. Bubble growth is due to the diffusion of volatile material from the liquid bulk and its vaporization at the bubble surface into a gaseous phase that stays within the confines of the growing bubble [70]. Bubble growth is usually controlled by mass transfer and both steady state and non-steady state mass transfer can be used to determine the approximate size of the bubbles [70]. Generally, in the study of bubble growth, heat transfer is neglected because the heat of vaporization has an insignificant effect on the temperature profile when the volatiles concentration is low [70].

The assumptions made when determining the bubble growth rate are [70]:

- Bubbles are spherical
- Vapor in a bubble is an ideal gas
- Pressure in a bubble is constant
- Isothermal process
- Large bubbles so that the surface tension does not contribute to pressure in bubble
- Negligible viscous normal stresses
- Newtonian fluid
- Constant diffusion coefficient
- Deformation from rotating equipment is not accounted for, which causes increase in surface area compared to the spherical bubble of the same shape

- Single bubble growth in a infinite medium; secondary bubbles that might coalesce are not accounted for.

Since there are so many assumptions, the following equation may have limited applicability and should only be used as a first approximation.

Upon integrating the continuity equation in spherical coordinates and substituting the radial velocity component, one gets the molar concentration of the volatile component, which is defined as [70]:

$$\frac{\partial C}{\partial t} + \frac{dR_b}{dt} \left(\frac{R_b}{r} \right)^2 \frac{\partial C}{\partial r} = D_f \left[\frac{1}{r} \frac{\partial}{\partial r} \left(r^2 \frac{\partial C}{\partial r} \right) \right] \quad 5. 110$$

with the initial and boundary conditions being:

$$C = C_s \text{ @ } r = R_b \quad 5. 111$$

$$C = C_\infty \text{ @ } r \rightarrow \infty \quad 5. 112$$

$$C = C_\infty \text{ @ } t = 0 \quad 5. 113$$

If one assumes steady state diffusional mass transfer then

$$\frac{\partial}{\partial r} \left(r^2 \frac{\partial C}{\partial r} \right) = 0 \quad 5. 114$$

and solving to get

$$C = C_\infty - (C_\infty - C_s) \frac{R_b}{r} \quad 5. 115$$

The flux is then defined as

$$N_f = \frac{D_f}{R_b} (C_\infty - C_s) \quad 5. 116$$

where, D_f is the diffusivity.

The size of the bubble at any given time is:

$$R(t) = \sqrt{R_0^2 + 2F_m Dt} \quad 5. 117$$

where,

$$F_m = \frac{RT(C_\infty - C_s)}{P} \quad 5. 118$$

F_m indicates the tendency to foam; high F_m enhances bubble growth, so one would want to have high temperature and low pressure and a large concentration difference between the bulk and the surface of the bubble [70].

If unsteady state diffusional and convective mass transfer is accounted for then the concentration in the bubble has to be solved for numerically, however the size of the bubble as a function of time can be approximated for two cases: slow growth and fast growth [70]:

$$R(t) = \sqrt{2FmDt} \quad 5. 119$$

and

$$R(t) = 2\sqrt{\frac{3}{\pi}Fm\sqrt{Dt}} \quad 5. 120$$

respectively.

The viscosity of the polymer melt may also control the growth of bubbles. For unsteady-state viscosity-controlled growth, the size of a bubble at any given time is:

$$R(t) = R_{cr} + (R_0 - R_{cr}) \exp \frac{(P_B - P_\infty)t}{4\mu} \quad 5.121$$

with,

$$R_{cr} = \frac{2\sigma}{P_B - P_\infty} \quad 5.122$$

where, subscripts B and ∞ indicate of the bubble and far away from the bubble, respectively.

5.8.3 Extruder configuration for devolatilization

In a typical vent zone, the screw channels are partially filled [70]. The screw section under the vent should not be filled; otherwise, there is no path for the volatiles to escape [85]. If there is a positive pressure in the vent region, the polymer will flow out of the vent [85]. In the apex region of a CRNI extruder, there is compression and decompression occurring, which allows improved surface renewal and hence the superior DV [70]. The stretching and extensional flows promote the bubble nucleation and growth. A large melt-gas interface can be provided by increasing the number of channels by using multiple flights, and only partially filling them through starve-feeding [66]. If the RPM is sufficiently high, one will get good “surface renewal” [66]. Tangential extruders provide large free volume for effective gas-melt interaction and enhanced traverse mixing with reorientation of streamlines [66].

Vent ports are usually elongated to increase the vapor release area and are “arranged tangentially above the down-going side of the screw”, while “the trailing edge is well chamfered to assist in re-entrainment” as shown in Figure 5.16 [67].

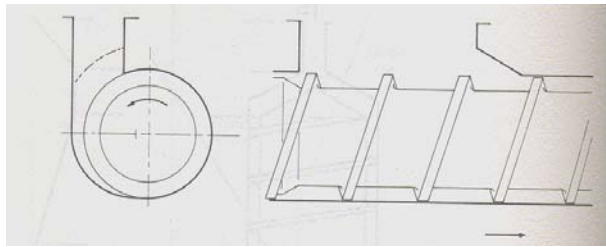


Figure 5.16: Design of vent for vacuum extraction [67]

The pressure is usually reduced to zero under the vent so a shallow channel section is usually put in to raise the pressure before the die [67]. An increase in die pressure will tend to cause vent blockage [67]. The screw channel must be only partially filled at the vents to allow vapor release [67].

Since the polymer melt has to adhere to the barrel in order to convey, it is inevitable that there is a build up of polymer in the vents, hence periodic cleaning is needed [71] to maintain DV efficiency. To minimize this buildup, the leading edge of the vent ports are undercut, see Figure 5.17 [71].

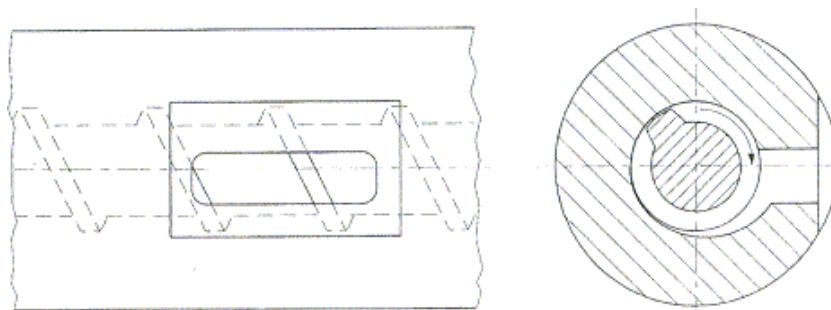


Figure 5.17: Vent port showing undercut [71]

5.8.4 Single screw DV

The exposure time of the wiped film, λ_f , is defined as [71]:

$$\lambda_f = \frac{1-Y}{N} \quad 5.123$$

where N is the screw speed and Y is the fraction of the channel width that is occupied by the melt pool (the degree of fill). Optimum screw speed for mixing and DV is around 400-500 rpm [70].

The exposure time of the melt pool λ_p , is defined as [70]:

$$\lambda_p = \frac{H}{V_{bx}} \quad 5.124$$

where, V_{bx} is the cross channel component of the barrel velocity

$$V_{bx} = pND_b \sin(\theta_b) \quad 5.125$$

If the backmixing effect is neglected, the dimensionless mass balance for the volatile component in the melt is

$$\frac{d\hat{C}}{d\hat{z}} = -E_x \hat{C} \quad 5.126$$

where, the $\hat{\cdot}$ represents the dimensionless variables and

$$\hat{C} = \frac{C - C_e}{C_o - C_e} \quad 5.127$$

$$\hat{z} = \frac{z}{L} \quad 5.128$$

$$E_x = n_f + k_p HL / Q_p \quad 5.129$$

$$n_f = \frac{v_{bx} H_f L}{\hat{V}} \quad 5.130$$

$$k_p = \left(\frac{4D'}{\pi \lambda_p} \right) \quad 5.131$$

$$\hat{C}(0) = 1 \quad 5.132$$

$$\hat{C} = \exp\left(-E_x \hat{z}\right) \quad 5.133$$

5.8.5 Twin screw devolatilization [71]

Currently, there aren't any models available for the DV of a CRNI extruder. However, there exists one for intermeshing co-rotating extruder. The following shows the derivation of this model.

The mass balance on volatile species around the first exposure, i.e. one flight, is:

$$Q_p C_o = Q_p C_1 + \dot{E}_1 \quad 5.134$$

where,

$$\dot{E}_1 = A_e C_o \left(\frac{4D'}{\pi\lambda} \right)^{1/2} \quad 5.135$$

C_o is the concentration of volatiles in the feed to the extruder; C_1 is the average concentration of volatiles remaining after the end of first exposure interval; Q_p is the volumetric flow rate; \dot{E}_1 is the average rate of evaporation in the first exposure interval; A_e is the area for evaporation [units of length squared for the time exposed].

For intermeshing extruders,

$$A_e = f_o A_t \quad 5.136$$

where, A_t is the total leading face of a 360° section of a single screw and f_o is the ratio of the channel area outside the intermeshing region to that of the area inside the intermeshing region.

In this case exposure time is:

$$\lambda_p = \frac{f_o}{N} \quad 5.137$$

and substituting in the above gives:

$$\dot{E}_1 = AC_o \left(\frac{4Df_o N'}{\pi} \right)^{1/2} \quad 5.138$$

Again substituting back into the mass balance one gets:

$$\frac{C_1}{C_o} = 1 - \frac{A_f}{Q_p} \left(\frac{4D'}{\pi\lambda} \right)^{1/2} \quad 5. 139$$

for the first exposure. For the sequence of n_e exposures, it yields:

$$\frac{C_n}{C_o} = \left[1 - \frac{A_f}{Q_p} \left(\frac{4D'}{\pi\lambda} \right)^{1/2} \right]^{L_e / \bar{b}} \quad 5. 140$$

where

$$n_e = \frac{L_e}{\bar{b}} \quad 5. 141$$

and L_e is the total exposure length of the screws and \bar{b} is the mean flight thickness.

Since there is no model for the non-intermeshing extruders, the above can be modified by using a different equation for the area for evaporation, A_e in equation 5. 136 by:

$$A_e = \left(W_a + 2 \frac{x_a}{360^\circ} \pi D_b \right) \Delta z \quad 5. 142$$

where x_a is the angle of one screw that is exposed and

$$\Delta z = Y \pi D \cos \theta \quad 5. 143$$

where Y is the degree of fill

The exposure time is

$$\lambda = \frac{H}{pND_b \sin(\theta_b)} \quad 5.144$$

which is taken from the definition of single screw. Therefore, for n exposures in a non-intermeshing extruder the concentration ratio is:

$$\frac{C_n}{C_o} = \left[1 - \frac{\left(W_a + 2 \frac{x_a}{360^\circ} \pi D_b \right) Y \pi D \cos \theta}{Q_p} \left(\frac{4D' pND_b \sin(\theta_b)}{\pi H} \right)^{1/2} \right]^{L_e / \bar{b}} \quad 5.145$$

5.9 Scale up

Scaling up reactive extrusion processes is very complicated [76]. The surface-to-volume ratio increases as the screw diameter decreases and is very large for small extruders [76]. So for big extruders the relative amount of heat transfer in large extruders is much lower than that of smaller ones [76]. Furthermore, larger machines tend to have a increasing radial temperature difference because the heat released in the middle of the channel has to be transferred over a larger distance [76]. Critical to scale up are: fluid mechanics, mass transfer, heat transfer, and mechanical integrity [70].

When scaling up, to have the same residence time in the large extruder as in the small extruder, the L/D ratio, mixing characteristic, and volume will increase with the cube of the diameter, but the surface only increases by the square of the diameter. Hence, as the diameter increases, the surface to volume ratio decreases inversely. It should be

noted that it is not a good practice to scale from 20 and 30 mm extruders to commercial extruders since capacity will usually be overstated. It is better to scale from 50 mm because the temperature distribution won't be that much different [66].

NFM Welding Engineering, Inc. experience is to “Scale H and W linearly with R , but decrease N slowly (but still increase $2RN$ or U) so that Q increases with the 2.5 power of screw radius” [69]. In the conventional scale up method for a CRNI extruder, the screw speed is held constant while the channel depth is increased as a ratio to the diameter (H/D is held constant) [74]. The flow rate is scaled as the 2.75 power of the diameter ratio. By doing this the shear rate in the screw channel is kept constant. The shear rate in the screw channel is defined as [74]:

$$\dot{\gamma} = \pi DN / H \quad 5. 146$$

With the conventional scale-up, even though the shear rate is kept constant, the filled length is not, so a new scale-up rule is presented that keeps both constant [74]. In this new scale up rule, the screw speed and the channel depth are both reduced in such a way that the ratio of ND/H is constant; i.e. the diameter ratio is raised to the 0.88 power for the channel depth and -0.12 for the screw speed [74].

For scaling the die, the following equations can be used to maintain a constant pressure drop so that operation would be under the same conditions [86]:

$$\frac{D}{D_0} = \left(\frac{Q}{Q_0} \right)^{0.333} \quad 5. 147$$

$$\frac{L}{L_0} = \left(\frac{Q}{Q_0} \right)^{0.333} \quad 5.148$$

Other scaling up relationships that are recommended are:

Capacity [66]:

$$\frac{Q_2}{Q_1} \propto \left(\frac{N_2}{N_1} \right) \left(\frac{D_2}{D_1} \right)^3 \quad 5.149$$

Power [66]:

$$\frac{E_2}{E_1} \propto \left(\frac{N_2}{N_1} \right)^2 \left(\frac{D_2}{D_1} \right)^3 \quad 5.150$$

Heat transfer area [66]:

$$\frac{A_2}{A_1} \propto \left(\frac{D_2}{D_1} \right)^2 \quad 5.151$$

Screw speed [66]:

$$N_2 \propto N_1 \left(\frac{D_2}{D_1} \right)^{-0.5} \quad 5.152$$

The scaling method used in modeling the process will be discussed in Chapter 6.

CHAPTER 6

MODEL DEVELOPMENT AND EXPERIMENT METHODS

Reactive extrusion is a very complex process with several variables that can affect the output of products. To understand how these different variables affect production and to determine ways to optimize the process, a model was made of the depolymerization of nylon 6 in an extruder. In this chapter, a description of the model is given then the methods used to verify the model is discussed.

6.1 Basis of the Extruder

The model developed in MATLAB for the depolymerization was done using the screw configuration of a 30 mm NFM counter rotating non-intermeshing twin screw extruder (CRNI). Figure 6.2 shows the screw profile of this extruder (the numbers indicate the different screw segments). The screw configuration includes: two cylinders, a reverse element, and three tapered elements. As stated in Chapter 5 on page 136, CRNI's screws have different lengths. The longer screw (single screw section) is used to build up pressure to pump/discharge the extrudate through the die [66, 70]. The pressure through the die affects the filled lengths of the screw sections. In this model, the die dimensions used are: length - two inches and the inner diameter - one inch.

Based on the operating range provided by NFM for the CRNI extruder, as shown in Figure 6.1, the capacity of this extruder is 100 lb/hr. Both ends of the operation limit (torque and excess surge) were tested in the model development to see how they affected

conversion; these results will be discussed below. Because of these results, in this model, if the throughput is greater than 10 lb/hr, the dimensions for the extruder were scaled up to ensure that there sufficient heat exchange area for the amount of material. The program for this model is applicable for flow rates between 10 and 1500 lb/hr.

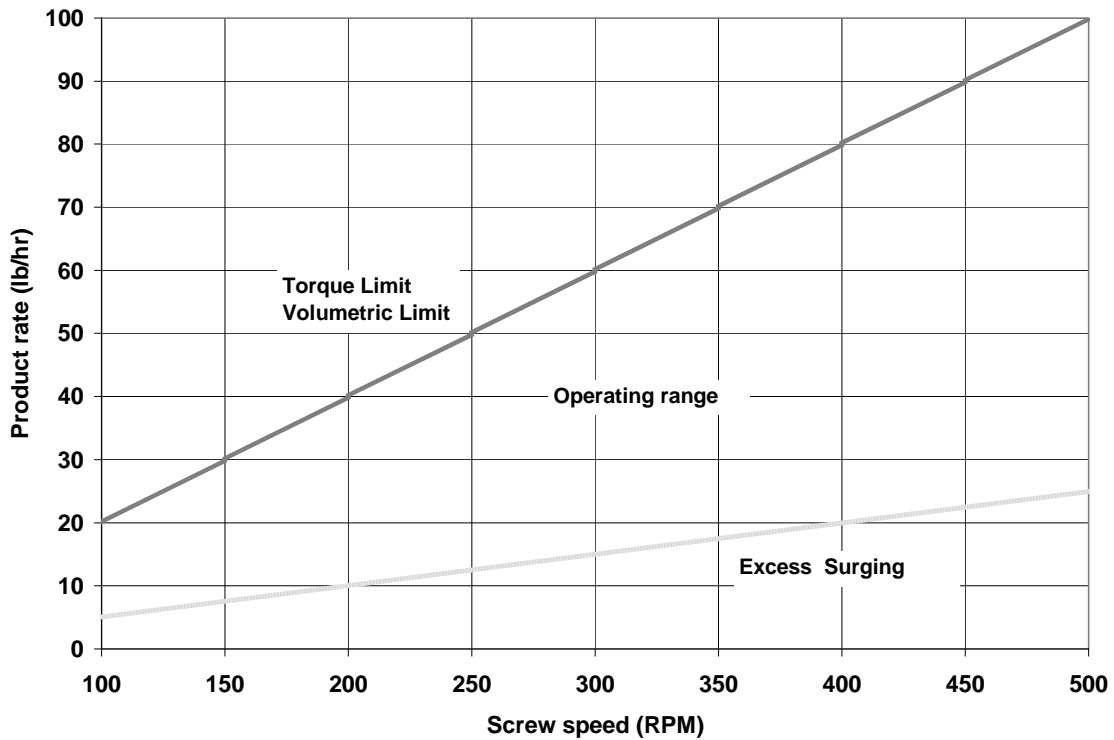


Figure 6.1: Operating range of the 30 mm NFM twin screw extruder

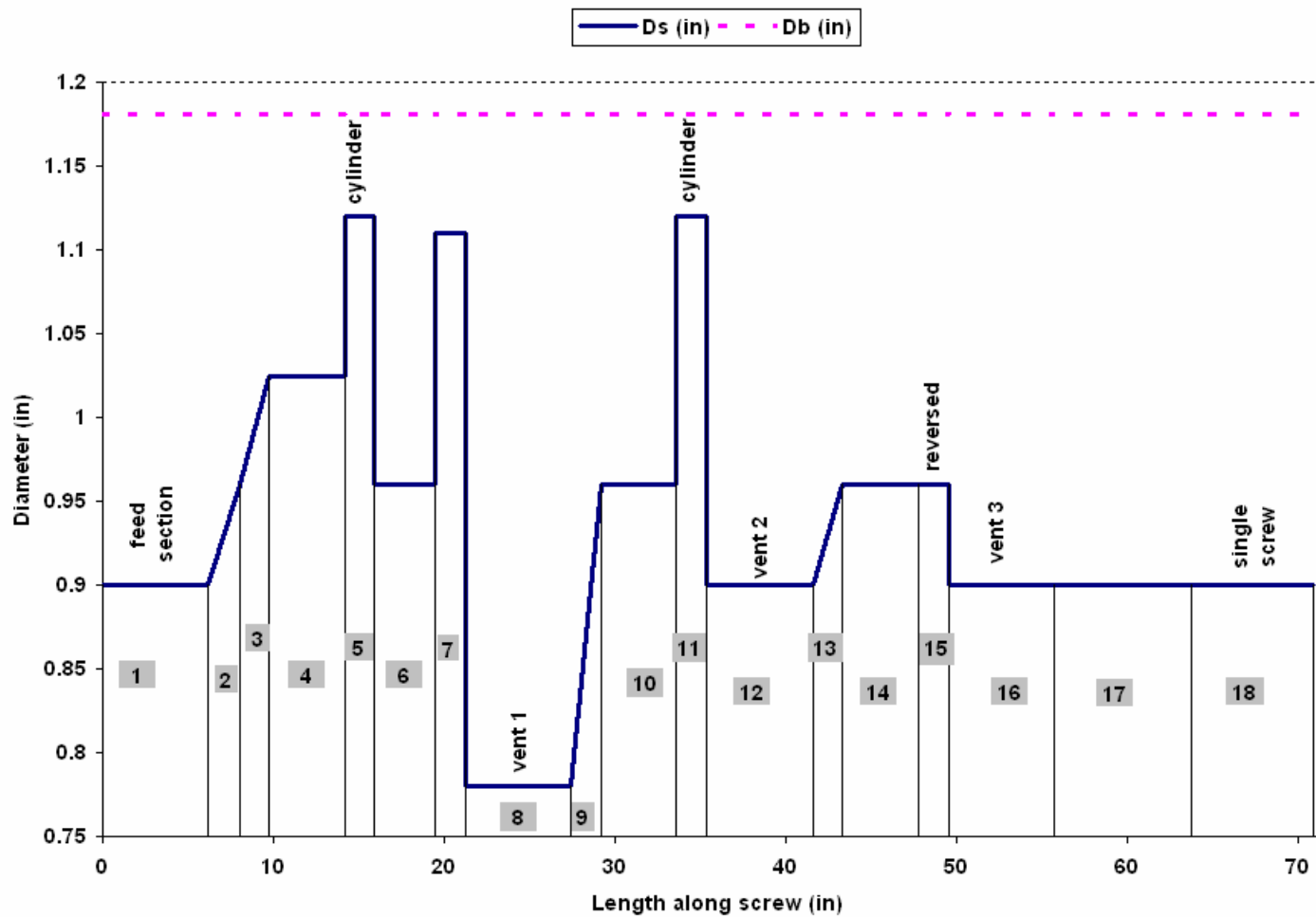


Figure 6.2: Screw profile of the 30 mm counter-rotating non-intermeshing twin screw NFM extruder used in the depolymerization process

6.2 Variables in the Model

Figure 6.3 shows the interrelations between some of the variables accounted for within this model. One of the most important variables in any extrusion process is the throughput. The throughput ultimately controls the product rate and profit through affecting the residence time, the die pressure, the backflow and the heat transfer coefficient. As shown in Figure 6.1, the throughput can also determine which screw speed is used. Together, the throughput and screw speed determine the amount of backflow, which in turn with the help of the screw speed shape the pressure gradient and influence mixing. In addition to controlling the backflow, pressure gradient and mixing, the screw speed also affects the heat transfer coefficient and ultimately the temperature. This temperature affects the viscosity, the speed of the reaction and the rate of devolatilization.

The die pressure (which is affected by the throughput, the die geometry, and the viscosity) along with the pressure gradient govern the fill length in the extruder. This fill length together with the throughput affects the residence time which in turn affects the conversion. The conversion also changes the viscosity. Initially as the reaction proceeds, lower molecular weight compounds are formed which will cause the average viscosity to decrease, but as they produce smaller molecules that are devolatilized, the cross-linked compounds and catalyst concentration increase and therefore increase the viscosity. As seen by this pattern, the rest of Figure 6.3 should be self explanatory.

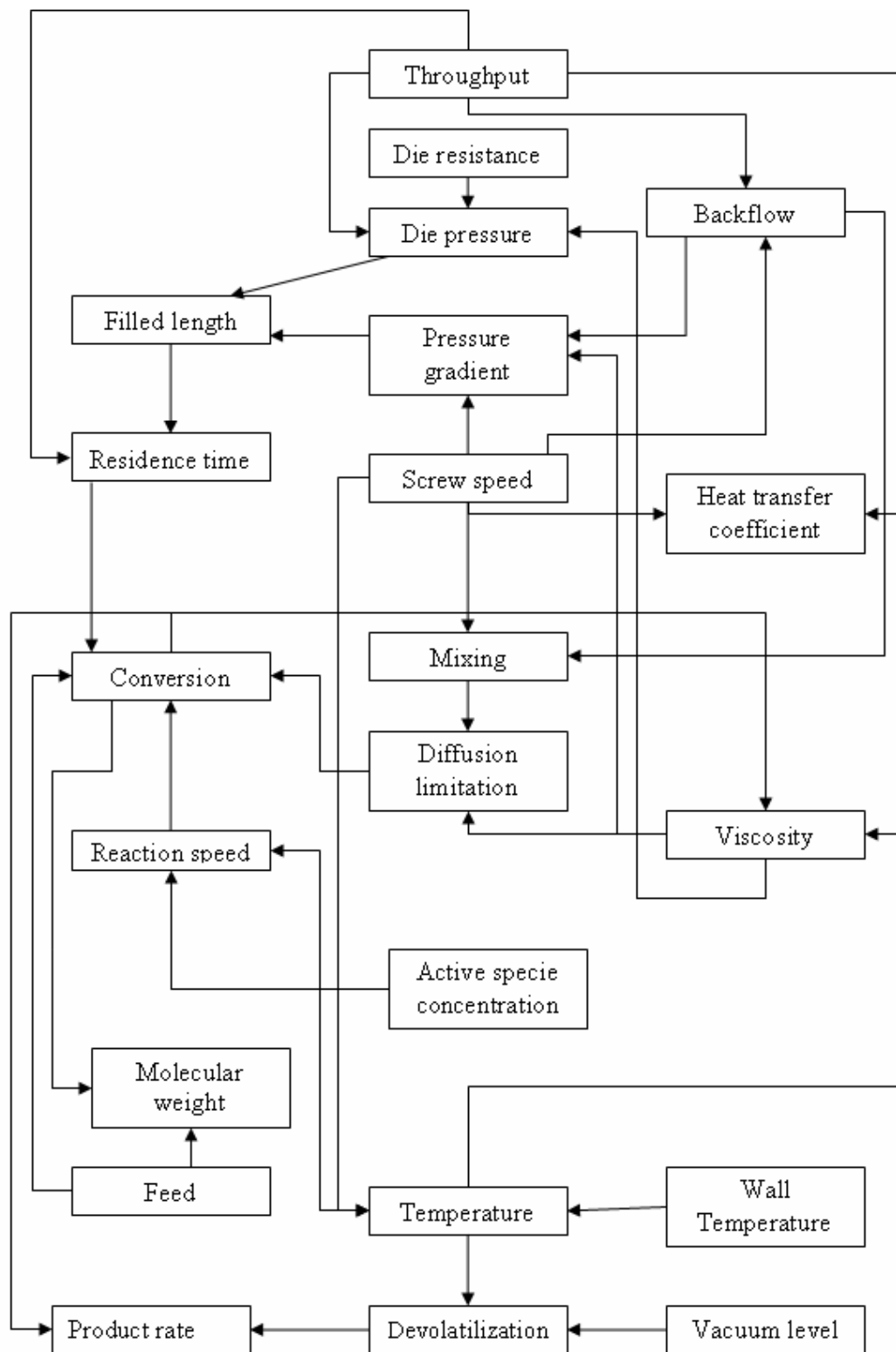


Figure 6.3: Variables accounted for in extruder depolymerization model (modified from reference [76])

6.3 Functions in the Model

The main function for the simulation is the “rxnzone2”. Figure 6.4 and Figure 6.5 show the flowchart of this function. “rxnzone2” calls several functions; the workings of these functions will be discussed later and their codes are given in the Appendix. The first function that “rxnzone2” calls is “feedinfo” then “screwdim” followed by “Meltzone”. With the returned information from the first three function, “rxnzone2” then predicts a value for the die flow rate and the other zones. Thereafter, it calls the “Pressure” which returns the filled volume for each segment. Then for each segment, beginning with segment four (where the reaction starts), “rxnzone2” calls “integrator3”, whose outputs include the temperature, conversion, and product flow rate.

After receiving the conversion for the first zone, “rxnzone2” then determines the flow rate of the next segment (taking into account if there is venting) and calls “integrator3” until the conversions for all the segments are found. Following the determination of the new flow rates, “rxnzone2” then compares them to the previously determined flow rates. If the flow rates do not agree within a certain error range, “rxnzone2” then uses the newly found flow rate as a prediction of the flow rate and recalculates the degree of fill and everything that follows that; this iteration is repeated until the difference between the new flow rates and the previous flow rates are within a certain error range. When they are within a certain error, “rxnzone2” then sends the dimensions, temperatures, conversions and flow rates for each zone to an Excel file called “Extrud sim results” on Sheet 1.

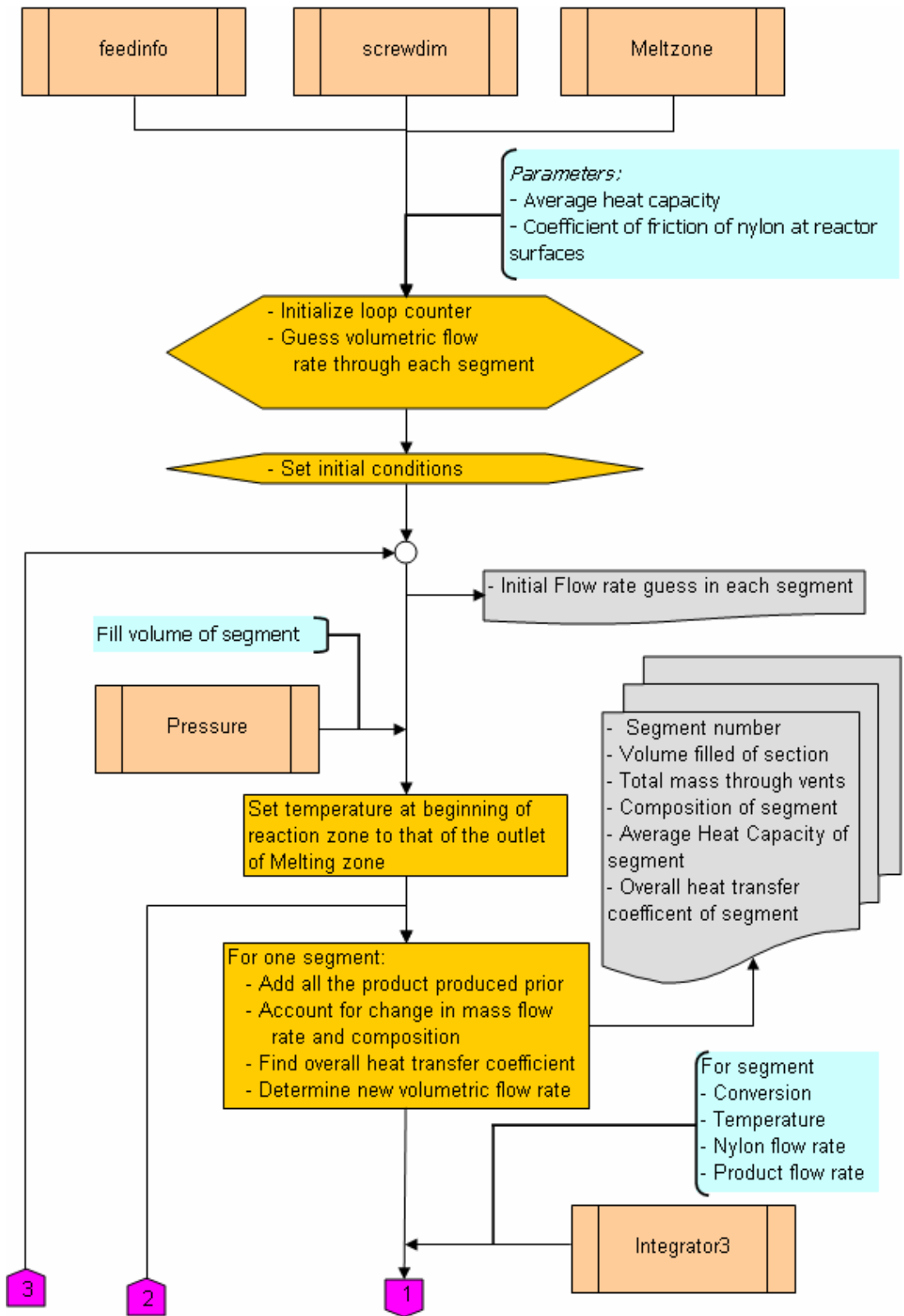


Figure 6.4: Part A of the Flowchart of the "rxnzone2" function

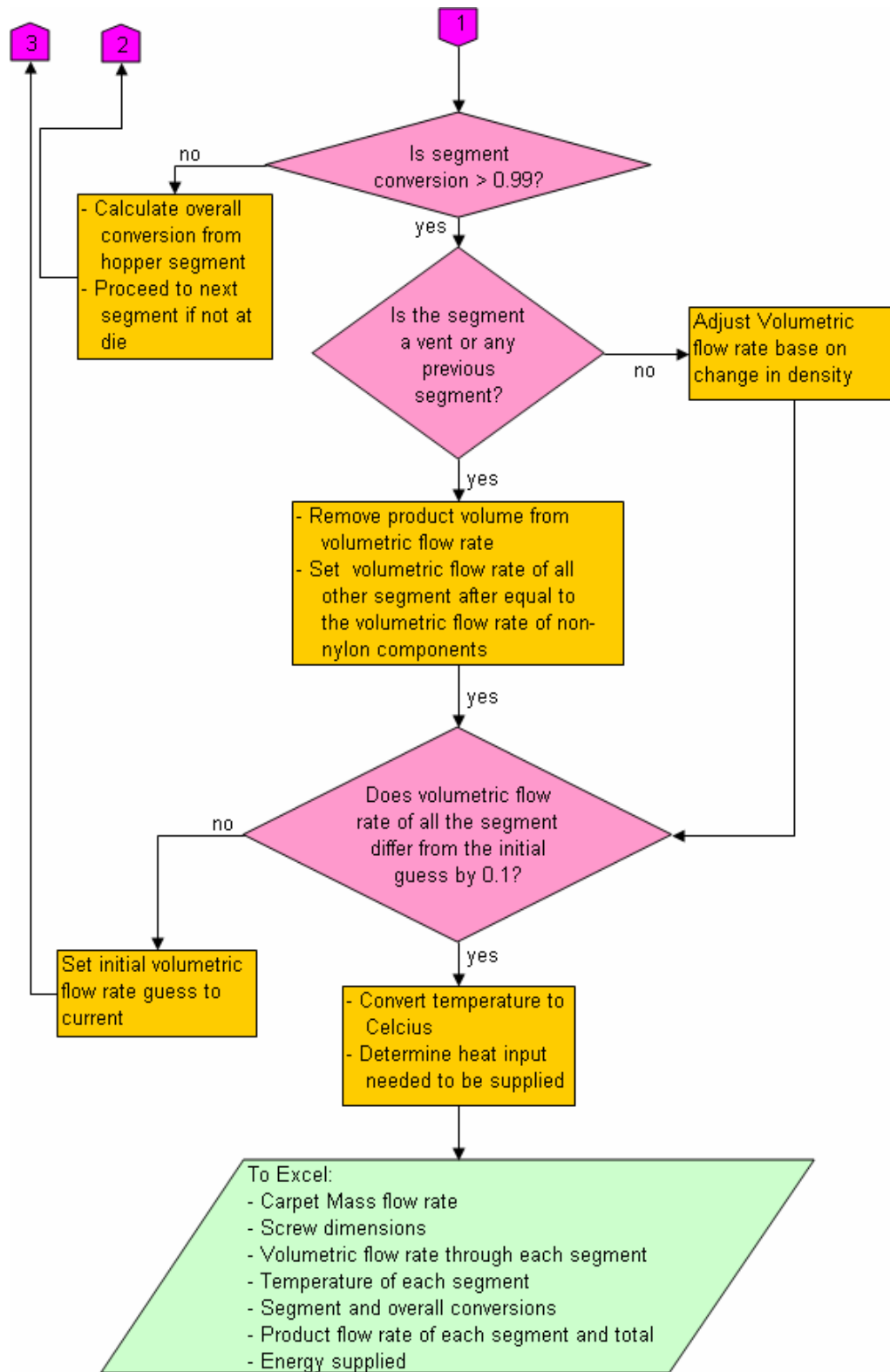


Figure 6.5: Part B of the Flowchart of the “rxnzone2” function

6.3.1 Function “feedinfo”

In the function “feedinfo” (flowchart in Figure 6.6), the carpet feed flow rate, its composition, as well as the physical properties of the components are listed. These parameters for the feed are also used in other functions. The compositions of post consumer carpet used in “feedinfo” were taken from the thesis of Jin who did DSC analysis of pelletized carpet and can be found in Table 6.1 [87].

Table 6.1: Composition of carpet used in model [87]

Carpet Face Yarn	wt % of components				
	Nylon 6	Nylon 6,6	Polypropylene	SBR	CaCO ₃
Nylon 6	77	0	11	6	6
Nylon 6,6	0	81	8	6	5

There is a discrepancy between these values and those reported by Wang given in Chapter 2 [5]. This discrepancy can be due to the shredding, extrusion and then pelletizing of the carpet. By shredding some of the backing material may fall out, as well as some dirt. During the extrusion process, there is a filter placed before die to remove solid components; hence, some CaCO₃ and dirt, which do not melt, will be removed. In the “feedinfo” function, the assumed inlet temperature of the carpet is 25 °C.

The barrel temperature for the reaction zone, T_b , is set for 325°C (the highest that could be reached in the lab), but can be changed for case studies. The temperature for the melting zone, T_{bmelt} , is set at 240 °C. “feedinfo” calculates the screw speed based on the mass flow rate of the carpet. If the mass is greater than 10 lb/hr, this value will not be used, but is determined in the function “screwdim”. In “feedinfo” there is the option to manually input the end of the operating range to use to test which end provided the better

yield. Depending on which limit is used, that line would be uncommented (removal of the % sign) and the other operating range lines would be commented.

As stated above, the “feedinfo” contains a few parameters for the components used in the model. The parameters, their values and the source from where they were taken are listed in the Appendix.

The outputs of “feedinfo” are the: feed temperature, total feed flow rate, temperatures of barrel sections, screw speed, solid total volumetric flow rate, and for each component: (composition, mass flow rate, solid and melt densities, heat capacity, and volumetric flow rate).

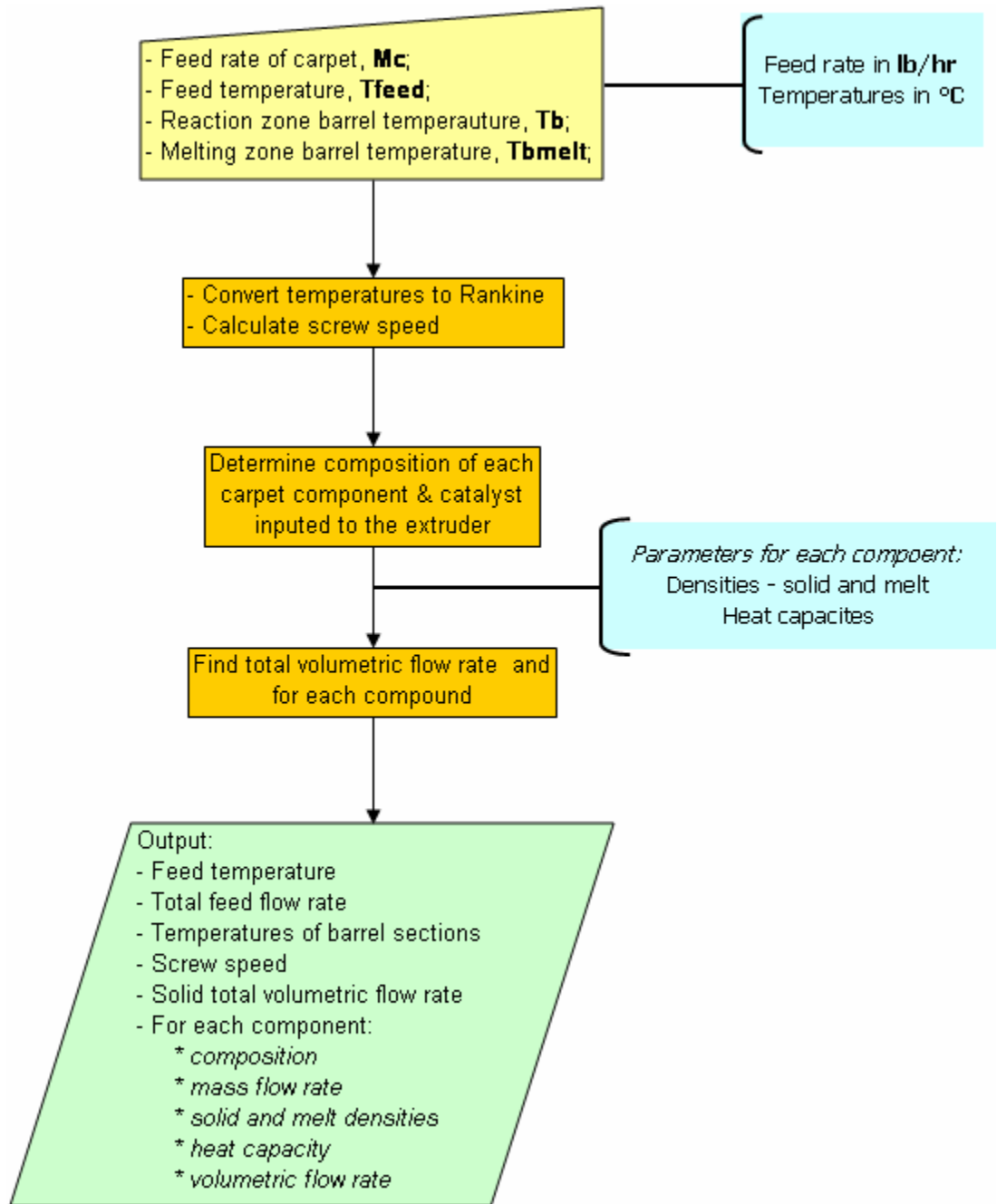


Figure 6.6: Flowchart of the “feedinfo” function

6.3.2 Function “screwdim”

The second function that “rxnzone2” calls is “screwdim” (see flowchart in Figure 6.8 and code in the appendix). “screwdim” in turn calls “feedinfo”. From the information of “feedinfo”, the function “screwdim” does the scaling dimension for the extruder at the capacity required by using the dimensions of the screw segments of the 30 mm extruder in the lab (see Figure 6.2 and the Appendix). (To test the limits of the extruder the non-scaling option was used as shown in the code.) In the traditional scaling factors presented in Chapter 5, the diameter is scaled based on a ratio of the volumetric throughput. When this was done for this reactive extrusion process, the temperature requirement was not met because of insufficient surface area. In addition, based on these scaling factors, the diameter of the barrel was outside the range of current commercial extruders. (Before scaling was done, it was found that the surface area of the 30 mm extruder was only sufficient to provide enough heat for 10 lbs/hr because of the endothermic nature of the reaction. This was one tenth of the capacity of that the machine.) To compensate for this, the diameter required was determined from Figure 6.7, which contains a plot of various barrel diameters and the corresponding flow rates that are available in commercial extruders. A power fit was best for the data and yielded the following:

$$D_b = 0.5211M^{0.376} \quad 6.153$$

where, D_b is the barrel diameter in inches and M is the mass flow rate in lb/hr.

Subsequently, the flight diameter was scaled. (The channel depth, H , was not scaled since the smaller H creates more friction, and hence, more heat for the endothermic reaction.)

Two different scaling ratios were used for the length. If the mass flow rate was less than 100 lb/hr, the following formula was used:

$$L_2 = L_1(D_2 / D_1)^2 \quad 6.154$$

where, subscripts 1 and 2 represent the un-scaled and scaled dimensions. This formula is inspired from the heat transfer scaling given in Chapter 5. However, when it was applied to higher flow rates, conversions were reached way before the single screw section, so the exponent 2 was reduced to 1.4, which allowed enough conversion while utilizing most of the extruder length.

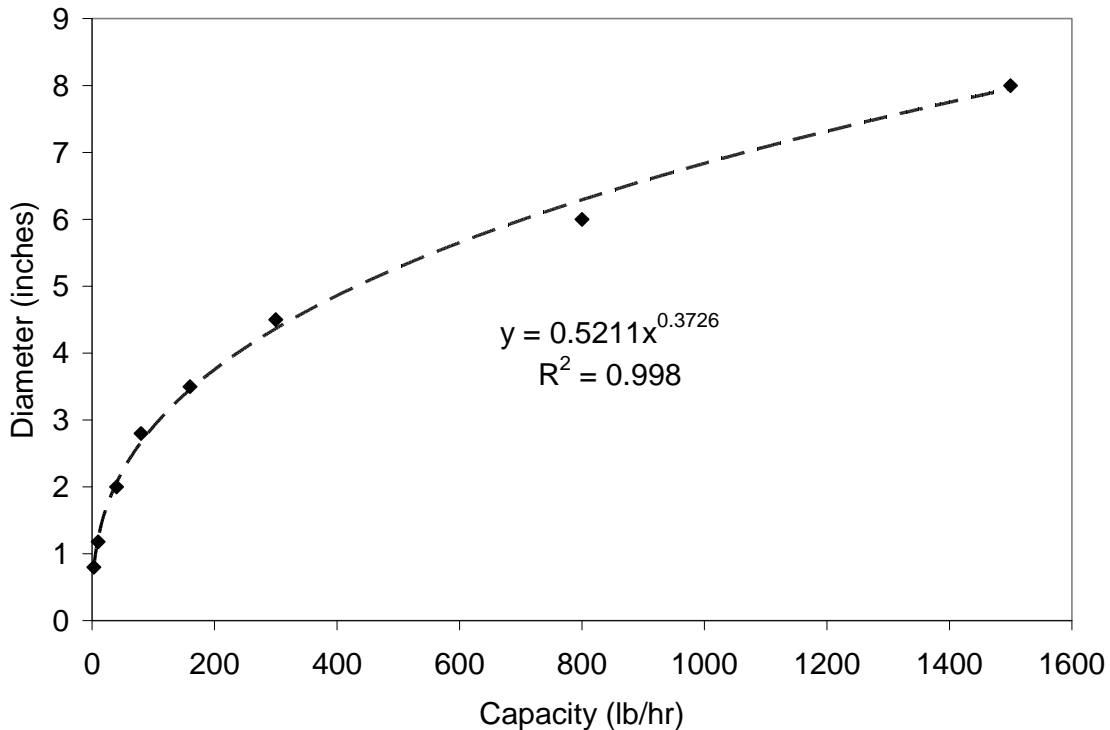


Figure 6.7: NFM/WE Machine diameter with one tenth of their regular capacity [88]

From these scaled lengths and diameters, the pitch, the flight width, the channel width, the helical length, the screw speed, and the angle of the screw helices were determined for each segment (the equations used to find these values can be found in section 5.1.2).

After scaling is completed, the next step is to find the volume in which the feed components can flow through. Since the length for each segment is given, the (average) cross-sectional area of each segment has to be found. To do this, the cross-sectional area of the screw is subtracted from that of the barrel (since the barrel is hollow and the screw is solid). Since the geometry of both is not common, the way in which this was done is presented on below. This function also determines the directional velocity of the barrel (based on the assumptions in modeling that the barrel instead of the screws is rotating as discussed in Chapter 5), the shear rate, the average viscosity based on shearing, and the energy dissipated. All these are the outlet of the function, “screwdim”.

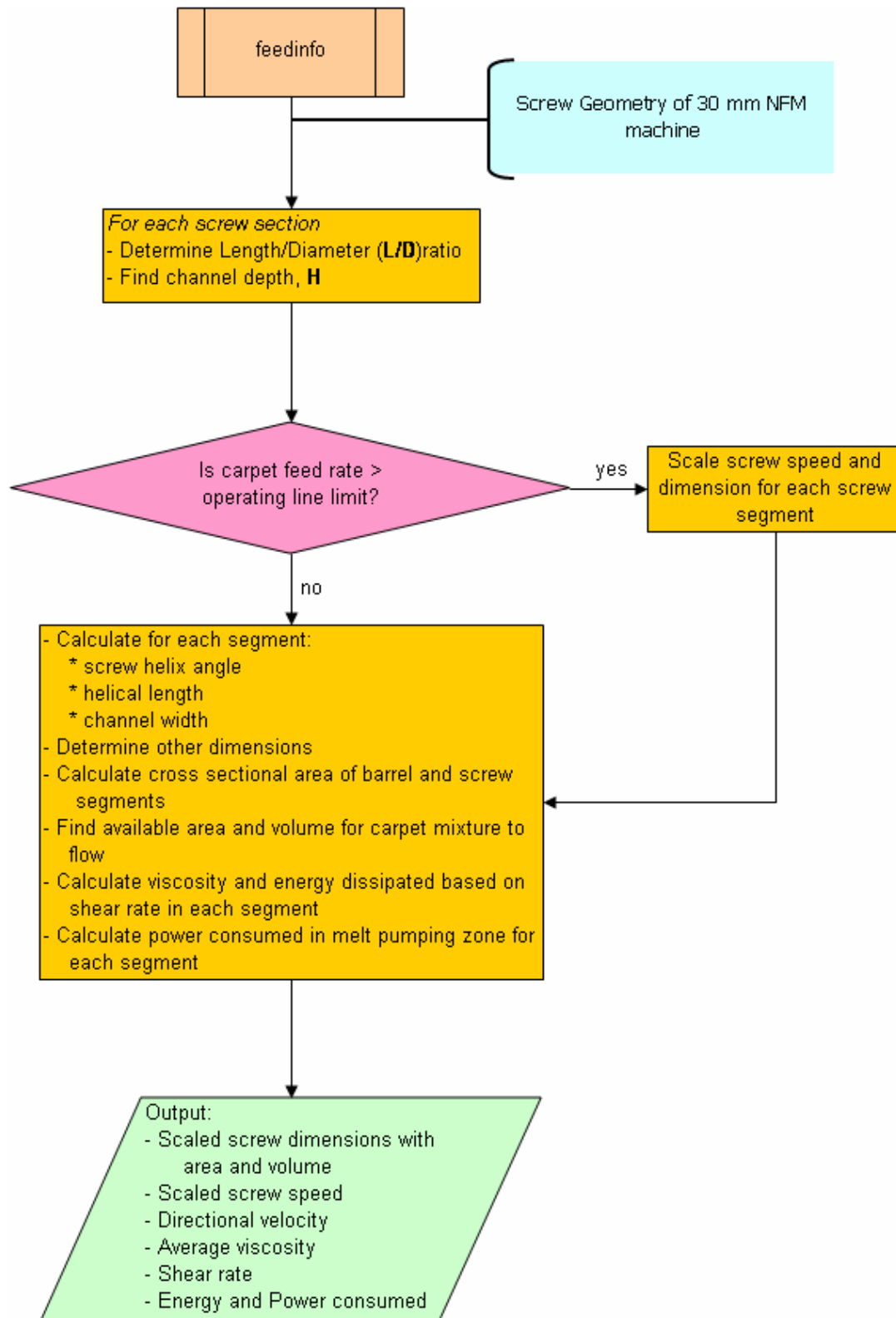


Figure 6.8: Flowchart of the “screwdim” function

6.3.2.1 *Finding the barrel cross-sectional area*

Figure 6.9 shows the cross sectional area of the barrel chamber. (The diameter of each chamber is 30mm.) Since the extruder is tangential, if these barrels were represented by two circles they would be touching each other tangentially. However, since plastic has to flow from one chamber to another, a gap (known as the apex) is made at this tangent, so one cannot see this tangential touching.

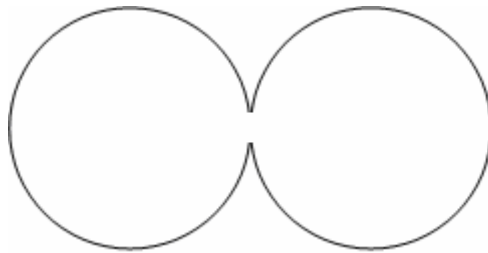


Figure 6.9: Cross-sectional area of the CRNI extruder barrel

Figure 6.10 shows this gap that is removed from the barrel wall. To find the cross-sectional area of the barrel this gap area has to be found by several geometric calculations. This gap is symmetrical along the tangent and so the derivation is done by considering the top section of the gap. Since the gap is not huge, one can approximate the gap using a triangle as shown in Figure 6.11.

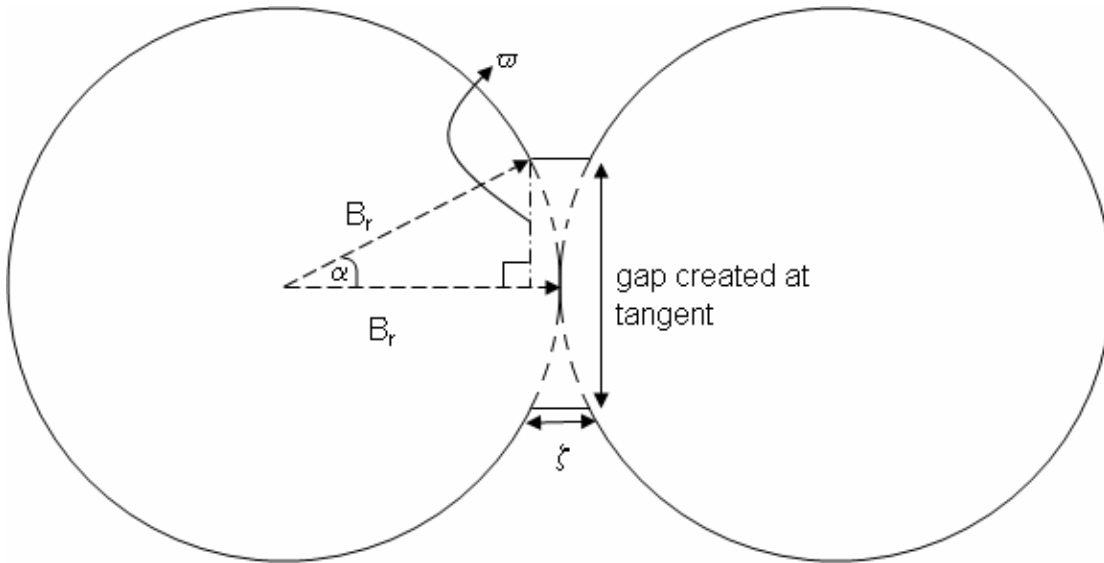


Figure 6.10: Barrel cross section showing the gap removed

In Figure 6.11, the gap area is represented by triangle *I*. To find the area of this triangle one must first find the height (which is equivalent to one half the gap length, w) and the base, ζ . w had to be measured in the lab since the length of this gap was not given by the manufacturer, and it was found to be 5 mm. The length of the base can be found thusly:

- Using w , the barrel radius (B_r), and the sine function, the value of ρ can be determined.
- With ρ in hand, c can be found using B_r and the cosine function.
- o is then the difference between B_r and c .

- Since triangle 1 is an isosceles, o is equivalent to 0.5ζ . (To verify, draw a vertical line from the center of ζ , to the base of triangle 3, this should be parallel to ϖ)

After finding the base length and height of the top portion of gap, the total gap area is approximated as $\zeta\varpi$. The total barrel cross sectional area is therefore going to be the area of two 30mm circles minus $\zeta\varpi$.

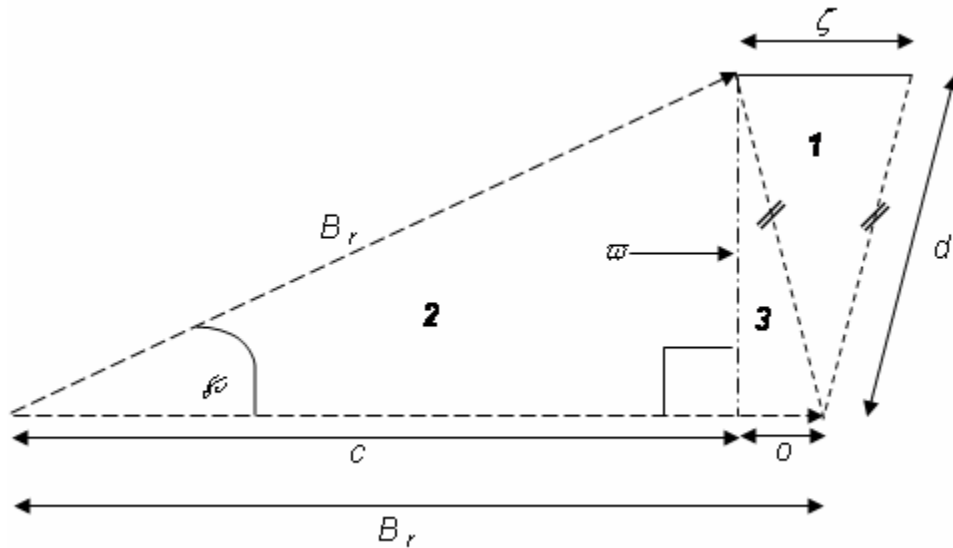


Figure 6.11: Geometry used in calculation of barrel gap area

6.3.2.2 Finding the screw cross-sectional area

The next step in finding the cross sectional area available for the reaction to occur is to find the cross-sectional area of the screws segment. For cylindrical segments, this is straight forward and will not be explained, but for the screw segments, the areas of the

flights have to be added to the base of the screw area. The cross-sectional area of the screw is shown in Figure 6.12. As one can see the base of the flight is curved at the screw root, but since the dimensions are small, this curvature can be approximated by a straight line. Therefore the cross-section, of the screw is:

$$A_s = \pi R^2 + e(0.06R + 0.03) \quad 6.1$$

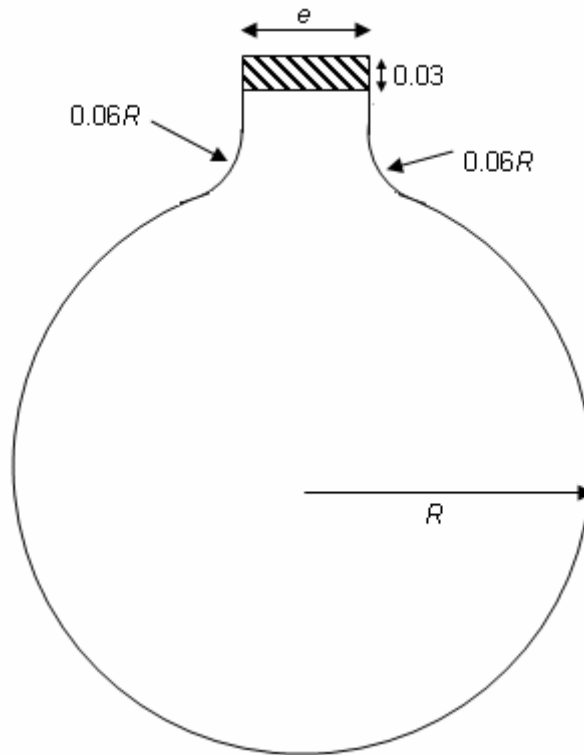


Figure 6.12: Shape of a flight, where R is the radius of the screw root, and $e=0.14''$ [89]

6.3.3 Function “Meltzone”

“Meltzone” (see flow chart in Figure 6.13 and the code in the appendix) is the third function that “rxnzone2” calls. The function “Meltzone” in turns also calls “feedinfo” and “screwdim”. Using the information from these two functions, the “Meltzone” function calculates and outputs the pressures, heat transfer from the barrel and the power consumed in the solid conveying and melting zones of the extruder. The equations used to calculate these outputs can be found in sections 5.3 and 5.7.1.

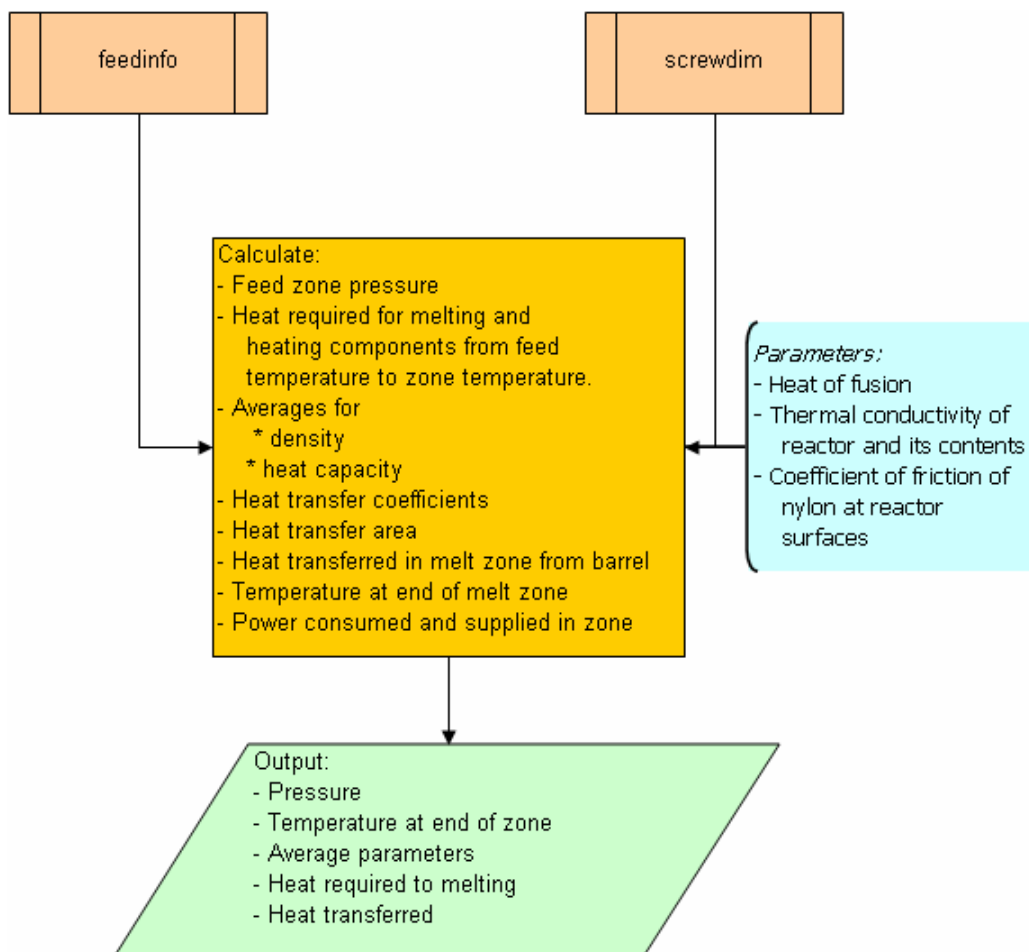


Figure 6.13: Flowchart of the “Meltzone” function

6.3.4 Function “Pressure”

With the returned information from the first three functions , “rxnzone2” then predicts a value for the die flow rate and for the other segments. Thereafter, it calls the “Pressure” function (see flowchart in Figure 6.14). The “Pressure” function uses these segment volumetric flow rates to calculate the pressure drop across each segment by using the following equations and their respective screw element:

Element	Equation
Twin screw segments	5. 41
Single screw segment	5. 54
Die	5. 59
Cylinders	5. 55

Starting at the die and working backwards towards the hopper, the pressure at the end of each segment is then found, given that the exit pressure at the die is 1 atm. With the pressure drop, the fill length of the segments were then determined using equations 5. 60 and 5.66. From these filled lengths the filled volume was determined and outputted.

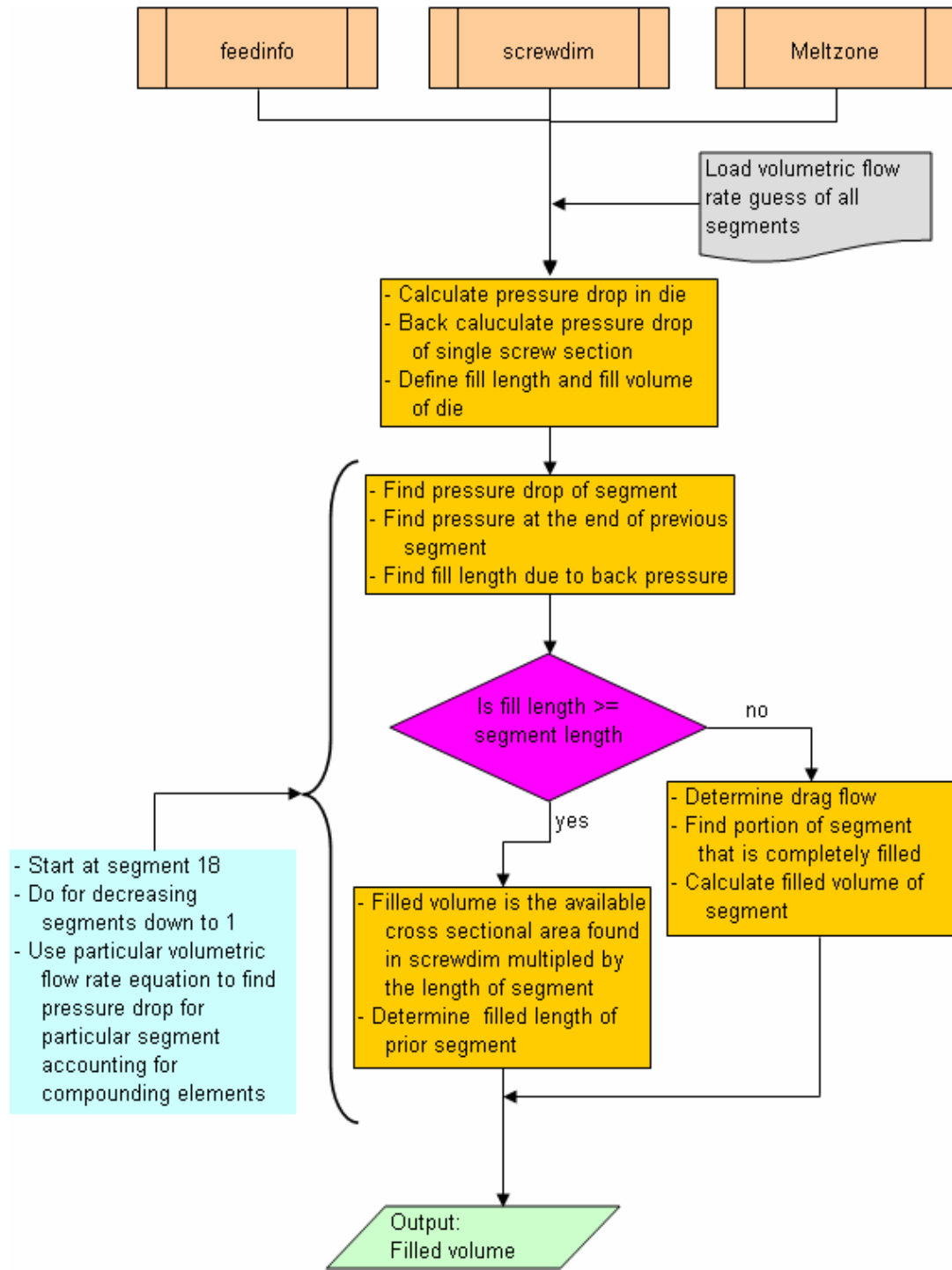


Figure 6.14: Flowchart of the “Pressure” function

6.3.5 Function “integrator3”

“integrator 3” (flowchart in Figure 6.15) is the last function that “rxnzone2” calls. “integrator3” contains the initial conditions for the conversion, temperature, nylon flow rate and product flow rate for that zone, which is used in solving their respective partial differential equations (PDEs) shown below. “integrator3” uses the built in MATLAB differential equation function “ode23s” to solve the PDEs contained in the function “Rxdiff2”. This “ode23s” functions further divides the given segment reaction volume into smaller sections to carryout the integration. The end result is that “integrator3” outputs: conversion, temperature, nylon flow rate, and product flow rate.

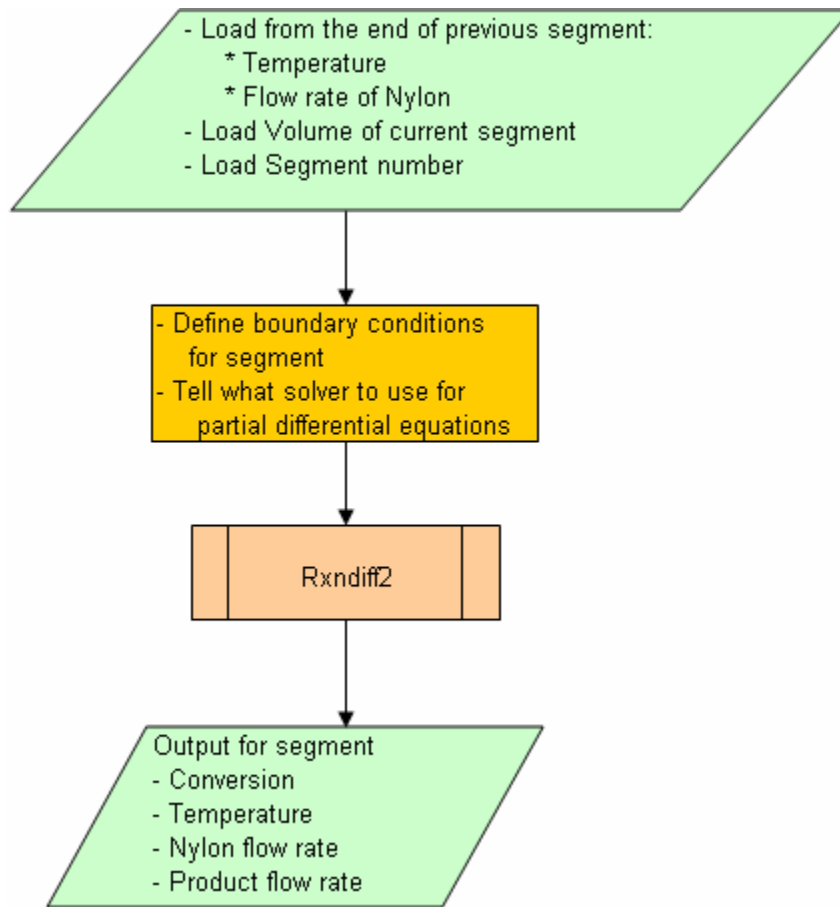


Figure 6.15: Flowchart of the “integrator3” function

6.3.6 Function “Rxdiff2”

“Rxdiff2” also calls some of the already mentioned functions and contains the heat of reaction with the activation and pre-exponential Arrhenius parameters for the depolymerization. As mentioned above “Rxdiff2” contains the partial differential equations (PDEs) describing the reaction conversion, temperature, product production, and reactant loss. These PDEs are derived from a plug flow reactor, which is a good approximation using the volume from the segments. The PDE for conversion is:

$$\frac{dX}{dV} = \frac{-r_p}{F_{po}} \quad 6.2$$

where, X is nylon conversion, r_p is the rate of the reaction, V is the filled volume and F_{po} is initial nylon feed rate into the segment.

As shown in Chapter 4, the global kinetics that fits the depolymerization of nylon 6 is first order and is the rate is defined as:

$$r_p = kC_{po}(1 - X) \quad 6.3$$

where, k is the rate constant (the parameters used to find this are in Chapter 4) and C_{po} is the concentration of nylon (i.e. the density of the nylon in the melt) at the beginning of the segment.

The PDE for temperature is [90]:

$$\frac{dT}{dV} = \frac{Q_w + E + [(-r_p)(-\Delta H_r)]}{F_{po}(\sum \Theta_i C_{pi} + X\Delta C_p)} \quad 5.155$$

where, T is reaction temperature, C_{pi} is the heat capacity, Θ_i are fractions of each feed component, and ΔC_p is the mean heat capacity of feed and product.

The rate of product formation is simply r_p while that of nylon 6 consumption is $-r_p$.

“Rxdiff2” then returns the outlet condition of the segment section being considered to “integrator3” which then returns them to “rxnzone2”. After receiving the conversion for the first zone, “rxnzone2” then determines the flow rate of the next zone (taking into account if there is venting) and calls “integrator3” until the conversion for all the zones are found.

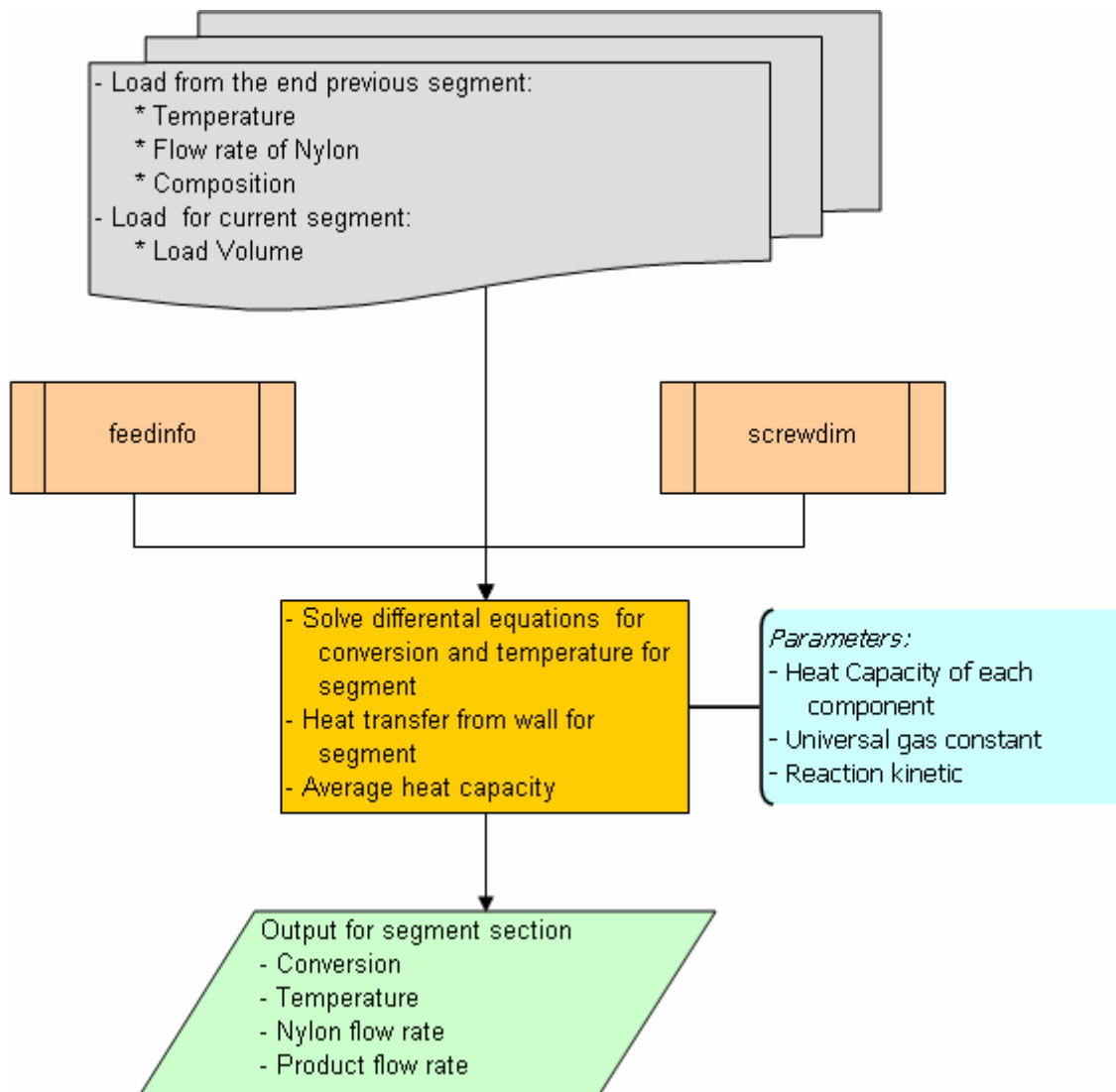


Figure 6.16: Flowchart of the “Rxdiff2” function

6.4 Cost Analysis

After “rxnzone2” sends its output to an Excel file called “Extrud sim results” on Sheet 1, in a separate Excel sheet, the predicted flow rate of caprolactam is used to give an estimate the cost of manufacturing and to determine the other economic factors. Using

the predicted conversion and flow rate of caprolactam, a stream factor of 0.96 was used to determine the flow rate of carpet required.

The capital cost of the extruder and the collection system was determined by using cost exponents. Since the heat transfer area determines the size of the extruder required, the cost exponent for heat exchangers, 0.44, was used instead of the six-tenths-rule as shown in the following equation [91]:

$$\frac{C_s}{C_b} = \left(\frac{F_s}{F_b} \right)^{0.44} \quad 6.156$$

where, F_b is the base capacity of the equipment, F_s is the desired capacity of equipment, C_b is the base cost of the equipment and C_s is the cost of the scaled equipment. (The base capacity of the extruder used was 10 lb/hr of carpet.) Using these purchase costs of these equipment, the capital cost of a plant running this process was determined by using a Lang factor of 3.63 [91] since the carpet enters as solid and the caprolactam leaves the extruder as a fluid.

For the manufacturing costs, it was assumed that the purchased price for the dry carpet pellets and KOH was \$0.05/lb and \$0.35/lb, respectively [92]. The cost of electricity was taken from the Department of Energy website for Georgia while most of the other costs associated with manufacturing (direct, fixed and general) were taken from reference [91]. The number of operators chosen for this process is only one because this process should be mostly automated.

With all the cost accounted for, the yearly gross profit was then determined and a 30% tax rate was used to find the net yearly profit. From these numbers and the market

value of caprolactam (\$0.98/lb [92]), a profitability analysis over a ten year period was performed to estimate items such as the Rate of Return on Investment (ROROI), Net Present Value (NPV), and the Present Value Ratio (PVR) using the methods given in reference [92].

6.5 Extrusion

The extruder used as the reactor for the depolymerization process is a 30mm counter rotating non-intermeshing twin screw extruder made by NFM Welding Engineers, Inc. shown in Figure 6.17. This extruder has three vent domes. Attached to the extruder vent domes is a vacuum collection system made by NFM as shown in Figure 6.18. The vacuum system as shown was also connected to a tank that collects the extrudate from the die that is shown in Figure 6.19. The set up of the coupled extrusion/vacuum collection system was further modified to include sample collection from each vent as shown in Figure 6.20 and Figure 6.21.

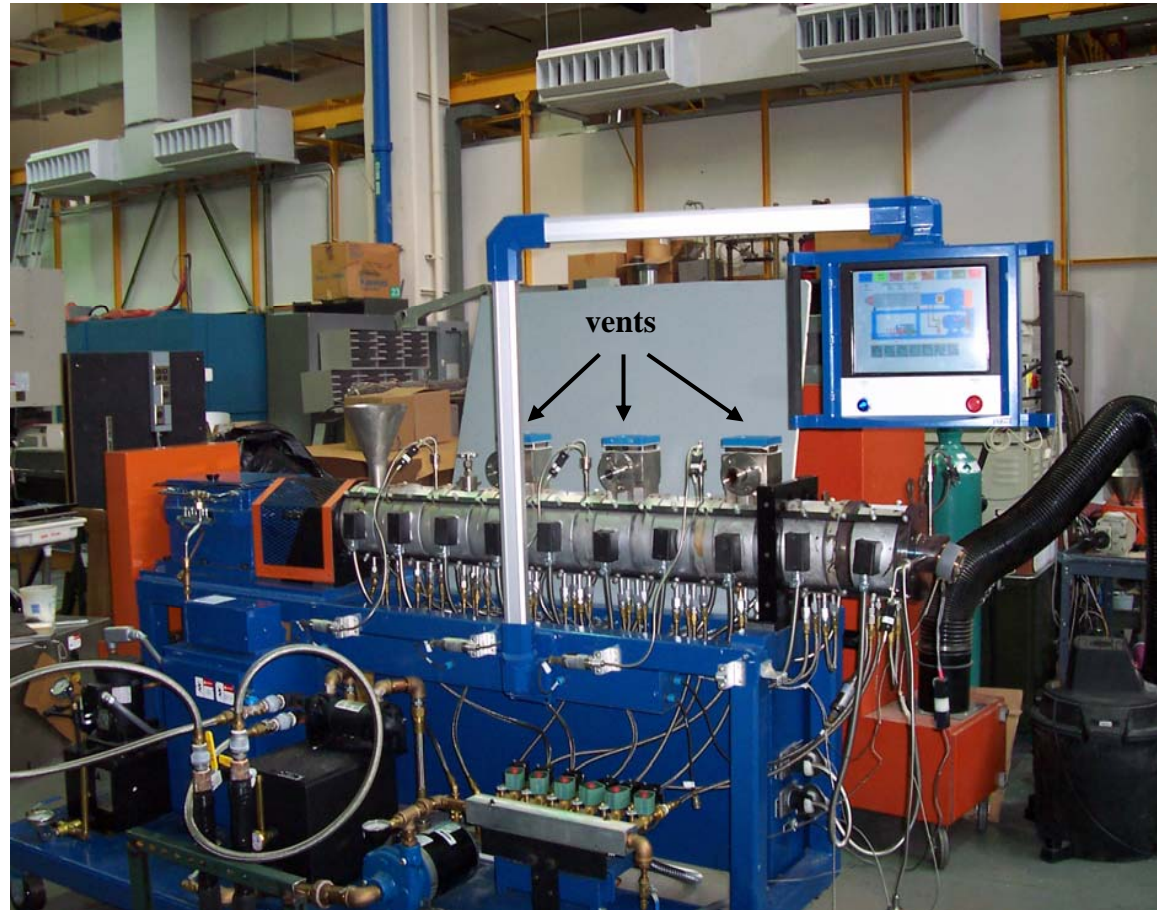


Figure 6.17: Picture of extruder without vacuum system attachment



Figure 6.18: Picture of extruder with vacuum system attachment 1



Figure 6.19: Picture of die attachment for collection of residual product

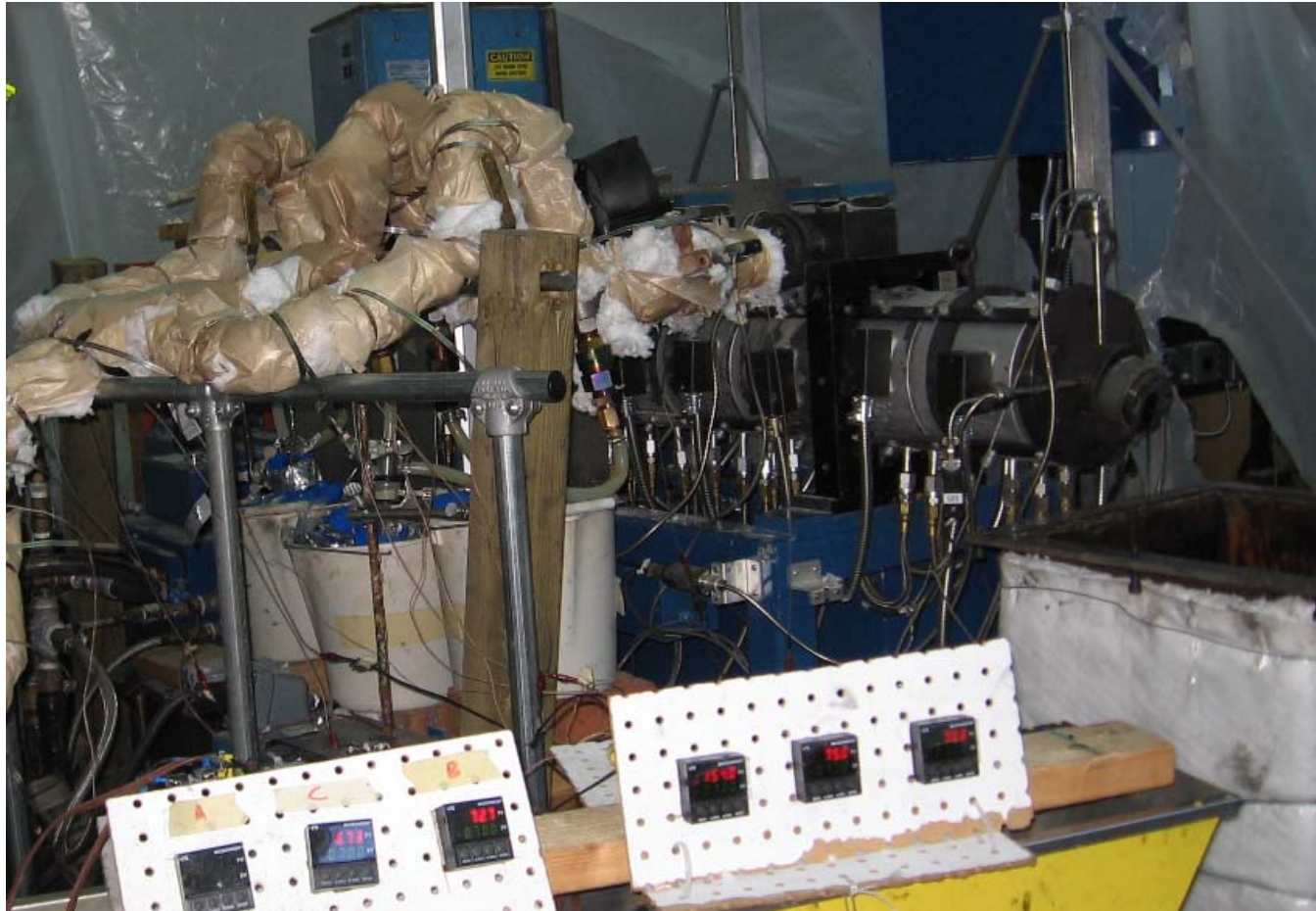


Figure 6.20: Picture of extruder with vacuum system with sample collection with bypass

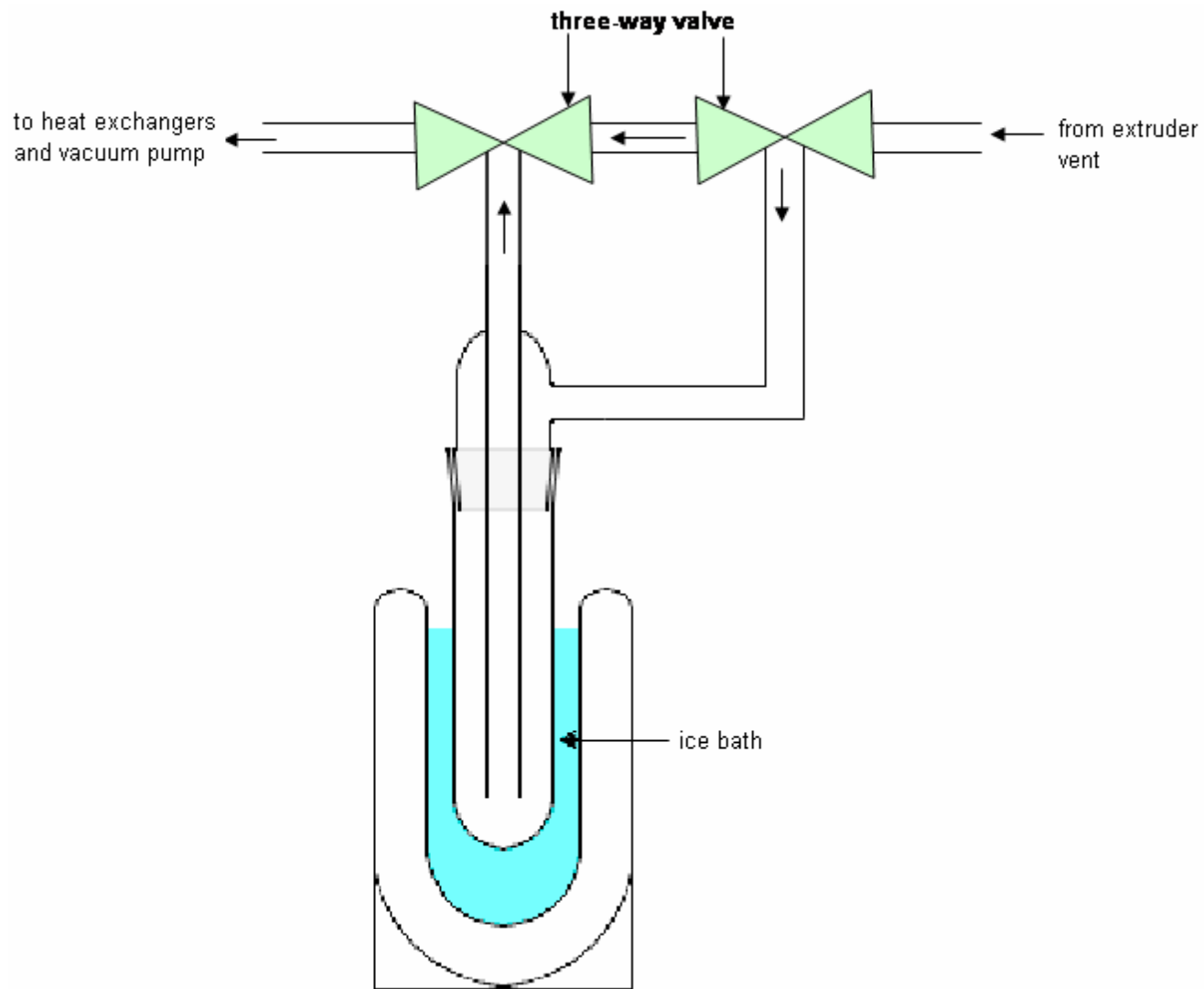


Figure 6.21: Schematic of the vacuum system with sample collection with bypass

The following conditions were used when running the extruder with pure nylon 6 and 100:1 N6:KOH:

Variables	Set points
Melt zone and die temperature	250°C
Reaction zone temperature	300 or 325°C
Flow rate	10 lb/hr
Screw Speed	100 or 150 RPM
Vent lines temperature	Various within the range of 25-300°C
Vacuum	Various within the range of -1 to -25 in Hg

The procedure used in operating the extrusion/vacuum system is as follows:

- Heat extruder zones to temperatures stated above
- Turn on cooling water to heat exchangers and load icepacks in sample collection tanks
- Turn vacuum pump on to warm it up (no vacuum to system).
- Start extruder at set screw speed and feeder at desired mass flow rate
- Wait until die has extrudate then open vacuum to the system
- Run for desired time.

CHAPTER 7

SIMULATION RESULTS AND VERIFICATION

7.1 *Effect of Screw Design and Operation Limit*

As noted earlier, the 30 mm NFM CRNI extruder has a wide operating range which is bounded by a volumetric/torque limit and an excess surging limit as shown in Chapter 6. To determine which section of the operating range was more efficient, the conversions at various carpet flow rates at each limit for both screw configurations were determined at a set barrel temperature of 325 °C and is shown in Figure 7.1. It should be noted that for an excess surge limit, the flow rates above 25 lb/hr require screw speeds that are above the limit of the extruder, but are included to show a theoretical comparison to the torque limit whose screw speed at these same flow rates did not surpass the extruder capability.

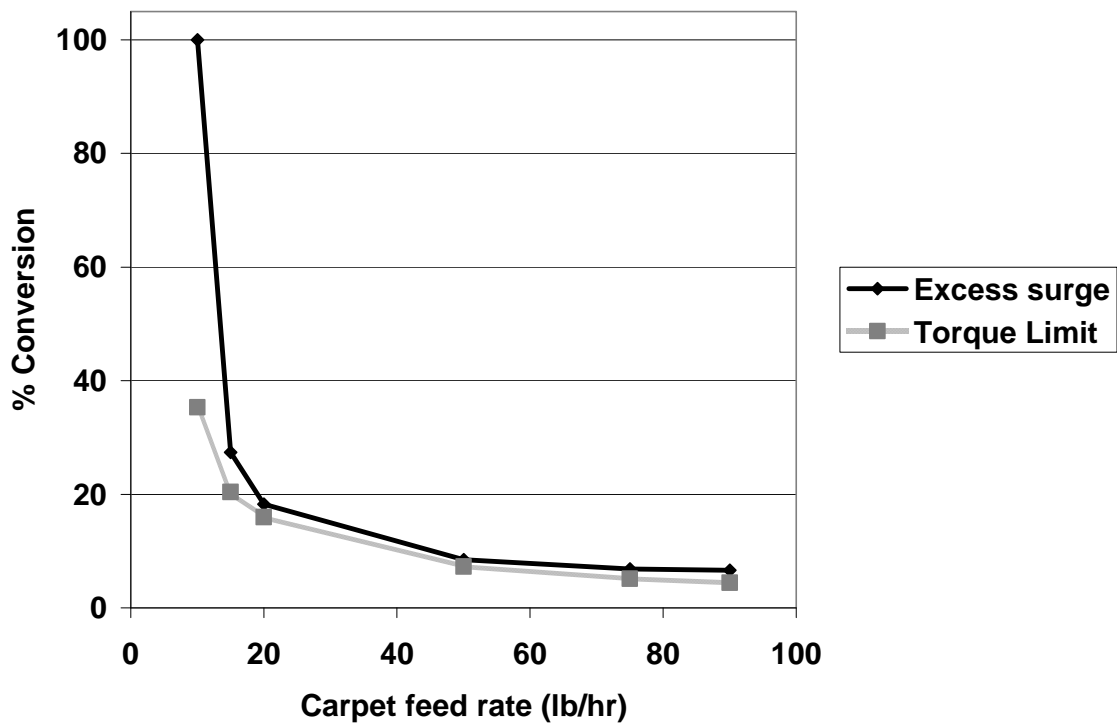


Figure 7.1: Conversion of N6 using the un-scaled extruder dimensions at the two boundary operating conditions at 325 (°C)

From Figure 7.1, the conversion for the excess surge limit is higher than at the torque condition, especially for 10 lb/hr. So ideally, it would be best to operate near the excess surge limit. For flow rates above 20 lb/hr, the conversion is under 40% which is quite low. This can be explained by the average temperature (shown in Figure 7.2) for the entire extruder in which the average temperature (which also includes the feed temperature) is much lower than the set barrel wall except for a flow rate of 10 lb/hr at the excess surge limit. This low conversion also has an impact on the cost of manufacturing shown in Figure 7.3. In general, the manufacturing cost of caprolactam associated with operating at the torque limit exceeds those when operating at the excess

surge limit. As can be seen in Figure 7.3, the per pound cost of manufacturing would amount to over \$10/lb and since the selling price of caprolactam is only \$0.98/lb [92], the process would be unprofitable.

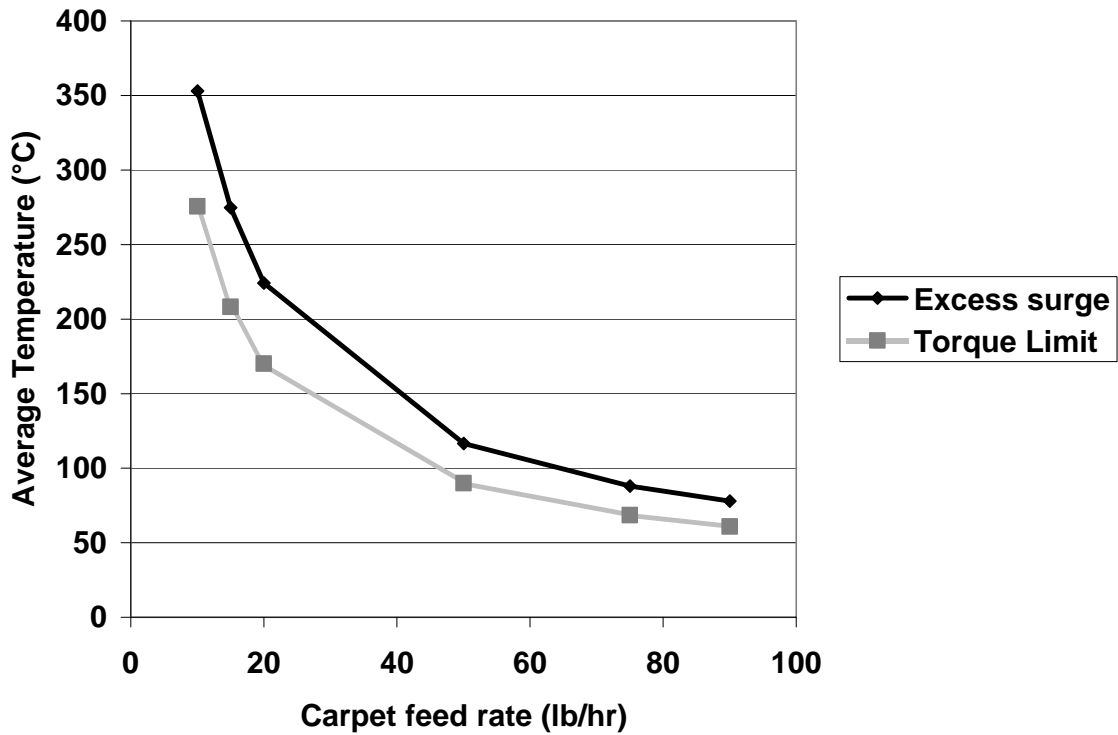


Figure 7.2: Average temperature in using the un-scaled extruder dimensions at the two boundary operating conditions at 325 (°C)

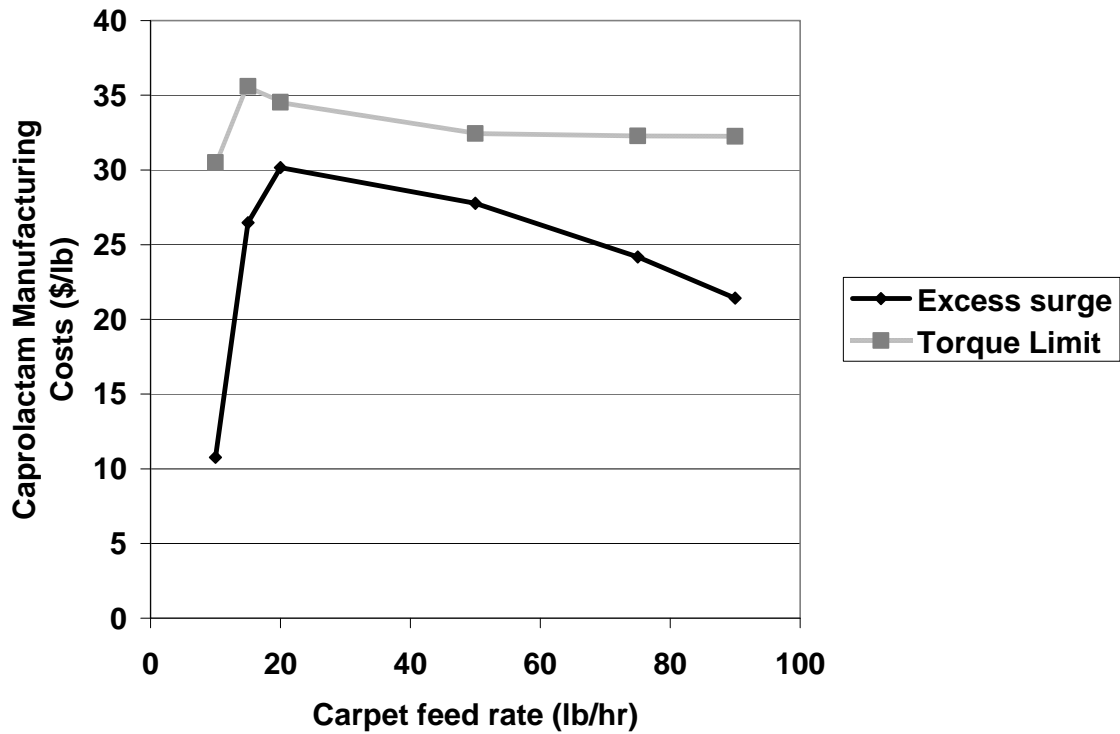


Figure 7.3: Cost of manufacturing of caprolactam using the un-scaled extruder dimensions at the two boundary operating conditions at 325 (°C)

7.2 Effect of Scaling on Cost

To make the process profitable, higher conversions and higher throughputs would be needed. In order to increase the conversion, the temperature of the extruder has to be increased. This was compensated for by increasing the heat transfer area and mechanical energy using scaled up factors discussed in Chapter 5 and 6 from the 10 lb/hr carpet feed rate operating close to the surge limit at 150 rpm. From using the scaled dimensions, enough energy was supplied to the reaction and conversions close to 100% were achieved for all the flow rates tested. Figure 7.4 and Figure 7.5 show how the conversion and temperature change along the screw length of the extruder for 10 lb/hr and 1500 lb/hr. With 10 lb/hr (no scaling), the temperature first surpasses that of the barrel wall, which

was set at 325° C, then became lower than the barrel wall temperature as the reaction proceeds down the reactor. At the same time, the conversion slowly increases down the reactor. With 1500 lb/hr (scaling used), the temperature only approaches the barrel temperature at the last segment. Despite the lower temperature at 1500 lb/hr, 100 % conversion was reached before the die.

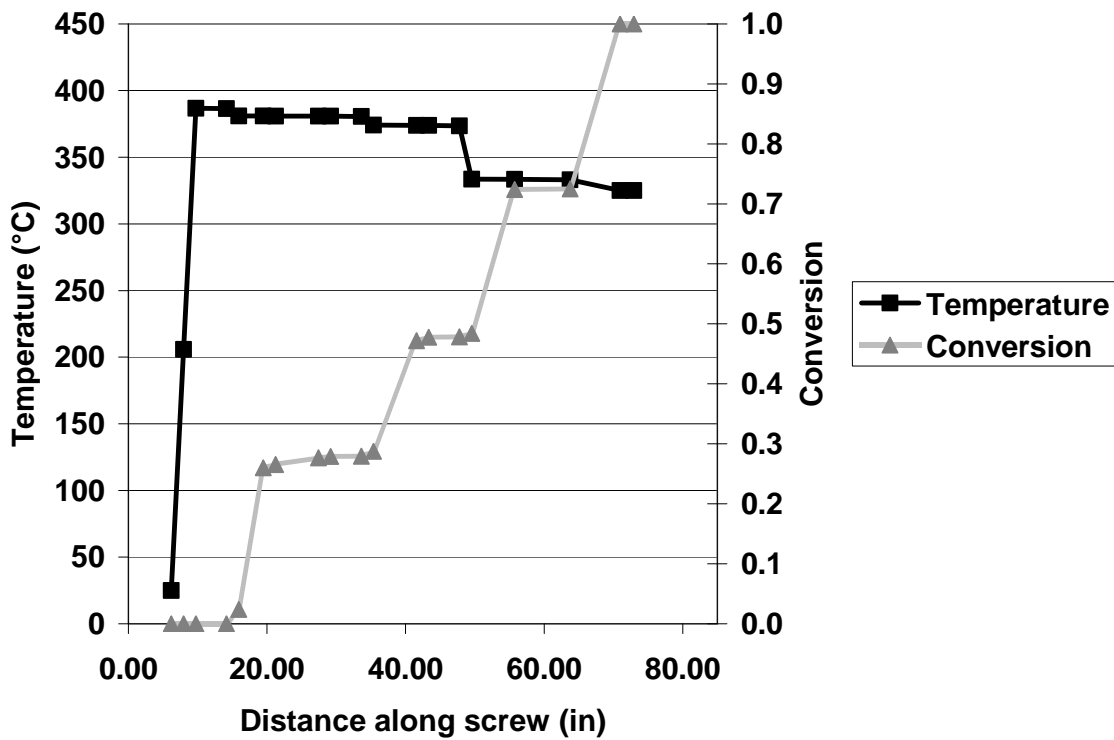


Figure 7.4: Temperature and N6 Conversion profile of 10 lb/hr of carpet using unscaled extruder dimensions at 325 (°C)

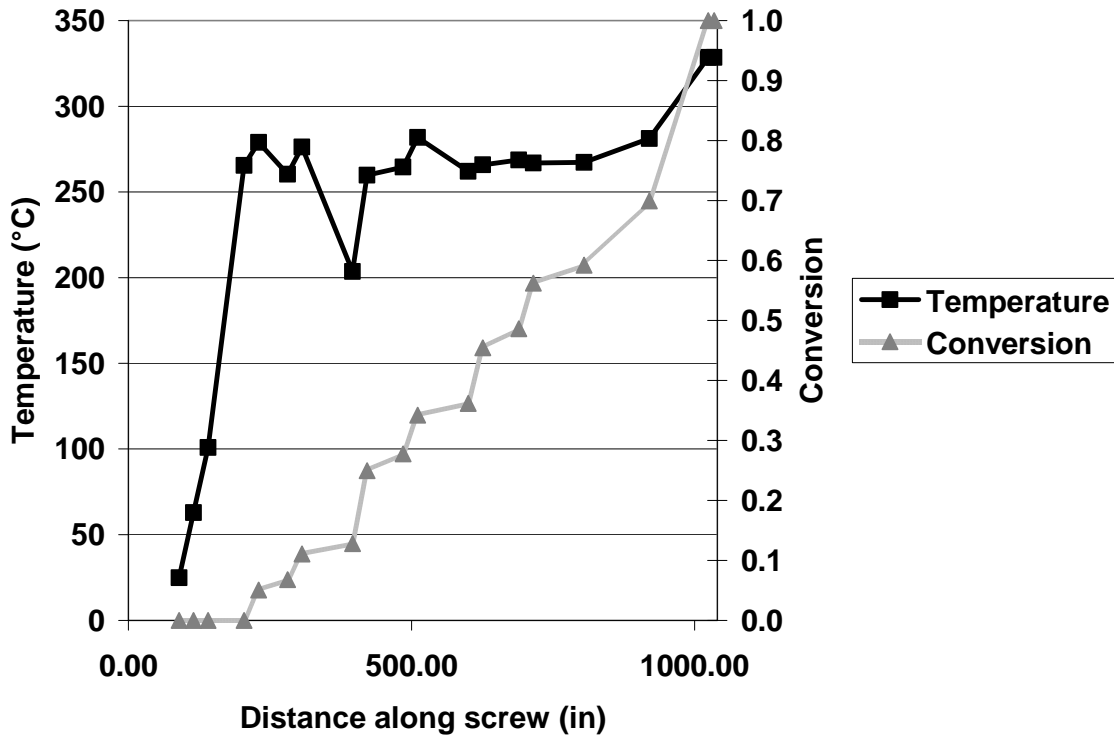


Figure 7.5: Temperature and N6 Conversion profile of 1500 lb/hr of carpet using scaled extruder dimensions at 325 (°C)

Since the assumed number of operators need for the process is one, the cost of manufacturing the caprolactam significantly decreases with increasing throughput as shown in Figure 7.6. At around 400 lb/hr, the cost becomes less than \$1.00/lb, but the Present Value Ratio (PVR) is below one. To get a PVR equal to 1, the flow rate has to be around 500 lb/hr. At 1500 lb/hr, which is the limit of this model, the PVR is 3.4 which shows that this process is economically viable.

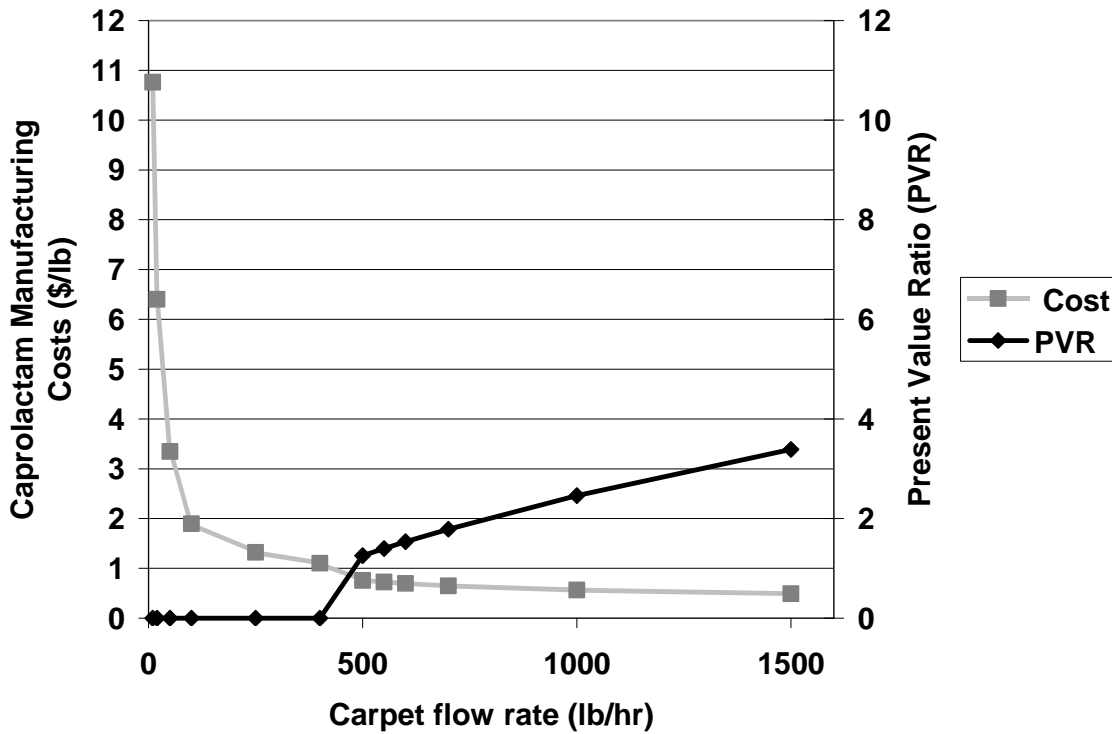


Figure 7.6: Cost of Manufacturing caprolactam and present value ratio of using scaled extruder dimensions at 325 (°C)

7.3 Extruder Results

Despite the results presented from the model, the results were not verified by the time of this writing. However, some of the findings and problems encountered while running this process will be discussed.

The first set of runs were done with the first set up shown in Figure 6.18. In the beginning, the temperature of the vent lines were set at 270°C (above the condensation temperature of caprolactam which is 267°C) to ensure that there were no condensation in the vent lines. However, the heat transfer capacity of the cooling tank was not adequate to condense/sublimate all the vapors exiting the extruder. Some of the vapors eventually

condensed/sublimated in the filter of the vacuum pump which clogged it; hence, suction was lost to the process. The temperature of the vent lines were lowered incrementally to room temperature to try to prevent this filter from clogging. However, since the vapor from the extruder was at 300°C or above, some vapor would condense and sublimate on the walls of the vent lines and the lines would become clogged and/or eventually the lines would get hotter and the filter would clog. Figure 7.7 shows the product that collected in the vent lines. This product was a white like pure caprolactam.



Figure 7.7: Pictures of vent lines clogged with product

In addition, products also collected in the cooling tank on the steel wool that was used in increase the heat transfer area/sublimation-nucleation sites. These can be seen in

Figure 7.8 and Figure 7.9. Some of this product was white just like pure caprolactam, however, because the tank's material of construction was carbon steel, rust from the metal can be found in the condensate hence some brown colored products. The product collected was then analyzed using a gas chromatograph – mass spectra (GC-MS) in tandem. Figure 7.10 and Figure 7.11 shows the GC-MS results. There was one primary peak in the GC and main molecular weight from that peak in the MS was 113, the molecular weight of caprolactam. The imine, found by NREL in reference [57], whose molecular weight is 111 was not found in this product.

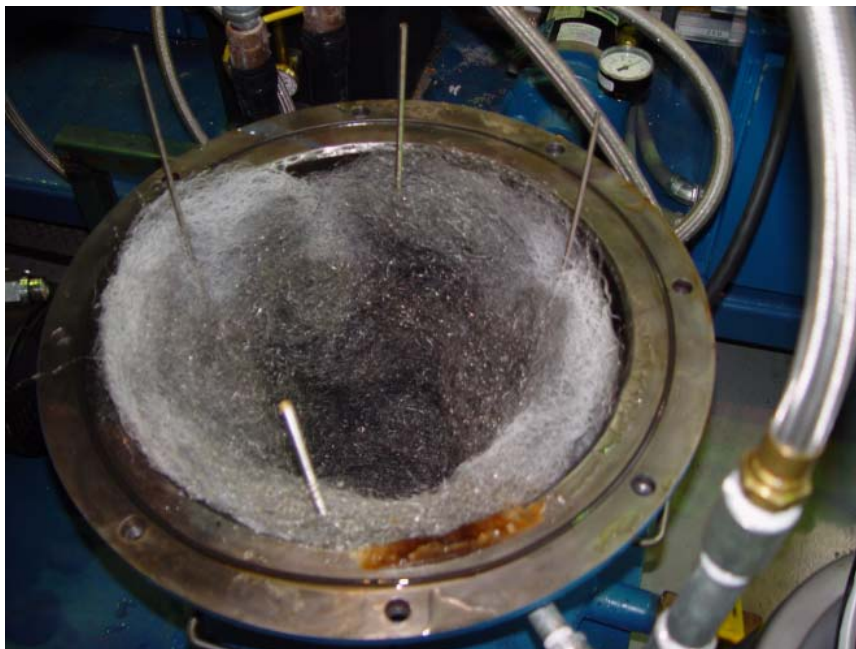


Figure 7.8: Product collected in the cooling tank



Figure 7.9: Close up on cooling collection tank product; the product collected on the steel wool

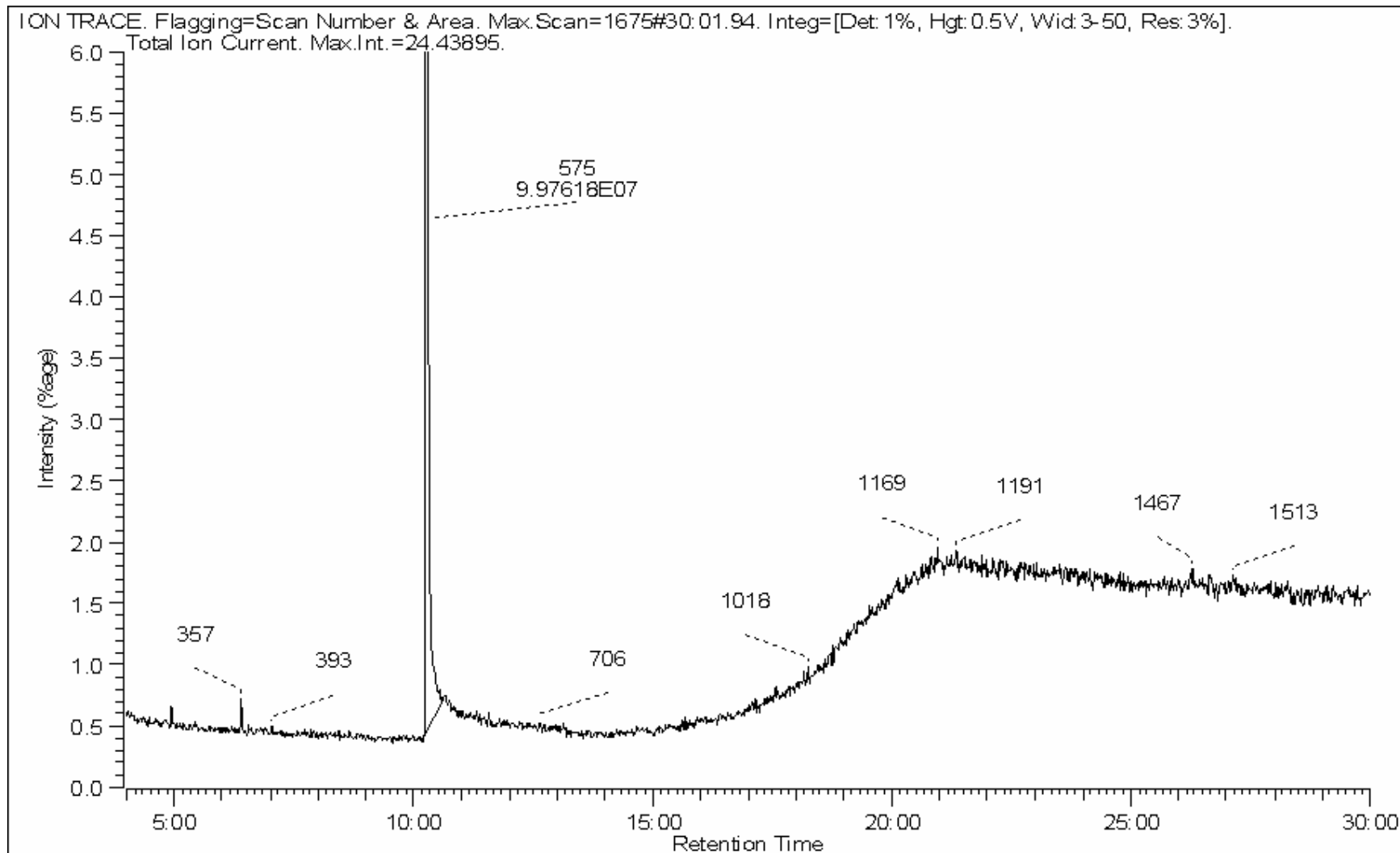


Figure 7.10: Gas chromatograph of the product collected from the extruder

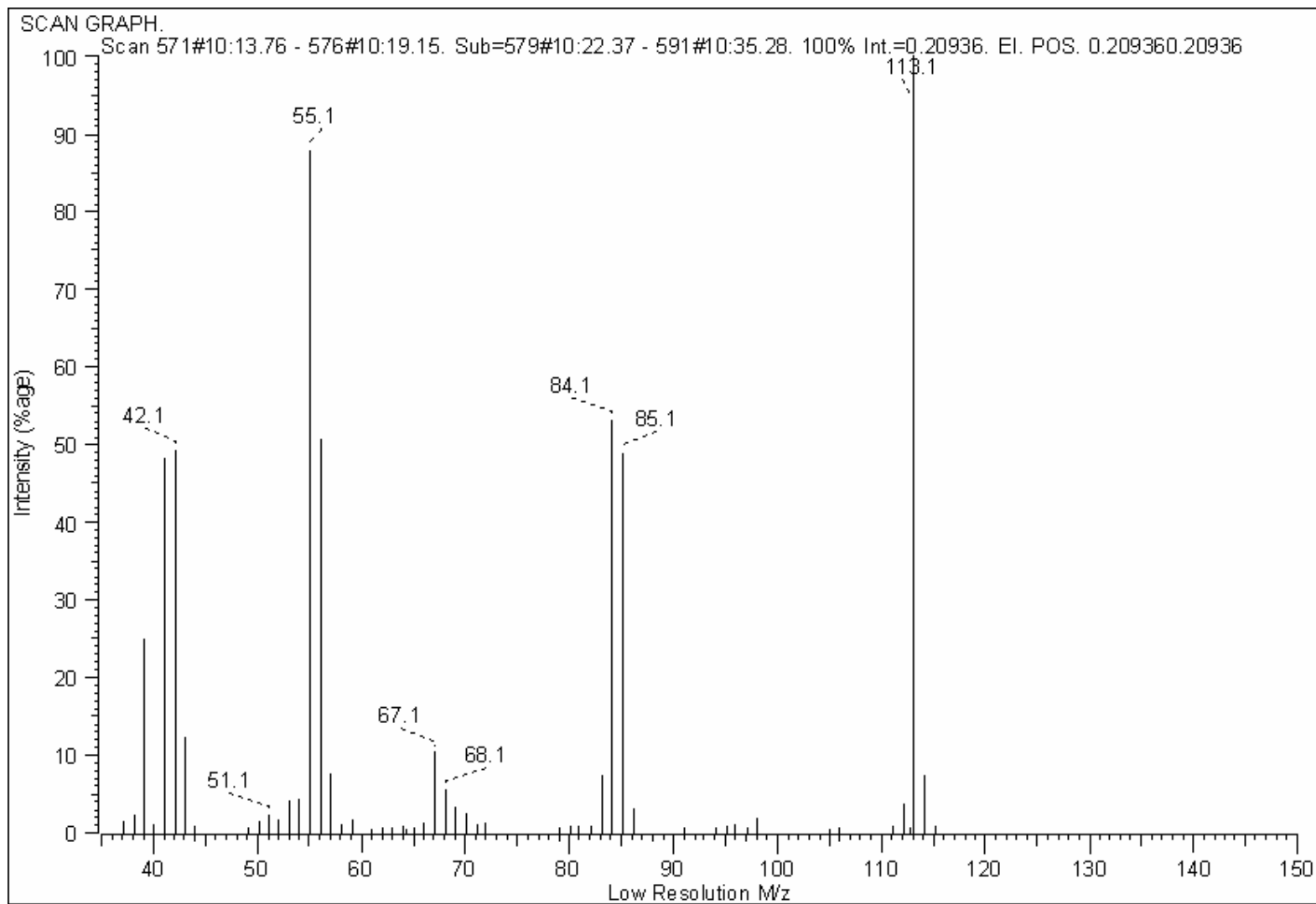


Figure 7.11: Mass spectra of the main peak from the gas chromatograph of the product collected from the extruder

Since there was insufficient cooling, an additional shell and tube heat exchanger was added to the system before the cooling tank. With the addition of the extra heat exchanger and keeping the vent lines at 70°C, the vacuum filter did not clog anymore. However, the readings of the vacuum in the vent lines would eventually go down to zero. During disassembling of the vent lines, it was discovered that the reacting mixture from the extruder was backing up into the vent lines. (This was not discovered earlier because the vacuum pump filter clogging prevent the process from being run long enough for this to occur.) It was thought that the die attachment was providing too much die resistance (pressure) causing the flow into the vents. Having used various vacuum pressure levels, the problem still occurred. So the die attachment was removed and die with less resistance was put in place. Another modification that was made at this time was the addition of sample collectors (as shown in Figure 6.20 and Figure 6.21) to measure independently the amount of products from each vent.

The new die did not prevent the extruder content from going into the vent lines. Before a steady state could be reached, the vacuum reading went to zero. Upon opening the sampling valve after the clog while the lines were still hot, the contents of the line collected was the same consistency as that in the extruder. Another observation: after turning off the vacuum and opening up the vent window while the extruder was still heating, one could see the contents of the vent receding from the vent lines down to the screws while some of the bubbles within were bursting. This indicates that the even though a low vacuum suction was being used, the material was still foaming. From the set up, there was not enough height provided for the foaming and hence the material foamed into the vent line. Once this problem of foaming into the vents is resolved, it is

anticipated that the catalytic depolymerization of nylon 6 in an extruder/reactor will work well.

CHAPTER 8

CONCLUSIONS AND RECOMMENDATIONS

It can be concluded that:

1. The use of base catalyst can lower the onset degradation temperature of Nylon 6 and 66 by 100 °C
2. Potassium hydroxide and sodium hydroxide were found to be the most effective catalysts at a concentration of 1 % by weight in nylon 6 and nylon 66, respectively
3. The mixing done by the Haake Rheomix ® gave good dispersion of the catalyst in the polymer matrix.
4. In the premixing of catalyst before TGA, the DSC indicate that some degradation may have occurred during mixing.
5. Comparison of different kinetic models indicate that kinetic parameters should be obtained using ASTM E 1641 – 99 method [49] since the kinetic parameters found were used to simulate other heating rates and they were in agreement with the experimental data
6. From GC-MS, the products from the extruder is caprolactam
7. Cost analysis of the extrusion process indicate that the process could be profitable

The following is recommended for further study:

1. Analyze the foaming of nylon carpet/catalyst mixture at reaction conditions to learn how to remove the vapor without clogging the vents. This may lead to

investigation of taller vent columns to facilitate the amount of foam formed and give enough time for the bubbles to burst. There may be the need to put an aid in to disrupt the foaming.

2. The use of cryogenics to cool the vapor product should be also explored.
3. An increase in the amount of heat transfer area for cooling the product should also be added to the process. The application of scraped-surface heat exchangers should be considered since there is sublimation.
4. Further investigation is needed to understand why there is melting point depression after mixing the catalyst with nylon since there could be possible applications developed from such a study.
5. To reduce the size of the extruder needed to get adequate the heat transfer, addition of heating elements/fluid within the screws may be considered.

APPENDIX

A.1 Parameters used in Modeling

Table A.1: Solid density and melt density of reactor components.

Material	Density at 70 °F (g/cm ³)	Melt Density (g/cm ³)	Reference
Calcium carbonate (CaCO ₃)	2.71	-	[93]
Potassium hydroxide (KOH)	2.04	-	[94]
Styrene butadiene rubber (SBR)	1.6		[95]
Nylon 6	1.13	0.97	[96]
Nylon 66	1.14	0.97	[96]
PP	0.9	0.7	[96]

Table A.2: Heat capacity of reactor component at room temperature.

Material	Heat Capacity		Reference
Calcium carbonate (CaCO ₃)	0.203	Btu/lbm*°F	[93]
Potassium hydroxide (KOH)	78.65	J/mol*K	[97]
Styrene butadiene rubber (SBR)	1.83	kJ/kg*K	[65]
Nylon 6	1.62	J/g*K	[98]

Table A.3: Heat capacity of reactor components at different temperature ranges

Material	Temperature range (K)	Heat Capacity		Source
Nylon 6	500-560	$1.236+2.73*10^{-3}T$	J/g*K	[99]
PP	290-380	$0.36+0.0023T(^{\circ}C)$	Cal/g*K	[100]
PP	450-500	$1.24+0.00304T$	J/g*K	[100]

Table A.4: Dimensions given by NFM used in the model [89]

Symbol	Description	Value for 30 mm NFM Extruder
<i>D</i>	diameter of the screw	See Figure 6.2
<i>D_b</i>	Diameter of barrel	30 mm
<i>e</i>	perpendicular width of the flights	0.14 inches
<i>S</i>	pitch	1.81 inches
<i>L_{die}</i>	Die length	2 inches
<i>R_{die}</i>	Die radius	0.5 inches

Other parameters:

- Coefficient of friction of N6 is equal to 0.6 (unitless) [73].
- Heat of fusion of polymers N6, PP are 55.08, 82.44 kJ/kg, respectively [65]
- Thermal conductivity of N6, PP, CaCO₃ are: 0.25, 0.14, 5.526 W(m K)⁻¹, respectively [67, 93]
- Thermal conductivity of barrel metal, stainless steel, is equal to 21.6 W(m K)⁻¹ [101]
- The ratio of uninterrupted barrel circumference to that of total barrel circumference is 0.85 [74]

A.2 Reactive Extrusion Model Codes

The code for each function can be found as follows:

function	Start Page #
rxnzone	252
feedinfo	268
screwdim	271
Meltzone	285
Pressure	293
integrator3	320
Rxndiff2	321

MATLAB Function “rxnzone2”

```
function rxnzone2=rxn()

warning off

%calling feedinfo function

feeds=feedinfo();

Tfeed=feeds(1,1);%(R)

Mc=feeds(2,1);%(lb/hr)

Tb=feeds(3,1);%(R)

TMassin=feeds(5,1);%(lb/hr)

Qs=feeds(7,1);%(lb/hr)

rhom(1)=feeds(13,1);%(lb/in^3)

rhom(2)=feeds(13,2);%(lb/in^3)

for x=1:5

    comp(x)=feeds(8,x);%(unitless)

    Massin(x)=feeds(9,x);%(lb/hr)

    rhos(x)=feeds(10,x);%(lb/in^3)

    Qscomp(x)=feeds(12,x);%(lb/hr)

end

%calling screwdim function

screws=screwdim();

Db=screws(1,1);%(inches)

N=screws(6,1);%(revolutions per hour)

alphaa=screws(16,1);%(radians)

mu=screws(18,1);%(lb/{in hr})

Ri=screws(19,1);%(inches)
```


MATLAB Function “rxnzone2”

```
Ro=screws(20,1);%(inches)

for x=1:19

    H(x)=screws(21,x);%(inches)

    R(x)=screws(22,x);%(inches)

    D(x)=screws(23,x);%(inches)

    L(x)=screws(24,x);%(inches)

    phi(x)=screws(25,x);%(radians)

    zb(x)=screws(26,x);%(inches)

    W(x)=screws(27,x); %(inches)

    Lsum(x)=screws(28,x);%(inches)

    Aavail(x)=screws(33,x);%(in^2)

    A(x)=screws(34,x);%(in^2)

    Vol(x)=screws(35,x);%(in^3)

    Mu(x)=screws(41,1);%(lb/{in hr})

    PWN(x)=screws(42,1);%(Btu/hr)

    Ener(x)=screws(43,1);%(Btu/hr)

end

thetab=screws(29,1);%(radians)

Ddie=screws(30,1);%(inches)

Rdie=screws(31,1);%(inches)

Ldie=screws(32,1);%(inches)

%calling meltzone

Melts=Meltzone();

Pfeed=Melts(1,1);%(lb/{ft hr^2})

P1=Melts(2,1);%(lb/{ft hr^2})

Tout=Melts(3,1); %(R)

QmeltT=Melts(4,1);%(btu/hr)
```

MATLAB Function “rxnzone2”

```
Qwmelt=Melts(7,1);%(btu/hr)

lambdam=Melts(8,1);%(btu/{hr in R})

N6meltT=Melts(11,1);%(R)

rhoavm=Melts(12,1);%(lb/in^3), average density

lambda(1)=Melts(14,1);%(btu/lb),heat of fusion of polymer
lambda(2)=Melts(14,2);%(btu/lb),heat of fusion of polymer

MechEn=Melts(15,1);%(Btu/hr), theoretical mechanical power supplied

for x=1:2 %for 1
    Qmelt(x)=Melts(9,x);%(btu/hr)
end %for 1
for x=1:3 %for 2
    lambdac(x)=Melts(10,x);%(btu/{hr in R})
end %for 2

f=alphaa/pi;%(unitless)

fs=0.6; %coefficient of friction at screw
fb=0.6; %coefficient of friction at barrel

%REACTION ZONE

%preloop initial values
j=2; %(unitless), counter
```

MATLAB Function “rxnzone2”

```
% initial guess of die volumetric flow rate, assume 90% conversion of
N6
Q(j,1:3)=Massin(1)/rhos(1)+Massin(2)/rhos(2)+Massin(3)/rhos(3)+...
    Massin(4)/rhos(4)+Massin(5)/rhos(5); %(in^3/hr)%just an
approximate,...
%not used in calculations below
Q(j,4)=Massin(1)/rhom(1)+Massin(2)/rhom(2)+Massin(3)/rhos(3)+...
    Massin(4)/rhos(4)+Massin(5)/rhos(5); %(in^3/hr)Assuming volume
additivity

cntr=1;

Q(j,5:7)=Q(j,4);
Q(j,8)=(Massin(1)/rhom(1))/(25*cntr)+Massin(2)/rhom(2)+Massin(3)/rhos(3)
)+...
    Massin(4)/rhos(4)+Massin(5)/rhos(5);
Q(j,9:11)=Q(j,8);
cntr=cntr+1;
Q(j,12)=(Massin(1)/rhom(1))/(25*cntr)+Massin(2)/rhom(2)+Massin(3)/rhos(
3)+...
    Massin(4)/rhos(4)+Massin(5)/rhos(5);
Q(j,13:15)=Q(j,12);
cntr=cntr+1;
Q(j,16)=(Massin(1)/rhom(1))/(25*cntr)+Massin(2)/rhom(2)+Massin(3)/rhos(
3)+...
    Massin(4)/rhos(4)+Massin(5)/rhos(5);
```

MATLAB Function “rxnzone2”

```
Q(j,17:19)=Q(j,16);

Qv=Q(j,:);

Qdie(j)=Q(j,19);%(in^3/hr)

Qse(j)=Q(j,18);%(in^3/hr); flow rate in single screw section

%looping to back calculate backpressure,degree fill etc
for j=j:1000 %for 4

    conversion(j,1:20)=0; %(unitless), initial condition
    ventflow(j,1:19)=0; %initial condition
    Tprod(j,3)=0;%(lb/hr), initial condition
    Prod(j,1:19)=0;%(lb/hr), initial condition
    prosum(j,1:19)=0;

    fid30=fopen('Q.txt','w');
    fprintf(fid30,'%6.4f\n', Qv);%(in^3/hr)
    fclose(fid30);
    Q(j,:)=Qv;

    Pres=Pressure(); %(in^3), pressure function calculates pressure,
    %filled length, and Volume filled but only returns volume filled

    for x=1:1:19 %for 5
        Vfil(j,x)=Pres(x);    %(in^3), volume filled
    end%for 5
```

MATLAB Function “rxnzone2”

```
%REACTION CALCULATIONS

%No reaction in sections 1-3, only melting

%section 1: feed

%section 2: taper1

%section 3:taper2

T(j,3)=Tout;%N6meltT; %(R),temperature at end of section 3

%section 4: forward1

for x=4:1:19 %for 7

    fid=fopen('x.txt','w');

    fprintf(fid,'%6.4f\n', x); %unitless

    fclose(fid);

    segment=x

    Volfil(x)=Vfil(j,x);%(in^3), volume filled

    fid=fopen('Vol.txt','w');

    fprintf(fid,'%6.4f\n', Volfil(x));%(in^3)

    fclose(fid);

    prosum(j,x)=Prod(j,x-1)+prosum(j,x-1);

    % account for the change in mass and composition
```

MATLAB Function “rxnzone2”

```
N6mass(j,x)=Massin(1)- prosum(j,x);

fid4=fopen('N6mass.txt','w');

fprintf(fid4,'%6.4f\n', N6mass(j,x));%(in^3/hr)

fclose(fid4);

%Mass inside segment of extruder along length, accounting for
%venting along the way

tank=sum(ventflow);

[tankr,tankc]=size(tank);

Tmass(j,x)=Tmassin-tank(tankr);%Tprod(j,x-1);

fid5=fopen('Tmass.txt','w');

fprintf(fid5,'%6.4f\n',Tmass(j,x));%(in^3/hr)

fclose(fid5);

comp1=[N6mass(j,x)/Tmass(j,x),Massin(2)/Tmass(j,x),Massin(3)/...
      Tmass(j,x),Massin(4)/Tmass(j,x),Massin(5)/Tmass(j,x),...
      Tprod(j,x-1)/Tmass(j,x)]; ...

%(unitless)

fid2a=fopen('comp1.txt','w');

fprintf(fid2a,'%6.4f\n', comp1);%(btu/lb R)

fclose(fid2a);

%Heat capacities

Cp(1)=(1.236+2.73*10^-3 *Tb)*0.239; %(btu/{lbm F}),n6 molten @ barrel
temp.

Cp(2)=0.26+0.0023*(Tb/1.8-273.15);%(btu/{lbm F}), molten PP
```

MATLAB Function “rxnzone2”

```
Cp(3)=.203; %(btu/{lbm F}), CaCO3,
Cp(4)=1.83/4.1868; %(btu/{lbm F}), SBR
Cp(5)=78.65920/(56.11*4.1868);%(btu/{lbm F}), KOH
Cp(6)=2.345/4.1868;%(btu/{lbm F}), caprolactam

Cpav(x)=1/(comp1(1)/Cp(1)+comp1(2)/Cp(2)+comp1(3)/Cp(3)+...
        comp1(4)/Cp(4)+comp1(5)/Cp(5)+comp1(6)/Cp(6)); %(btu/lb R)
fid2=fopen('Cp.txt','w');
fprintf(fid2,'%6.4f\n', Cpav(x));%(btu/lb R)
fclose(fid2);

capdensity=3.91;%(g/cc,Relative vapour density (air = 1)...
%http://www.inchem.org/documents/icsc/icsc/eics0118.htm
capdensity=capdensity*(28317/(453.593*1728));%(lb/in^3)

rhoav(x)=1/(comp1(1)/rhom(1)+comp1(2)/rhom(2)+comp1(3)/rhos(3)+...
        comp1(4)/rhos(4)+comp1(5)/rhos(5)+comp1(6)/capdensity);
%(lb/in^3)

lambdac(6)=0.5*1000/(39.37*1.8*1055.06); %(btu/{hr in R}),
%thermal conductivity of caprolactam
lambdacav(x)=1/(comp1(1)/lambdac(1)+comp1(2)/lambdac(2)+...
        comp1(3)/lambdac(3)+comp1(6)/lambdac(6));%(btu/{hr in R})
alphai(x)= 0.94*lambdacav(x)/D(x)*((rhoav(x)*N*(D(x)^2)/mu)^...
        0.28)*(Cpav(x)*mu/lambdacav(x))^0.33; %(btu/{hr in^2 R})
```

MATLAB Function “rxnzone2”

```
U(x)=1/((Ri*(log(Ro/Ri))/lambdam)+(1/alphai(x)));%(btu/{hr in^2
R)

fid3=fopen('U.txt','w');

fprintf(fid3,'%6.4f\n',U(x));%(btu/{hr in^2 R})

fclose(fid3);

%Tp=470; % need to use differential

fid6=fopen('Temp.txt','w');

fprintf(fid6,'%6.4f\n',T(j,x-1));%(R)

fclose(fid6);

Q(j,x)=Tmass(j,x)/rhoav(x);

%% or should I use?

%Q(j,x)=Qv(x)-(ventflow(j-1,x)/capdensity);

fid30=fopen('Q2.txt','w');

fprintf(fid30,'%6.4f\n',Q(j,x));%(in^3/hr)

fclose(fid30);

%Calling the function integrators to get conversion,
temperature
%and flow rates

integrators=integrator3();

conversion(j,x)=integrators(:,1); % conversion of segment

Prod(j,x)=integrators(:,4); %(in^3/hr),product flow
```


MATLAB Function "rxnzone2"

```
if conversion(j,x)>0.99 %if all reacted b4 die

    if x<=8
        for ww=(x+1):1:8
            Q(j,ww)=Q(j,x);
        end
        Q(j,9:19)=Massin(2)/rhom(2)+Massin(3)/rhos(3)+...
            Massin(4)/rhos(4)+Massin(5)/rhos(5); %(in^3/hr)
    end

    %after venting,
    if x==9
        Q(j,(x+1):19)=Massin(2)/rhom(2)+Massin(3)/rhos(3)+...
            Massin(4)/rhos(4)+Massin(5)/rhos(5); %(in^3/hr)
    end

    if (x<=12 && x>9)
        for ww=(x+1):1:12
            Q(j,ww)=Q(j,x);
        end
        Q(j,13:19)=Massin(2)/rhom(2)+Massin(3)/rhos(3)+...
            Massin(4)/rhos(4)+Massin(5)/rhos(5); %(in^3/hr)
    end

    %after venting,
```

MATLAB Function “rxnzone2”

```
if x==13

    Q(j,(x+1):19)=Massin(2)/rhom(2)+Massin(3)/rhos(3)+...
        Massin(4)/rhos(4)+Massin(5)/rhos(5); %(in^3/hr)

end

if (x<=16 && x>13)

    for ww=(x+1):1:16

        Q(j,ww)=Q(j,x);

    end

    Q(j,17:19)=Massin(2)/rhom(2)+Massin(3)/rhos(3)+...
        Massin(4)/rhos(4)+Massin(5)/rhos(5); %(in^3/hr)

end

%after venting,

if x>=17

    Q(j,(x+1):19)=Massin(2)/rhom(2)+Massin(3)/rhos(3)+...
        Massin(4)/rhos(4)+Massin(5)/rhos(5) ;%(in^3/hr)

end

if x<19

    prosum(j,x:19)=Prod(j,x)+prosum(j,x-1);

end

Prod(j,x+1:19)=0;

T(j,x:19)=integrators(:,2); %Temperature

Esect(j,x)=load('Qwf.txt');% (Btu/hr), heat input required

for segment
```

MATLAB Function “rxnzone2”

```
Tprod(j,x:19)=Tprod(j,x-1)+ Prod(j,x);%(in^3/hr),total
product

    %flow rate

Oconversion(j,x:19)=1;%overall conversion of nylon
break %for 7
else
T(j,x)=integrators(:,2); %Temperature
%F=integrators(:,3); %nylon flow

Tprod(j,x)=Tprod(j,x-1)+ Prod(j,x); %(in^3/hr),total
product

Oconversion(j,x)=(Massin(1)-
N6mass(j,x))/Massin(1);%overall...
    %cnvrnsn of nylon
end %if 1

%venting,
if x== 8 %if 2 (vent 1)
    ventflow(j,x)=Tprod(j,x); %Vent 1
    Tprod(j,x)=0;
end %if 2

if x==12 %if 3 (vent 2)
    ventflow(j,x)=Tprod(j,x); %Vent 2
```

MATLAB Function “rxnzone2”

```
Tprod(j,x)=0;
end %if 3

if x== 16 %if 4 (vent 3)
    ventflow(j,x)=Tprod(j,x); %Vent 3
    Tprod(j,x)=0;
end %if 4

end %for 7

if Q(j,:)-Q(j-1,:)<.1 %if 2
    break %for 7
else

    Qv=Q(j,:);
    j=j+1;%(unitless)
    Qdie(j)=Q(j-1,19);%(in^3/hr), x =19
    Qse(j)=Q(j-1,18);%(in^3/hr), x-1=18
end %if 2

end %while,or for 4
pprodsum(j,1:19)=0;
for zx=4:19
    pprodsum(j,zx)=pprodsum(j,zx-1)+Prod(j,zx);
end
```

MATLAB Function “rxnzone2”

```
T(j,1)=Tfeed;%(R)
T(j,2)=(Tfeed+Tout)/2; %(R)
T(j,3)=Tout;%(R)
for x=1:19
T(j,x)=T(j,x)/1.8; %K
T(j,x)=T(j,x)-273.15; %C
end
Esect(j,3)=Qwmelt;%(Btu/hr)
EsectB=Esect(j,:);%(Btu/hr)
EsectB(19)=0;%(Btu/hr)
The=sum(EsectB);%(Btu/hr), theoretical heat input required
TheS=The*100/61;%(Btu/hr), heat input need to be supplied

for x=1:1:19
    z=6;
    rxnzone2(4,x)=D(x);%in
    rxnzone2(5,x)=L(x); %in
    rxnzone2(z,x)=Lsum(x); %(inches)
    rxnzone2(z+1,x)=Q(j,x);%(in^3/hr)
    rxnzone2(z+2,x)=T(j,x);%(C)
    rxnzone2(z+3,x)=conversion(j,x);% overall conversion
    rxnzone2(z+4,x)=Oconversion(j,x);% segment conversion
    rxnzone2(z+5,x)=Prod(j,x);%(in^3/hr)
    rxnzone2(z+6,x)=pprodsum(j,x);%prosum(j,x);%(in^3/hr)
```

MATLAB Function “rxnzone2”

```
end

rxnzone2(1,1)=Mc;%(lb/hr)

rxnzone2(2,1)=N/60;%(1/min)

rxnzone2(z+1,1)=Db

sections={'1: feed','2: taper1',' 3:taper2',...
          '4: forward1', '5: cylinder1', '6: injection port?? forward2',...
          '7: forward3','8: vent1','9: taper2'...
          '10: forward4','11: cylinder2','12: vent2'...
          '13: taper3','14: forward5','15: reverse'...
          '16: vent3','17: forward6','18: single'...
          '19:die'};

M={'Inlet Carpet Mass Flow Rate (lb/hr)';'Screw speed (1/min)'; ...
  'sections';'Section diameter (in)';'Section length (in)';...
  'Distance from hopper (in)';...
  'Total Volume Flow rate (in^3/hr)';...
  'Temperature (C)';'Segment Conversion';'Overall Conversion';...
  'Product flow (lb/hr)';'Cumulative Product flow (lb/hr)'};

Config={'Barrel diameter (in)';'Total Screw length (in)';...
        'Thermal energy input (Btu/hr)'; 'Mechanical Energy input
(Btu/hr)'};
```

MATLAB Function “rxnzone2”

```
Cvals=[Db; Lsum(18);ThEs;MechEn];

w=xlswrite('Extrud sim results.xls', M, 'Sheet1', 'A1');
excl=xlswrite('Extrud sim results.xls', rxnzone2, 'Sheet1', 'B1');
secciones=xlswrite('Extrud sim results.xls', sections, 'Sheet1', 'B3');
wm=xlswrite('Extrud sim results.xls', Config,'Sheet1', 'A16');
wm0=xlswrite('Extrud sim results.xls', Cvals,'Sheet1', 'B16');
```

MATLAB Function “feedinfo”

```
function feedinfo=feed()

%Inputs

Mc=50; % (lb/hr), carpet mass flow rate

Tfeed=25; %(C), Feed temperature

Tb=325; %(C), barrel temperature of reaction zone

Tbmelt=240; %(C) barrel temperature of melting zone

%Determining screw speed

Nset=15*Mc; %rpm, %nearer to excess surge limit

    %Nset=20*Mc; % rpm, excess surge limit

    %Nset=5*Mc; %rpm, torque limit

Nset=Nset*60; %(revolutions per hour)

%Convert temperature to Rankine

Tfeed=Tfeed+273.15; %(K), Feed temperature

Tfeed=Tfeed*1.8; %(R), Feed temperature

Tb=Tb+273.15; %(K), barrel temperature of reaction zone

Tb=Tb*1.8; %(R),barrel temperature of reaction zone

Tbmelt=Tbmelt+273.15; %(K), barrel temperature of melting zone

Tbmelt=Tbmelt*1.8;%(R),barrel temperature of melting zone

%Carpet composition

comp=[0.77, 0.11, 0.06, 0.06];%(unitless), for PCCN6wt%[n6, PP, CaCO3,
SBR]

%comp=[0.8,0.11,0.06, 0.05];%(unitless), for PCCN66 wt%[n66,...]
```


MATLAB Function “feedinfo”

```
%Finding mass or each compound in the extruder
Massin=comp.*Mc; %(lb/hr),[n6, PP, CaCO3, SBR]mass of each component
Massin(5)=0.01*Massin(1);%(lb/hr),5th position = mass catalyst (1%of N6
wt)

    %if using pure then change 0.01 to 1e-20 or smaller
TMassin=sum(Massin);%(lb/hr),Total Mass feed to extruder

%Evaluate the composition of each compound in the extruder
comp=Massin./TMassin;%(unitless,Total feed comp'tion
[n6,pp,caco3,sbr,koh]

%Densities
rhos=[1.13, 0.9, 2.71, 1.6,2.04];%(g/cc),solid density
%[n6,pp,caco3,sbr,koh], n6= 1.13; n6/6= 1.14
rhos=rhos.*(28317/(453.593*1728));%(lb/in^3)
rhom=[0.97, 0.7];%(g/cc),melt density [n6, pp]same for nylon 6 and 6,6
rhom=rhom.*(28317/(453.593*1728));% (lb/in^3)

%Heat capacities, sources listed in appendix
Cp(1)=1.62/4.1868; %(btu/{lbm F}),n6 solids
Cp(2)=(1.24+0.00304*300)/4.1868;%(btu/{lbm F}), polypropylene solid
Cp(3)=.203; %(btu/{lbm F}),heat capacity of CaCO3,
Cp(4)=1.83/4.1868; %(btu/{lbm F}), heat capacity of SBR,
Cp(5)=78.65920/(56.11*4.1868);%(btu/{lbm F}), heat capacity of KOH

%Volumetric flow rate of solid
```

MATLAB Function “feedinfo”

```
for x=1:5
    Qscomp(x)= Massin(x)/rhos(x); %(in^3/hr),Volumetric flow rate of
each
    %solid component [n6, PP, CaCO3, SBR, koh]
end
Qs=sum(Qscomp); %(in^3/hr),volumetric flow rate of all solids

%Output
feedinfo(1,1)=Tfeed; %(R)
feedinfo(2,1)=Mc; %(lb/hr)
feedinfo(3,1)=Tb; %(R)
feedinfo(4,1)=Tbmelt; %(R)
feedinfo(5,1)=TMassin; %(lb/hr)
feedinfo(7,1)=Qs; %(lb/hr)
feedinfo(13,1)=rhom(1); %(lb/in^3)
feedinfo(13,2)=rhom(2); %(lb/in^3)
feedinfo(14,1)=Nset; %(revolutions per hour)
for x=1:5
    feedinfo(8,x)=comp(x); %(unitless)
    feedinfo(9,x)=Massin(x); %(lb/hr)
    feedinfo(10,x)=rhos(x); %(lb/in^3)
    feedinfo(11,x)=Cp(x); %(btu/lb R)
    feedinfo(12,x)=Qscomp(x); %(lb/hr)
end
```

MATLAB Function “screwdim”

```
function screwdim=screw()  
  
%calling feedinfo function  
feeds=feedinfo();  
Tfeed=feeds(1,1); %(R)  
Mc=feeds(2,1); %(lb/hr)  
Tb=feeds(3,1); %(R)  
Tbmelt=feeds(4,1); %(R)  
TMassin=feeds(5,1); %(lb/hr)  
Qs=feeds(7,1); %(lb/hr)  
rhom(1)=feeds(13,1); %(lb/in^3)  
rhom(2)=feeds(13,2); %(lb/in^3)  
Nset=feeds(14,1); %(revolutions per hour)  
  
for x=1:5  
    comp(x)=feeds(8,x); %(unitless)  
    Massin(x)=feeds(9,x); %(lb/hr)  
    rhos(x)=feeds(10,x); %(lb/in^3)  
    Cp(x)=feeds(11,x); %(btu/lb R)  
    Qscomp(x)=feeds(12,x); %(lb/hr)  
end  
  
%Screw Geometry of 30 mm NFM machine,for definitions of terminology see  
% in chapter 5 and drawing provided; source[89].  
Dbnfm=30; %(mm), barrel diameter  
Dbnfm=Dbnfm*39.37/1000; %(inches), barrel diameter  
Rbnfm=Dbnfm/2;%(inches),barrel radius  
enfm=0.14; %(inches),flight thickness  
Snfm=1.181; %(inches),pitch
```

MATLAB Function “screwdim”

```
thetab=atan(Snfm/(pi*Dbnfm)); %barrel helix angle

Fldnfm=1.170; %(inches),screw + flight diameter

p=1; %(dimensionless),number of flights in parallel

fu=0.85;%(unitless), ratio of uninterrupted barrel circumference to
%that of total barrel circumference, [74]

%Screw segment lengths & diameters of depolymerization twin-screws as
...
%designed by NFM
%segment 1: feed
%segment 2: taper1
%segment 3:taper2
%segment 4: forward1
%segment 5: cylinder1
%segment 6: forward2 with an injection port
%segment 7: forward3
%segment 8: vent1
%segment 9: taper2
%segment 10: forward4
%segment 11: cylinder2
%segment 12: vent2
%segment 13: taper3
%segment 14: forward5
%segment 15: reverse
%segment 16: vent3
%segment 17: forward6
%segment 18: single
%segment 19:die
```

MATLAB Function “screwdim”

```
Lnfm=[6.2 1.77 1.77 4.42 1.77 3.54 1.77 6.19 1.77 4.42 1.77 6.2 1.77
...
4.42 1.77 6.2 8 7.2];%(inches), segment lengths % die not included
Dnfm=[0.9 0.93 1.06 1.025 1.12 0.96 1.11 0.78 0.87 0.96 1.12 0.9
0.93...
0.96 0.96 0.9 0.9 0.9];%(inches) %die not included
%average taken for tapered sections

Rnfm=Dnfm./2;%(inches)

Ldienfm=2; %(inches)
Ddienfm=1; % (inches)
Rdienfm=Ddienfm/2; %(inches)
L(19)= Ldienfm;%(inches)
R(19)=Rdienfm;%(inches)
D(19)=2*R(19);%(inches)

%Finding length to diameter ratio (L/D) for each segment
g2=length(Lnfm); %finding the amount of numbers in the Lnfm array
for x=1:g2
    %LoverD(x)=Lnfm(x)/Dnfm(x);%(dimensionless), L/D for each segment
    LoverD(x)=Lnfm(x)/Dnfm(x); %(dimensionless), L/D for each segment
    Hnfm(x)=Rnfm-Rnfm(x);% (inches), channel depth for each segment
end

%Defining screw speed based on operating line choosen
```

MATLAB Function “screwdim”

```
Nnfm=150;%500 %(rpm), 500 is the maximum given on NFM chart,...
%but can be changed depending operating line used
Nnfm=Nnfm*60; %(revolutions per hour)
Mcnfm=10; %90; %(lb/hr) this is below the maximum before
torque/volumetric
%limit which is 100lb/hr, but can be changed depending
%operating line used
Mnfm=comp.*Mcnfm;%(lb/hr) %mass of each component if max flow rate was
used

%Determining the flow rate of each component when not scaling up
for x=1:5
    Qnfm(x)= Mnfm(x)/rhos(x);%(in^3/hr),(NFM capacity) volumetric flow
    %rate of each component [n6, PP, CaCO3, SBR]
end
Qnfm=sum(Qnfm);%(in^3/hr),(NFM capacity)Vol flow rate of all solids

%Scaling up
if Mc>10 %default
    %if Mc>100, %limit of 30 mm extruder, used when NOT scaling up

    Db=0.5211*Mc^0.3726;% (inches), barrel diameter
    Rb=Db/2; % (inches), barrel radius
    %Fld=Fldnfm*(Qs/Qnfm)^(1/2.75); %(inches),flight diameter
    Fld=Fldnfm*(Db/Dbnfm); %(inches),flight diameter
    S=pi*Db*tan(thetab);%(inches),pitch
    e=enfm*S/Snfm; %(inches),flight width,
```

MATLAB Function “screwdim”

```
for x=1:18

    %Scaling

    % H(x)=Hnfm(x)*(Db/Dbnfm)^0.88; %(inches),channel depth,
traditional

    %no scaling done since smaller provide more friction hence more
    %heat for endothermic reaction

    H(x)=Hnfm(x); %(inches),channel depth

    D(x)=Dnfm(x)*Db/Dbnfm;%(inches),

    R(x)=D(x)/2;%(inches),

    if Mc>=100

        L(x)=Lnfm(x)*(Db/Dbnfm)^1.4;

    else

        L(x)=Lnfm(x)*(Db/Dbnfm)^2;

    end

end

Ddie=(Mc/Mcnfm)^0.333*Ddienfm; %Scaled die diameter

Rdie=Ddie/2; %(inches)

Ldie=(Mc/Mcnfm)^0.333*Ldienfm; %Scaled die length

L(19)= Ldie;%(inches)

R(19)=Rdie;%(inches)

D(19)=2*R(19);%(inches)

N=Nnfm*(Db/Dbnfm)^(-0.12); %(revolutions per hour), scaling screw
speed
```

MATLAB Function “screwdim”

```
else

    Db=Dbnfm;% (inches), barrel diameter

    Rb=Db/2; % (inches), barrel radius

    Fld=Fldnfm; %(inches),flight diameter

    S=pi*Db*tan(thetab);%(inches),pitch

    e=enfm;  %(inches),flight width

    for x=1:18

        H(x)=Hnfm(x); %(inches),channel depth

        R(x)=Rb-H(x);%(inches),screw root radius

        D(x)=Dnfm(x);%(inches),screw root diameter

        L(x)=Lnfm(x); %(unitless), L/D for each segment

    end

    N=Nset; %(revolutions per hour), scaling screw speed

end

for x=1:18

    %calculating the angle of the screw helices phi=tan-1(S/pi*D)

    phi(x)=atan(S/(pi*D(x)));%(radians)

    zb(x)=L(x)/sin(phi(x)); %(inches),helical length, inches

    W(x)=S*cos(phi(x))-e; %(inches,)channel width

end

% Screw helix angles for cylindrical and reverse elements

%phi(15)=-phi(15); % uncomment when forward screw element used instead

of
```


MATLAB Function "screwdim"

```
%reverse

phi(5)=0; %cylinder

phi(11)=0; %cylinder

zb(5)=L(5); %cylinder

zb(11)=L(11); %cylinder

%Other extruder variables/parameters

B=S-e; %(inches), axial distance between the flights

Wb=B*cos(thetab); %(inches), at barrel channel width

deltaf=Db-Fld;%(inches), deltaf clearance between the screw flight and
%the barrel

Ri=2*Rb; %(inches), barrel inner radius approximation for energy
balance

Ro=Ri+2; %(inches), barrel outer radius approximation, assuming
thickness

%is two inches % used in energy balance

alphaa=pi*fu; %(radians), apex angle

%Calculating cumulative sum of length after each segment

Lsum(1)=L(1); %(inches)

for x=2:19

    Lsum(x)=L(x)+Lsum(x-1);%(inches), cumulative length after each
segment

end

Ltotal=sum(L);%(inches), shoud equal Lsum(19)

%"Barrel" velocity in various directions, z=length screw axis, x=cross
```

MATLAB Function “screwdim”

```
axis
Vbz=p*N*Db*cos(thetab); %(inches/hr)
Vbx=p*N*Db*sin(thetab);%(inches/hr)
Vb=p*N*Db;%(inches/hr)

%calculating cross-sectional barrel area, as mentioned in Chapter 6
seglength=10; %(mm) from measurement, gap/apex length, measured in lab
seglength=seglength/1000*39.37; %(inches), converting to inches
hslength=seglength/2; %(inches)
thetal=asin(hslength/Rb); %apex angle
csm=Rb*cos(thetal);%(inches)
o=Rb-csm;%(inches)
topdist=2*o;%(inches)
segarea=Rb*topdist; %(in^2), approximate gap/apex area
areabarrel=2*(pi*(Rb^2)+10*topdist^2-(2*segarea)); %(in^2)

%calculating cross sectional area of screw in the different segment
for x=1:17
    %area of helix attached to rod segment of screw
    Ac(x)= e*(0.06*R(x)+0.03); %(in^2), area of flight
    % calculating screw segment area
    rodarea(x)=R(x)^2*pi;%(in^2), one screw
    Ascrew(x)=2*(rodarea(x)+Ac(x));%(in^2),two screws: rxn cross sec.
area
    Ascrew(x)=2*(rodarea(x));%(in^2), two screws
    %reaction cross sec area
    Aavail(x)=areabarrel-Ascrew(x); %(in^2), area available for
reaction
```

MATLAB Function “screwdim”

```
% Volume of segment,
Vol(x)=L(x)*Aavail(x); % (in^3), volume available for reaction

%for energy balance on segment
A(x)=pi*Ri*L(x); %(in^2), heat transfer area of segment
end

for x=[5,11]
    % calculating and correcting cylindrical segments areas
    rodarea(x)=R(x)^2*pi;%(in^2), one screw
    Ascrew(x)=2*(rodarea(x));%(in^2), two screws
    %reaction cross sec area
    Aavail(x)=areabarrel-Ascrew(x); %(in^2), area available for
reaction
    % Volume of segment
    Vol(x)=L(x)*Aavail(x); % (in^3), volume available for reaction
    TVolume=sum(Vol);

    % For energy balance of segment
    A(x)=pi*Ri*L(x); %(in^2), heat transfer area of segment using the
...
    %approximated inner diameter discribed in chapter 5 energy segment
end

for x=18
    %calculating cross sectional area of screw
    %area of helix attached to rod segment of screw Ah=e/sin
```

MATLAB Function “screwdim”

```
phi*(.06R+.03)

    a1(x)=R(x)*.06; %(inches),account for curvature 0.06 from screw
diagram

    b1(x)=a1(x)+.03; %(inches),inches

    y1(x)=sin(phi(x)); %(unitless), intermediate

    z1(x)=((y1(x))^-1)*e; %(inches),flight projection in X direction

    Ac(x)= b1(x)*z1(x); %(in^2),area of flight

    % calculating screw segment area

    rodarea(x)=(R(x))^2*pi; %(in^2), one screw

    Ascrew(x)=(rodarea(x)+Ac(x));%(in^2), one screws

    %reaction cross sec area

    Aavail(x)=areabarrel-Ascrew(x); %(in^2),area available for reaction

    % Volume of segment x

    Vol(x)=L(x)*Aavail(x);% (in^3), volume available for reaction

    % for energy balance on segment

    A(x)=pi*Ri*L(x); %(in^2),heat transfer area of segment

end

for x=19 %Die

    %reaction area of die

    Aavail(x)=pi*R(19)^2;%(in^2),area available for reaction

    Vol(x)=Aavail(x)*L(19);% (in^3), volume available for reaction

    A(x)=pi*R(19)*L(19); %(in^2),heat transfer area of segment

end
```

MATLAB Function “screwdim”

```
%Calculating shear viscosity and energy dissipated using equations ...
%from Chapter 5.7.1

for x=1:17

    shear(x)=pi*D(x)*N/H(x);%(hr^-1),each segment shear rate

    Mu(x)=2.62*10^-3*7.2330/39.37^2*12*(shear(x))^(0.63-1)*3600^(2-
.63);...

        %(lb/{in hr}), shear viscosity

    visdis(x)=2*(2.62*10^-
3*(shear(x))^(1+0.63)*0.028317/(1055.06*3600^...
0.63*36)); %BTU/(hr in^3) %Chris Rauwendaal page 332.

    Ener(x)=visdis(x)*Vol(x);%BTU/hr
end

for x=18

    shear(x)=pi*D(x)*N/H(x);%(hr^-1),

    Mu(x)=2.62*10^-3*7.2330/39.37^2*12*(shear(x))^(0.63-1)*3600^(2-
.63);...

        %(lb/{in hr})

    visdis(x)=2.62*10^-
3*(shear(x))^(1+0.63)*0.028317/(1055.06*3600^0.63*36);...

        %BTU/(hr in^3) %Chris Rauwendaal page 332.

    Ener(x)=visdis(x)*Qs;%BTU/hr

    %Ener(x)=visdis(x)*Vol(x);%BTU/hr
end

Shear=mean(shear);%(hr^-1), average shear rate of extruder
mu=2.62*10^-3*7.2330/39.37^2*12*(Shear)^(0.63-1)*3600^(2-.63);...

    %(lb/{in hr}), average viscosity
```

MATLAB Function “screwdim”

```
%Drive Power using equations from Chapter 5.7.1
for x=2:18

    %Power consumed in each melt pumping zone, reference:[66]

    PWC(x)=pi^2*(D(x))^3*N^2*L(x)*Mu(x)/(2*(Db-Fld)); %(lb in^2/hr^3)

    PWC(x)=2*PWC(x)*100*9.486*10^(-4)/(7.233*10^-
5*3600^2*12*10^7*39.37);...

    %(Btu/hr)

end

screwdim(1,1)=Db;%(inches)
screwdim(2,1)=Rb;%(inches)
screwdim(3,1)=Fld;%(inches)
screwdim(4,1)=S;%(inches)
screwdim(5,1)=e;%(inches)
screwdim(6,1)=N;%(revolutions per hour)
screwdim(7,1)=B;%(inches)
screwdim(8,1)=Wb;%(inches)
screwdim(9,1)=deltaf;%(inches)
screwdim(10,1)=Ltotal;%(inches)
screwdim(11,1)=p;%(unitless)
screwdim(12,1)=fu;%(unitless)
screwdim(13,1)=Vbz;%(in/hr)
screwdim(14,1)=Vbx;%(in/hr)
screwdim(15,1)=Vb;%(in/hr)
screwdim(16,1)=alphaa;%(radians)
```

MATLAB Function “screwdim”

```
screwdim(17,1)=areabarrel;%(in^2)

screwdim(18,1)=mu;%(lb/{in hr})

screwdim(19,1)=Ri;%(inches)

screwdim(20,1)=Ro;%(inches)

for x=1:18

    screwdim(21,x)=H(x);%(inches)

    screwdim(22,x)=R(x);%(inches)

    screwdim(23,x)=D(x);%(inches)

    screwdim(24,x)=L(x);%(inches)

    screwdim(25,x)=phi(x);%(radians)

    screwdim(26,x)=zb(x);%(inches)

    screwdim(27,x)=W(x);%(inches)

    screwdim(28,x)=Lsum(x);%(inches)

    screwdim(33,x)=Aavail(x);%(in^2)

    screwdim(34,x)=A(x);%(in^2)

    screwdim(35,x)=Vol(x);%(in^3)

    screwdim(40,x)=shear(x);%(hr^-1)

    screwdim(41,x)=Mu(x);%(lb/{in hr})

    screwdim(42,x)=PWC(x);%(Btu/hr)

    screwdim(43,x)=Ener(x);%Btu/hr

end

for x=19

    screwdim(33,x)=Aavail(x);%(in^2)

    screwdim(34,x)=A(x);%(in^2)

    screwdim(35,x)=Vol(x);%(in^3)

    screwdim(22,x)=R(x);%(inches)

    %screwdim(23,x)=D(x);%(inches)
```

MATLAB Function “screwdim”

```
screwdim(24,x)=L(x);%(inches)

screwdim(28,x)=Lsum(x);%(inches)

screwdim(40,x)=shear(18);%(hr^-1)

end

screwdim(29,1)=thetab;%(radians)

screwdim(30,1)=D(19);%(inches)

screwdim(31,1)=R(19);%(inches)

screwdim(32,1)=L(19);%(inches)
```


MATLAB Function “Meltzone”

```
function Meltzone=melt()  
  
%calling feedinfo function  
feeds=feedinfo();  
  
Tfeed=feeds(1,1);  
Mc=feeds(2,1);  
Tb=feeds(3,1);  
Tbmelt=feeds(4,1);  
TMassin=feeds(5,1);  
Qs=feeds(7,1);  
rhom(1)=feeds(13,1);  
rhom(2)=feeds(13,2);  
  
for x=1:5  
    comp(x)=feeds(8,x);  
    Massin(x)=feeds(9,x);  
    rhos(x)=feeds(10,x);  
    Cp(x)=feeds(11,x);  
    Qscomp(x)=feeds(12,x);  
  
end  
  
%calling screwdim function  
screws=screwdim();  
Db=screws(1,1);%(inches)  
Rb=screws(2,1);%(inches)  
Fld=screws(3,1);%(inches)  
S=screws(4,1);%(inches)  
e=screws(5,1);%(inches)  
N=screws(6,1);%(revolutions per hour)
```

MATLAB Function “Meltzone”

```
B=screws(7,1);%(inches)
Wb=screws(8,1);%(inches)
deltaf=screws(9,1);%(inches)
Ltotal=screws(10,1);%(inches)
p=screws(11,1);%(unitless)
fu=screws(12,1);%(unitless)
Vbz=screws(13,1);%(in/hr)
Vbx=screws(14,1);%(in/hr)
Vb=screws(15,1);%(in/hr)
alphaa=screws(16,1);%(radians)
areabarrel=screws(17,1);%(in^2)
mu=screws(18,1);%(lb/{in hr})
Ri=screws(19,1);%(inches)
Ro=screws(20,1);%(inches)
for x=1:19
    H(x)=screws(21,x);%(inches)
    R(x)=screws(22,x);%(inches)
    D(x)=screws(23,x);%(inches)
    L(x)=screws(24,x);%(inches)
    phi(x)=screws(25,x);%(radians)
    zb(x)=screws(26,x);%(inches)
    W(x)=screws(27,x); %(inches)
    Lsum(x)=screws(28,x);%(inches)
    Aavail(x)=screws(33,x);%(in^2)
    A(x)=screws(34,x);%(in^2)
    Vol(x)=screws(35,x);%(in^3)
    shear(x)=screws(40,1);%(hr^-1)
    Mu(x)=screws(41,1);%(lb/{in hr})
```

MATLAB Function “Meltzone”

```
PWC(x)=screws(42,1);%(Btu/hr)

Ener(x)=screws(43,1);%(Btu/hr)

end

thetab=screws(29,1);%(radians)

%FEED and MELTING ZONE

%section 3:taper2   %section 2: taper1   %section 1: feed

%Assumed that the polymer is fully melted by the end of section 3
since

%the temperature will increase to reaction temperature in zone 4 and
%will be well above the melting temperature

%Heat of fusion of polymer [n6, pp]
lambda=[55.08,82.44];%(kJ/kg),
lambda=lambda.*453.59/1055.06; %(btu/lb)

%Thermal conductivity [n6, pp, caco3]
lambdac=[.25, .14, 5.526]; % (W {m K}^-1), %couldn't find for KOH
lambdac=lambdac./(1.73073*12); %(btu/{hr in R})

lambdacmelt=1/(comp(1)/lambdac(1)+comp(2)/lambdac(2)+comp(3)/lambdac(3)
);
%(btu/{hr ft R}), average thermal conductivity

%thermal conductivity of barrel metal
lambdam=21.6; %(W {m K}^-1), %Stainless Steel
```

MATLAB Function “Meltzone”

```
lambdam=lambdam/(1.73073*12); %(btu/{hr in R})

fs=0.6; %(unitless), coefficient of friction of nylon at screw
fb=0.6; %(unitless), coefficient of friction of nylon at barrel
N6meltT=Tb;%(R)

%Calculating feed zone pressure
avtheta=(thetab+phi(1))/2; %(unitless)
Kd(1)=(D(1)*sin(avtheta)+fs*cos(avtheta))/(Db*cos(avtheta)-fs*...
    sin(avtheta)); %(inches)
phip=90-thetab;%(unitless),assuming negligible friction b/c phip is
unknown

%intermediates to find Pressure
A1(1)=fb*Wb*sin(phip)+2*H(1)*fs*sin(thetab)+W(1)*fs*sin(thetab);%(inche
s)
A2(1)= H(1)*((W(1)+Wb)/2)*sin(avtheta);%(in^2)
B1(1)=fb*Wb*cos(phip)-2*H(1)*fs*sin(thetab)*cot(avtheta)*
((D(1)+Db)/2)/...
    Db - W(1)*fs*sin(thetab)*cot(phi(1))*D(1)/Db;%(inches)
B2(1)=H(1)*(W(1)+Wb)/2*cos(avtheta)*((D(1)+Db)/2)/Db;%(in^2)
Pfeed= 1; %(atm), assuming starved feed
Pfeed=Pfeed *1.01325*10^5*7.233*12*3600^2/39.37^2; %(lb/{in hr^2})
P1=Pfeed*exp(((B1(1)-A1(1)*Kd(1))/(B2(1)+A2(1)*Kd(1)))*zb(1));
    %(lb/{in hr^2}),pressure at end of feed zone

for x=1:2
```

MATLAB Function “Meltzone”

```
Qmelt(x)=(Massin(x)*(Cp(x)*(N6meltT-Tfeed))+ Massin(x)*lambda(x));  
    %(btu/hr), heat required for melting and heating N6 and PP from  
    %feed temp to reaction zone start temp.  
end  
for x=3:5  
    Qmelt(x)=Massin(x)*Cp(x)*(N6meltT-Tfeed);  
    %(btu/hr), heat required for heating of other components from  
feed...  
    %temp to reaction zone start temp.  
end  
  
QmeltT=sum(Qmelt); %(btu/hr), total heat required for melting and  
heating..  
    % up to reaction zone start temp.  
  
rhoavm=1/(comp(1)/rhom(1)+comp(2)/rhom(2)+comp(3)/rhos(3)+comp(4)/rhos.  
..  
    (4)+comp(5)/rhos(5)); %(lb/in^3), average density  
  
Cpm=1/(comp(1)/Cp(1)+comp(2)/Cp(2)+comp(3)/Cp(3)+comp(4)/Cp(4)+comp...  
    (5)/Cp(5));%(btu/lb R), average solid heat capacity  
  
%Finding heat transfer coefficient (HTC)  
    alphamelt=  
0.94*lambda(melt)/((D(2)+D(3))/2)*(((rhoavm*N*((D(2)+D(3))...
```

MATLAB Function “Meltzone”

```

/2)^2)/mu)^0.28)*(Cpm*mu/lambdacmelt)^0.33; %(btu/{hr in^2 R})

    % HTC if polymer and barrel wall

Umelt=1/((Ri*(log(Ro/Ri))/lambdam)+(1/alphamelt));%(btu/{hr in^2
R})

    % overall HTC
Amelt= pi*Ri*(L(1)+L(2)+L(3));%(in^2), heat transfer area
Qwmelt=Umelt*Amelt*(Tb-Tfeed);%(btu/hr), heat transferred to melt from
barrel

%section 1: feed
%All the equations to find power can be found in Chapter 5.7.1
%power consumed by solid conveying
for x=1 %for 8
    theta=90-phi(x);
    Ew=pi*N*D(x)*cos(theta)*fb*Wb(x)*zb(x)*(P1-Pfeed)/...
        log(P1/Pfeed);%(lb in^2/hr^3)%power consumed by solid conveying
    Ew=Ew*100*9.486*10^-4/(7.233*10^-5*3600^2*12*10^7*39.37);%(Btu/hr)

    Eh=pi*N*D(x)*sin(thetab)/(sin(thetab-theta))*fb*Wb(x)*zb(x)*...
        (P1-Pfeed)/log(P1/Pfeed);%(lb in^2/hr^3)% power turned into
heat from solid conveying
    Eh=abs(Eh*100*9.486*10^-4/(7.233*10^-
5*3600^2*12*10^7*39.37));%(Btu/hr)

```

MATLAB Function “Meltzone”

```
end %for 8

%section 2: taper1 & %section 3:taper2
% Average screw dimensions in tapered segments
Dav=(D(2)+D(3))/2; %(inches)
Wav=(W(2)+W(3))/2;%(inches)
phiav=(phi(2)+phi(3))/2;%(unitless)

%power supplied for solid conveying
Esolid= Eh+Ener(1)+Ener(2)+Ener(3);%(Btu/hr)
EsolidS=Esolid*100/61;%(Btu/hr)

% temperature leaving meltzone
Tout=(Umelt*Amelt*(Tb-Tfeed)+Esolid-(Massin(1)*lambda(1)+Massin(2)*...
    lambda(2))+Mc*Cpm*Tfeed)/(Mc*Cpm);
%Power consumed
    PC=sum(PWC)+abs(Ew);%(Btu/hr), PWC is tanken from screwdim and Ew
above

%Power needed to be supplied for melt pumping
PWN(x)=100*PC/61;  %(Btu/hr)
%[83] - 61%
%[71] -80-90%
PWNT=sum(PWN);%(Btu/hr)
MechEn=PWNT+EsolidS;%(Btu/hr)

%end of FEED and MELTING zone
```

MATLAB Function “Meltzone”

```
Meltzone(1,1)=Pfeed;%(lb/{in hr^2})
Meltzone(2,1)=P1;%(lb/{in hr^2})
Meltzone(3,1)=Tout;% (R)
Meltzone(4,1)=QmeltT;%(btu/hr)
Meltzone(7,1)=Qwmelt;%(btu/hr)
Meltzone(8,1)=lambdam;%(btu/{hr in R})
for x=1:2
Meltzone(9,x)=Qmelt(x);%(btu/hr)
end
for x=1:3
    Meltzone(10,x)=lambdac(x);%(btu/{hr in R})
end
Meltzone(11,1)=N6meltT;%(R)
Meltzone(12,1)=rhoavm;%(lb/in^3), average density
Meltzone(13,1)=Cpm;%(btu/lb R), aveage heat capacity
Meltzone(14,1)=lambda(1);%(btu/lb),heat of fusion of polymer
Meltzone(14,2)=lambda(2);%(btu/lb),heat of fusion of polymer
Meltzone(15,1)=MechEn;%(Btu/hr), mechanical power supplied
Meltzone(16,1)=Qwmelt;%(Btu/hr), heat transferred to melt from barrel
```


MATLAB Function “Pressure”

```
function Pressure=press()  
  
%calling feedinfo function  
  
feeds=feedinfo();  
Tfeed=feeds(1,1);%(R)  
Mc=feeds(2,1);%(lb/hr)  
Tb=feeds(3,1);%(R)  
Tbmelt=feeds(4,1);%(R)  
TMassin=feeds(5,1); %(lb/hr)  
Qs=feeds(7,1);%(lb/hr)  
rhom(1)=feeds(13,1);%(lb/in^3)  
rhom(2)=feeds(13,2);%(lb/in^3)  
  
for x=1:5  
    comp(x)=feeds(8,x);%(unitless)  
    Massin(x)=feeds(9,x);%(lb/hr)  
    rhos(x)=feeds(10,x);%(lb/in^3)  
    Cp(x)=feeds(11,x);%(btu/lb R)  
    Qscomp(x)=feeds(12,x);%(lb/hr)  
  
end  
  
%calling screwdim function  
  
screws=screwdim();  
Db=screws(1,1);%(inches)  
Rb=screws(2,1);%(inches)  
Fld=screws(3,1);%(inches)  
S=screws(4,1);%(inches)  
e=screws(5,1);%(inches)  
N=screws(6,1);%(revolutions per hour)  
B=screws(7,1);%(inches)
```

MATLAB Function “Pressure”

```
Wb=screws(8,1);%(inches)

deltaf=screws(9,1);%(inches)

Ltotal=screws(10,1);%(inches)

p=screws(11,1);%(unitless)

fu=screws(12,1);%(unitless)

Vbz=screws(13,1);%(in/hr)

Vbx=screws(14,1);%(in/hr)

Vb=screws(15,1);%(in/hr)

alphaa=screws(16,1);%(radians)

areabarrel=screws(17,1);%(in^2)

mu=screws(18,1);%(lb/{in hr})

Ri=screws(19,1);%(inches)

Ro=screws(20,1);%(inches)

for x=1:19

    H(x)=screws(21,x);%(inches)

    R(x)=screws(22,x);%(inches)

    D(x)=screws(23,x);%(inches)

    L(x)=screws(24,x);%(inches)

    phi(x)=screws(25,x);%(radians)

    zb(x)=screws(26,x);%(inches)

    W(x)=screws(27,x); %(inches)

    Lsum(x)=screws(28,x);%(inches)

    Aavail(x)=screws(33,x);%(in^2)

    A(x)=screws(34,x);%(in^2)

    Vol(x)=screws(35,x);%(in^3)

end

thetab=screws(29,1);%(radians)

Ddie=screws(30,1);%(inches)
```

MATLAB Function “Pressure”

```
Rdie=screws(31,1);%(inches)
Ldie=screws(32,1);%(inches)

%calling meltzone
Melts=Meltzone();
Pfeed=Melts(1,1);%(lb/{in hr^2})
P1=Melts(2,1);%(lb/{in hr^2})
QmeltT=Melts(4,1);%(btu/hr)
Qwmelt=Melts(7,1);%(btu/hr)
lambdam=Melts(8,1);%(btu/{hr in R})
N6meltT=Melts(11,1);%(R)
for x=1:2
    Qmelt(x)=Melts(9,x);%(btu/hr)
end
for x=1:3
    lambdac(x)=Melts(10,x);%(btu/{hr in R})
end

%All pressure/flow, filled length equation used therein can be ...
%found in Chapter 5.5

f=alphaa/pi; %(unitless)
% loading initial guess of die volumetric flow rate that was put in a
file
% by rxnzone2
Q=load('Q.txt'); %(in^3/hr)
```

MATLAB Function “Pressure”

```
Qdie=Q(19);%(in^3/hr)

Qse=Q(18);% (in^3/hr), flow rate in single screw segment

% Determining segment pressure and degree filled starting from die

% segment 19:die

deltaPdie=(8*Qdie*Ldie*mu)/(pi*Rdie^4); %(lb/{in hr^2})

P(19)= 1; %atm,

P(19)=P(19)*1.01325*10^5*7.233*12*3600^2/39.37^2; %(lb/{in hr^2})

P(18)=P(19)-deltaPdie; %(lb/{in hr^2})

Vfil(19)=Aavail(19)*Ldie;%(in^3)

filL(19)=Ldie;%(inches)

%segment 18: single

for x=18

    deltaP(x)=(Lsum(x)-Lsum(17))*(-

Qse+0.5*W(x)*H(x)*N*D(x)*cos(phi(x))*...

    (1-0.57*H(x)/W(x))/((W(x)*(H(x))^3)*(1-

0.62*(H(x)/W(x)))/(12*mu)));

    %(lb/{in hr^2})

    P(x-1)=P(x)-deltaP(x); %(lb/{in hr^2})

    vf=P(19)/deltaP(x); %(unitless)

    % filL(x)=vf*S;%(inches) %check where this came from

    kN(x)=W(x)*H(x)*D(x)*pi*cos(phi(x))*(1-0.57*H(x)/W(x))/2;%(in^3)

    kp(x)=(1-.62*H(x)/W(x))*W(x)*(H(x)^3)/12;%(in^4)
```

MATLAB Function “Pressure”

```
fillL(x)=kp(x)*deltaP(x)/(mu*(kN(x)*N-Qse)); %(inches)

%Determining if fill length is more than length of segment or if
there
%is any filled length
if fillL(x)>= L(x)
    Vfil(x)=Aavail(x)*L(x);%(in^3)
    fillL(x-1)=L(x-1)-L(x); %(inches)
else
    pDf(x)=(Qse/N)/kN(x); % (unitless), drag flow
    pVfil(x)=pDf(x)*pi*H(x)^2*(L(x)-fillL(x))*(360-45)/360;%(in^3)
    Vfil(x)=fillL(x)*A(x)+pVfil(x);%(in^3)
end
end

%segment 17: forward6
for x=17
    %calculating pressure drop
    Wa(x)=D(x)*(1-cos(alphaa))+2*deltaf;%(inches)
    %using intermediates to find deltaP
    Ap(x)=0.5*fu*W(x)*H(x)*Vbz;%(in^3/hr)
    Bp(x)=W(x)*(H(x))^3/(12*mu);%(in^5 hr/lb)
    Cp1(x)=(pi*D(x)*(deltaf^3)*cos(phi(x)))/(12*mu*e);%(in^4 hr/lb)
    Cp2(x)=pi*D(x)*cos(phi(x))/p; %(inches)
    Cp3(x)=6*mu*Vbx*W(x)/((H(x))^2);%(lb/in hr^2)
    Dp(x)=p*e*(deltaf^3)/(12*mu);%(in^5 hr/lb)
    Ep(x)=.5*(1-fu)*pi*D(x)*(H(x)+.5*Wa(x))*Vb*sin(phi(x));% (in^3/hr)
    Fp(x)=.5*(1-fu)*pi*D(x)*((H(x)+.5*Wa(x))^3)/(12*mu); %(in^5 hr/lb)
```

MATLAB Function “Pressure”

```
gz(x)=(Ap(x)-Cp1(x)*Cp3(x)-Ep(x)-
Q(x))/(Bp(x)+Cp1(x)*Cp2(x)+Dp(x)+...
    Fp(x)/sin(phi(x))); %(lb/{in^2 hr^2})
deltaP(x)=(Lsum(x)-Lsum(x-1))*gz(x);%(lb/{in hr^2})
P(x-1)=P(x)-deltaP(x);%(lb/{in hr^2})

kN(x)=f*W(x)*H(x)*pi*D(x)*cos(phi(x))-
(pi*D(x)*W(x)*sin(phi(x)))/...
    (e*H(x)^2);%(in^3)
kc12(x)=pi^2*D(x)^2*deltaf^3/(6*e*p)+p*e*deltaf^3/6; %(in^4)
Wa(x)=D(x)*(1-cos(alphaa))+2*deltaf; %(inches)
Ha(x)=0.5*D(x)*sin(alphaa);%(inches)
hem(x)=Wa(x)/(2*H(x)); %(unitless)

ka(x)=2*(7*hem(x)^3*Ha(x)^4*(27*hem(x)^4+5))/(90*(55*hem(x)^4+38*...
    hem(x)^4+3)); %(in^4)
kch(x)=W(x)*(H(x)^3)/6;%(in^4)
kp(x)=kch(x)+ka(x)+kc12(x);%(in^4)
filL(x)=kp(x)*deltaP(x)/(mu*(kN(x)*N-Q(x)));%+ filL(x);%(inches)
%determining if fill length is more than length of segment or if
there
%is any filled length
if filL(x)>= L(x)
    Vfil(x)=Aavail(x)*L(x);%(in^3)
    filL(x-1)=L(x-1)-L(x);%(inches)
else
    pDf(x)=(Q(x)/N)/kN(x); % (unitless),drag flow
    pVfil(x)=pDf(x)*pi*H(x)^2*(L(x)-filL(x))*(360-45)/360;%(in^3)
```

MATLAB Function “Pressure”

```
Vfil(x)=fill(x)*A(x)+pVfil(x);%(in^3)

end

end

%segment 16: forward with vent3

for x=16

    %calculating presure drop

    Wa(x)=D(x)*(1-cos(alphaa))+2*deltaf;%(inches)

    %using intermediates to find deltaP

    Ap(x)=0.5*fu*W(x)*H(x)*Vbz;%(in^3/hr)

    Bp(x)=W(x)*(H(x))^3/(12*mu);%(in^5 hr/lb)

    Cp1(x)=(pi*D(x)*(deltaf^3)*cos(phi(x)))/(12*mu*e);%(in^4 hr/lb)

    Cp2(x)=pi*D(x)*cos(phi(x))/p; %(inches)

    Cp3(x)=6*mu*Vbx*W(x)/((H(x))^2);%(lb/in hr^2)

    Dp(x)=p*e*(deltaf^3)/(12*mu);%(in^5 hr/lb)

    Ep(x)=.5*(1-fu)*pi*D(x)*(H(x)+.5*Wa(x))*Vb*sin(phi(x));% (in^3/hr)

    Fp(x)=.5*(1-fu)*pi*D(x)*((H(x)+.5*Wa(x))^3)/(12*mu); %(in^5 hr/lb)

    gz(x)=(Ap(x)-Cp1(x)*Cp3(x)-Ep(x)-
Q(x))/(Bp(x)+Cp1(x)*Cp2(x)+Dp(x)+...

    Fp(x)/sin(phi(x))); %(lb/{in^2 hr^2})

    deltaP(x)=(Lsum(x)-Lsum(x-1))*gz(x);%(lb/{in hr^2})

    P(x-1)=P(x)-deltaP(x);%(lb/{in hr^2})

    kN(x)=f*W(x)*H(x)*pi*D(x)*cos(phi(x))-
(pi*D(x)*W(x)*sin(phi(x)))/...

    (e*H(x)^2);%(in^3)

    kc12(x)=pi^2*D(x)^2*deltaf^3/(6*e*p)+p*e*deltaf^3/6; %(in^4)

    Wa(x)=D(x)*(1-cos(alphaa))+2*deltaf; %(inches)
```

MATLAB Function “Pressure”

```
Ha(x)=0.5*D(x)*sin(alphaa);%(inches)

hem(x)=Wa(x)/(2*H(x)); %(unitless)

ka(x)=2*(7*hem(x)^3*Ha(x)^4*(27*hem(x)^4+5))/(90*(55*hem(x)^4+38*...
    hem(x)^4+3)); %(in^4)

kch(x)=W(x)*(H(x)^3)/6;%(in^4)

kp(x)=kch(x)+ka(x)+kc12(x);%(in^4)

filL(x)=kp(x)*deltaP(x)/(mu*(kN(x)*N-Q(x)));%(inches),

    %determining if fill length is more than length of segment or if
there
    %is any filled length
    if filL(x)>= L(x)
        Vfil(x)=Aavail(x)*L(x);%(in^3) %shouldnt need this
    else
        pDf(x)=(Q(x)/N)/kN(x); % (unitless),drag flow
        pVfil(x)=pDf(x)*pi*H(x)^2*(L(x)-filL(x))*(360-45)/360;%(in^3)
        Vfil(x)=filL(x)*A(x)+pVfil(x);%(in^3)
    end
end

%segment 15: reverse
for x=15
    %calculating presure drop

    Wa(x)=D(x)*(1-cos(alphaa))+2*deltaf;

    %using intermediates to find deltaP
```


MATLAB Function “Pressure”

```
Ap(x)=0.5*fu*W(x)*H(x)*Vbz;%(in^3/hr)

Bp(x)=W(x)*(H(x))^3/(12*mu);%(in^5 hr/lb)

Cp1(x)=(pi*D(x)*(deltaf^3)*cos(phi(x)))/(12*mu*e);%(in^4 hr/lb)

Cp2(x)=pi*D(x)*cos(phi(x))/p; %(inches)

Cp3(x)=6*mu*Vbx*W(x)/((H(x))^2);%(lb/in hr^2)

Dp(x)=p*e*(deltaf^3)/(12*mu);%(in^5 hr/lb)

Ep(x)=.5*(1-fu)*pi*D(x)*(H(x)+.5*Wa(x))*Vb*sin(phi(x));% (in^3/hr)

Fp(x)=.5*(1-fu)*pi*D(x)*((H(x)+.5*Wa(x))^3)/(12*mu); %(in^5 hr/lb)

gz(x)=(Ap(x)-Cp1(x)*Cp3(x)-Ep(x)-
Q(x))/(Bp(x)+Cp1(x)*Cp2(x)+Dp(x)+...

    Fp(x)/sin(phi(x))); %(lb/{in^2 hr^2})

deltaP(x)=(Lsum(x)-Lsum(x-1))*gz(x);%(lb/{in hr^2})

P(x-1)=P(x)-deltaP(x);%(lb/{in hr^2})

Vfil(x)=Aavail(x)*L(x);%(in^3)

filL(x)=L(x);%(inches

% intermediate for length of filled segment

kkN(x)=f*W(x)*H(x)*pi*D(x)*cos(phi(x))-
(pi*D(x)*W(x)*sin(phi(x)))/...

    (e*H(x)^2);%(in^3)

kc12(x)=pi^2*D(x)^3*deltaf^3/(6*e*p)+p*e*deltaf^3/6; %(in^5 or
in^4)check please

Wa(x)=D(x)*(1-cos(alphaa))+2*deltaf; %(inches)

Ha(x)=0.5*D(x)*sin(alphaa);%(inches)

hem(x)=Wa(x)/(2*H(x)); %(unitless)

ka(x)=2*(7*hem(x)^3*Ha(x)^4*(27*hem(x)^4+5))/(90*(55*hem(x)^4+38*...
```

MATLAB Function “Pressure”

```
hem(x)^4+3)); %(in^4)

kch(x)=W(x)*(H(x)^3)/6;%(in^4)

kp(x)=-(kch(x)+ka(x)+kc12(x));%(in^4) pressure term; hence negative
in front

%      filL(x-1)=kp(x)*deltaP(x)/(mu*(kN(x)*N-Q(x)));%(inches)
end

%segment 14: forward5
for x=14

    %for x=17:-1:4

    %calculating presure drop

    Wa(x)=D(x)*(1-cos(alphaa))+2*deltaf;%(inches)

    %using intermediates to find deltaP

    Ap(x)=0.5*fu*W(x)*H(x)*Vbz;%(in^3/hr)

    Bp(x)=W(x)*(H(x))^3/(12*mu);%(in^5 hr/lb)

    Cp1(x)=(pi*D(x)*(deltaf^3)*cos(phi(x)))/(12*mu*e);%(in^4 hr/lb)

    Cp2(x)=pi*D(x)*cos(phi(x))/p; %(inches)

    Cp3(x)=6*mu*Vbx*W(x)/((H(x))^2);%(lb/in hr^2)

    Dp(x)=p*e*(deltaf^3)/(12*mu);%(in^5 hr/lb)

    Ep(x)=.5*(1-fu)*pi*D(x)*(H(x)+.5*Wa(x))*Vb*sin(phi(x));% (in^3/hr)

    Fp(x)=.5*(1-fu)*pi*D(x)*((H(x)+.5*Wa(x))^3)/(12*mu); %(in^5 hr/lb)

    gz(x)=(Ap(x)-Cp1(x)*Cp3(x)-Ep(x)-
Q(x))/(Bp(x)+Cp1(x)*Cp2(x)+Dp(x)+...

    Fp(x)/sin(phi(x))); %(lb/{in^2 hr^2})

    deltaP(x)=(Lsum(x)-Lsum(x-1))*gz(x);%(lb/{in hr^2})
```

MATLAB Function “Pressure”

```
P(x-1)=P(x)-deltaP(x);%(lb/{in hr^2})

%      length of filled segment before reverse

kN(x)=f*W(x)*H(x)*pi*D(x)*cos(phi(x))-
(pi*D(x)*W(x)*sin(phi(x)))/...
    (e*H(x)^2);%(in^3)

kc12(x)=pi^2*D(x)^2*deltaf^3/(6*e*p)+p*e*deltaf^3/6; %(in^4)

Wa(x)=D(x)*(1-cos(alphaa))+2*deltaf; %(inches)

Ha(x)=0.5*D(x)*sin(alphaa);%(inches)

hem(x)=Wa(x)/(2*H(x)); %(unitless)

ka(x)=2*(7*hem(x)^3*Ha(x)^4*(27*hem(x)^4+5))/(90*(55*hem(x)^4+38*...
    hem(x)^4+3)); %(in^4)

kch(x)=W(x)*(H(x)^3)/6;%(in^4)

kp(x)=kch(x)+ka(x)+kc12(x);%(in^4)

filL(x)=kp(x)*deltaP(x)/(mu*(kN(x)*N-Q(x)));%(inches)

%determining if fill length is more than length of segment or if
there
%is any filled length
if filL(x)>= L(x)
    Vfil(x)=Aavail(x)*L(x); %(in^3)
    filL(x-1)=L(x-1)-L(x);%(inches)
else
    pDf(x)=(Q(x)/N)/kN(x); % (unitless),drag flow
    pVfil(x)=pDf(x)*pi*H(x)^2*(L(x)-filL(x))*(360-45)/360;%(in^3)
    Vfil(x)=filL(x)*A(x)+pVfil(x);%(in^3)
end
```

MATLAB Function “Pressure”

```
end

%segment 13: tapered3 %took average screw diameter
for x=13
    %for x=17:-1:4
    %calculating presure drop
    Wa(x)=D(x)*(1-cos(alphaa))+2*deltaf;%(inches)
    %using intermediates to find deltaP
    Ap(x)=0.5*fu*W(x)*H(x)*Vbz;%(in^3/hr)
    Bp(x)=W(x)*(H(x))^3/(12*mu);%(in^5 hr/lb)
    Cp1(x)=(pi*D(x)*(deltaf^3)*cos(phi(x)))/(12*mu*e);%(in^4 hr/lb)
    Cp2(x)=pi*D(x)*cos(phi(x))/p; %(inches)
    Cp3(x)=6*mu*Vbx*W(x)/((H(x))^2);%(lb/in hr^2)
    Dp(x)=p*e*(deltaf^3)/(12*mu);%(in^5 hr/lb)
    Ep(x)=.5*(1-fu)*pi*D(x)*(H(x)+.5*Wa(x))*Vb*sin(phi(x));% (in^3/hr)
    Fp(x)=.5*(1-fu)*pi*D(x)*((H(x)+.5*Wa(x))^3)/(12*mu); %(in^5 hr/lb)
    gz(x)=(Ap(x)-Cp1(x)*Cp3(x)-Ep(x)-
Q(x))/(Bp(x)+Cp1(x)*Cp2(x)+Dp(x)+...
    Fp(x)/sin(phi(x))); %(lb/{in^2 hr^2})
    deltaP(x)=(Lsum(x)-Lsum(x-1))*gz(x);%(lb/{in hr^2})
    P(x-1)=P(x)-deltaP(x);%(lb/{in hr^2})
    % length of filled segment before reverse
    kN(x)=f*W(x)*H(x)*pi*D(x)*cos(phi(x))-
(pi*D(x)*W(x)*sin(phi(x)))/...
    (e*H(x)^2);%(in^3)
    kc12(x)=pi^2*D(x)^2*deltaf^3/(6*e*p)+p*e*deltaf^3/6; %(in^4)
    Wa(x)=D(x)*(1-cos(alphaa))+2*deltaf; %(inches)
    Ha(x)=0.5*D(x)*sin(alphaa);%(inches)
```

MATLAB Function “Pressure”

```
hem(x)=Wa(x)/(2*H(x)); %(unitless)

ka(x)=2*(7*hem(x)^3*Ha(x)^4*(27*hem(x)^4+5))/(90*(55*hem(x)^4+38*...
    hem(x)^4+3)); %(in^4)

kch(x)=W(x)*(H(x)^3)/6;%(in^4)

kp(x)=kch(x)+ka(x)+kc12(x);%(in^4)

filL(x)=kp(x)*deltaP(x)/(mu*(kN(x)*N-Q(x)));%(inches)

%determining if fill length is more than length of segment or if
there

%is any filled length

if filL(x)>= L(x)

    Vfil(x)=Aavail(x)*L(x);%(in^3)

    filL(x-1)=L(x-1)-L(x);%(inches)

else

    pDf(x)=(Q(x)/N)/kN(x);% (unitless),drag flow

    pVfil(x)=pDf(x)*pi*H(x)^2*(L(x)-filL(x))*(360-45)/360;%(in^3)

    Vfil(x)=filL(x)*A(x)+pVfil(x);%(in^3)

end

end

%segment 12: forward with vent2

for x=12

    %calculating presure drop

    Wa(x)=D(x)*(1-cos(alphaa))+2*deltaf;%(inches)

    %using intermediates to find deltaP

    Ap(x)=0.5*fu*W(x)*H(x)*Vbz;%(in^3/hr)

    Bp(x)=W(x)*(H(x))^3/(12*mu);%(in^5 hr/lb)

    Cp1(x)=(pi*D(x)*(deltaf^3)*cos(phi(x)))/(12*mu*e);%(in^4 hr/lb)
```

MATLAB Function “Pressure”

```
Cp2(x)=pi*D(x)*cos(phi(x))/p; %(inches)

Cp3(x)=6*mu*Vbx*W(x)/((H(x))^2);%(lb/in hr^2)

Dp(x)=p*e*(deltaf^3)/(12*mu);%(in^5 hr/lb)

Ep(x)=.5*(1-fu)*pi*D(x)*(H(x)+.5*Wa(x))*Vb*sin(phi(x));% (in^3/hr)

Fp(x)=.5*(1-fu)*pi*D(x)*((H(x)+.5*Wa(x))^3)/(12*mu); %(in^5 hr/lb)

gz(x)=(Ap(x)-Cp1(x)*Cp3(x)-Ep(x)-
Q(x))/(Bp(x)+Cp1(x)*Cp2(x)+Dp(x)+...
    Fp(x)/sin(phi(x))); %(lb/{in^2 hr^2})

% P(x)=1; %atm, change to that of vacuum

% P(x)=P(x)*1.01325*10^5*7.233*12*3600^2/39.37^2; %(lb/{in hr^2})

deltaP(x)=(Lsum(x)-Lsum(x-1))*gz(x);%(lb/{in hr^2})

P(x-1)=P(x)-deltaP(x);%(lb/{in hr^2})

kN(x)=f*W(x)*H(x)*pi*D(x)*cos(phi(x))-
(pi*D(x)*W(x)*sin(phi(x)))/...
    (e*H(x)^2);%(in^3)

kc12(x)=pi^2*D(x)^2*deltaf^3/((6*e*p)+p*e*deltaf^3/6); %(in^4)

Wa(x)=D(x)*(1-cos(alphaa))+2*deltaf; %(inches)

Ha(x)=0.5*D(x)*sin(alphaa);%(inches)

hem(x)=Wa(x)/(2*H(x)); %(unitless)

ka(x)=2*(7*hem(x)^3*Ha(x)^4*(27*hem(x)^4+5))/(90*(55*hem(x)^4+38*...
    hem(x)^4+3)); %(in^4)

kch(x)=W(x)*(H(x)^3)/6;%(in^4)

kp(x)=kch(x)+ka(x)+kc12(x);%(in^4)

fill(x)=kp(x)*deltaP(x)/(mu*(kN(x)*N-Q(x)));%+fill(x);%(inches),
    %determining if fill length is more than length of segment or if
there
```

MATLAB Function “Pressure”

```
%is any filled length

if fillL(x)>= L(x)

    Vfil(x)=Aavail(x)*L(x);%(in^3)

else

    pDf(x)=(Q(x)/N)/kN(x); % (unitless),drag flow

    pVfil(x)=pDf(x)*pi*H(x)^2*(L(x)-fillL(x))*(360-45)/360;%(in^3)

    Vfil(x)=fillL(x)*A(x)+pVfil(x);%(in^3)

end

end

%segment 11: cylinder2

for x=11

    k(x)=D(x)/Db; %(unitless)

    alffa=pi*((R(x))^4)*(1-(k(x))^4+((k(x))^4-2*(k(x))^2+1)/log(k(x))));

    Wa(x)=D(x)*(1-cos(alphaa))+2*deltaf;%(inches)

    Ha(x)=0.5*D(x)*sin(alphaa);%(inches)

    hem(x)=Wa(x)/(2*H(x));%(unitless)

    beeta=Ha(x)^4*(189*(hem(x))^5+35*(hem(x))^2)/(2475*(hem(x))^4+1710*...

        (hem(x))^2+135);%(inches)

    deltaP(x)=L(x)*mu*Q(x)/(alffa+beeta);%(lb/{in hr^2})

    P(x-1)=P(x)-deltaP(x);%(lb/{in hr^2})

    fillL(x-1)=kp(x)*deltaP(x)/(mu*(kN(x)*N-Q(x)));%(inches)

    %determining if fill length is more than length of segment or if
there
```

MATLAB Function “Pressure”

```
%is any filled length

Vfil(x)=Aavail(x)*L(x);%(in^3)

fillL(x)=L(x);%(inches)

end

%segment 10: forward4
for x=10
    %for x=17:-1:4
    %calculating presure drop
    Wa(x)=D(x)*(1-cos(alphaa))+2*deltaf;
    %using intermediates to find deltaP
    Ap(x)=0.5*fu*W(x)*H(x)*Vbz;%(in^3/hr)
    Bp(x)=W(x)*(H(x))^3/(12*mu);%(in^5 hr/lb)
    Cp1(x)=(pi*D(x)*(deltaf^3)*cos(phi(x)))/(12*mu*e);%(in^4 hr/lb)
    Cp2(x)=pi*D(x)*cos(phi(x))/p; %(inches)
    Cp3(x)=6*mu*Vbx*W(x)/((H(x))^2);%(lb/in hr^2)
    Dp(x)=p*e*(deltaf^3)/(12*mu);%(in^5 hr/lb)
    Ep(x)=.5*(1-fu)*pi*D(x)*(H(x)+.5*Wa(x))*Vb*sin(phi(x));% (in^3/hr)
    Fp(x)=.5*(1-fu)*pi*D(x)*((H(x)+.5*Wa(x))^3)/(12*mu); %(in^5 hr/lb)
    gz(x)=(Ap(x)-Cp1(x)*Cp3(x)-Ep(x)-
Q(x))/(Bp(x)+Cp1(x)*Cp2(x)+Dp(x)+...
    Fp(x)/sin(phi(x))); %(lb/{in^2 hr^2})
    deltaP(x)=(Lsum(x)-Lsum(x-1))*gz(x);%(lb/{in hr^2})
    P(x-1)=P(x)-deltaP(x);%(lb/{in hr^2})
```


MATLAB Function “Pressure”

```
%length of filled segment before cylinder

kN(x)=f*W(x)*H(x)*pi*D(x)*cos(phi(x))-
(pi*D(x)*W(x)*sin(phi(x)))/...
    (e*H(x)^2);%(in^3)

kc12(x)=pi^2*D(x)^2*deltaf^3/(6*e*p)+p*e*deltaf^3/6; %(in^4)

Wa(x)=D(x)*(1-cos(alphaa))+2*deltaf; %(inches)

Ha(x)=0.5*D(x)*sin(alphaa);%(inches)

hem(x)=Wa(x)/(2*H(x)); %(unitless)

ka(x)=2*(7*hem(x)^3*Ha(x)^4*(27*hem(x)^4+5))/(90*(55*hem(x)^4+38*...
    hem(x)^4+3)); %(in^4)

kch(x)=W(x)*(H(x)^3)/6;%(in^4)

kp(x)=kch(x)+ka(x)+kc12(x);%(in^4)

filL(x)=kp(x)*deltaP(x)/(mu*(kN(x)*N-Q(x)));%+ filL(x);%(inches)

%determining if fill length is more than length of segment or if
there

%is any filled length
if filL(x)>= L(x)
    Vfil(x)=Aavail(x)*L(x);%(in^3)
    filL(x-1)=L(x-1)-L(x);%(inches)
else
    pDf(x)=(Q(x)/N)/kN(x); % (unitless),drag flow
    pVfil(x)=pDf(x)*pi*H(x)^2*(L(x)-filL(x))*(360-45)/360;%(in^3)
    Vfil(x)=filL(x)*A(x)+pVfil(x);%(in^3)
end
end

%segment 9: tapered2
```

MATLAB Function “Pressure”

```
%took average screw diameter

for x=9

    %for x=17:-1:4

    %calculating presure drop

    Wa(x)=D(x)*(1-cos(alphaa))+2*deltaf;

    %using intermediates to find deltaP

    Ap(x)=0.5*fu*W(x)*H(x)*Vbz;%(in^3/hr)

    Bp(x)=W(x)*(H(x))^3/(12*mu);%(in^5 hr/lb)

    Cp1(x)=(pi*D(x)*(deltaf^3)*cos(phi(x)))/(12*mu*e);%(in^4 hr/lb)

    Cp2(x)=pi*D(x)*cos(phi(x))/p; %(inches)

    Cp3(x)=6*mu*Vbx*W(x)/((H(x))^2);%(lb/in hr^2)

    Dp(x)=p*e*(deltaf^3)/(12*mu);%(in^5 hr/lb)

    Ep(x)=.5*(1-fu)*pi*D(x)*(H(x)+.5*Wa(x))*Vb*sin(phi(x));% (in^3/hr)

    Fp(x)=.5*(1-fu)*pi*D(x)*((H(x)+.5*Wa(x))^3)/(12*mu); %(in^5 hr/lb)

    gz(x)=(Ap(x)-Cp1(x)*Cp3(x)-Ep(x)-
Q(x))/(Bp(x)+Cp1(x)*Cp2(x)+Dp(x)+...

    Fp(x)/sin(phi(x))); %(lb/{in^2 hr^2})

    deltaP(x)=(Lsum(x)-Lsum(x-1))*gz(x);%(lb/{in hr^2})

    P(x-1)=P(x)-deltaP(x);%(lb/{in hr^2})

    %length of filled segment before cylinder

    kN(x)=f*W(x)*H(x)*pi*D(x)*cos(phi(x))-
(pi*D(x)*W(x)*sin(phi(x)))/...

    (e*H(x)^2);%(in^3)

    kc12(x)=pi^2*D(x)^2*deltaf^3/(6*e*p)+p*e*deltaf^3/6; %(in^4)

    Wa(x)=D(x)*(1-cos(alphaa))+2*deltaf; %(inches)

    Ha(x)=0.5*D(x)*sin(alphaa);%(inches)

    hem(x)=Wa(x)/(2*H(x)); %(unitless)
```

MATLAB Function “Pressure”

```
ka(x)=2*(7*hem(x)^3*Ha(x)^4*(27*hem(x)^4+5))/(90*(55*hem(x)^4+38*...
    hem(x)^4+3)); %(in^4)
kch(x)=W(x)*(H(x)^3)/6;%(in^4)
kp(x)=kch(x)+ka(x)+kc12(x);%(in^4)
filL(x)=kp(x)*deltaP(x)/(mu*(kN(x)*N-Q(x)));%+ filL(x);%(inches)

%determining if fill length is more than length of segment or if
there
%is any filled length
if filL(x)>= L(x)
    Vfil(x)=Aavail(x)*L(x);%(in^3)
    filL(x-1)=L(x-1)-L(x);%(inches)
else
    pDf(x)=(Q(x)/N)/kN(x); % (unitless),drag flow
    pVfil(x)=pDf(x)*pi*H(x)^2*(L(x)-filL(x))*(360-45)/360;%(in^3)
    Vfil(x)=filL(x)*A(x)+pVfil(x);%(in^3)
end
end

%segment 8: forward with vent1
for x=8
    %calculating presure drop
    Wa(x)=D(x)*(1-cos(alphaa))+2*deltaf;%(inches)
    %using intermediates to find deltaP
    Ap(x)=0.5*fu*W(x)*H(x)*Vbz;%(in^3/hr)
    Bp(x)=W(x)*(H(x))^3/(12*mu);%(in^5 hr/lb)
    Cp1(x)=(pi*D(x)*(deltaf^3)*cos(phi(x)))/(12*mu*e);%(in^4 hr/lb)
```

MATLAB Function “Pressure”

```
Cp2(x)=pi*D(x)*cos(phi(x))/p; %(inches)

Cp3(x)=6*mu*Vbx*W(x)/((H(x))^2);%(lb/in hr^2)

Dp(x)=p*e*(deltaf^3)/(12*mu);%(in^5 hr/lb)

Ep(x)=.5*(1-fu)*pi*D(x)*(H(x)+.5*Wa(x))*Vb*sin(phi(x));% (in^3/hr)

Fp(x)=.5*(1-fu)*pi*D(x)*((H(x)+.5*Wa(x))^3)/(12*mu); %(in^5 hr/lb)

gz(x)=(Ap(x)-Cp1(x)*Cp3(x)-Ep(x)-
Q(x))/(Bp(x)+Cp1(x)*Cp2(x)+Dp(x)+...
    Fp(x)/sin(phi(x))); %(lb/{in^2 hr^2})

% P(x)=1; %atm, change to that of vacuum

% P(x)=P(x)*1.01325*10^5*7.233*12*3600^2/39.37^2; %(lb/{in hr^2})

deltaP(x)=(Lsum(x)-Lsum(x-1))*gz(x);%(lb/{in hr^2})

P(x-1)=P(x)-deltaP(x);%(lb/{in hr^2})

kN(x)=f*W(x)*H(x)*pi*D(x)*cos(phi(x))-
(pi*D(x)*W(x)*sin(phi(x)))/...
    (e*H(x)^2);%(in^3)

kc12(x)=pi^2*D(x)^2*deltaf^3/((6*e*p)+p*e*deltaf^3/6); %(in^4)

Wa(x)=D(x)*(1-cos(alphaa))+2*deltaf; %(inches)

Ha(x)=0.5*D(x)*sin(alphaa);%(inches)

hem(x)=Wa(x)/(2*H(x)); %(unitless)

ka(x)=2*(7*hem(x)^3*Ha(x)^4*(27*hem(x)^4+5))/(90*(55*hem(x)^4+38*...
    hem(x)^4+3)); %(in^4)

kch(x)=W(x)*(H(x)^3)/6;%(in^4)

kp(x)=kch(x)+ka(x)+kc12(x);%(in^4)

fill(x)=kp(x)*deltaP(x)/(mu*(kN(x)*N-Q(x)));%+fill(x);%(inches),
%last term added recently

%determining if fill length is more than length of segment or if
```

MATLAB Function “Pressure”

```
there

%is any filled length
    if filL(x) >= L(x)
        Vfil(x) = Aavail(x) * L(x); % (in^3)
        filL(x-1) = L(x-1) - L(x); % (inches)
    else
        pDf(x) = (Q(x)/N)/kN(x); % (unitless), drag flow
        pVfil(x) = pDf(x) * pi * H(x)^2 * (L(x) - filL(x)) * (360-45)/360; % (in^3)
        Vfil(x) = filL(x) * A(x) + pVfil(x); % (in^3)
    end
end

%segment 7: forward3
for x=7
    %calculating presure drop
    Wa(x) = D(x) * (1 - cos(alphaa)) + 2 * deltaf;
    %using intermediates to find deltaP
    Ap(x) = 0.5 * fu * W(x) * H(x) * Vbz; % (in^3/hr)
    Bp(x) = W(x) * (H(x))^3 / (12 * mu); % (in^5 hr/lb)
    Cp1(x) = (pi * D(x) * (deltaf^3) * cos(phi(x))) / (12 * mu * e); % (in^4 hr/lb)
    Cp2(x) = pi * D(x) * cos(phi(x)) / p; % (inches)
    Cp3(x) = 6 * mu * Vbx * W(x) / ((H(x))^2); % (lb/in hr^2)
    Dp(x) = p * e * (deltaf^3) / (12 * mu); % (in^5 hr/lb)
    Ep(x) = .5 * (1 - fu) * pi * D(x) * (H(x) + .5 * Wa(x)) * Vb * sin(phi(x)); % (in^3/hr)
    Fp(x) = .5 * (1 - fu) * pi * D(x) * ((H(x) + .5 * Wa(x))^3) / (12 * mu); % (in^5 hr/lb)
    gz(x) = (Ap(x) - Cp1(x) * Cp3(x) - Ep(x) -
Q(x)) / (Bp(x) + Cp1(x) * Cp2(x) + Dp(x) + ...
        Fp(x) / sin(phi(x))); % (lb/{in^2 hr^2})
end
```

MATLAB Function “Pressure”

```
deltaP(x)=(Lsum(x)-Lsum(x-1))*gz(x);%(lb/{in hr^2})

P(x-1)=P(x)-deltaP(x);%(lb/{in hr^2})

%length of filled segment before cylinder

kN(x)=f*W(x)*H(x)*pi*D(x)*cos(phi(x))-
(pi*D(x)*W(x)*sin(phi(x)))/...
    (e*H(x)^2);%(in^3)

kc12(x)=pi^2*D(x)^2*deltaf^3/(6*e*p)+p*e*deltaf^3/6; %(in^4)

Wa(x)=D(x)*(1-cos(alphaa))+2*deltaf; %(inches)

Ha(x)=0.5*D(x)*sin(alphaa);%(inches)

hem(x)=Wa(x)/(2*H(x)); %(unitless)

ka(x)=2*(7*hem(x)^3*Ha(x)^4*(27*hem(x)^4+5))/(90*(55*hem(x)^4+38*...
    hem(x)^4+3)); %(in^4)

kch(x)=W(x)*(H(x)^3)/6;%(in^4)

kp(x)=kch(x)+ka(x)+kc12(x);%(in^4)

filL(x)=kp(x)*deltaP(x)/(mu*(kN(x)*N-Q(x)));%+ filL(x);%(inches)

%determining if fill length is more than length of segment or if
there
%is any filled length
if filL(x)>= L(x)
    Vfil(x)=Aavail(x)*L(x);%(in^3)
    filL(x-1)=L(x-1)-L(x);%(inches)
else
    pDf(x)=(Q(x)/N)/kN(x); % (unitless),drag flow
    pVfil(x)=pDf(x)*pi*H(x)^2*(L(x)-filL(x))*(360-45)/360;%(in^3)
    Vfil(x)=filL(x)*A(x)+pVfil(x);%(in^3)
```

MATLAB Function “Pressure”

```
end

end

%segment 6: forward2 (with injection port)
for x=6

    %calculating presure drop

    Wa(x)=D(x)*(1-cos(alphaa))+2*deltaf;

    %using intermediates to find deltaP

    Ap(x)=0.5*fu*W(x)*H(x)*Vbz;%(in^3/hr)

    Bp(x)=W(x)*(H(x))^3/(12*mu);%(in^5 hr/lb)

    Cp1(x)=(pi*D(x)*(deltaf^3)*cos(phi(x)))/(12*mu*e);%(in^4 hr/lb)

    Cp2(x)=pi*D(x)*cos(phi(x))/p; %(inches)

    Cp3(x)=6*mu*Vbx*W(x)/((H(x))^2);%(lb/in hr^2)

    Dp(x)=p*e*(deltaf^3)/(12*mu);%(in^5 hr/lb)

    Ep(x)=.5*(1-fu)*pi*D(x)*(H(x)+.5*Wa(x))*Vb*sin(phi(x));% (in^3/hr)

    Fp(x)=.5*(1-fu)*pi*D(x)*((H(x)+.5*Wa(x))^3)/(12*mu); %(in^5 hr/lb)

    gz(x)=(Ap(x)-Cp1(x)*Cp3(x)-Ep(x)-
Q(x))/(Bp(x)+Cp1(x)*Cp2(x)+Dp(x)+...

    Fp(x)/sin(phi(x))); %(lb/{in^2 hr^2})

    deltaP(x)=(Lsum(x)-Lsum(x-1))*gz(x);%(lb/{in hr^2})

    P(x-1)=P(x)-deltaP(x);%(lb/{in hr^2})

    %length of filled segment before cylinder

    kN(x)=f*W(x)*H(x)*pi*D(x)*cos(phi(x))-
(pi*D(x)*W(x)*sin(phi(x)))/...

    (e*H(x)^2);%(in^3)

    kc12(x)=pi^2*D(x)^2*deltaf^3/(6*e*p)+p*e*deltaf^3/6; %(in^4)

    Wa(x)=D(x)*(1-cos(alphaa))+2*deltaf; %(inches)
```

MATLAB Function “Pressure”

```
Ha(x)=0.5*D(x)*sin(alphaa);%(inches)

hem(x)=Wa(x)/(2*H(x)); %(unitless)

ka(x)=2*(7*hem(x)^3*Ha(x)^4*(27*hem(x)^4+5))/(90*(55*hem(x)^4+38*...
    hem(x)^4+3)); %(in^4)

kch(x)=W(x)*(H(x)^3)/6;%(in^4)

kp(x)=kch(x)+ka(x)+kc12(x);%(in^4)

filL(x)=kp(x)*deltaP(x)/(mu*(kN(x)*N-Q(x)));%+ filL(x);%(inches)

%determining if fill length is more than length of segment or if
there
%is any filled length
if filL(x)>= L(x)
    Vfil(x)=Aavail(x)*L(x);%(in^3)
    filL(x-1)=L(x-1)-L(x);%(inches)
else
    pDf(x)=(Q(x)/N)/kN(x); % (unitless),drag flow
    pVfil(x)=pDf(x)*pi*H(x)^2*(L(x)-filL(x))*(360-45)/360;%(in^3)
    Vfil(x)=filL(x)*A(x)+pVfil(x);%(in^3)
end
end

%segment 5: cylinder1
for x=5
    k(x)=D(x)/Db; %(unitless)
    alffa=pi*((R(x))^4)*(1-(k(x))^4+((k(x))^4-2*(k(x))^2+1)/log(k(x)));
    Wa(x)=D(x)*(1-cos(alphaa))+2*deltaf;%(inches)
    Ha(x)=0.5*D(x)*sin(alphaa);%(inches)
```


MATLAB Function “Pressure”

```
hem(x)=Wa(x)/(2*H(x));%(unitless)

beeta=Ha(x)^4*(189*(hem(x))^5+35*(hem(x))^2)/(2475*(hem(x))^4+1710*...
    (hem(x))^2+135);%(inches)

deltaP(x)=L(x)*mu*Q(x)/(alfa+beeta);%(lb/{in hr^2})

P(x-1)=P(x)-deltaP(x);%(lb/{in hr^2})

fillL(x-1)=kp(x)*deltaP(x)/(mu*(kN(x)*N-Q(x)));%(inches)

%determining if fill length is more than length of segment or if
there
%is any filled length

Vfil(x)=Aavail(x)*L(x);%(in^3)

filL(x)=L(x);%(inches)

%length of filled segment before cylinder

end

%segment 4: forward1
for x=4

    %calculating presure drop

    Wa(x)=D(x)*(1-cos(alphaa))+2*deltaf;%(inches)

    %using intermediates to find deltaP

    Ap(x)=0.5*fu*W(x)*H(x)*Vbz;%(in^3/hr)

    Bp(x)=W(x)*(H(x))^3/(12*mu);%(in^5 hr/lb)

    Cp1(x)=(pi*D(x)*(deltaf^3)*cos(phi(x)))/(12*mu*e);%(in^4 hr/lb)

    Cp2(x)=pi*D(x)*cos(phi(x))/p; %(inches)
```

MATLAB Function “Pressure”

```

Cp3(x)=6*mu*Vbx*W(x)/((H(x))^2);%(lb/in hr^2)

Dp(x)=p*e*(deltaf^3)/(12*mu);%(in^5 hr/lb)

Ep(x)=.5*(1-fu)*pi*D(x)*(H(x)+.5*Wa(x))*Vb*sin(phi(x));% (in^3/hr)

Fp(x)=.5*(1-fu)*pi*D(x)*((H(x)+.5*Wa(x))^3)/(12*mu); %(in^5 hr/lb)

gz(x)=(Ap(x)-Cp1(x)*Cp3(x)-Ep(x)-
Q(x))/(Bp(x)+Cp1(x)*Cp2(x)+Dp(x)+...

    Fp(x)/sin(phi(x))); %(lb/{in^2 hr^2})

deltaP(x)=(Lsum(x)-Lsum(x-1))*gz(x);%(lb/{in hr^2})

P(x-1)=P(x)-deltaP(x);%(lb/{in hr^2})

%length of filled segment before cylinder

kN(x)=f*W(x)*H(x)*pi*D(x)*cos(phi(x))-
(pi*D(x)*W(x)*sin(phi(x)))/...

    (e*H(x)^2);%(in^3)

kc12(x)=pi^2*D(x)^2*deltaf^3/(6*e*p)+p*e*deltaf^3/6; %(in^4)

Wa(x)=D(x)*(1-cos(alphaa))+2*deltaf; %(inches)

Ha(x)=0.5*D(x)*sin(alphaa);%(inches)

hem(x)=Wa(x)/(2*H(x)); %(unitless)

ka(x)=2*(7*hem(x)^3*Ha(x)^4*(27*hem(x)^4+5))/(90*(55*hem(x)^4+38*...

    hem(x)^4+3)); %(in^4)

kch(x)=W(x)*(H(x)^3)/6;%(in^4)

kp(x)=kch(x)+ka(x)+kc12(x);%(in^4)

fill(x)=kp(x)*deltaP(x)/(mu*(kN(x)*N-Q(x)));%+ fill(x);%(inches)

%determining if fill length is more than length of segment or if
there

%is any filled length

if fill(x)>=L(x)

    Vfil(x)=Aavail(x)*L(x);

```

MATLAB Function “Pressure”

```
    fillL(x-1)=L(x-1)-L(x);  
  
    else  
  
        pDf(x)=(Q(x)/N)/kN(x); % %drag flow  
  
        pVfil(x)=pDf(x)*pi*H(x)^2*(L(x)-fillL(x))*(360-45)/360;  
  
        Vfil(x)=fillL(x)*A(x)+pVfil(x);  
  
    end  
  
end  
  
Pressure=Vfil; %(in^3)
```

MATLAB Function “Integrator3”

```
function integrator3=inte()

%inputs:

%x=segment #

%To= temperature at end of previous segment

%Fo= nylon flow rate at end of previous segment

%Volume = segment volume

x=load('x.txt'); %(unitless), segment number

To=load('Temp.txt');%(R)

Fo=load('N6mass.txt');%(lb/hr)

Volume=load('Vol.txt');%(in^3)

Xo=0;%conversion at beginning of section

Po=0;%product flow at beginning of section

    options=odeset('RelTol',1e-5, 'AbsTol',[1e-5 1e-5 1e-5 1e-5]);

    [Vx,z]=ode23s('Rxxdiff2',[0 Volume],[Xo To Fo Po],options);

    [r,c]=size(z);

    Xc=z(r,1); % conversion%(unitless)

    Tp=z(r,2); %Temperature%(R)

    F=z(r,3); %nylon flow %(lb/hr)

    P=z(r,4); %product flow %(lb/hr)

integrator3=[Xc,Tp,F,P]
```

MATLAB Function “Rxndiff2”

```
function Rxndiff2=Diffe(Vx,z)

%inputs
x=load('x.txt'); %(unitless), segment number
comp1=load('comp1.txt'); %(unitless), composition
U=load('U.txt');%(btu/{hr in^2 R}), overall heat transfer coefficient
Fo=load('N6mass.txt');%(lb/hr), nylon flow rate at end of previous
segment
Volume=load('Vol.txt');%(in^3), volume of segment
To=load('Temp.txt');%(R), temperature at the end of pervious segment

feeds=feedinfo();
rhom(1)=feeds(13,1);%(lb/in^3)
Tb=feeds(3,1);%(R)

screws=screwdim();
Aavail(x)=screws(33,x);%(in^2)
RxnArea=Aavail(x);%(in^2)
A(x)=screws(34,x);%(in^2)
Ener(x)=screws(43,x);%(Btu/hr)
SArea=A(x);%(in^2)

%Heat capacities
Cp(1)=(1.236+2.73*10^-3 *Tb)*0.239; %(btu/{lbm F}),n6 molten @ barrel
temp.
Cp(2)=0.26+0.0023*(Tb/1.8-273.15);%(btu/{lbm F}), molten PP
Cp(3)=.203; %(btu/{lbm F}), CaCO3,
```

MATLAB Function "Rxndiff2"

```
Cp(4)=1.83/4.1868; %(btu/{lbm F}), SBR
Cp(5)=78.65920/(56.11*4.1868);%(btu/{lbm F}), KOH
Cp(6)=2.345/4.1868;%(btu/{lbm F}), caprolactam

for xxt=1:6

    Thetar(xxt)=comp1(xxt)/comp1(1);
Cptheta(xxt)=Cp(xxt)*Thetar(xxt);

end

Cpthetasum=sum(Cptheta)-Cptheta(1);% sum except for N6

R=1.987; %universal gas constant, BTU/(lbmol R)

%kinetic constants, to be corrected

    no=1; %order of reaction

%Activation energy

    Ea=131000; %J/mol

    Ea=Ea*453.593*9.486*10^-4; %(Btu/lbmole), conversion

% preexponential

    ko=9.68E+10; %(min^-1)

    ko=ko*60; %(hr^-1)

k=ko*exp((-Ea/(R*z(2))));%(hr^-1)

rP=k*rhom(1)*(1-z(1))^no;%(conversion per hr)%definition -rp=+kCa(1-
alpha)

%calculating heat of rxn
```

MATLAB Function “Rxndiff2”

```
dHrxnTref= 340; %(kJ/kg), look up from DTA data
dHrxnTref= dHrxnTref*1000*9.486*10^-4/2.20462; %(Btu/lb)
Trefd=350; %(C)
Trefd=Trefd+273.15; %(K)
Trefd=Trefd*1.8; %(R)
DeltaCp=Cp(6)-Cp(1);%check units
dHrxnT=dHrxnTref+DeltaCp*(z(2)-Trefd);%(Btu/lb)
Hrxn=rP.*(dHrxnT)*Volume;%(Btu/hr)..check

%Qw=U*SArea*(Tb-To);%(btu/{hr } )
Qw=U*SArea*(Tb-z(2));%(btu/{hr } ), heat transferred from wall
    fid=fopen('Qwf.txt','w');
    fprintf(fid,'%6.4f/n',Qw);
    fclose(fid);

Fcon=Fo*(Cp(1)+Cpthetasum);

Rxndiff2(1,:)=rP./Fo;
Rxndiff2(2,:)=(-Hrxn+Qw+Ener(x))/Fcon;
Rxndiff2(3,:)=-(rP);
Rxndiff2(4,:)=rP;
Rxndiff2;
```

REFERENCES

1. MinHut, C., D. K. Captain, F. Gadala-Maria and D. Amiridis., *Review: Recycling of Nylon from Carpet Waste*. Polymer Engineering and Science, 2001. **41**(9): p. 1457-1470.
2. Zhang, Y., *Manufacturing of Glass Mat Reinforced Thermoplastics from Carpet Waste*, in *School of Textile and Fiber Engineering*. 1999, Georgia Institute of Technology: Atlanta.
3. www.carpertrecovery.org, *Carpet America Recovery Effort 2006 Annual Report*. 2007.
4. Wang, Y., Y. Zhang, M. Polk, S. Kumar, and J. Muzzy, *Chapter 16: Recycling of Carpet and Textile Fibers*, in *PLASTICS AND THE ENVIRONMENT: A Handbook*, A.L. Andrady, Editor. 2003, John Wiley & Sons: New York. p. 697-725.
5. Wang, Y., *Recycling Technologies for Fibrous Textile & Carpet Waste and Research Activities at Georgia Tech*. 1998:
<http://www.tfe.gatech.edu/faculty/wang/fiberrecycle/sld006.htm>.
6. McKinney, R.J., *Ammonolysis of Nylon*. 1994: U.S.
7. Bodrero, S., et al. *Chemical recycling of polyamide 6,6 and polyamide 6 through a two step AMI-/ammonolysis process*. in *4th Annual conference on Recycling of Fibrous Textile and Carpet Waste*. 1999. Dolton, Georgia.
8. Hendrix, J.A., et al., *Depolymerization of Polyamides*. 1997: U.S.
9. Bonfield, J.H., et al., *Polycaprolactam Depolymerization*: U.S.
10. Braun, M., et al., *Recycling Nylon 6 Carpet to Caprolactam*. Polym.-Plastics Tech. & Engr., 1999. **38**(3): p. 471-484.
11. Jenczewshi, T.J., et. al. AlliedSignal Inc., *Monomer Recovery From Multi-Component Materials*. 1997.

12. Chaupart, N., et al., *Molecular weight distribution and mass changes during polyamide hydrolysis*. *Polymer Engineering and Science*, 1998. **39**(6-7): p. 1375-1380.
13. Bassler, P., et al., *Producing caprolactam through hydrolytic cleavage of molten polycaprolactam*. 1996.
14. Bajaj, P., et al., *Reuse of polymer and fibre waste*, in *Manufactured Fibre Technology*, V.K.K. V.B. Gupta, Editor. 1997, Chapman & Hall: New York.
15. Corbin, T., et. al, *Reclaiming epsilon-caprolactam from nylon 6 carpet with use of auxiliary streams*. 1999: US.
16. Moran, E.F., E.I. Dupont de Nemours., *Conversion of nylon 6 and/or nylon 66 to monomers*. 1994: US.
17. Moran, E.F., et al., E.I. Dupont de Nemours., *Conversion of nylon 6 and/or nylon 6,6 to adipic acid*. 1995.
18. Kotek, R.B.C., *Semi-continuous depolymerization of nylon 6 polymer*. 1994: US.
19. Myers, C.D., *Recovery of nylon ingredients*. 1946: U.S.
20. Schut, J.H. *Big German Plant may Relieve US Bottleneck in Recycling Carpet nylon*. 2002 [cited; Available from: www.plasticstechnology.com].
21. Rice, S., and R. MacLean, *Ask the Expert*. greenbiz.com, November 2001.
22. Thomissen, P.J.H., *Depolymerization of Polyamides*. 1965.
23. Herra, M., et al., *Main Products and kinetics of thermal degradation of polyamides*. *Chemosphere*, 2001. **42**: p. 601-607.
24. Lehrle, R.S., *Thermal degradation mechanism of nylon 6 deduced from kinetic studies by pyrolysis-g.c*. *Polymer Degradation and Stability*, 2000. **67**: p. 21-33.

25. Won, C.-Y., *Depolymerization of nylon 6,6 in the Presence of Phase Transfer Catalyst.*, in *School of Textile and Fiber Engineering*. 1994, Georgia Institute of Technology: Atlanta.
26. Polk, M.B., et.al., *Nylon 66, nylon 46, and PET phase-transfer-catalyzed alkaline depolymerization at atmospheric pressure*. *Polym.-Plast. Technol. Eng.*, 1999. **38**(3): p. 459.
27. Mukherjee, A.K., et. al., *Depolymerization of Poly-caprolactam Catalyzed by Sodium Hydroxide*. *Journal of Applied Polymer Science*, 1978. **22**: p. 361-368.
28. Nielinger, W., et.al. , *Process for the recovery of caprolactam by pyrolysis of polyamide 6*, B. Aktiengesellschaft, Editor. 1993: U.S.
29. Czernik, S., et. al., *Catalytic pyrolysis of nylon-6 to recover caprolactam*. *Journal of Analytical and Applied Pyrolysis*, 1998. **46**: p. 51-51.
30. Bockhorn, H., et al., *Kinetic study on the non-catalysed and catalysed degradation of polyamide 6 with isothermal and dynamic methods*. *Thermochimica Acta*, 1999. **337**: p. 97-110.
31. Bockhorn, H., et al., *Pyrolysis of polyamide 6 under catalytic conditions and its application to reutilization of carpets*. *Journal of Analytical and Applied Pyrolysis*, 2001. **58-59**: p. 79-94.
32. Takahashi, Y., M. Kamimoto, Y. Abe, R. Sakamoto, K. Kanari, and T. Ozawa, *Investigation of Latent Heat-thermal Energy Storage Materials. IV. Thermoanalytical Evaluation of Binary Eutectic Mixtures of NaOH with LiOH or KOH*. *Thermochimica Acta*, 1987. **121**: p. 193-202.
33. Bale, C.W., and Arthur D. Pelton *Coupled phase diagram and thermodynamic analysis of the 18 binary systems formed among Li₂CO₃, K₂CO₃, Na₂CO₃, LiOH, KOH, NaOH, Li₂SO₄, K₂SO₄ and Na₂SO₄*. *Calphad* 1982. **6**(4): p. 255-278.
34. *KOH-NaOH: Data from FTsalt-FACT salt Databases*, Facility for the Analysis of Chemical Thermodynamics.
<http://www.crct.polymtl.ca/fact/documentation/FTsalt/KOH-NaOH.jpg>.

35. Dauby, C., J. Glibert and P. Claes, *Electrical Conductivity and Specific Mass of the molten NaOH-KOH Eutectic Mixture*. Ekcmchimics Arm., 1979. **24**: p. 35-39.
36. Price, D.M., Douglas J. Hourston, and Fabrice Dumont. *Thermogravimetry of Polymers*. Encyclopedia of Analytical Chemistry 2000 pp. 8094–8105 [cited; Available from: <http://www.sump4.com/publications/book001.pdf>].
37. Beyler, C.L., and M.M. Hirschler. *SECTION ONE : Chapter 7: Thermal Decomposition of Polymers*. [cited; Available from: http://www.gbhinternational.com/papers_5_13_02/368_Beyler_Hirschler_SFPE_Handbook_3.pdf].
38. Ortega, A., *The Kinetics of Solid-State Reactions Towards Consensus - Part 3. Searching for consistent kinetic results: SCTA vs. conventional thermal analysis*. Int J Chem Kinet, 2002. **34**(4): p. 223 - 236.
39. Khawam, A., and Douglas R. Flanagan, *Basics and Applications of Solid-State Kinetics: A Pharmaceutical Perspective*. Journal of Pharmaceutical Sciences, 2006. **95**(3): p. 472-498.
40. Ortega, A., *The Kinetics of Solid-State Reactions Towards Consensus - Part 1: Uncertainties, Failures, and Successes of Conventional Methods*. Int J Chem Kinet, 2001. **33**(6): p. 334-352.
41. Minying, L., G. Lijun, Z. Qingxiang, W. Yudong, Y. Xiaojuan, and C. Shaokui. *Thermal degradation process and kinetics of poly(dodecamethyleneisophthalamide)*. 2003 Jun. 1, 2003 [cited; Available from: <http://www.chemistrymag.org/cji/2003/056043pe.htm>].
42. Ortega, A., *The Kinetics of Solid-State Reactions Towards Consensus - Part 2: Fitting Kinetics Data in Dynamic Conventional Thermal Analysis*. Int J Chem Kinet, 2002. **34**(3): p. 193-208.
43. Galwey, A.K., and M. E. Brown, *Thermal Decomposition of Ionic Solids*. 1999, New York: Elsevier.
44. Capart, R., L. Khezami, and A.K. Burnham, *Assessment of various kinetic models for the pyrolysis of a microgranular cellulose*. Thermochemica Acta, 2004. **47**: p. 79-89.

45. Wang, X., X. Li, D. Yan, *Isothermal Gravimetric Analysis of Poly(trimethylene terephthalate)*. J App Polym Sci, 2002. **84**: p. 1600-1608.
46. Tang, W., X. Li, D. Yan, *Thermal Decomposition Kinetics of Thermotropic Copolyesters Made from trans-p-Hydroxycinnamic Acid and p-Hydrobenzoic Acid*. Journal of Applied Polymer Science, 2004. **91**: p. 445-454.
47. Bockhorn, H., A. Hornung, U. Hornung, S. Teepe and J. Weichmann, *Investigation of the Kinetics of Thermal Degradation of Commodity Plastics*. Combust. Sci. and Tech., 1996. **116-117**: p. 129-151.
48. Criado, J.M., and M. Gonzalez *The Methos of Calculation of Kinetic Parameters as a Possible cause of Apparent Compensation Effects*. Thermochemica Acta, 1981. **46**: p. 201-207.
49. *ASTM Test Method E1641, "Standard Test Method for Decomposition Kinetics by Thermogravimetry"*, in *ASTM Book of Standards*. 1994, American Society for Testing and Materials. p. 1042-1046.
50. Ozawa, T., *A New Method of Analyzing Thermogravimetric Data*. Bulletin of the Chemical Society of Japan, 1965. **38**: p. 1881-1886
51. Flynn, J.H., and L. A. Wall, *A Quick, Direct Method for the Determination of Activation Energy from Thermogravimetric Data*. Polymer Letters 1966. **4** p. 323-328
52. Scott, S.A., J.S. Dennis, J.F. Davidson, and A. N. Hayhurst, *An algorithm for determining the kinetics of devolatilisation of complex solid fuels from thermogravimetric experiments*. Chemical Engineering Science, 2006. **61**: p. 2339-2348.
53. *CHAPTER 3. EXPERIMENTAL DESIGN AND METHODOLOGY: Thermal Analysis* [cited 2006 June 5]; Available from: <http://etd02.lnx390.lsu.edu/docs/available/etd-0409102-112238/unrestricted/Di-3.pdf>.
54. *Chapter 3. Thermal Analysis (Chapter 12 Campbell & White)* . <http://www.eng.uc.edu/~gbeauca/Classes/Analysis/Chapter3.pdf>.

55. Nairn, J.A., *Chapter 11: Differential Scanning Calorimetry*:
<http://www.mse.utah.edu/~nairn/classes/mse5473/Notes/11DSC.pdf>.
56. Melling, R., F.W. Wilburn, and R.M. McIntosh, *Study of Thermal Effects Observed by Differential Thermal Analysis: Theory and Its Application to Influence of Sample Parameters on a Typical DTA Curve*. Analytical Chemistry, 1969. **41**(10): p. 1275-1286.
57. Evans, R., J. Scahill, M. Looker, and S. Czernik, *Conversations on waste carpet recycling*. 2003, National Research Energy Laboratory (NREL): Golden, CO.
58. Nawrath, D., *Diaminoketone aus Lactamen*. Angew. Chem., 1960. **72**(24): p. 1002.
59. Holland, B.J., and J. N. Hay, *Thermal degradation of nylon polymers*. Polymer International, 2000. **49**: p. 943-948.
60. Kamerbeek B., G.H.K., and W. Grolle *Thermal Degradation of Polymers*. Society of Chemical Industry, Monograph, 1961. **13**: p. 357
61. Peebles, L.H., and M.W. Huffman, J. Polym. Sci. , 1971. **9**: p. 1807.
62. Ravve, A., *Principles of Polymer Chemistry*. 2nd ed. 2000, New York: Kluwer Academic/ Plenum Publishers.
63. Tiedt, L.R., and W.E. Pretorius. *An Introduction to Electron Microscopy and X-ray Microanalysis*. [cited 2006 April]; Available from:
http://www.puk.ac.za/fakulteite/natuur/lem/LEM_diktaat.pdf.
64. chemfinder.com.
65. Brandrup, J., and E. H. Immergut, ed., *Polymer Handbook, 2nd ed*. 1975, New York: John Wiley & Son Inc.
66. Xanthos, M., *Reactive extrusion: Principles and Practice*. 1992, New York: Hanser.

67. Stevens, M.J., and J. A. Covas, *Extruder Principles and Operations*. 1995, London: Chapman & Hall.
68. Cheremisinoff, N.P., *Polymer Mixing and Extrusion Technology*. 1987, New York: Marcel Dekker, Inc.
69. White, J., L., *Twin Screw Extruders: Technology and Principles*. 1991, New York: Hanser.
70. Albalak, R.J., *Polymer Devolatilization*. 1996, New York: Marcel Dekker, Inc.
71. Rauwendaal, C., *Polymer Extrusion*. 4th ed. 2001, Cincinnati: Hanser.
72. Thompson, M.R., A. N. Hrymak and A. E. Hamielec, *Modeling the Reactive Modification of HDPE in a Nonintermeshing Twin Screw Extruder*. *Advances in Polymer Technology*, 1995. **14**(2): p. 87-96.
73. Tadmor, Z., and Imrich Klein, *Engineering Principles of Plasticating Extrusion*. Polymer Science and Engineering Series. 1970, New York: van Nostrand Reinhold.
74. Hagberg, C.G., and Eugene R. Uhl, *Scaleup of melt conveying parameters in counter-rotating non-intermeshing twin screw extruders*. ANTEC, 2001. **59th**: p. 206-214.
75. Min, K., M.H. Kim, and J. L. White, *Int. Polym. Proc*, 1988. **3**: p. 165.
76. Janssen, L.P.B.M., *Reactive Extrusion Systems*. 2004, New York: Marcel Dekker, Inc.
77. Pinto, G., and Tadmor, Z. , *Polym. Eng. Sci.*, 1970. **29**: p. 709.
78. Lu, Y., Biesenberger, J. A., and Todd, D. B., ANTEC 1993: p. 27.
79. Darnell, W.H., and E. A. J. Mol, *SPE Journal*, 1956. **12**(April): p. 21.
80. Kaplan, A., and Z. Tadmor, *Polym. Eng. Sci.* , 1974. **14**: p. 58.

81. Nichols, R.J., and J. Yao, SPE ANTEC Tech. Papers, 1982. **28**: p. 416.
82. Mudalamane, R., David I. Bigio, David C. Tomayko. Marcel Meissel. , *Behavior of fully filled regions in a non-intermeshing twin-screw extruder*. Polymer Engineering and Science, 2003. **43**(8): p. 1466-1476.
83. Giles, H.F., Jr., J. R. Wagner Jr, and E. M. Mount III, *Extrusion - The definitive Processing Guide and Handbook*. 2005, Norwich, NY: William Andrew Pub.
84. Jepson, C.H., Ind. Eng. Chem., 1953. **45**: p. 992.
85. Cheremisinoff, N.P., *Guidebook to extrusion technology*. 1993, Englewood Cliffs, NJ: Prentice-Hall.
86. Potente, H., and S. Kramme, *Scale-Up in the Design of Extrusion Dies*. Macromol. Mater. Eng., 2002. **287**(11): p. 745 - 749.
87. Jin, K., *Processing Characteristics and Properties of Glass Fiber Reinforced Composites from Post Consumer Carpets*, in *School of Polymer, Textile and Fiber Engineering*. 2003, Georgia Institute of Technology: Atlanta, GA.
88. *NFM/WE Machine Capabilities and Specifications in* http://www.nfm.net/products_we_specs.html. 1998-2007, NFM Welding Engineers.
89. *Installation, Operation and Maintenance Instruction Manual for Twin Screw Extruder*. 2004, Massillon, OH: NFM Welding Engineers.
90. Fogler, S., *Elements of Chemical Reaction Engineering*. 3rd ed. 1998, Upper Saddle River, NJ: Prentice Hall Ptr
91. Turton, R., R. C. Bailie, W. B. Whiting, J. A. Shaeiwitz, *Analysis, Synthesis, and Design of Chemical Processes*. 1998, Upper Saddle River, NJ: Prentice Hall.
92. *Chemical market reporter* 2004.
93. Almaz Optics, *Calcium Carbonate (Calcite), CaCO₃*: <http://www.almazoptics.com/CaCO3.htm>.

94. Safety Officer in Physical Chemistry at Oxford University, *Safety data for potassium hydroxide*:
http://physchem.ox.ac.uk/MSDS/PO/potassium_hydroxide.html.
95. EC21, *SBR(Styrene Butadiene) Rubber Sheet, Rubber Mats*:
[http://skypro.en.ec21.com/product_detail.jsp?group_id=GC00793336&product_id=CA00793386&product_nm=SBR\(Styrene_Butadiene\)_Rubber_Sheet,_Rubber_Mats,](http://skypro.en.ec21.com/product_detail.jsp?group_id=GC00793336&product_id=CA00793386&product_nm=SBR(Styrene_Butadiene)_Rubber_Sheet,_Rubber_Mats,).
96. Stelray Plastic Products, *Density Values- Selected Resins*:
http://www.stelray.com/density_val.htm.
97. National Institute of Standards and Technology:
<http://webbook.nist.gov/cgi/cbook.cgi?Name=koh&Units=SI&cTC=on>.
98. Yutopian, *Thermal and Mechanical Properties of Nylon*. 2000:
<http://www.yutopian.com/Yuan/prop/Nylon.html>.
99. Gaur, U., S. Lau, B. B. Wunderlich, B. Wunderlich, *Heat Capacity and Other Thermodynamic Properties of Linear Macromolecules. VIII. Polyesters and Polyamides*. J. Phys. Chem. Ref. Data. , 1983. **12**(1): p. 65-89.
100. Gaur, U., B. Wunderlich, *Heat Capacity and Other Thermodynamic Properties of Linear Macromolecules IV. Polypropylene*. J. Phys. Chem. Ref. Data, 1981. **10**(4): p. 1051-1064.
101. Geankoplis, C.J., *Transport Processes and Unit Operation, 3rd ed.* 1993, Englewood Cliffs, NJ: Prentice Hall P T R.